OCS Report
MMS 92-0024

Straits of Florida
Physical Oceanographic Field Study

Final Interpretive Report
Volume II: Technical Report

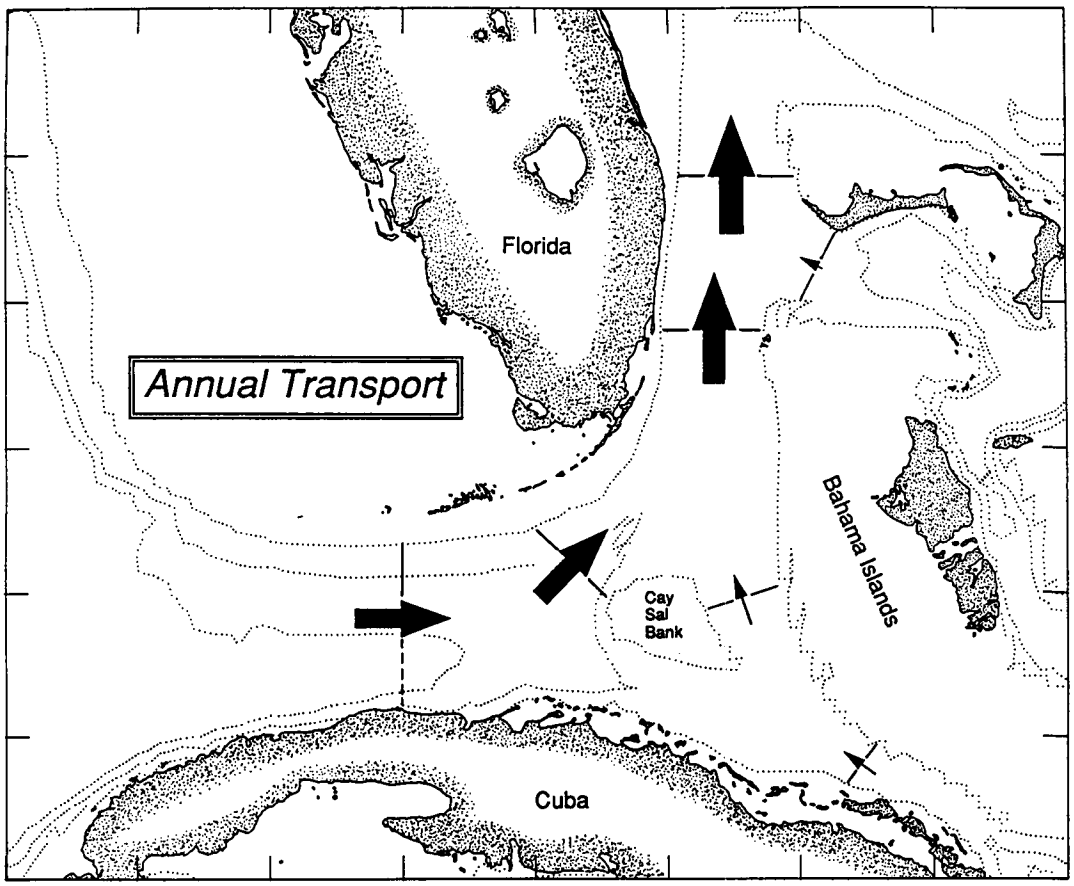

U.S. Department of the Interior
Minerals Management Service
Atlantic OCS Region

OCS Report
MMS 92-0024

Straits of Florida Physical Oceanographic Field Study

Final Interpretive Report
Volume II: Technical Report

Author:

Science Applications International Corporation

Prepared under MMS Contract
14-35-0001-30493
by
Science Applications International Corporation
Raleigh, North Carolina 27605

Program Manager: Evans Waddell, Ph.D.
Science Applications International Corporation
Raleigh, North Carolina 27605

Project Officer: Robert Miller, Ph.D.
Minerals Management Service
Atlantic OCS Regional Office

Published by:

U.S. Department of the Interior
Minerals Management Service
Atlantic OCS Regional Office

Herndon
1992

DISCLAIMER

This report was prepared under contract between the Minerals Management Service (MMS) and Science Applications International Corporation (SAIC). This report has been technically reviewed by the MMS and approved for publication. Approval does not signify that the contents necessarily reflect the views and policies of the Service, nor does mention of trade names or commercial products constitute endorsement or recommendation for use. It is, however, exempt from review and compliance with MMS editorial standards.

REPORT AVAILABILITY

Extra copies of the report may be obtained from the Public Information Unit (Mail Stop OPS-3-4) at the following address:

U.S. Department of the Interior
Minerals Management Service
Atlantic Region (LE-4)
381 Elden Street
Suite 1109
Herndon, VA 22070-4817

Telephone Number: (504) 736-2519

CITATION

Science Applications International Corporation, 1992, Straits of Florida Physical Oceanographic Field Study, Final Interpretive Report. Volume II: Technical Report. OCS Report/MMS 92-0024. U.S. Dept. of the Interior, Minerals Management Service, Gulf of Mexico OCS Regional Office, New Orleans, LA. 179 pp.

ABOUT THE COVER

The cover illustration suggests the relative scale of annual transport through the various channels in the general study area.

ABSTRACT

The Straits of Florida Physical Oceanographic Field Study was initiated by the MMS to develop a data base which would support future numerical modeling of the study area and allow an improved understanding of the circulation and transport patterns and their causative mechanisms. A one-year field measurement program initiated in November 1992 included the following observations:

- Subsurface currents/temperature
- Velocity profiles using Pegasus technology
- Hydrographic surveys (CTD/XBT)
- Lagrangian drifters
- Winds
- Satellite Imagery
- Water levels

In addition, MMS arranged for NOAA to provide voltages on across channel telephone cables which can be used for independent estimates of net transport.

A successful field program provided the basis for improved documentation and understanding of the magnitude and variability of current and hydrographic fields as well the time varying transport over a series of eight transects on the primary and lateral channels in the study area.

Results showed that configuration of the Loop Current can affect flow throughout the study area including bifercating the Florida Current flow around Cay Sal Bank. Old Bahama Channel contributes a relatively substantial transport volume as well as water mass characteristics not found in water entering from the Gulf of Mexico.

TABLE OF CONTENTS

Section		Page
	List of Figures	iv
	List of Tables	xiii
	Acknowledgements	xv
I.	INTRODUCTION	1
	1.1 Study Objectives	1
	1.2 Scope of the Study	1
	1.3 Approach and Methodology	4
	1.3.1 Introduction	4
	1.3.2 Study Area Description	4
	1.3.3 Program Sampling Design	4
	1.3.4 PEGASUS Profiling	6
	1.3.5 Drifters	6
	1.3.6 Hydrography	6
	1.3.7 Ancillary Data	6
	1.3.7.1 Satellite Imagery	6
	1.3.7.2 Meteorological Observation	7
	1.3.7.3 Water Level Observations	7
II.	TIDES	9
	2.1 Tidal Currents and Elevations	9
	2.2 Tidal Transport	11
III.	HYDROGRAPHY	15
	3.1 Introduction	15
	3.1.1 Sampling Locations and Time	15
	3.2 Hydrographic Conditions - Cruise One (90-35)	15
	3.2.1 Temperature, Salinity and Density Sections	15
	3.3 Hydrographic Conditions - Cruise Two (91-03)	23
	3.3.1 Temperature, Salinity and Density Sections	23
	3.4 Hydrographic Conditions - Cruise Three (91-12)	30
	3.4.1 Temperature, Salinity and Density Sections	30
	3.5 Hydrographic Conditions - Cruise Four (91-17)	38
	3.5.1 Temperature, Salinity and Density Sections	38

TABLE OF CONTENTS (CONT.)

Section		Page
3.6	Hydrographic Conditions - Cruise Five (91-20)	46
3.6.1	Temperature, Salinity and Density Sections	54
3.7	Mean Temperatures	54
3.8	Seasonal Patterns	61
3.8.1	Comments	62
IV.	**FLORIDA CURRENT VARIABILITY AND CIRCULATION**	66
4.1	Introduction	66
4.1.1	Northern Straits of Florida	66
4.1.2	Eastern Gulf of Mexico	68
4.1.3	Southern Straits of Florida	69
4.2	Low-Frequency Variability	70
4.2.1	Southern Straits of Florida	70
4.2.1.1	Spatial and Temporal Variability	70
4.2.1.2	Energy Distribution and Coherence Scales	87
4.2.2	Northern Straits of Florida	93
4.2.2.1	Spatial and Temporal Variability	93
4.2.2.2	Energy Distribution and Coherence Scales	93
4.2.2.3	Northwest Providence Channel	93
4.3	First Order Statistics of Moored Current and Temperature Fields	100
4.3.1	Mean Properties	100
4.3.2	Standard Deviation Fields	111
4.4	Forcing Mechanisms	111
4.4.1	Florida Current Meanders, Eddies and Gyres	111
4.4.2	Wind Forcing	115
4.4.3	Circulation in the Old Bahama Channel	123
4.5	Summary	125
V.	**SECTIONAL VELOCITIES AND TRANSPORT**	131
5.1	Introduction	131
5.2	Velocity and Transport Based on PEGASUS Technology	131

TABLE OF CONTENTS (CONT.)

Section		Page
	5.2.1 Velocity Cross Sections	131
	5.2.2 Average Velocity/Temperature Cross Sections	133
	5.2.2.1 Northwest Providence Channel	133
	5.2.2.2 Santaren Channel	137
	5.2.2.3 Transect B	142
	5.2.3 Transports	147
	5.2.4 Comparison to Other Observations	148
5.3	Transport Estimates Based on Current-Meter Data	150
	5.3.1 Methods of Estimation	150
	5.3.2 Subtidal Transport	155
	5.3.3 Transport Spectra and Coherence	160
	5.3.4 Wind Forcing	166
VI.	**SUMMARY**	172
6.1	Introduction	172
6.2	Current Patterns	172
6.3	Transport	173
6.4	Hydrography	174
6.5	Tides	175
REFERENCES		176

LIST OF FIGURES

Figure No.	Caption	Page
1.1-1	Map of the general study area	2
1.3-1	Locations of moorings deployed on the indicated sections (Transects A, B, C, D, E, F, G and H)	5
1.3-2	Map showing the location of meteorological and water level measurement sets	8
2.1-1	Hodographs for M_2 tidal constituent. Ellipse boundary describes tidal vector terminus path over a cycle. Rotational sense is indicated by arrow head. A 6 cm sec^{-1} vector is shown for scale. Diamonds show water level measurement sites with associated tidal phase and amplitude in boxes	10
2.1-2	Hodographs and tidal water level information for K_1 tidal constituent. For an explanation of information contained in this figure, see caption of Figure 2.1-1	12
2.1-3	Hodographs and tidal water level information for O_1 tidal constituent. For an explanation of information contained in this figure, see caption of Figure 2.1-1	13
3.2-1.	Location of stations during Cruise I. Squares (□) indicate CTD stations. Crosses (x) are XBT stations	16
3.2-2.	Composite T/S plot for Cruise I	17
3.2-3.	Temperature, salinity and density sections, Transect B (Big Pine Key to Cay Sal)	18
3.2-4.	Temperature, salinity and density sections, Transect C (Miami to Bimini)	20
3.2-5.	Temperature sections, Transect D (Jupiter to Settlement Point)	21
3.2-6.	Temperature sections, Transect E (Northwest Providence Channel)	22
3.2-7.	Temperature, salinity, density sections, Transect F (Santaren Channel)	24
3.3-1.	Station locations for Cruise II. Squares (□) indicate CTD stations. Crosses (x) are XTB stations	25
3.3-2.	Composite T/S plot for Cruise II	26

LIST OF FIGURES (CONT.)

Figure No.	Caption	Page
3.3-3.	Temperature section, Transect A (Marguesas Keys to Havana)	27
3.3-4.	Temperature, salinity, density section, Transect B	28
3.3-5.	Temperature, salinity and density section, Transect C	29
3.3-6.	Temperature section, Transect D	31
3.3-7.	Temperature, salinity, density section, Transect E	32
3.3-8.	Temperature, salinity, and density section, Transect F (Santaren Channel)	33
3.4-1.	Station locations for Cruise III. Squares (□) indicate CTD stations. Crosses (x) are XBT stations	34
3.4-2.	Composite T/S plot for Cruise III	35
3.4-3.	Temperature, salinity, and density sections, Transect A	36
3.4-4.	Temperature, salinity, and density sections, Transect B	37
3.4-5.	Temperature, salinity, and density sections, Transect C	39
3.4-6.	Temperature sections, Transect D	40
3.4-7.	Temperature, salinity and density sections, Transect E	41
3.4-8.	Temperature, salinity and density sections, Transect F	42
3.5-1.	Location of stations for Cruise IV. Squares (□) indicate CTD stations. Crosses (x) are XBT stations	43
3.5-2.	Composite T/S plot for Cruise IV	44
3.5-3.	Temperature, salinity and density sections, Transect A	45
3.5-4.	Temperature, salinity and density sections, Transect B	47
3.5-5.	Temperature, salinity and density sections, Transect C	48
3.5-6.	Temperature section, Transect D	49
3.5-7.	Temperature, salinity and density sections, Transect E	50
3.5-8.	Temperature section, Transect F	51

LIST OF FIGURES (CONT.)

Figure No.	Caption	Page
3.6-1.	Location of stations for Cruise V. Squares (□) indicate CTD stations. Crosses (x) are XBT stations	52
3.6-2.	Composite T/S plot for Cruise V	53
3.6-3.	Temperature, salinity, and density sections, Transect A . . .	55
3.6-4.	Temperature, salinity, and density sections, Transect B . . .	56
3.6-5.	Temperature, salinity, and density sections, Transect C . . .	57
3.6-6.	Temperature section, Transect D	58
3.6-7.	Temperature, salinity and density sections, Transect E . . .	59
3.6-8.	Temperature, salinity and density sections, Transect F . . .	60
3.8-1.	Maximum temperature at Transects B, C, and F	63
3.8-2.	Maximum salinity at Transects B, C, and F	64
4.2-1.	40-HLP filtered temperature and velocity for the entire measurement period at Mooring A1, instrument at 145 m below the surface. Data from the beginning of the study period is at the top and data from the end of the study period, at the bottom	72
4.2-2.	40-HLP filtered temperature and velocity for the period March 1991 through August 1991 for instruments at 300 m on Moorings A2 and A3. The first half of the record is at the top and the second half at the bottom	73
4.2-3.	40-HLP filtered temperature and velocity data for the entire measurement period at 75 m on Mooring B1. The total record is divided into three periods and presented. See the axis just below each stick plot for time	74
4.2-4.	40-HLP velocity for the indicated moorings and depths. Time interval presented is from March through April 1991 . .	75
4.2-5	Composite thermal image for week of Dec. 16-22, 1991. Vectors are as of noon GMT, December 19, 1991	76
4.2-6	Composite thermal image for week of Feb. 17-23, 1991. Vectors are as of noon GMT, February 20, 1991	77

LIST OF FIGURES (CONT.)

Figure No.	Caption	Page
4.2-7a	Composite thermal image for week of March 3-9, 1991. Vectors are as of noon GMT, March 5, 1991	78
4.2-7b	Composite thermal image for week of March 10-16, 1991. Vectors are as of noon GMT, March 12, 1991	78
4.2-7c	Composite thermal image for week of March 17-23, 1991. Vectors are as of noon GMT, March 19, 1991	79
4.2-7d	Composite thermal image for week of March 24-30, 1991. Vectors are as of noon GMT, March 26, 1991	79
4.2-7e	Composite thermal image for week of March 31-April 6, 1991. Vectors are as of noon GMT, April 2, 1991	80
4.2-7f	Composite thermal image for week of April 7-13, 1991. Vectors are as of noon GMT, April 9, 1991	80
4.2-7g	Composite thermal image for week of April 21-27, 1991. Vectors are as of noon GMT, April 23, 1991	81
4.2-8	Cross section of temperatures in the upper 200 m on Line A	83
4.2-9	40-HLP velocity and temperature records for Moorings F1, F2 and F3 at 300 m for the period March-May 1991	85
4.2-10	40-HLP velocity and temperature records for Mooring G1 at 50, 250 and 450 m depths over the period from March-May, 1991	86
4.2-11a	Spectra of 3-HLP normal velocity components. Records analyzed were made by the uppermost instrument on Moorings A1, B1, B4, and F4 as noted in the figure	88
4.2-11b	Spectra for 3-HLP normal velocity components. Record analyzed was made by the uppermost instrument on Mooring G1. The time interval analyzed is the same as in Figure 4.2-11a	89
4.2-12	Spectra for 3-HLP temperature records as measured on Moorings B1, B2 and B3. The time period analyzed is the same as in Figure 4.2-11	90
4.2-13	Phase and coherence plots for a) normal velocity components at the upper instrument (75m) on B1 and B2, and b) the normal velocity components as measured by the instrument on Moorings B1 (150 m) and B4 (145 m)	91

LIST OF FIGURES (CONT.)

Figure No.	Caption	Page
4.2-14a,b	Phase and coherence for a) uppermost instrument on 1) Mooring F1 and F3 and 2) A1 and B1, and b) uppermost instruments on Moorings F1 and B4	92
4.2-15	40-HLP filtered temperature and velocity records for the upper instruments on Moorings C1, C2 and C3 for the period from December 1990 - March 1991	94
4.2-16	40-HLP filtered temperature and velocity records for the upper instruments on Moorings D1, D2 and D3 for the period from December 1990 - March 1991	95
4.2-17	Spectra of 3-HLP velocity components for instruments at a) 100 m on Mooring C1 and b) 145 m on Mooring D1	96
4.2-18	Phase and coherence for 40-HLP filtered normal (v) components of velocity between a) the upper instruments on Moorings C1 and C2, and b) the instruments at 250 m and 300 m on Moorings C1 and C2, respectively	97
4.2-19	Phase and coherence for 40-HLP filtered transect normal (v) velocity components between a) instruments on C1 at 250 m and D1 at 300 m, and b) instruments on F3 at 50 m and C3 at 145 m	98
4.2-20	40-HLP temperature and velocity records from Mooring E1 (300 m) and E3 (300 m) for the period from January to March 1991	99
4.2-21	Phase and coherence between like components at 100 m on Moorings E1 and E3	101
4.3-1	Plot of the mean vector for current velocities measured at the upper instrument on each mooring. The notation for 145 m is provided since that is the upper instrument depth for many of the moorings. Note the scale vector drawn on the west Florida shelf	102
4.3-2	Plot of the mean vector for current velocities measured at approximately 300 m. below the surface. Note the scale vector drawn on the west Florida shelf	103
4.3-3	Plot of the mean vector for current velocities measured at approximately 600 m. below the surface. For those moorings having no instrument that deep, no vector is drawn. Note the scale vector drawn on the west Florida shelf	104

LIST OF FIGURES (CONT.)

Figure No.	Caption	Page
4.3-4	Contours of means for a) transect-normal velocity and b) temperature. Mean values were computed using the complete available time series on Transect A	105
4.3-5	Contours of means for a) transect-normal velocity and b) temperature. Mean values were computed using the complete available time series on Transect B	106
4.3-6	Contours of means for a) transect-normal velocity and b) temperature. Mean values were computed using the complete available time series on Transect C	107
4.3-7	Contours of means for a) transect-normal velocity and b) temperature. Mean values were computed using the complete available time series on Transect D	108
4.3-8	Contours of means for a) transect-normal velocity and b) temperature. Mean values were computed using the complete available time series on Transect E	109
4.3-9	Contours of means for a) transect-normal velocity and b) temperature. Mean values were computed using the complete available time series on Transect F	110
4.3-10	Contours of standard deviations of transect-normal velocity for a) Transect A and b) Transect B	112
4.3-11	Contours of standard deviations of transect-normal velocity for a) Transect C and b) Transect D	113
4.3-12	Contours of standard deviations of transect-normal velocity for a) Transect E and b) Transect F	114
4.4-1	Spectra for the indicated components of 40-HLP filtered wind stress at Key West, Miami and W. Palm Beach FL. All units are dyne cm^{-2}	117
4.4-2	Spectra of transport over the indicated transects	118
4.4-3	Spectra of transport over the indicated transects	119
4.4-4	Phase and coherence between 1) Section D transport as computed from current meter data and along-channel component of wind stress at W. Palm Beach, and 2) Section D transport as estimated from cable voltages and along-channel component of wind stress at W. Palm Beach.	120

LIST OF FIGURES (CONT.)

Figure No.	Caption	Page
4.4-5	Phase and coherence between transport over Transect C and the along-channel component of wind stress from 1) W. Palm Beach and 2) Miami	121
4.4-6	Phase and coherence between transport as estimated by the cable at Transect A and 1) along-channel component of wind stress and 2) water level at Key West	122
4.4-7	Profiles of temperature, salinity and density taken at Mooring G in Old Bahama Channel. One set of profiles is given for each cruise. Note the mid-depth (100-300 m) salinity maximum which is commonly found	124
4.4-8a	Time series (3-HLP) of pressure, temperature and along-channel current speed at the indicated depths. The time interval presented is from June to September 1991. Note the large pressure changes in June and July as strong currents caused the top of the mooring to be drawn down . . .	126
4.4-8b	The same time series presented in Figure 4.4-8a but for the period from September to November 1991. Note the absence of large pressure fluctuations after the mooring was stiffened. Note the episodes of very high currents at mid-depth in October	127
4.4-9	Spectra of 3-HLP along-channel velocity component showing the strong tidal and inertial signals	128
5.2-1	Area maps showing PEGASUS station locations and identifiers .	132
5.2-2	Average velocity component normal (a) and parallel (b) to Section E, and temperature (c): November 1990	134
5.2-3	Average velocity component normal (a) and parallel (b) to Section E, and temperature (c): February 1991	135
5.2-4	Average velocity component normal (a) and parallel (b) to Section E, and temperature (c): September 1991	136
5.2-5	Average velocity component normal (a) and parallel (b) to Section F, and temperature (c): November 1990	138
5.2-6	Average velocity component normal (a) and parallel (b) to Section F, and temperature (c): February 1991	139
5.2-7	Average velocity component normal (a) and parallel (b) to Section F, and temperature (c): May 1991	140

LIST OF FIGURES (CONT.)

Figure No.	Caption	Page
5.2-8	Average velocity component normal (a) and parallel (b) to Section F, and temperature (c): September 1991	141
5.2-9	Average velocity component normal (a) and parallel (b) to Section B, and temperature (c): November 1990	143
5.2-10	Average velocity component normal (a) and parallel (b) to Section B, and temperature (c): February 1991	144
5.2-11	Average velocity component normal (a) and parallel (b) to Section B, and temperature (c): May 1991	145
5.2-12	Average velocity component normal (a) and parallel (b) to Section B, and temperature (c): September 1991	146
5.3-1	Time series of along-channel velocity components at the indicated depths, the actual (solid line) and estimated (dashed line) pressure used in the transport computation scheme, and transport based on current meters (solid) and the cable (dashed)	151
5.3-2	Time series of transport as based on cable voltages at the north end of the study area (solid line), the west end of the study area (dotted line/Key West to Havana) and the annual signal at the northern line. The larger dots show transports as estimated using PEGASUS technology. See text for further information	153
5.3-3	Time series plots of transport based on current meters (solid lines) and cables (dashed line) on the indicated transects for the period from December 1990 to November 1991	154
5.3-4	Transport time series estimated by sums or differences (solid line) and cable-based or current meter-based estimates on the indicated transect. The bottom plot shows the complete estimate of transport on Transect A using both cable and sums and differences of transport in other channels	157
5.3-5a,b	Spectra of 40-HLP transport over the indicated transects: a) transport over Transect D based on current meters and cable, b) transport over Transects B and C	161

LIST OF FIGURES (CONT.)

Figure No.	Caption	Page
5.3-5c,d	Spectra of 40-HLP transport over the indicated transects: c) transport over A with 1) cable, and 2) and 3) sums and differences, d) transport over Transects 1) E, 2) F and 3) G. Note that (B+F) estimates Transect A without consideration of input from OBC. B+F-G is the complete estimate of transport over Transect A	162
5.3-6a,b	Phase and coherence between the indicated time series. (a) shows results for various methods of estimating transport on Transect A; (b) shows relation between 1) Transects B and C, and 2) Transects C and D	163
5.3-6c,d	Phase and coherence between the indicated time series. (c) shows (1) Transects F vs. C and (2) sum of B+F vs. C; (b) shows (1) Transects C vs. E and (2) Transects E vs. D	164
5.3-6e	Phase and coherence between 1) transport on Transect D as estimated by the cable and current meters, and 2) transport as estimated by cables on Transects A and D	165
5.3-7	a) Spectra of along-channel wind stress for the indicated locations, b) Phase and coherence between 1) along-channel components at Key West and Miami and 2) N-S (along-channel) components at Miami and West Palm Beach	167
5.3-8a,b	Phase and coherence for: a) transport over Transect A (cable) vs. 1) along-channel wind stress and 2) water level at Key West; b) transport over Transect B vs. 1) cross-channel (N-S) wind stress at Key West and 2) along-channel water level gradient between Miami and Key West . . .	168
5.3-8c,d	Phase and coherence for: c) transport over Transect C vs. along-channel wind stress at 1) W. Palm Beach and 2) Miami; d) transport over Transect D vs. along-channel wind stress at 1) W. Palm Beach and 2) Miami	169
5.3-9	Phase and coherence for: a) transport over Transect E and 1) along-channel wind stress and 2) water level at Settlement Point, and b) transport over Transect F and 1) along-channel wind stress at Miami and 2) water level at Settlement Point	171

LIST OF TABLES

Table No.	Caption	Page
2.2-1	Tidal Constituent Transports	11
3.1-1	Summary listing of hydrographic profiles by transect, cruise and type	19
3.7-1	Mean Maximum Salinity by Section	61
5.2-1	Average Sectional Transports	147
5.3-1	Comparison of 1991 Transport Measurements. October 10, 15, 18, 28, 31 and November 2, 4, 6	155
5.3-2	Transport Statistics and Correlations	159

Acknowledgements

The success of a complex undertaking such as the Straits of Florida Physical Oceanographic Field Study results from the diligent support of a number of skilled and dedicated individuals. Thanks are extended to those who went to sea aboard the **M/V Seaward Explorer** and the **R/V Calanus**. The excellence and continuity of data resulting from these field activities were the foundation of the program. Dr. Robert Miller (MMS/Atlantic Region) provided valuable program support and guidance which is much appreciated. An Interagency Agreement between MMS and NOAA provided for participation in the program of Dr. James Larsen, PMEL, and incorporation of transport estimates based on his cross-channel cable measurements. He also made us aware of additional Pegasus-based transport estimates at 27°N made by M. Bushnell (AOML) which provided program principal investigators with increased confidence in the computational scheme for estimating transport from current-meter time series.

I. INTRODUCTION

1.1 Study Objectives

The Minerals Management Service (MMS), through its Outer Continental Shelf (OCS) Environmental Studies Program, funds various projects that support the MMS's statutory requirement to understand and describe "environmental impacts on the human, marine, and coastal environments of the OCS and coastal areas that might be affected by oil and gas development" (43 U.S.C. 1346). It is in this context that the MMS contracted with Science Applications International Corporation (SAIC) to conduct the Physical Oceanographic Field Study of the Straits of Florida (SoF).

The specific objectives of this study were twofold:

1) To acquire data sets that provide initial and boundary conditions for a numerical circulation model as well as information that can be used for model validation and verification.

2) To develop an improved understanding of primary circulation patterns in the study area and the responsible forcing mechanisms.

The overall rationale for the SoF project, which both these objectives support, is development of a numerical circulation model which will provide improved input to and hence reliability of the Oil Spill Risk Assessment (OSRA) model results. OSRA is used to provide a probabilistic characterization of potential adverse impacts of activities linked directly to offshore oil and gas development, production, and transportation.

The study area is the path followed by the Florida Current/Gulf Stream (Figure 1.1-1). Effective and compatible modeling of the Loop Current and the Gulf Stream is essential to a proper characterization of linked circulation patterns in the Gulf of Mexico and the South Atlantic Bight. This points to the importance of having a circulation model that can adequately reflect conditions and patterns in this key waterway. An improved documentation and understanding of the expected transport and current patterns is also important to the overall MMS objectives since knowledge of the dynamics governing circulation provides guidance in developing an appropriate model and provides a basis for evaluating model performance (skill assessment).

1.2 Scope of the Study

The SoF Physical Oceanography Study involved one year of coordinated observations of those variables determined to be of key importance to subsequent circulation modeling and to the present and any future process synthesis. The specific experimental design was developed in keeping with the RFP requirements and after discussion with numerical circulation modelers as well as this program's principal investigators.

Of primary concern to the modelers, and hence a major thrust of this study, is documentation of volume transport as it varies in time at the boundaries of the study area, in particular along 82°W and 27°N. In addition, water level

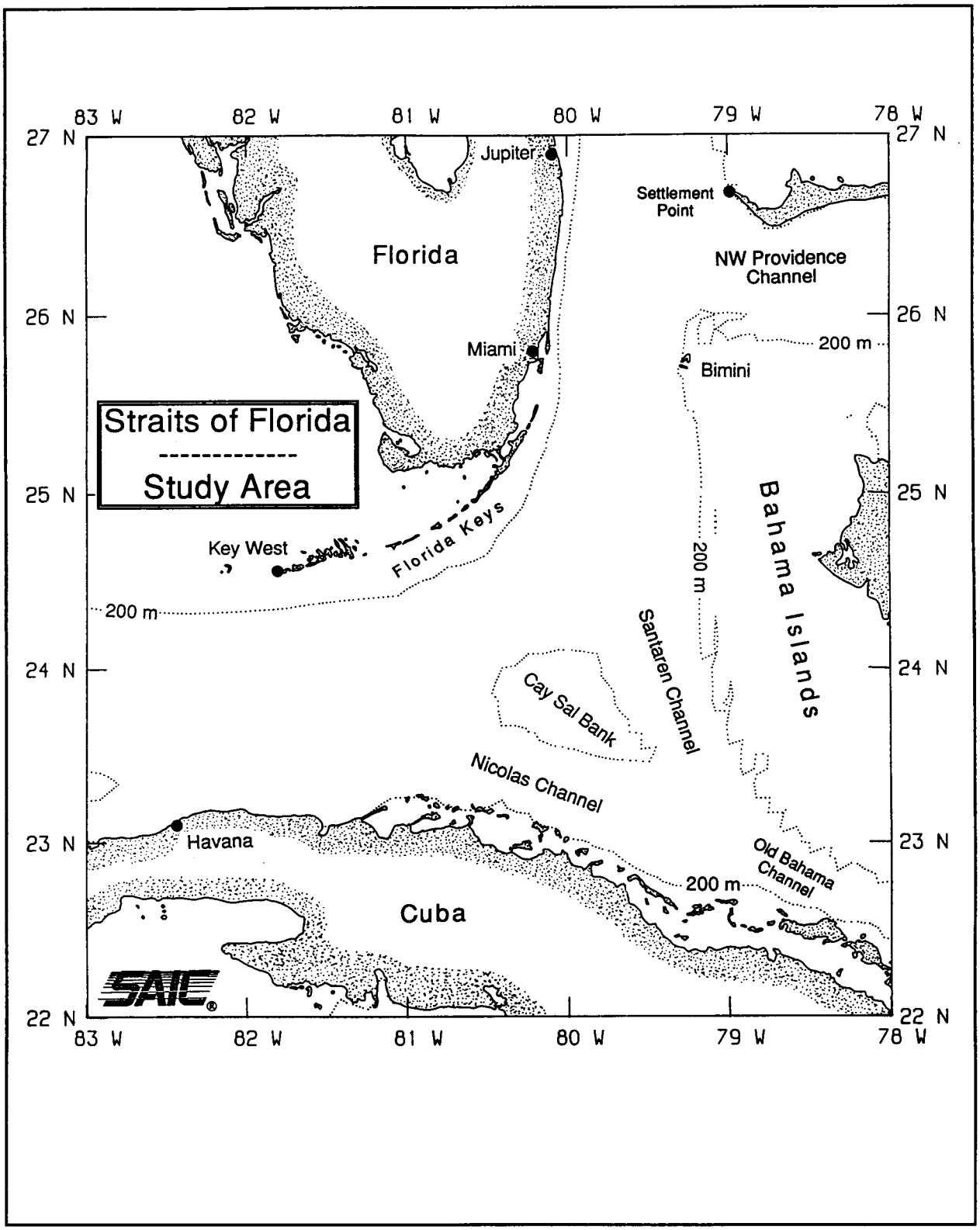

Figure 1.1-1 Map of the general study area.

gradients along and across the primary and secondary channels are of interest to support modeling. To document mass transport requires information on the time varying density and current velocity fields at the domain boundaries.

The following primary and ancillary variables were either measured as part of the field program or acquired from other sources:

1) Subsurface currents (velocity, temperature)

2) Surface currents velocity (lagrangian)

3) Hydrographic measurements - temperature and salinity

4) Ancillary Data

- Satellite thermal imagery
- Meteorological observation (wind velocity, air temperature, and atmospheric pressure).
- Water levels

The above data were supplemented with detailed vertical profiles of horizontal velocity as determined with PEGASUS technology.

Generally, field activities occurred as follows: Five seasonal cruises were made during which all field equipment (current meters and water level sensors) were either deployed, rotated or retrieved. On each cruise, conductivity, temperature and depth profiler (CTD) and expendable bathythermograph (XBT) profiles were used to measure profiles along each mooring transect in such a way as to support and complement subsurface current velocity data. During each cruise, three ARGOS-tracked surface drifters were to be released and tracked for 50 days. PEGASUS-based velocity profiles were measured during four separate cruises, which occurred approximately quarterly. Satellite thermal imagery was obtained for the study area. The meteorological observations were obtained from existing NOAA measurement sites as were some of the water level data.

Transport time series were computed using subsurface current data. These estimates were compared with transport computed using PEGASUS velocity profiles that were made on three primary cross-channel transects.

Key program scientific participants are:

Dr. L. Atkinson (Old Dominion University)
Dr. T. Berger (SAIC)
Dr. P. Hamilton (SAIC)
Dr. K. Leaman (U. of Miami)
Dr. T. Lee (U. of Miami)

Primary program support personnel from SAIC include:

Dr. E. Waddell, Program Manager
Mr. J. Singer, Logistics Manager
Dr. R. Wayland, Data Manager

One contract deliverable that the reader is directed to is the Program Data Report, which describes in detail data taken (when, where and what), data return and data processing procedures. These topics will be included in the present report only to the extent that is necessary to present program results in an appropriate framework.

1.3 Approach and Methodology

1.3.1 Introduction

1.3.2 Study Area Description

The Gulf Stream (GS) has a major role in maintaining a meridional heat transport as well as being a primary influence on circulation patterns along the Atlantic coast of the United States (US). The precursor of the Gulf Stream, the Loop Current, enters the Gulf of Mexico via the Yucatan Straits and exits by the SoF. While in the Straits of Florida, this major western boundary current is called the Florida Current (FC). The study area (Figure 1.1-1) for the present program is the SoF, and the primary oceanographic features to be documented are the FC and related circulation patterns in the region.

The southern or western end of the SoF is a 150 km wide, steep-sided channel between the Florida Keys and Cuba. In this approach, water depths shoal until they are approximately 1500m on a line between Key West and Havana. Further eastward, the main channel turns 90° to the north. In this area of channel curvature, maximum water depths continue to shoal with the deepest part of the channel skewed to the offshore.

After the northward turn, the main FC channel remains steep-sided with the Florida Keys and mainland Florida on the west and the Bahama Islands to the east. Northwest Providence Channel (NWPC), which opens into this channel at about 26°N, connects the SoF with the Atlantic. Water depths in this northern section of the SoF are generally less than 800 m or about half that found at 82°N.

In the area where the main channel turns to the north is Cay Sal Bank, a large but shallow (water depths $\leq$ 30m) reef whose presence creates two other channels - Nicholas Channel toward Cuba and Santaren Channel (SC) towards the Bahamas Islands (Great Bahama Bank). Southeast of Cay Sal Bank is the Old Bahama Channel (OBC), a narrow passage separating Great Bahama Bank from Cuba and connecting the SoF with the Caribbean Sea.

1.3.3 Program Sampling Design

Moored current meter arrays were placed on four approximately equally spaced cross-channel transects (A, B, C and D) as well as in NWPC (E), SC (F) and OBC (G) as shown in Figure 1.3-1. An additional mooring (H) was placed between the Dry Tortugas and the Marquesas Keys to provide an indication of the flow through the deeper portion of the intervening channel.

These instrumented transects provide the velocity data that was used to estimate transport through the main and lateral channels as well as providing information needed to document FC dynamics. The various sectional transport estimates can be combined to compute and check input and outputs for the total study area as well as subunits (control volumes). The approximate along-channel separation of

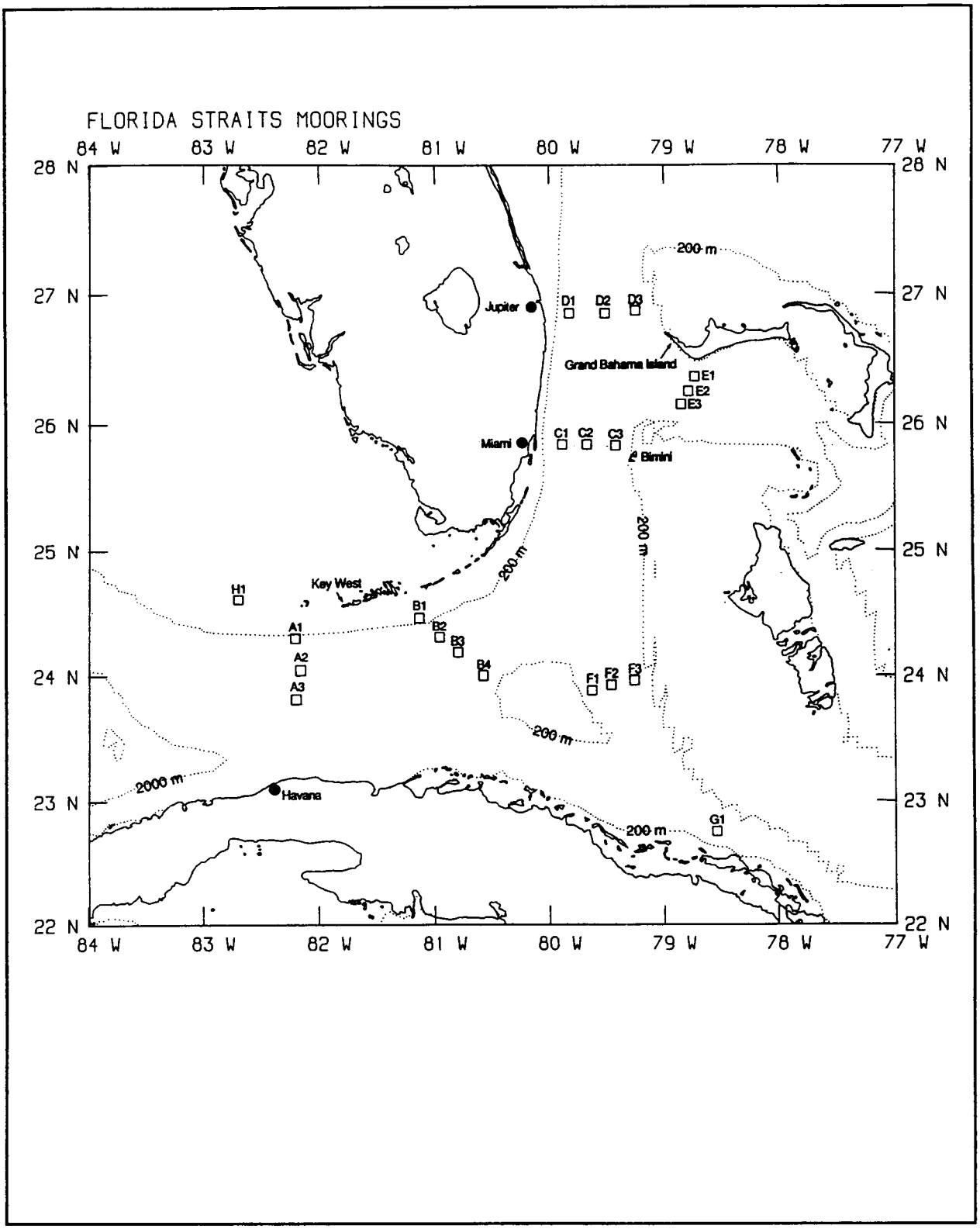

Figure 1.3-1 Locations of moorings deployed on the indicated sections (Transects A, B, C, D, E, F, G and H).

Transects A, B, C and D is 60 to 80 nautical miles, which provides appropriate resolution of the expected wave length of meanders that occur in the SoF. This distribution of transects also provides two sets of observations on both sides of the northward 90° turn of the main channel in the middle of the study area. The location of Transects A and B also allows coordination and incorporation of selected data with an overlapping NOAA-funded study (SEFCAR) being conducted by Dr. T. Lee (U. of Miami), a principal investigator on the present study.

1.3.4 PEGASUS Profiling

A key element in the present study was development of methods by which measured velocity time series could be used to estimate the volume of water being transported through each instrumented transect. On Transect D, voltage, which was measured on an abandoned phone cable, was calibrated using PEGASUS technology during the Subtropical Atlantic Climate Study (STACS) to provide sectional transport estimates. Via an Interagency Agreement with NOAA, the MMS arranged for Dr. J. Larsen (NOAA/PMEL) to provide these cable-based transport estimates as well as those for a cable between Key West and Havana for the present study period. During the present study, PEGASUS was again used to provide accurate transport estimates through Transects B, E and F (Figure 1.3-1). With these and cable data from Transect D, transports computed from current meter time series through all key transects could be calibrated/evaluated.

1.3.5 Drifters

Three ARGOS-tracked, near-surface drifters, which were to be released during each of the five quarterly mooring deployment, rotation or recovery cruises, provided information having several uses. The resulting drifter trajectories are a good indicator of the movement of a surface-constrained water parcel as it responds to the time varying balance of forces. They also provide information which, when combined with subsurface current data, may enhance documentation of the vertical structure of the velocity field.

1.3.6 Hydrography

During each of the five quarterly mooring cruises, hydrographic profiles were measured along all of the mooring transects (Figure 1.3-1). These profiles were obtained with either a CTD profiler or XBTs. An examination of the temperature/salinity (TS) structure within the LC and GS shows the consistently strong correlation of these two variables. Within the LC/GS, knowledge of temperature provides an excellent indication of salinity. With this knowledge, SAIC proposed to rely more on XBTs at stations well inside the main LC/GS water mass. CTD observations were used more extensively near the GS boundary, especially near the surface where water masses may not conform to the documented TS correlation.

1.3.7 Ancillary Data

1.3.7.1 Satellite Imagery

During part of each year, sea surface temperature fields reflect some of the characteristics of the underlying water mass distribution. This is particularly true along the northern side of the Gulf Stream during the cooler months. During these periods the FC boundary at the surface can be located by looking for a

marked temperature gradient between the FC and the cooler water to the north. These data are more useful for the region south or west of the northward channel curvature where the west Florida shelf water tends to be cooler and the GS boundary position has substantial N-S variability in response to passage of features such as meanders.

1.3.7.2 Meteorological Observations

Previous studies, e.g. STACS, have shown some relationship between local currents and transport, and wind stress on the water surface (Lee and Williams, 1988). Consequently, local wind data was to be acquired from sites where observations were already being made. Of particular interest were those measurements made immediately adjacent to or over the water at the coast. This coastal proximity was important so the observations more adequately reflected conditions which existed over the water in the study area. A number of NOAA maintained sites exist along the U.S. coast between Key West in the south and Jupiter, Florida in the north (Figure 1.3-2).

1.3.7.3 Water Level Observations

The potential relation between transport and water level gradients was the rationale for these measurements. A series of existing NOAA-maintained measurement sites were located along the Florida Key and at one site in the Bahama Islands (Figure 1.3-2). These were supplemented with water level measurement at two sites as part of the present program. When the entire set of water level observations are grouped, water level gradients can be computed across many of the major channels (Transects B, C, D and E). Current meter-based transport estimates were also made on all four of these channels with PEGASUS or cable calibration data being available for three transects (B, D and E).

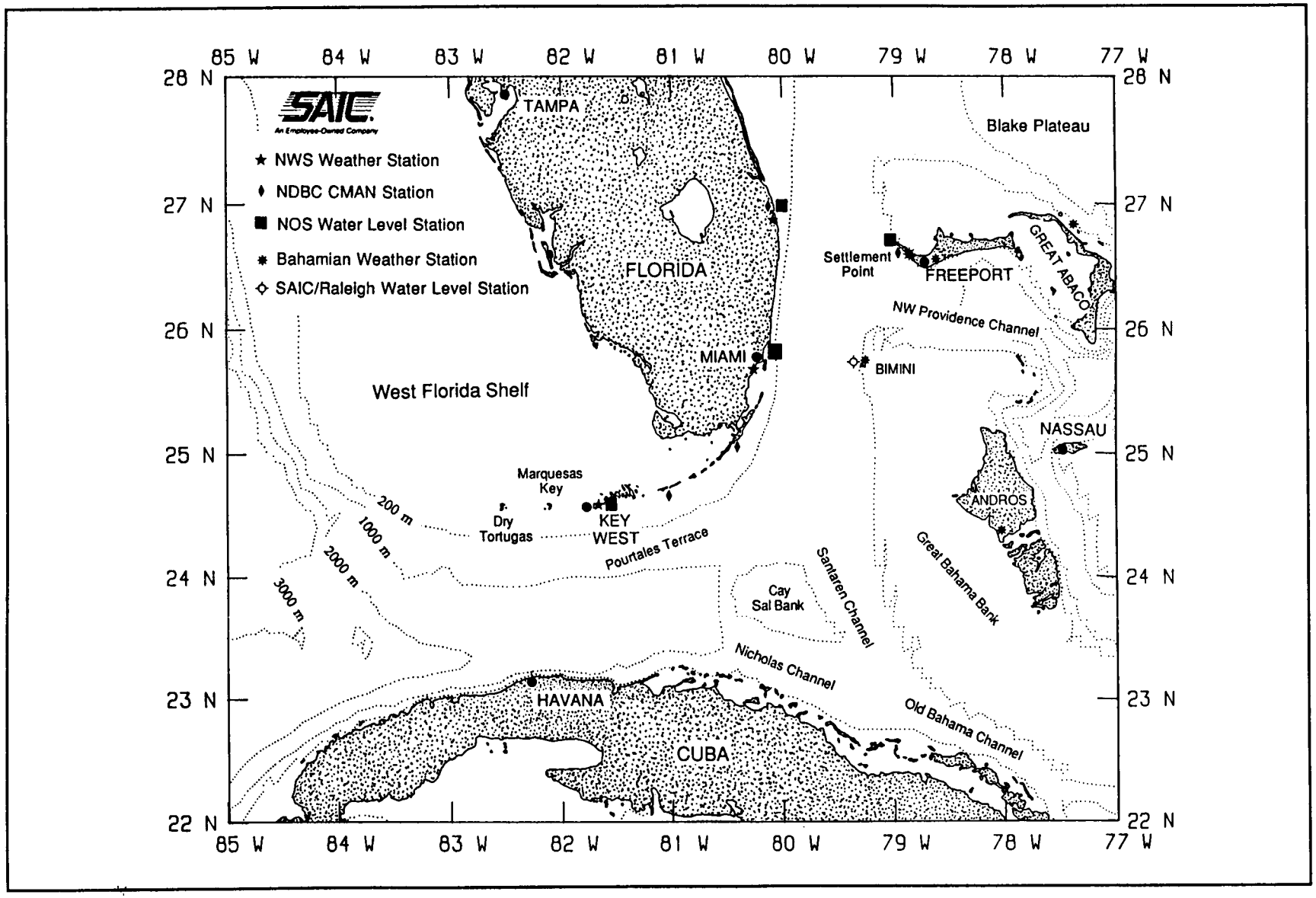

Figure 1.3-2 Map showing the location of meteorological and water level measurement sets.

II. TIDES

2.1 Tidal Currents and Elevations

Analyses of tidal currents in the Florida Straits have been previously restricted to the Miami-Cat Cay (Wunsch and Wimbush, 1977) and the STACS (Jupiter to Settlement Point) transect at about 27°N (Mayer et al., 1984). Both studies showed that the tidal currents are complex across the Florida Current with evidence of baroclinic internal motions, probably generated by the shelf topography of the western side of the Straits.

Tidal motions at 27°N have an rms amplitude for volume transport of 1.5 Sv with twice a year extremes of about 5 Sv (Mayer et al., 1984). The rms value is approximately half the annual signal and should be considered in the PEGASUS sampling schemes so as to minimize any tidal biases to the calculated transports.

The extensive nature of the current meter data base in this study allows a more comprehensive analysis of tidal currents between 27°N and Key West including the subsidiary SC, OBC and NWPC. The sea level and current meter records were analyzed using the standard harmonic analysis package developed by Foreman (1979), which is based on Godin's (1972) treatise. The principal constituents that dominate the tidal sea-level signal are the O_1, K_1, and M_2 with periods of 25.82, 23.93 and 12.42 hours respectively. The M_2 constituent dominates sea-level fluctuations at all stations. There are minor contributions from the Q_1, P_1, N_2 and S_2 constituents (Mayer et al., 1984).

Figure 2.1-1 shows the M_2 tidal hodographs for the uppermost current meter on each mooring. In the Florida Current, this is nominally 145m. On A1, B1, and B2, the depth is nominally 75m. In the SC and NWPC, the instruments are at a nominal 100m depth, and in the OBC (Mooring G), the mid-depth instrument of 250m was used because of the large depth excursions of the uppermost instrument, which caused large apparent diurnal fluctuations in current in some parts of the record (see Section 5). The analyses were performed on the longest possible records, generally 11 months. For a few instruments, shorter six-month records were used because of data gaps, and for the tide gauge on Cay Sal Bank (ZB51), only a three-month record was available.

The amplitude of M_2 sea-level signal decreased from 41 cm at 27°N to 17.7 cm at Key West. The propagation of the M_2 tide is also from the north towards the southwest (Figure 2.1-1). Despite the decrease in the M_2 elevations, the current velocity amplitudes have similar magnitudes at Transect B as at Transects D and C (3 to 4 cm s^{-1}). There is some decrease in amplitude at Transect A, where the FC is less constricted and channel depths are greater. M_2 currents at Transect D lead currents at Transect B, and the phase difference with nearby elevation stations is about a 50 to 60° lag, which indicates a mixed progressive (phase difference≈0) and standing (phase difference≈90°) wave. However, the relatively weak M_2 currents in the NWPC are close to being in-phase with Settlement Point, thus indicating a more purely progressive wave. This shows that the M_2 tidal characteristics in the NWPC and in the FC between 26 and 27°N may have quite complicated interactions. The M_2 tidal currents in the SC and OBC, which are relatively weak (1-2 cm s^{-1}), tend to be in-phase with current at B4 and therefore close to 90° out-of-phase with the sea level elevation on Cay Sal Bank (ZB51). However, the phase structure across Transect F shows a 90° phase shift, indicating further complexities around Cay Sal Bank.

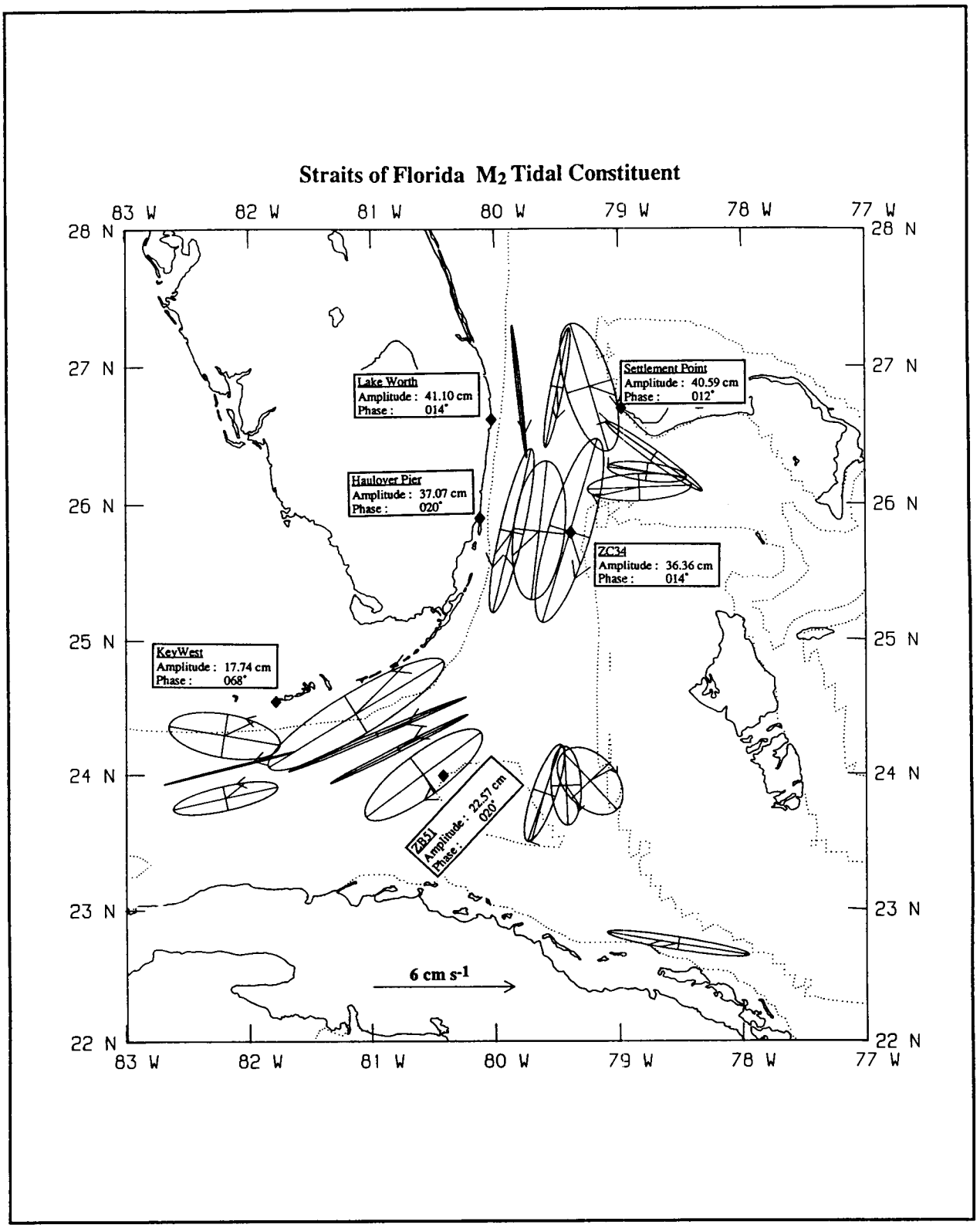

Figure 2.1-1 Hodographs for M_2 tidal constituent. Ellipse boundary describes tidal vector terminus path over a cycle. Rotational sense is indicated by arrow head. A 6 cm sec^{-1} vector is shown for scale. Diamonds show water level measurement sites with associated tidal phase and amplitude in boxes.

The K_1 constituent generates the largest tidal currents over most of the region (Figure 2.1-2). Tidal elevations decrease towards the southeast from 27°N and increase markedly towards the west. However, like the M_2 constituent, there is not a similar variation in K_1 tidal current amplitudes. The largest current amplitudes in the FC are at Transect C (≈5 cm s^{-1}). Tidal current amplitudes are also large in the NWPC (≈4 cm s^{-1}) and the Old Bahama Channel (≈8 cm s^{-1}). The propagation of phase from the elevation records is towards the southwest with marked cross channel differences on Transects C, D and E. On Transects A, B, C and E, the K_1 currents are approximately in-phase with each other despite the 119° phase difference in Miami and Key West sea level signals. This means that the tides have a more standing wave characteristic on Transects A and B and a more mixed characteristic with southwards propagation on Transects C and D. Transect E, on the other hand, shows a standing wave elevation and current phase difference on the north side but a mixed characteristic on the southside, where the currents have the largest amplitude. This again indicates that the character of the K_1 tide, like the M_2 tide, is particularly complex in its interaction with the FC and NWPC topography in the region 26° to 27°N.

The O_1 tide, shown here for completeness in Figure 2.1-3, shows characteristics in both sea level and currents that are similar to the K_1 constituent. The largest currents are found on Transects C and E and have similar phase relationships to each other and sea level as the K_1. The only significant difference is that the O_1 current amplitudes in the SC and OBC are not as strong as the K_1 (6 cm s^{-1} versus 8 cm s^{-1} in the OBC).

2.2 Tidal Transport

The contribution of the major constituents to the tidal transport through each transect can be estimated from the mean amplitude of the along-channel component multiplied by the cross-sectional area normal to the direction of the isobaths. These are given in Table 2.2-1.

Table 2.2-1 Tidal Constituent Transports

Transect	Cross-Sectional Area (km^2)	Constituent Transports (Sv)		
		M_2	K_1	O_1
B	59	1.8	1.9	2.2
C	46	1.3	2.1	1.7
D	48	1.2	0.9	1.5
E	27	0.4	0.9	0.9
F	31	0.2	0.3	0.3
G	11	0.3	0.9	0.6

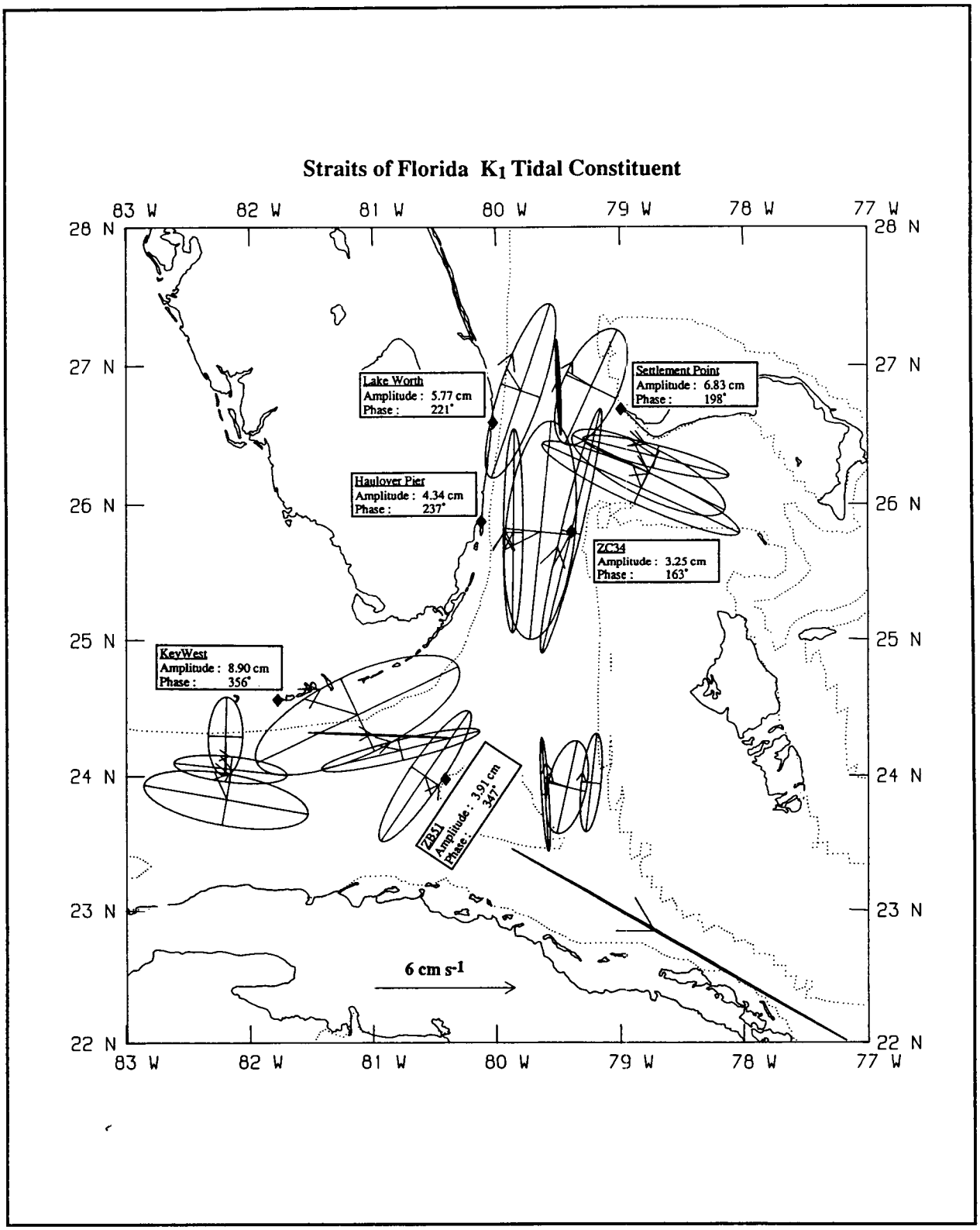

Figure 2.1-2 Hodographs and tidal water level information for K_1 tidal constituent. For an explanation of information contained in this figure, see caption of Figure 2.1-1.

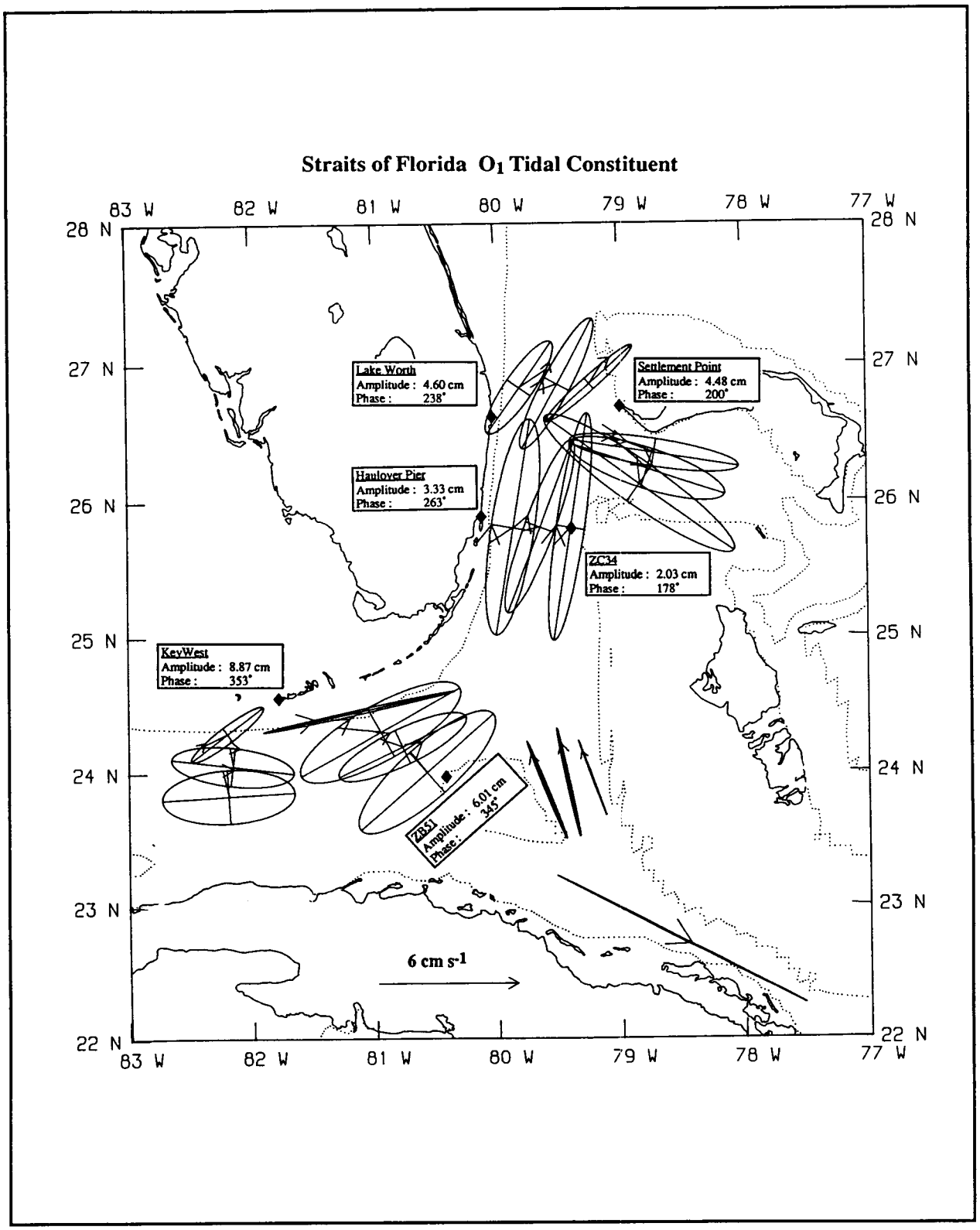

Figure 2.1-3 Hodographs and tidal water level information for O_1 tidal constituent. For an explanation of information contained in this figure, see caption of Figure 2.1-1.

The largest tidal transports in the FC occur through Transects B and C. The tidal transports through NWPC (Transect E) are larger than the mean flow frequency transport. Transect F has very small tidal transports, but the OBC (Transect G) has tidal transports comparable to the mean long term transport. Comparing these results for Transect D with those of Mayer et al. (1984) shows a discrepancy of about 1 Sv for the maximum tidal transport. This occurs because the semi-diurnal and diurnal bands have been broken down into separate constituents as required by an harmonic analysis method. Neglect of the subsidiary constituents (P_1, Q_1, N_2 and S_2) approximately accounts for the maximum transport being about 1 Sv less in the above analysis than estimated by the spectral methods of Mayer et al. (1984).

III. HYDROGRAPHY

3.1 Introduction

This report section presents hydrographic data taken during this study. The section first presents the sampling plan and schedule and then focuses on the salinity, temperature, and density fields. Following that, mean fields are presented, followed by a short discussion of variability. In the Program Data Report (SAIC, 1992), there is a detailed presentation of specific procedures, locations and times for all hydrographic observations.

3.1.1 Sampling Locations and Time

The general location of the standard hydrographic stations is shown in Figure 1.1-1. The pattern reveals the goal of making sections across the SoF at four sections in the main channel (Transects A, B, C and D) and across two of the primary lateral channels (Transects E and F). Additional samples were taken in OBC and at a location west of the Dry Tortugas. The sample spacing along the sections was well within the correlation length scales; thus, the sampling is sufficient to describe the data accurately. The one or two OBC stations obviously provide information only on the types of water that may be in that Channel. No Transect G sections have been provided.

The hydrographic samples were taken during five cruises. The timing of the cruises is sufficient to detect the seasonal signal but may not have sampled the extremes that may have occurred. Also, because of the relatively short sampling period (1.0 year) no estimate of longer term changes can be made.

Table 3.1-1 shows the details of each cruise and section.

3.2 Hydrographic Conditions - Cruise One (90-35)

Stations occupied during the first cruise are shown in Figure 3.2-1. Transect A was not occupied, Transect D was all XBT's, Transects E and G had one CTD Station. The composite T/S plot (Figure 3.2-2) shows the typical T/S pattern plus some unusual exceptions. First, note the high salinity water (almost 37 psu) at 26°C. Normally, Subtropical Underwater (SUW) may reach 37 psu at a maximum at 22.5°C. In this station 37 psu occurs in 26°C water. There are many stations where salinity is up to 0.6 psu lower than expected with some exhibiting considerable structure. Note that even below 15°C one station had salinities which were low by 0.5 psu. In the following discussion these station locations will be identified.

3.2.1 Temperature, Salinity and Density Sections

Transect B (Big Pine Key to Cay Sal Bank) - The temperature section shows a 100m mixed layer with a 2°C gradient in surface temperature across the channel (Figure 3.2-3a). The temperature ranged from 6.4 to 27.3°C. There appeared to be thermostads in the 16 to 20°C range in the eastern part of the channel. The thermocline was especially strong over the Portales Terrace on the western Margin. A slight eddy structure was evident at 100m, 60 km from the western edge. Salinities ranged from 34.90 to 36.83

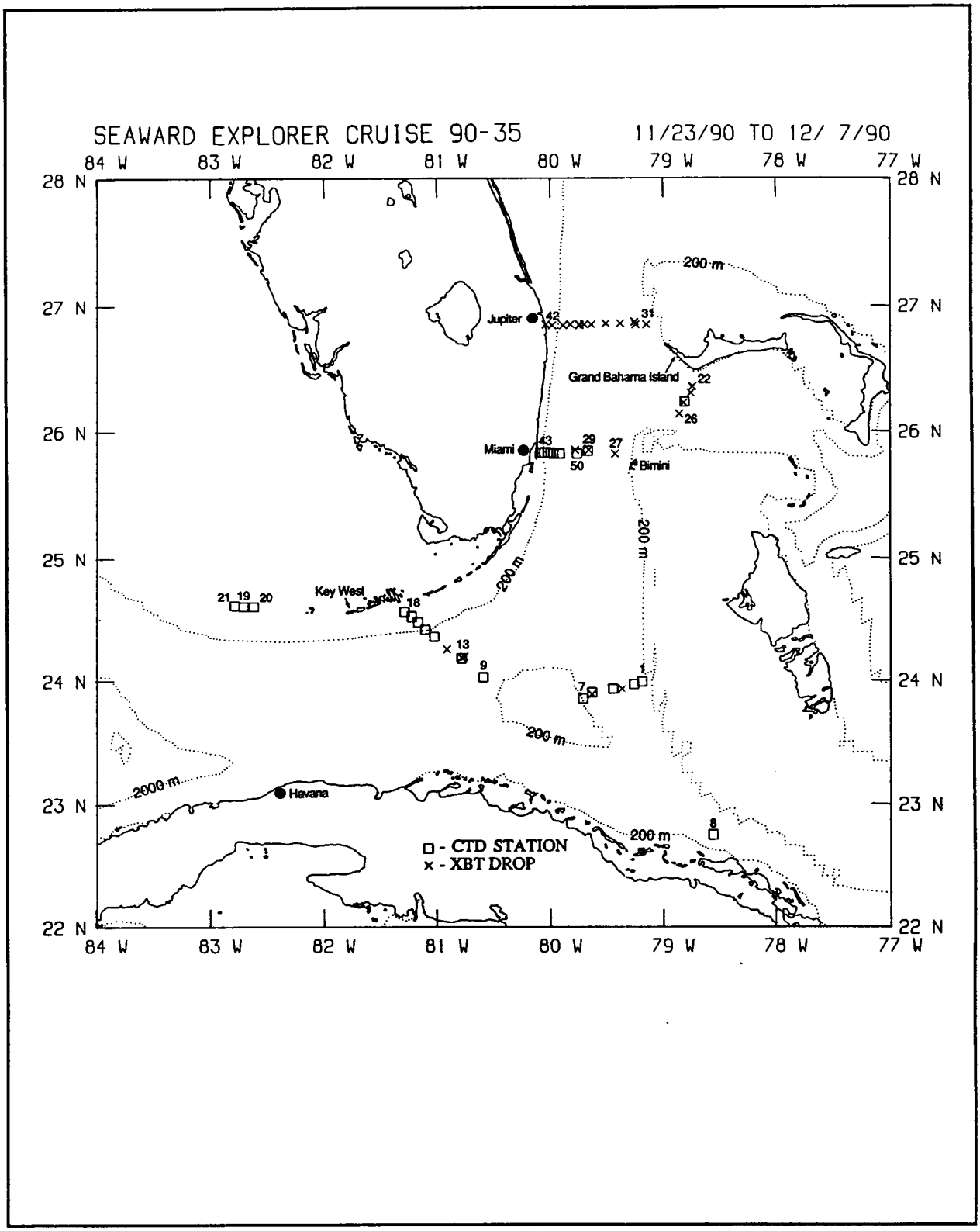

Figure 3.2-1. Location of stations during Cruise I. Squares (□) indicate CTD stations, crosses (x) are XBT stations.

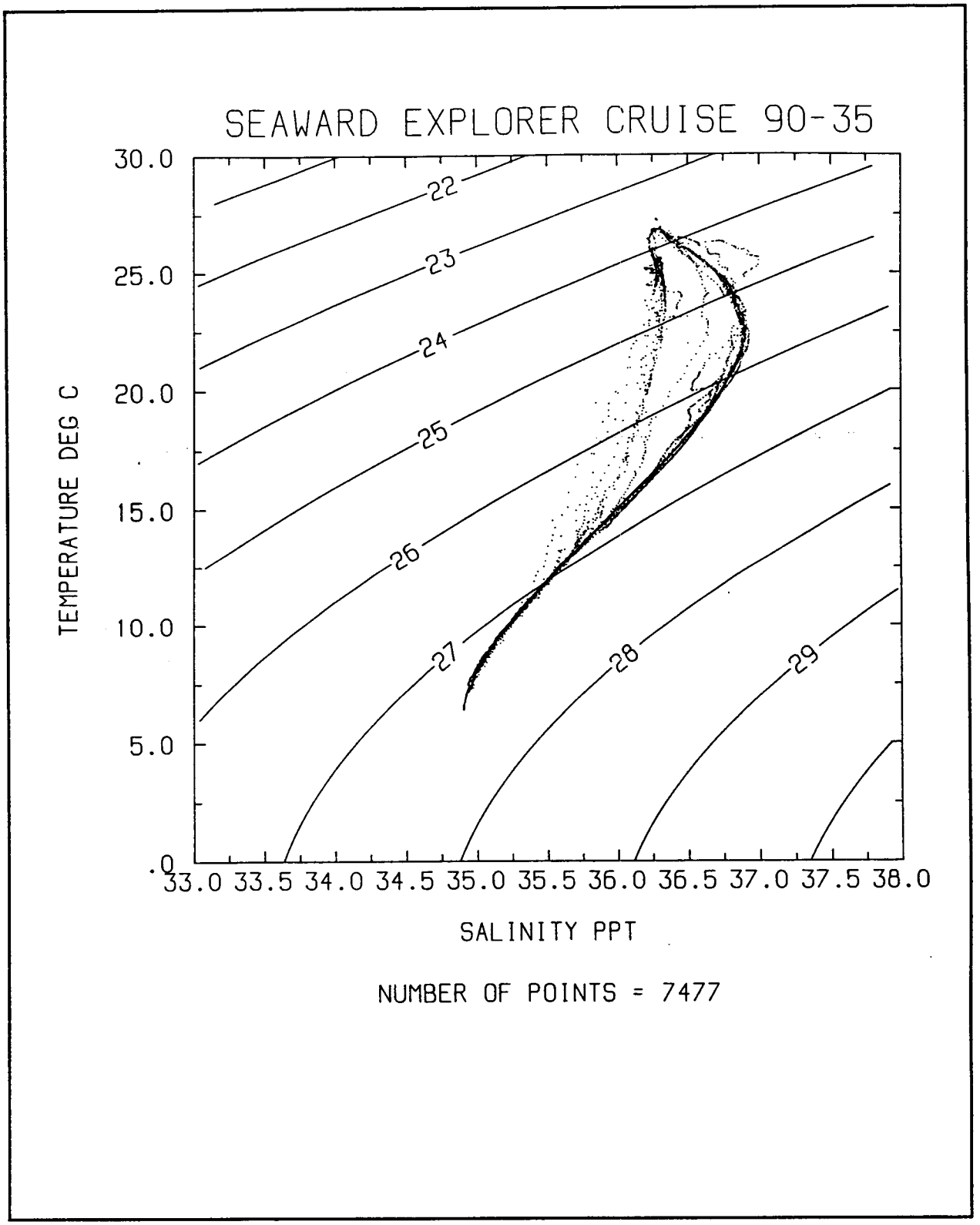

Figure 3.2-2. **Composite T/S plot for Cruise I.**

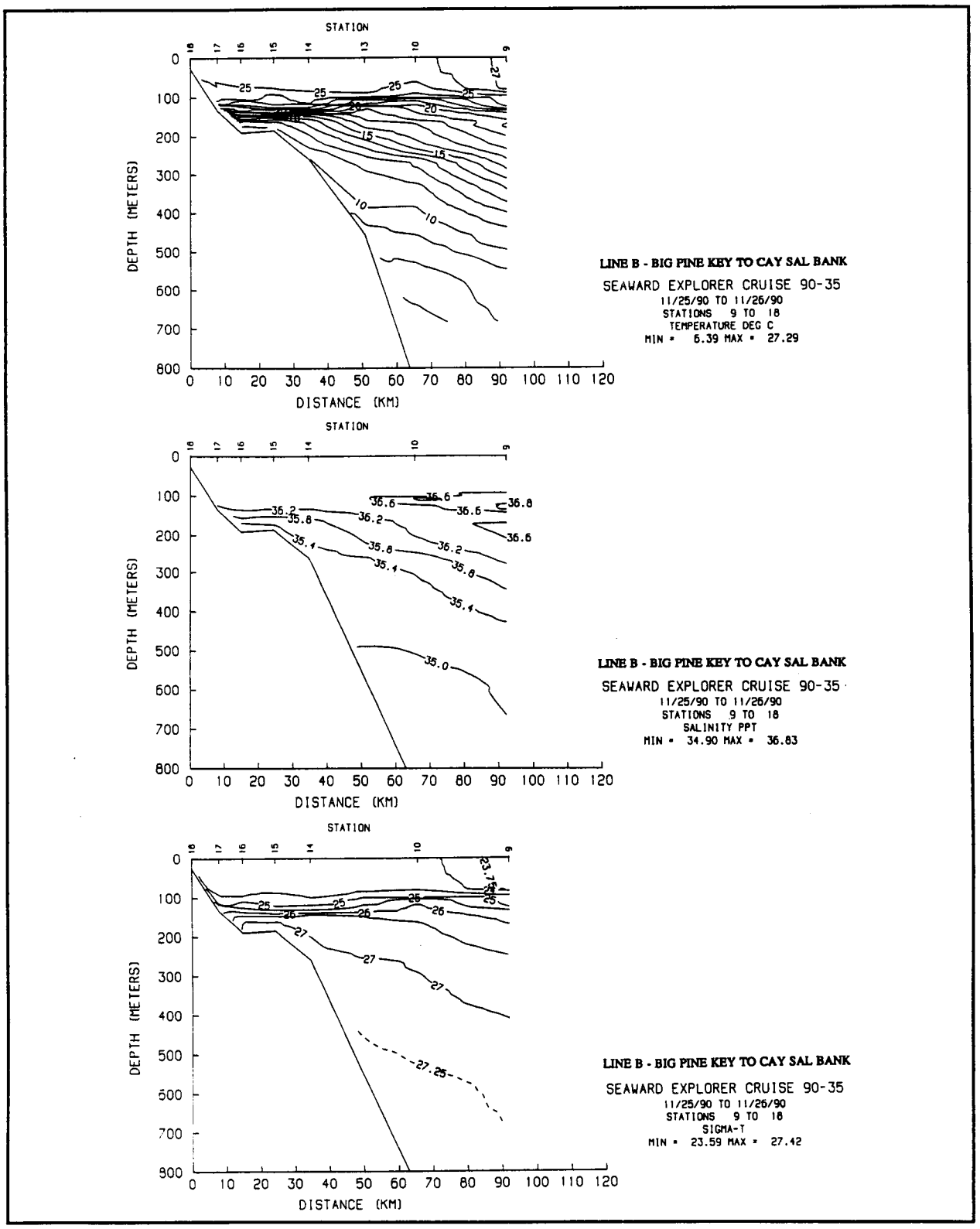

Figure 3.2-3. Temperature, salinity and density sections, Transect B (Big Pine Key to Cay Sal).

Table 3.1-1 Summary listing of hydrographic profiles by transect, cruise and type.

TRANSECT	CRUISE 1		CRUISE 2		CRUISE 3		CRUISE 4		CRUISE 5	
	Station Nos.	CTD/ XBT	Station Nos.	CTD/ XBT	Station Nos.	CTD/ XBT	Station Nos.	CTD/ XBT	Station Nos.	CTD/ XBT
A	–	–	1-9	1/8	1-9	7/12	4-13	7/3	4-14	7/3
B	9-18	7/3	13-24	9/3	13-16 18-24	7/14	14-19 21-25	8/3	14-16 18-24	5/5
C	27-30 43-50	8/4	57-68	8/4	32-34 36-44	8/4	33-44	10/2	32-43	10/2
D	31-42	0/12	36-56	1/20	52-63	0/12	52-62	0/11	51-57 59-62	0/11
E	22-26	1/4	31-35	5/0	45-51	5/2	45-51	5/2	44-50	5/2
F	1-7	5/2	26-30	5/0	27-31	5/0	28-32	1/4	27-31	5/0
G	8	1/0	25	1/0	25-26	2/0	26-27	1/1	25-26	2/0
H	19-21	3/0	10-12	0/3	10-12	0/3	1-3	3/0	1-3	3/0
TOTAL	50	22/28	68	30/38	61	34/27	61	35/26	60	37/23

psu (Figure 3.2-3b). The lowest salinities were at 200m along the western margin corresponding to the coldest water in the section (10.69°C). The salinity maximum was a coherent structure at 100m in the eastern part of the section. Density showed weak horizontal gradients above 150m with a suggestion of a countercurrent over the terrace (Figure 3.2-3c). A "typical" Gulf Stream structure appears below 150m.

Transect C (Miami to Bimini) - The temperature section is similar to Transect D (Figure 3.2-4a). Temperature ranged from 5.9 to 27.5°C . There were no thermostads and colder waters appeared more prevalent. Mixed layer depths were about 100m. Salinity shows clearly the SUW salinity maximum. Salinity ranged from 34.9 to 36.9 psu (Figure 3.2-4b). The low values were in 8°C waters at 150 - 200m over the Miami Terrace. The density section reveals a northward current with only the suggestion of a counter current at 300m on the eastern margin of the Straits (Figure 3.2-4c).

Transect D (Jupiter to Settlement Point). This temperature section shows a typical Gulf Stream structure (Figure 3.2-5). A frontal eddy may be present about 20 km from the western margin. There is no apparent countercurrent on the eastern side of the channel. The temperature ranged from 6.3°C to 27.1°C. There were no obvious thermostads although colder waters appeared more volumous. The upper layer appeared well mixed to nearly 100m.

Transect E (Northwest Providence Channel) - The temperature section shows a definite thermostad in the 17 to 19°C range (Figure 3.2-6). This is much in

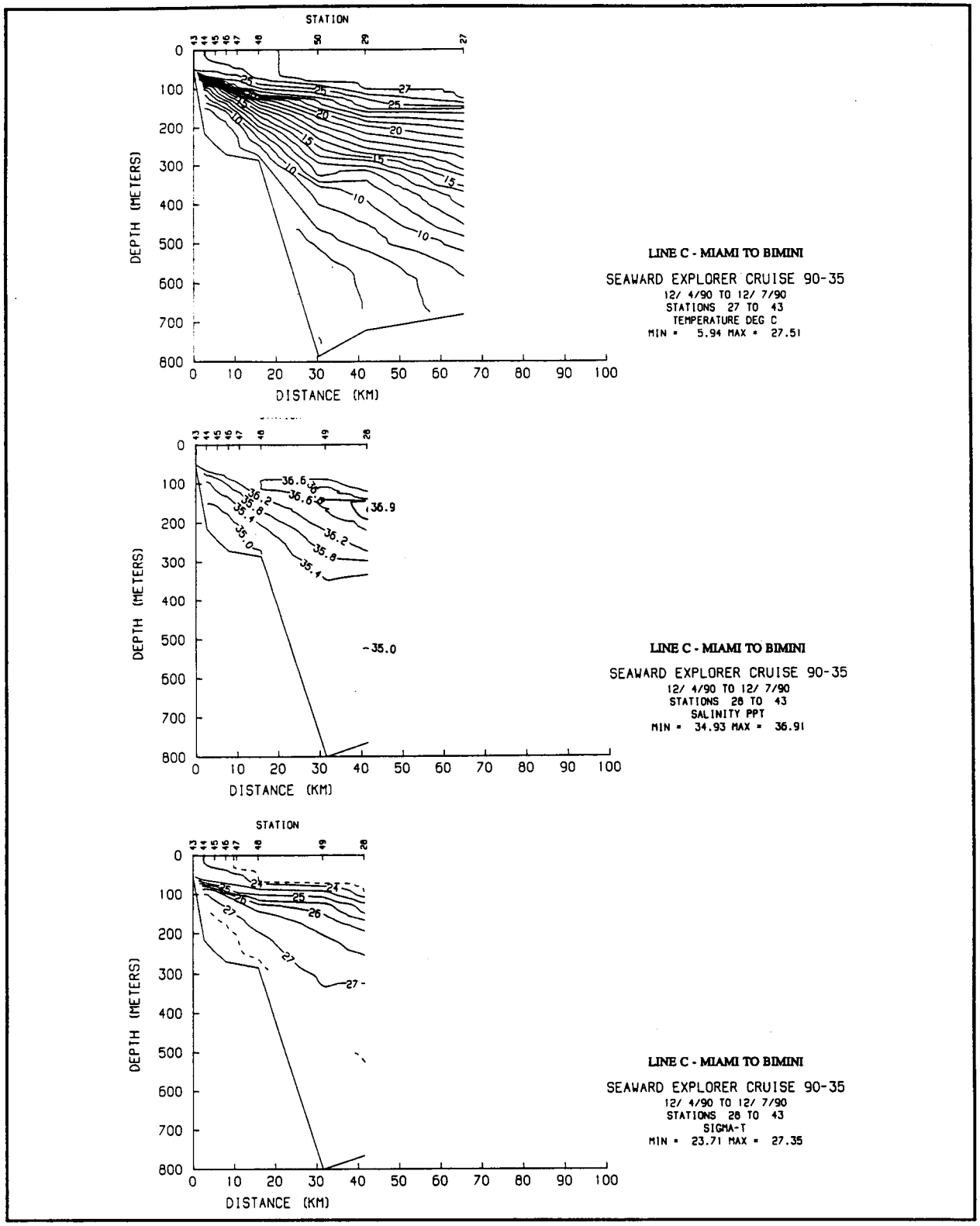

Figure 3.2-4. Temperature, salinity and density sections, Transect C (Miami to Bimini).

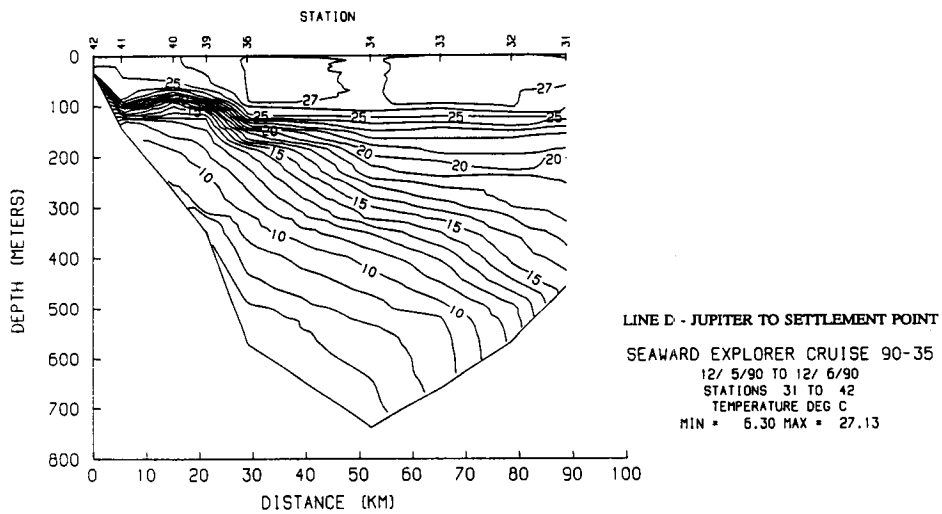

Figure 3.2-5. Temperature sections, Transect D (Jupiter to Settlement Point).

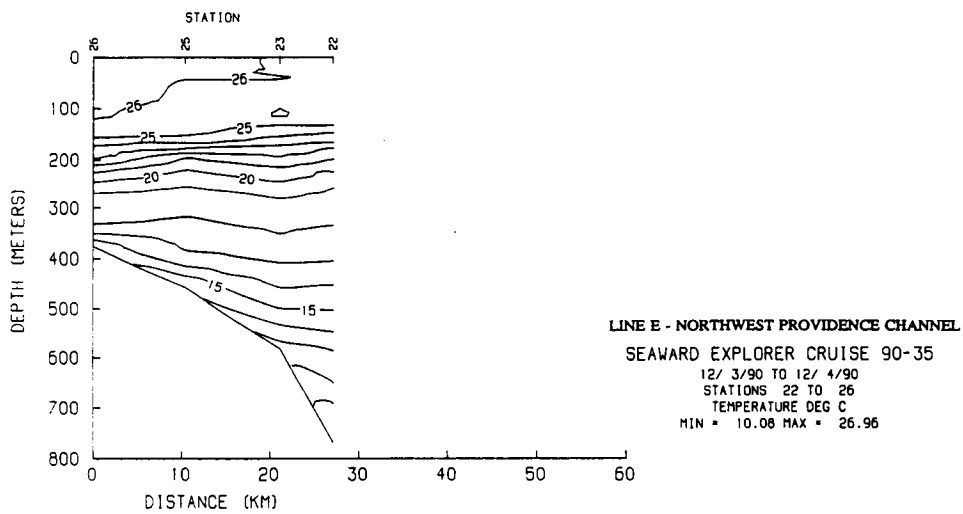

Figure 3.2-6. Temperature sections, Transect E (Northwest Providence Channel).

contrast to the other sections. The mixed layer is over 100m thick, just as it was at the other sections. Temperature ranged from 10.08 to 26.96°C, which is generally warmer than the other channels during this cruise.

Transect F (Santaren Channel) - The first striking feature is the constant vertical temperature gradient especially below 100m (Figure 3.2-7a). Temperatures ranged from 8.57 to 26.95°C. As with the other sections, the upper 100m was mixed. The salinity section showed the same gradient as the temperature section (Figure 3.2-7b). The salinity maximum extended across the Channel, but highest salinities were found on the eastern margin. Salinity ranged from 36.3 to 37.0 psu. This range is higher than any in the Straits. The lack of low salinities suggests that little or no water of Gulf of Mexico origin is present. The 37.00 psu water, higher than any water in Transect B section, suggests another source. The density section shows weak horizontal gradients with a counter flow indicated over the western half of the channel (Figure 3.2-7c).

Station G (Old Bahama Channel) - Salinity approached 37 psu in the SUW layer.

3.3 Hydrographic Conditions - Cruise Two (91-03)

The stations occupied on the second cruise are shown in Figure 3.3-1. Note that an additional section was added between Key West and Havana, Transect A. The composite T/S plot (Figure 3.3-2) is somewhat different from the previous cruise. While standard Gulf Stream water occurs, the warm, high salinity water noted previously is not present. Below 15°C there are two slightly different water types with a salinity difference of about 0.1 psu.

3.3.1 Temperature, Salinity and Density Sections

Transect A - Temperature ranged from 5.52 to 24.2°C. The section shows a decreasing temperature gradient with depth (Figure 3.3-3). No thermostad is obvious in the 15 to 20°C range. A doming structure in the 50 to 100m depth 20 to 40 km offshore suggests a frontal eddy structure.

Transect B - This section showed a prominent thermostad at 22°C and a less pronounced one between 16 and 20°C over the western part of the section (Figure 3.3-4a). Temperature ranged from 5.66 to 26.05°C. Salinity showed the typical salinity maximum restricted to the western part of the channel with maximum values of 36.87 psu (Figure 3.3-4b). Low salinity water was found at two places. At the deepest part of the section, water of 34.87 psu occurred. This represents Antarctic Intermediate Water that is slightly lower in salinity than water of the same temperature from the North Atlantic. The second area of low salinity was found between 0 and 200 meters just off the Keys. This no doubt represents water coming from the Gulf of Mexico, where it was modified by mixing with runoff entering the Gulf. This is Wennekins' [1959] Continental Edge Water. The density section shows inclined isopycnals over nearly the whole field with no evidence of eddy activity (Figure 3.3-4c).

Transect C - The temperature section had a slightly colder upper layer thermostad (20°C) and another at 17°C (Figure 3.3-5a). Temperatures ranged from 6.06 to 26.05°C. Salinity ranged from 34.9 to 36.87 psu with the high salinity core on the Bimini side of the channel (Figure 3.3-5b). No low salinity surface

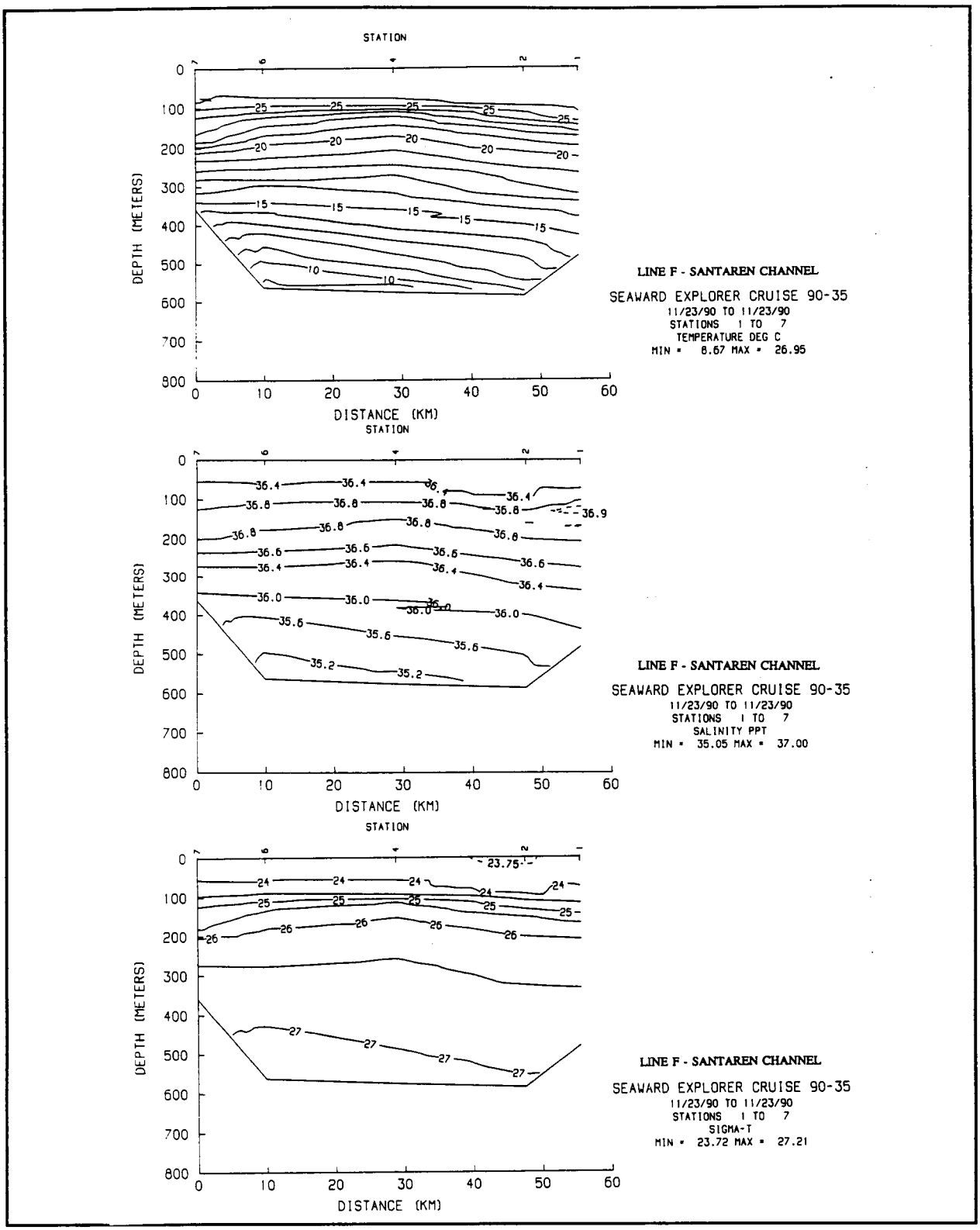

Figure 3.2-7. Temperature, salinity, density sections, Transect F (Santaren Channel).

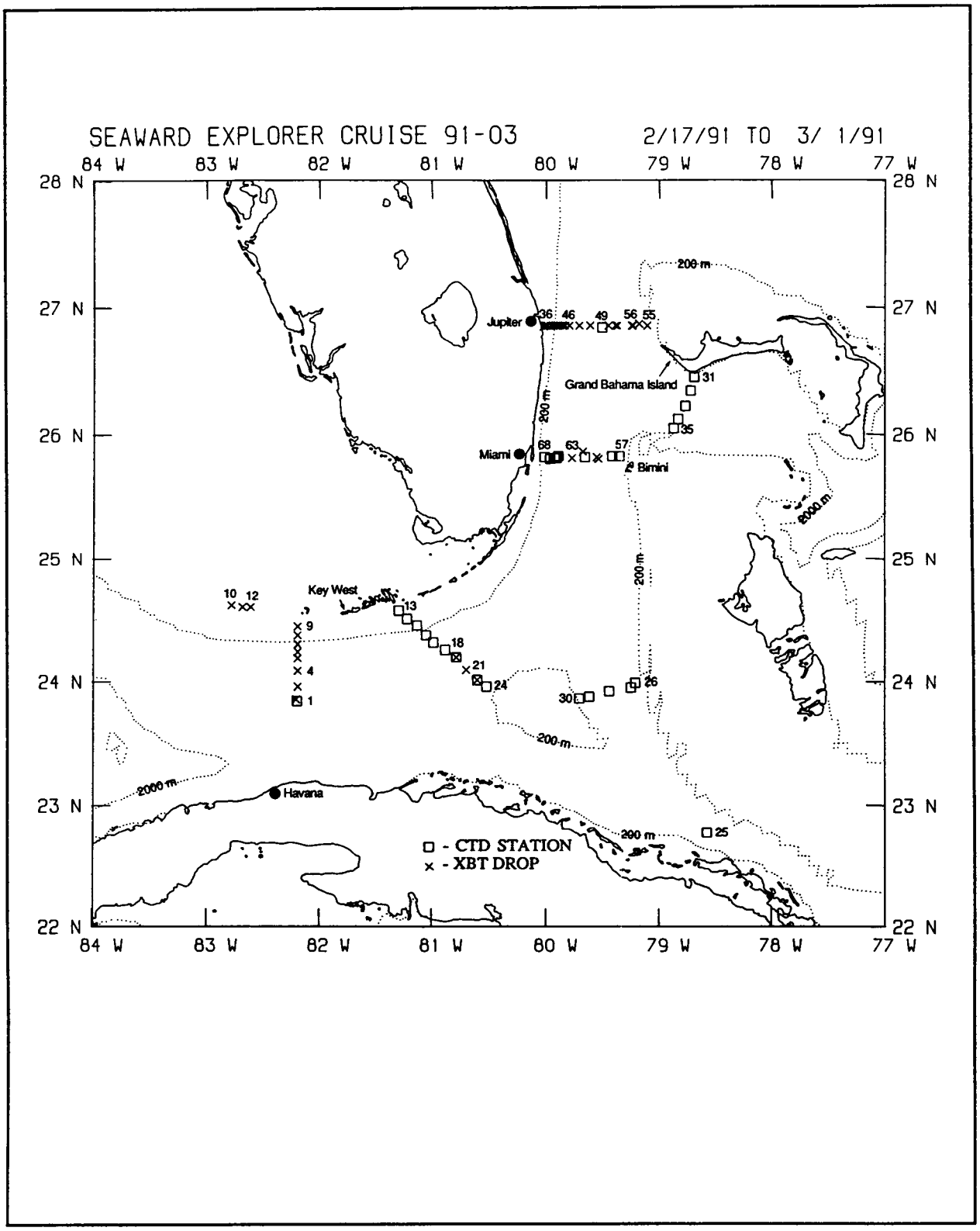

Figure 3.3-1. Station locations for Cruise II. Squares (□) indicate CTD stations crosses (x) are XTB stations.

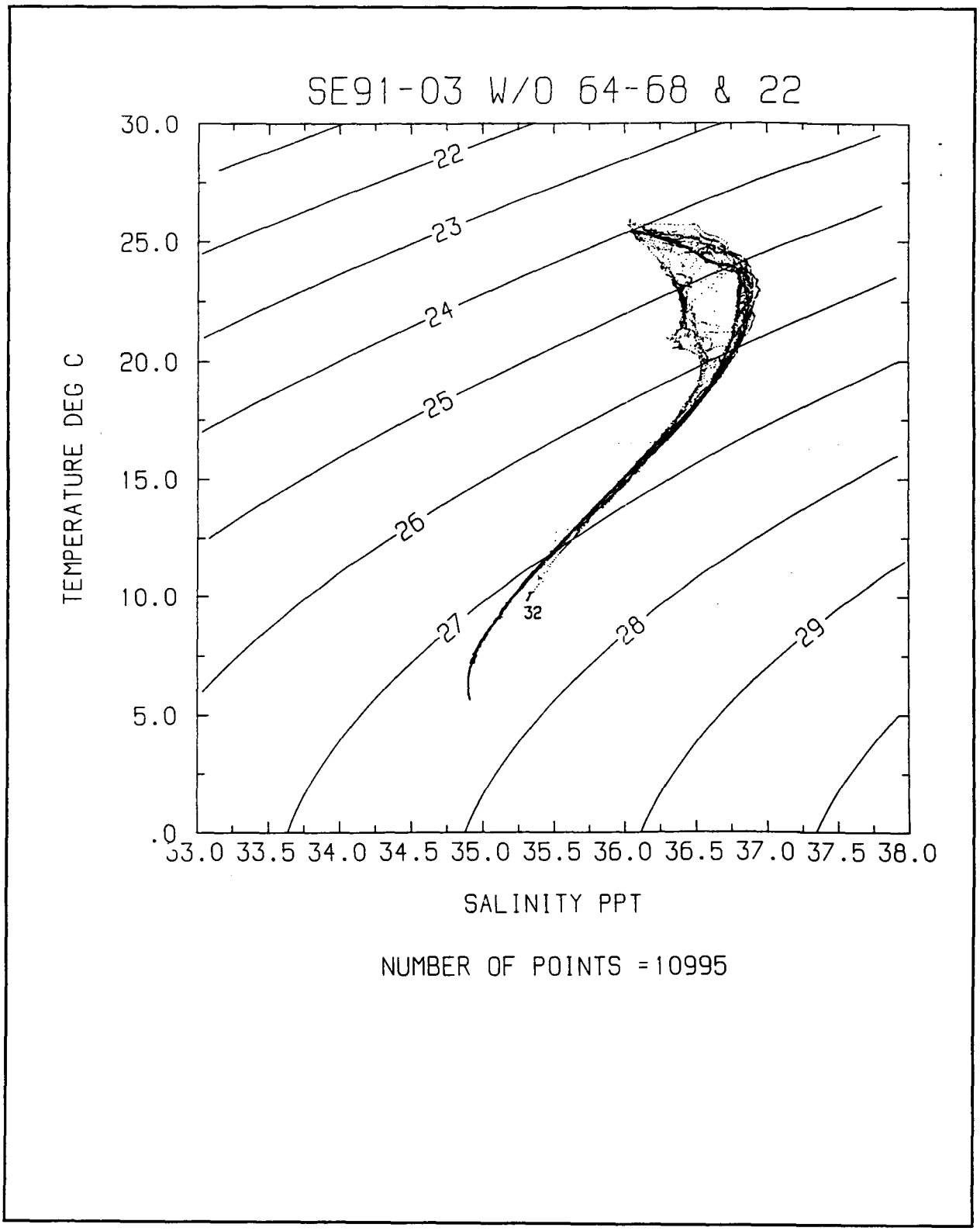

Figure 3.3-2. Composite T/S plot for Cruise II.

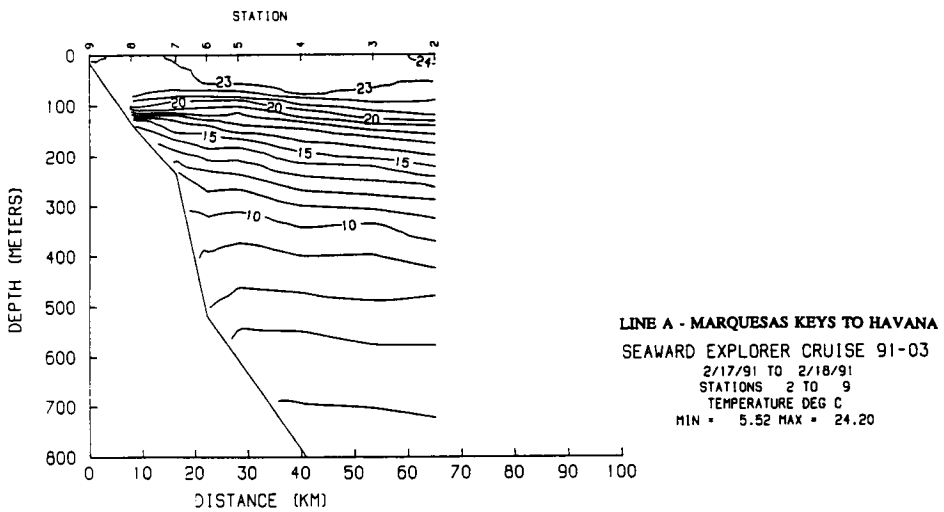

Figure 3.3-3. Temperature section, Transect A (Marguesas Keys to Havanna).

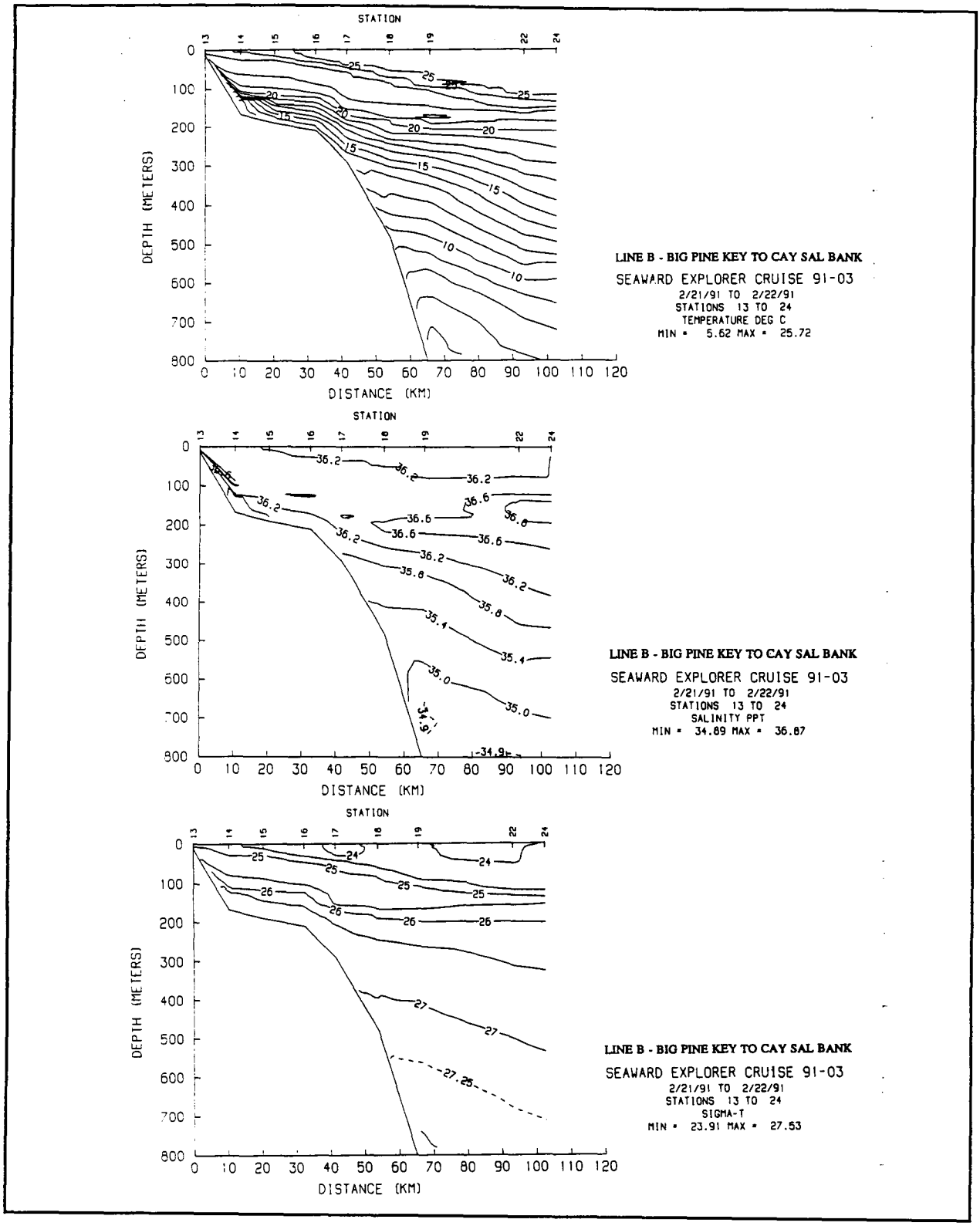

Figure 3.3-4. Temperature, salinity, density section, Transect B.

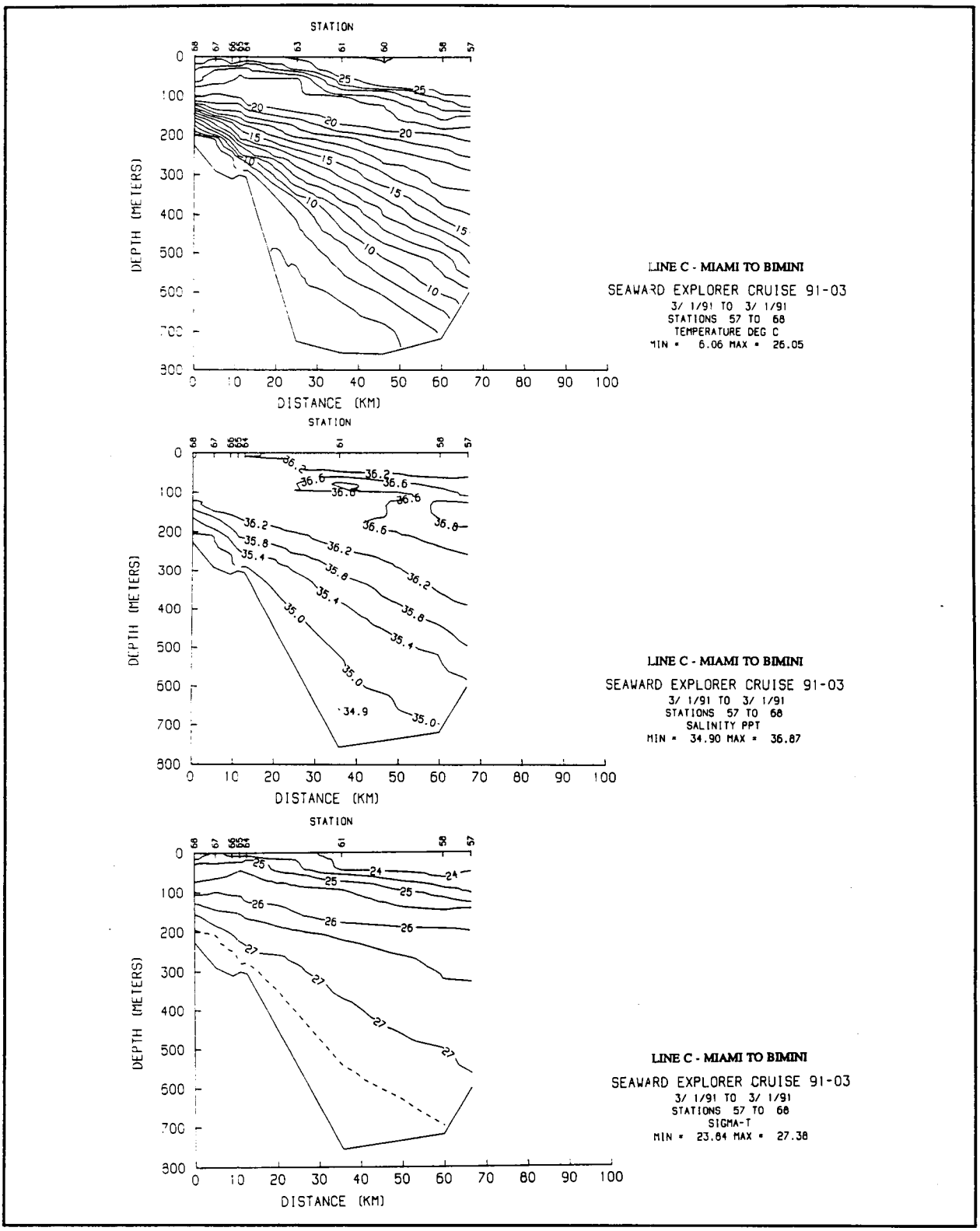

Figure 3.3-5. Temperature, salinity and density section, Transect C.

layer was present. The density field showed steeper horizontal density gradients with depth (Figure 3.3-5c). A dome structure was evident over the terrace off Miami.

Transect D - Notable features were the deepening surface layer to the east, strong thermal gradients over the terrace off Jupiter, and thermostads at 17 - 18°C (Figure 3.3-6). The temperature field suggests southward currents at several depths on the Settlement Point side of the Straits.

Transect E - The temperature section shows slight structure with minimum temperatures in the deepest part of the Channel (Figure 3.3-7a). Temperatures ranged from 9.77 to 25.41°C. Salinity ranged from 35.3 to 36.86 psu with the salinity maximum lying at 175m (Figure 3.3-7b). The density field suggested an eastward current in the upper layer and westward in the lower layer (Figure 3.3-7c).

Transect F - Temperature ranged from 11.24 to 25.51°C (Figure 3.3-8a). Minimum temperatures were found on the western side of the channel. The surface layer appeared to be deeper over the western part of the channel also. A thermostad appeared at 17 to 18°C. Salinity ranged from 35.39 to 36.95 psu (Figure 3.3-8b). The high salinity core was on the eastern side of the Channel. The density field suggests a southward current in the upper layer and a northward current below about 300m (Figure 3.3-8c).

Transect G - The typical subsurface salinity maximum and a surface mixed layer are present.

3.4 Hydrographic Conditions - Cruise Three (91-12)

The stations occupied on the third cruise are shown in Figure 3.4-1. Complete CTD sections were done on Transects A, B, C, E, F, and G. For the other sections (D and H) only XBT's were used. The composite T/S plot (Figure 3.4-2) shows the standard Gulf Stream pattern. Note that the tight T/S lines vary slightly again as they did during Cruise two. There are a few high salinity layers and the typical lower salinity stations.

3.4.1 Temperature, Salinity and Density Sections

Transect A - Temperature ranged from 5.99 to 27.79°C (Figure 3.4-3a). The section shows strongest temperature gradients in the 50 - 200 meter depth ranges. No thermostad is obvious in the 15 to 20°C range. No significant doming structures were observed. The salinity ranged from 34.89 to 36.89 psu (Figure 3.4-3b). The somewhat high salinity (36.89 psu) maximum is on the Havana side of the channel. The lower salinities were found on the Marquesas Keys side no doubt resulting from drainage out of Florida Bay. The density section showed constant downward sloping isotherms across the channel (Figure 3.4-3c). A slight dome structure appeared at Station 3 at 100m.

Transect B - The temperature section showed a warm surface layer and slight thermostad at 20 to 22°C at Stations 16-18 and at 18°C at Stations 18-21 (Figure 3.4-4a). Temperature ranged from 5.93 to 27.98°C. Salinity showed the typical salinity maximum restricted to the western half of the Channel (Figure 3.4-4b). Maximum values were 36.89 psu, only .02 higher than the previous

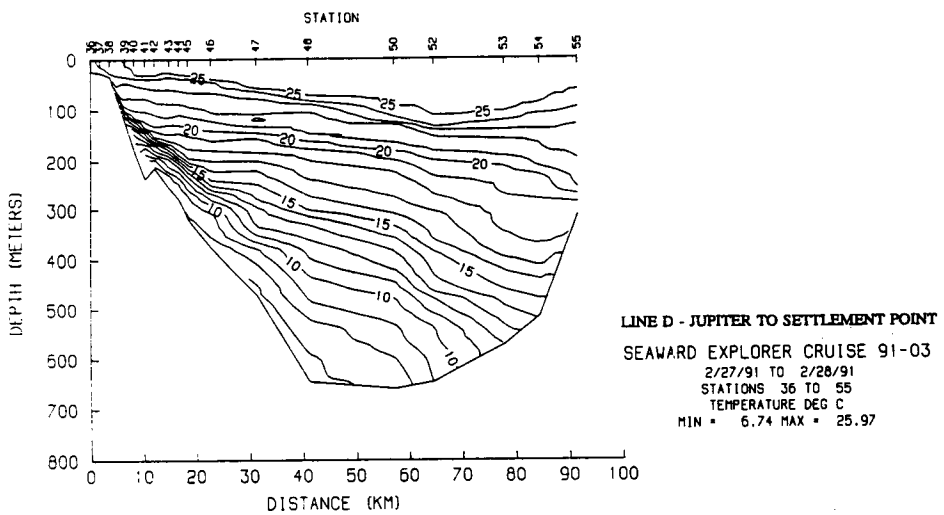

Figure 3.3-6. Temperature section, Transect D.

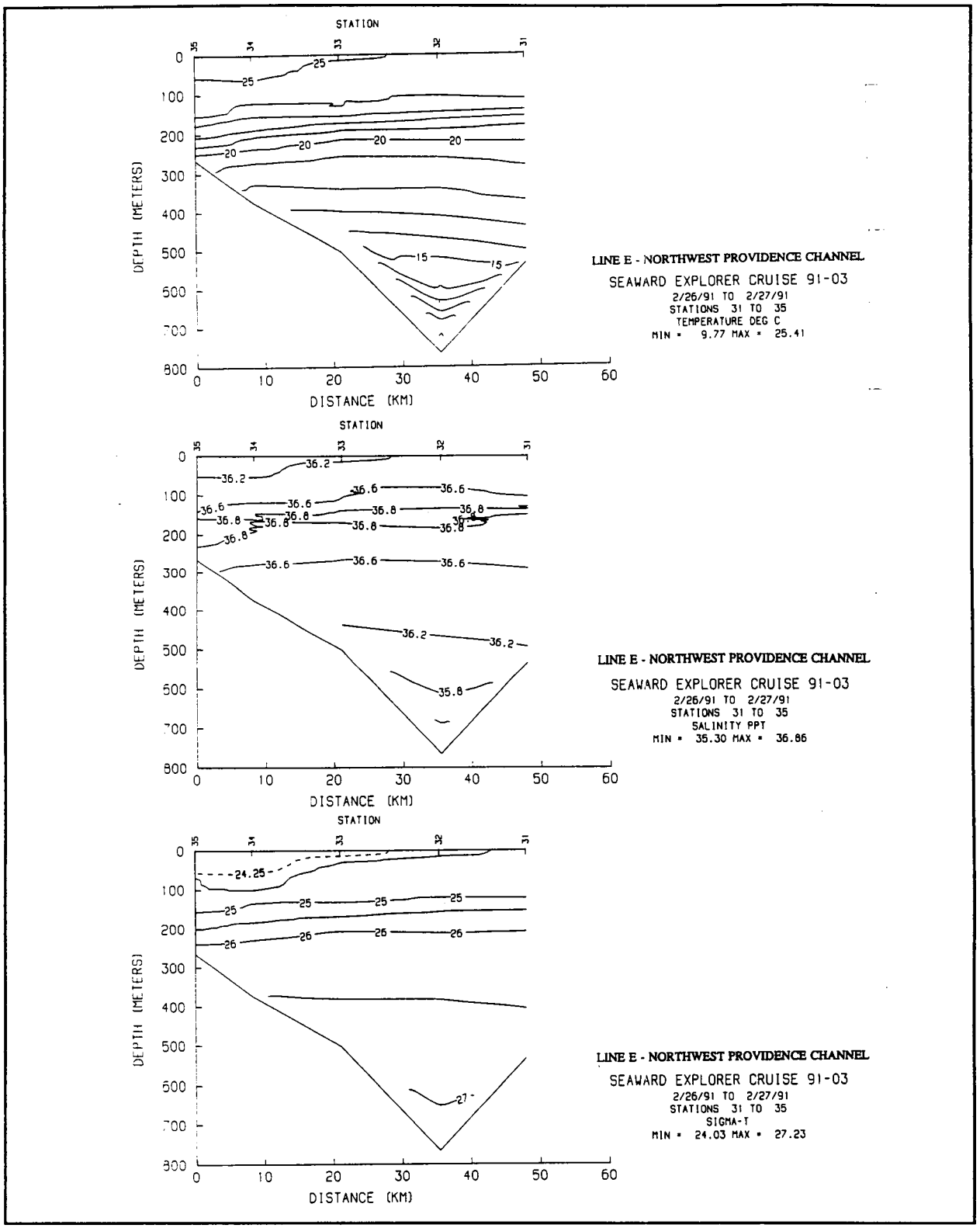

Figure 3.3-7. Temperature, salinity, density section, Transect E.

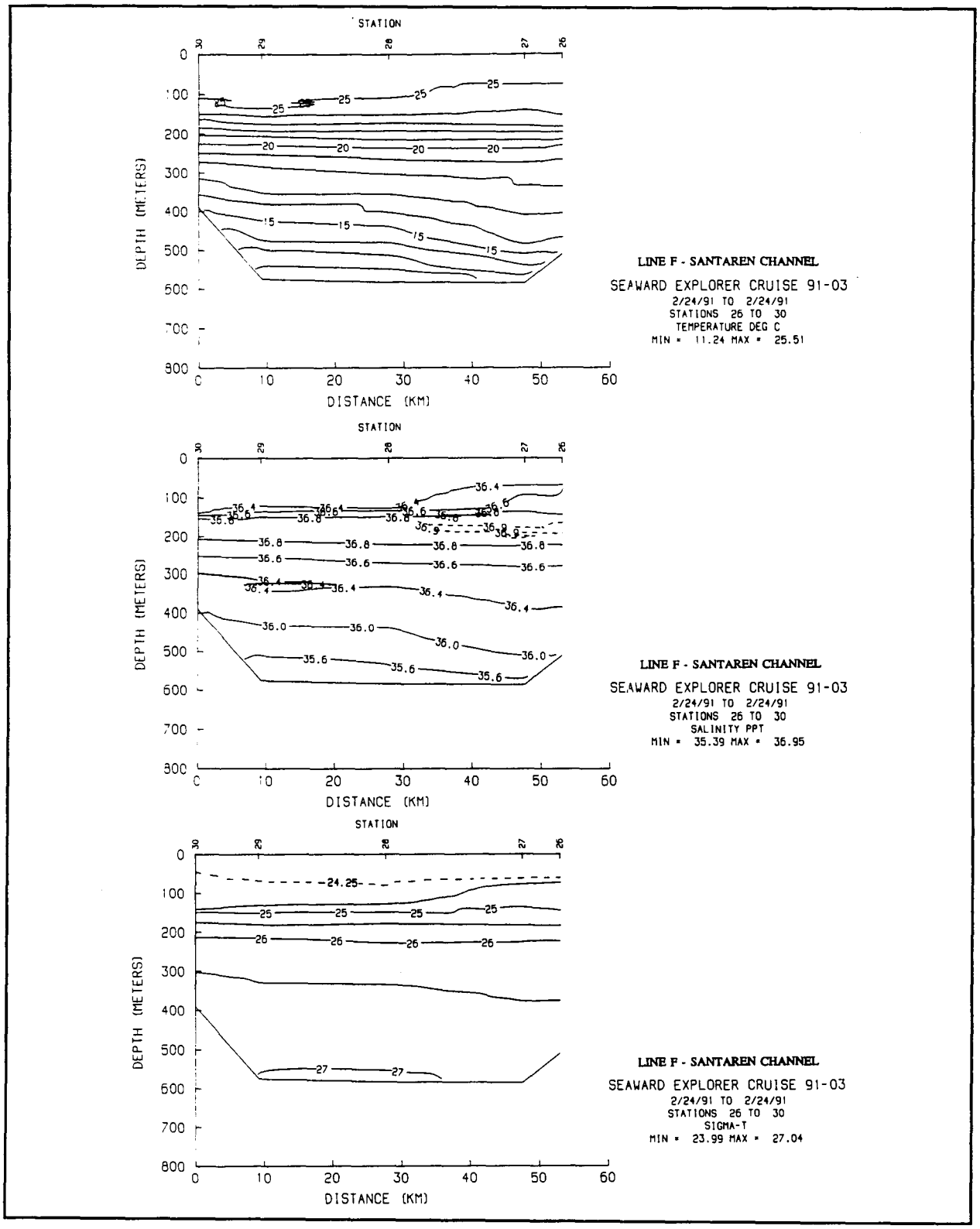

Figure 3.3-8. Temperature, salinity, and density section, Transect F (Santaren Channel).

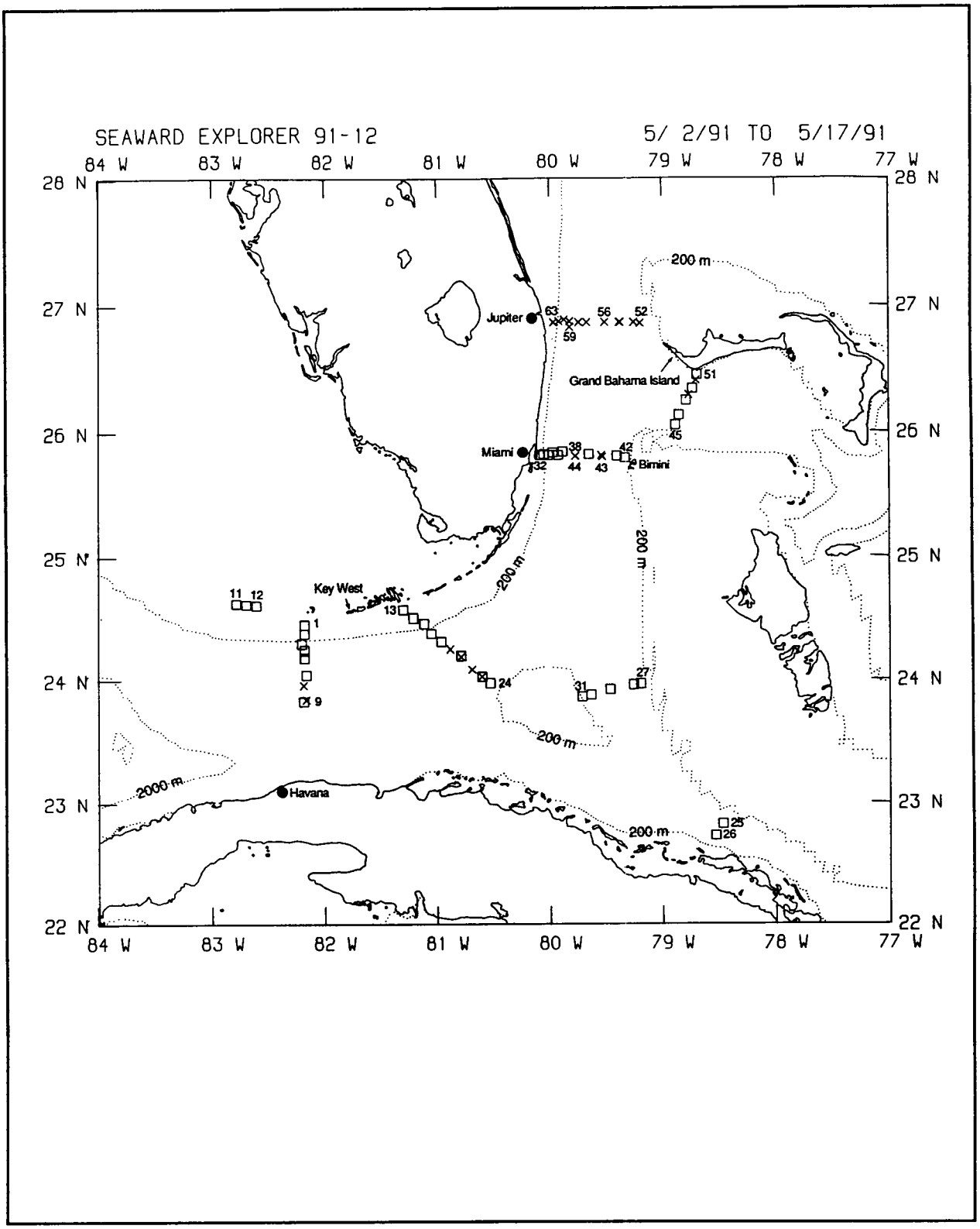

Figure 3.4-1. Station locations for Cruise III. Squares (□) indicate CTD stations. Crosses (x) are XBT stations.

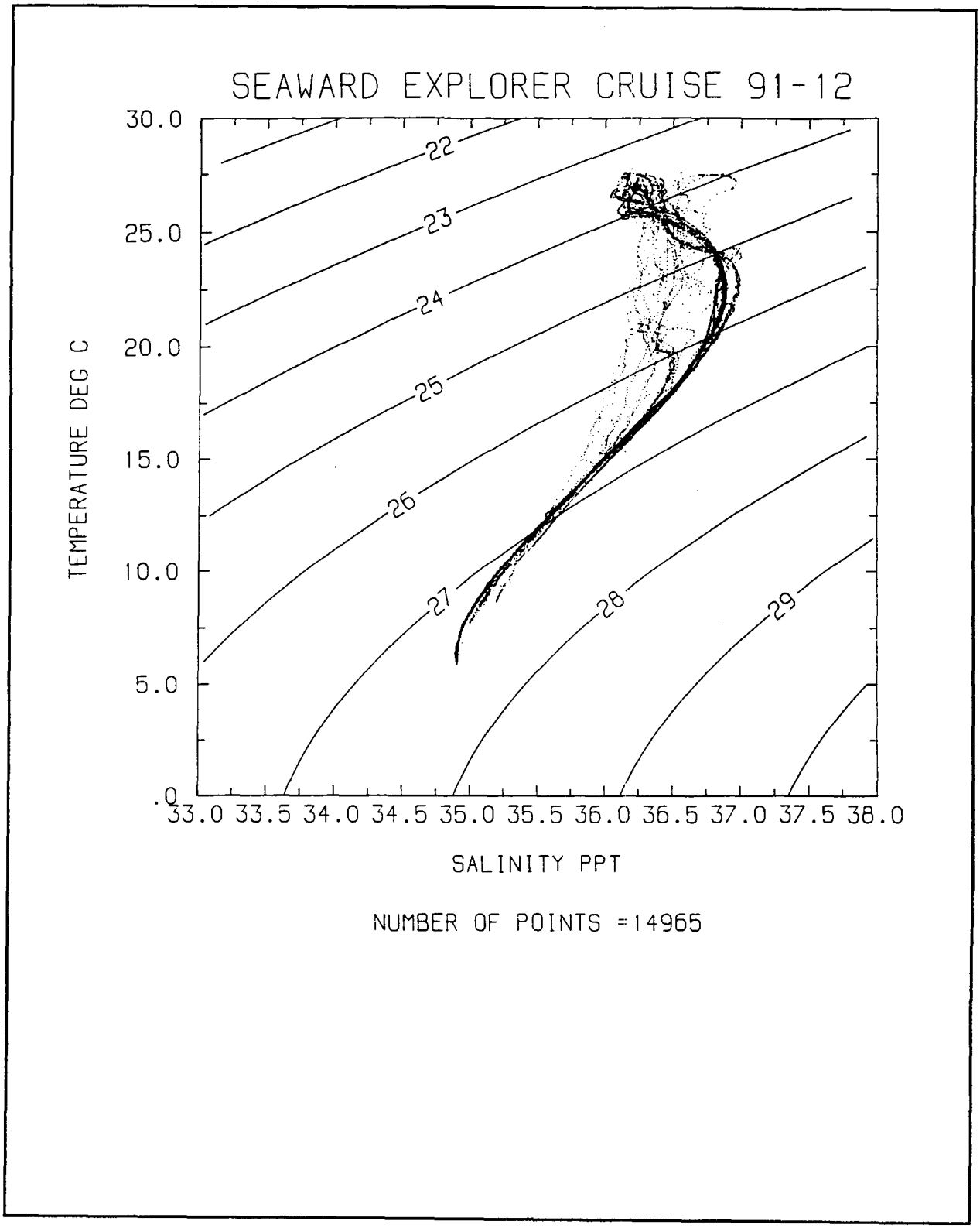

Figure 3.4-2. Composite T/S plot for Cruise III.

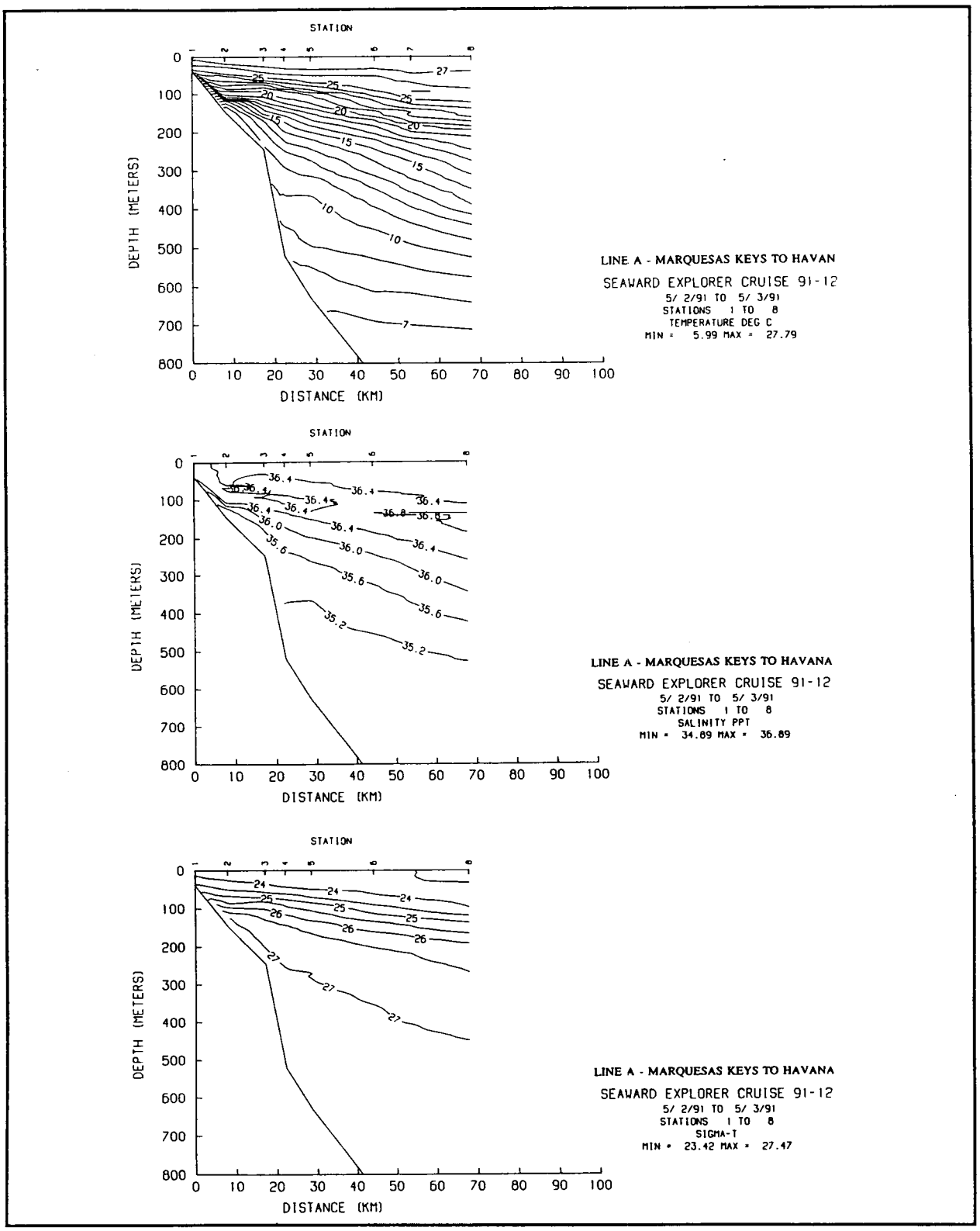

Figure 3.4-3. Temperature, salinity, and density sections, Transect A.

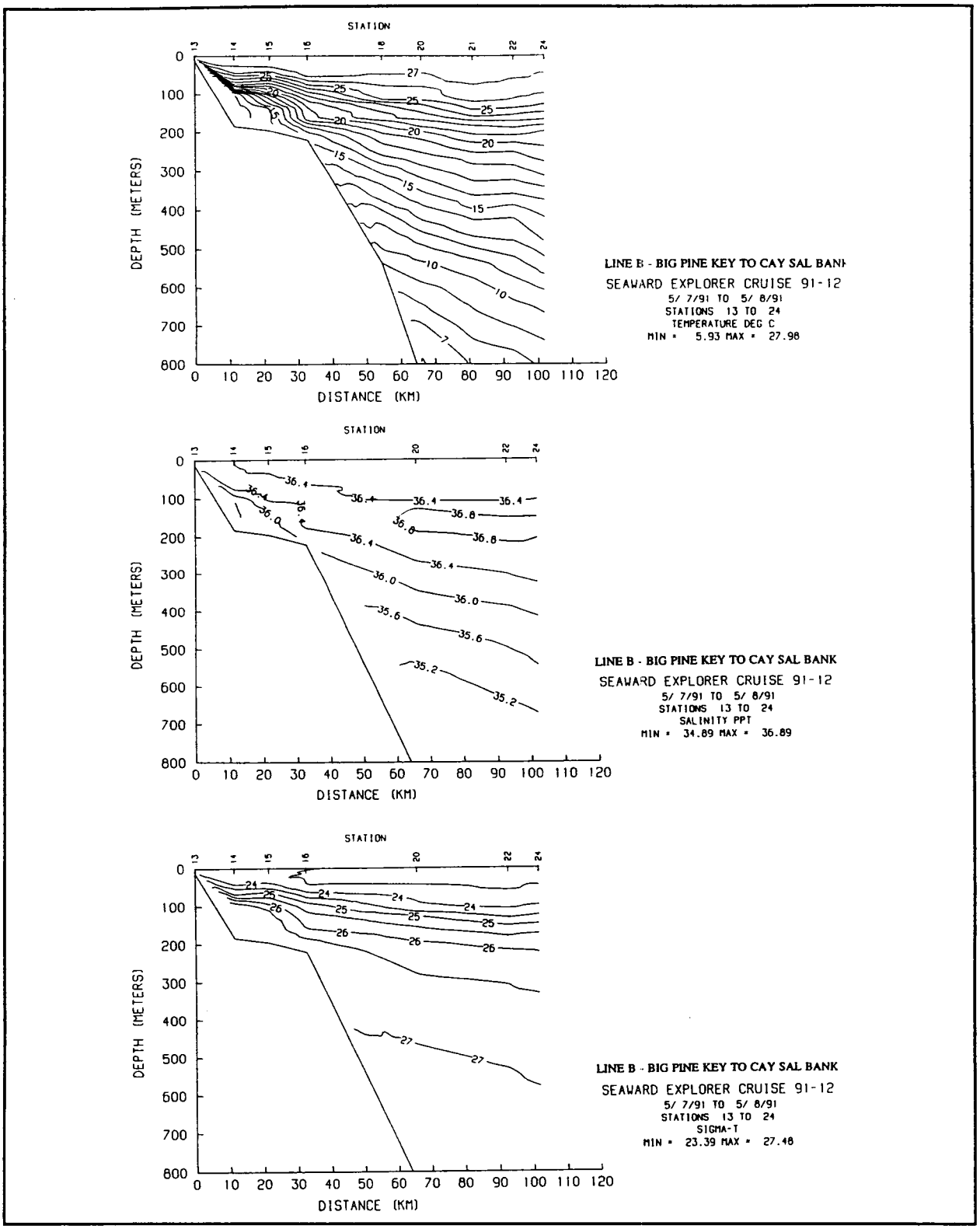

Figure 3.4-4. Temperature, salinity, and density sections, Transect B.

cruise. Low salinity water was found at two places. At the deepest part of the section, water of 35.1 psu was found. This is higher salinity than normally expected for Antarctic Intermediate Water; thus, there apparently was little AIW present. The second area of low salinity was found between 0 and 200 meters just off the Keys. This is Continental Edge Water. The density section shows inclined isopycnals over nearly the whole field with evidence of an eddy over the Portales Terrace (Figure 3.4-4c).

Transect C - The temperature section ranged from 6.04 to 28.01°C (Figure 3.4-5a). The minimum was only .04 colder than the previous cruise. The maximum was about 2°C warmer because of the season. There was a slight thermostad at 18°C. The salinity section showed values ranging from 34.9 to 36.89 psu. The high salinity layer occupied the western half of the section at 150m (Figure 3.4-5b). The density section showed no evidence for eddy activity (Figure 3.4-5c). The dome in the 23.5 isopycnal is no doubt a mixed layer anomaly.

Transect D - Temperature ranged from 6.45 to 28.62°C (Figure 3.4-6). A thermostad was present in the 18°C range. The isotherms show that no eddies are present. Note the intense thermocline over the shelf off Jupiter (Station 63). Cold water was flooding the shelf and no doubt affected circulation in the area.

Transect E - Temperature ranged from 8.66 to 27.36°C (Figure 3.4-7a). The lack of structure easily differentiates this section from the others. Salinity ranged from 35.19 to 36.99 psu in the Channel (Figure 3.4-7b). The high salinity layer spread across the center two thirds of the Channel. Lowest salinity was found at the bottom of the channel. Density shows little structure (Figure 3.4-7c).

Transect F - Temperature ranged from 10.95 to 27.47°C (Figure 3.4-8a). Salinity ranged from 35.35 to 36.96 psu (Figure 3.4-8b). Highest salinities were in the Subtropical Underwater at 200 meter. There is some structure in the density field with a low point at station 30 (Figure 3.4-8c)

Transect G - The mixed layer was about 75m, below which the high salinity layer dominated, causing a very strong vertical density gradient.

3.5 Hydrographic Conditions - Cruise Four (91-17)

The stations occupied on the fourth cruise are shown in Figure 3.5-1. Complete CTD sections were made on Transects A, B, C, E and H. The composite T/S plot (Figure 3.5-2) shows the standard Gulf Stream pattern. Note that the tight T/S lines vary slightly again as they did in previous cruises. Few high salinity layers occur, and the typical lower salinity stations are seen again.

3.5.1 Temperature, Salinity and Density Sections

Transect A - Temperature ranged from 5.65 to 33.64°C (Figure 3.5-3a). The section shows strongest temperature gradients in the upper 100 meters. No thermostad is obvious in the 15 to 20°C range. No significant doming structures were observed. There was a significant warm layer centered at Station 6. This could be related to the XBT sampling versus the CTD. The

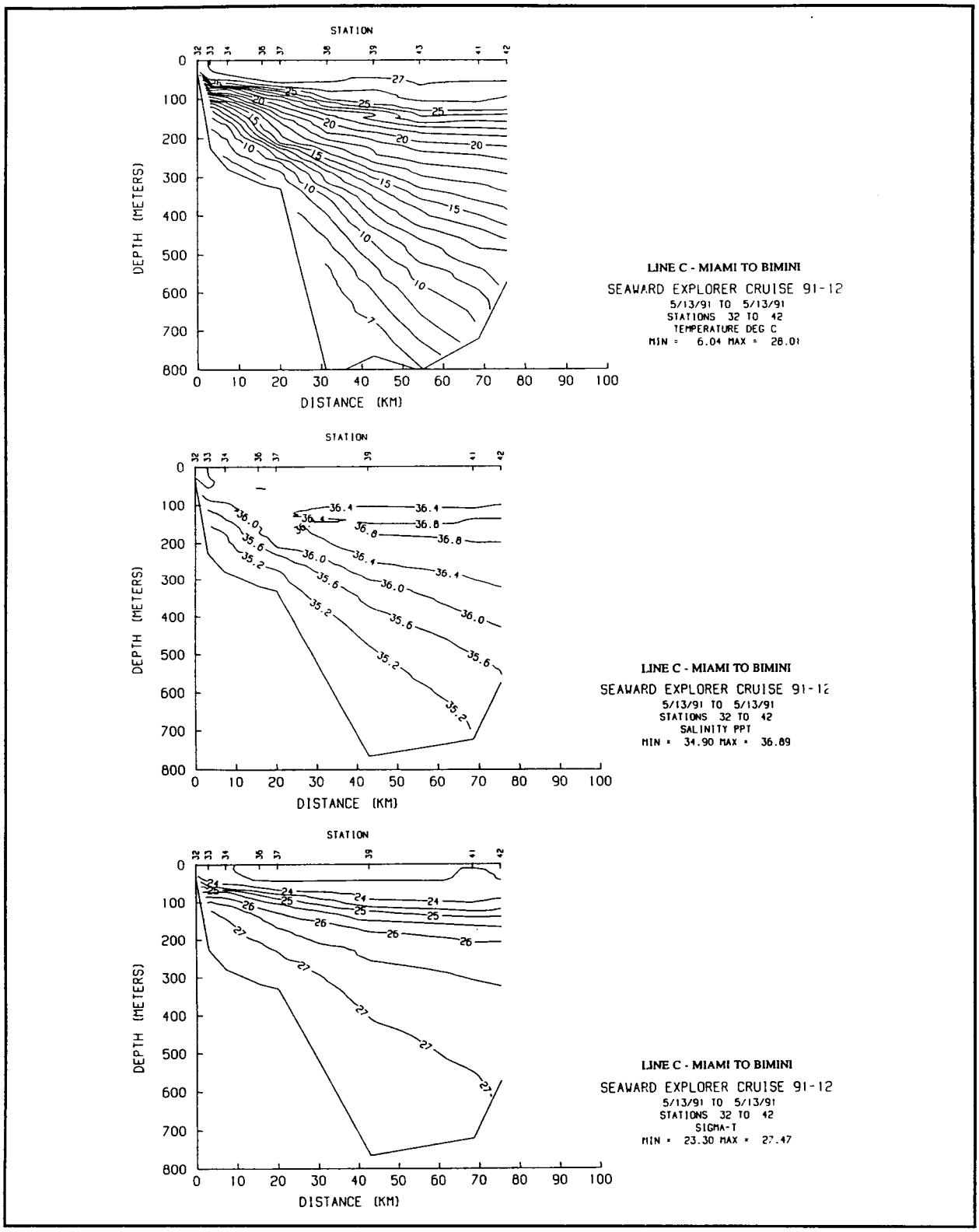

Figure 3.4-5. Temperature, salinity, and density sections, Transect C.

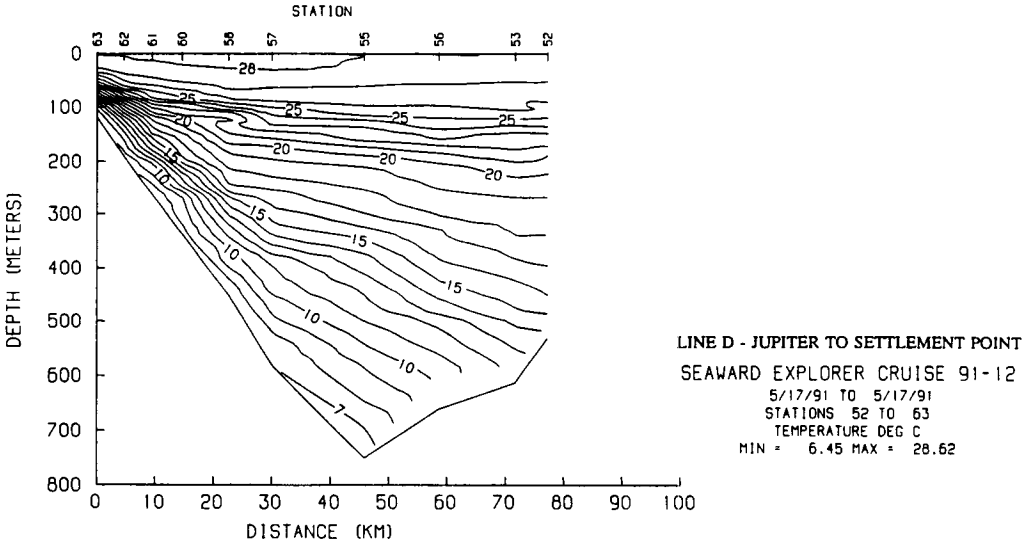

Figure 3.4-6. Temperature sections, Transect D.

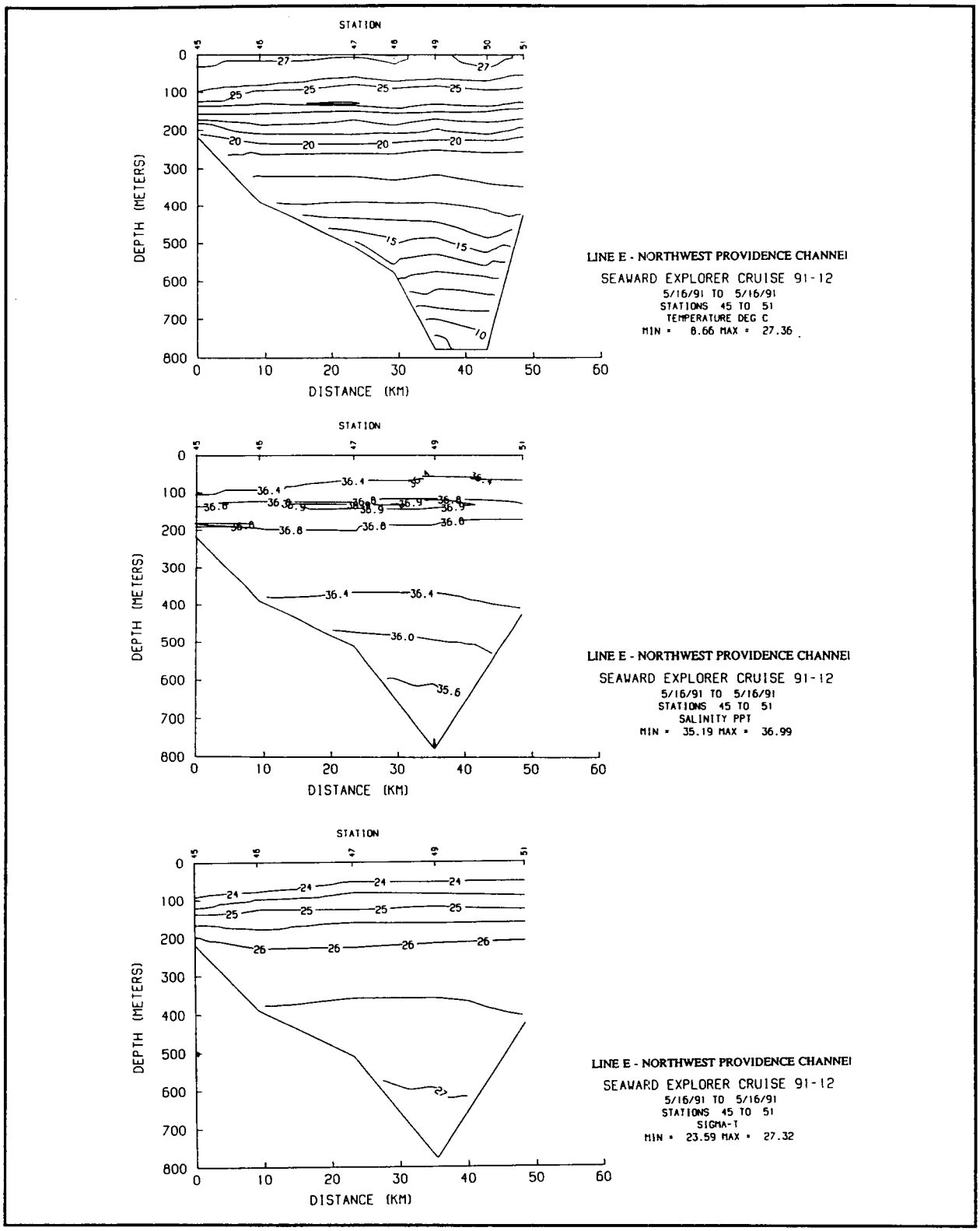

Figure 3.4-7. Temperature, salinity and density sections, Transect E.

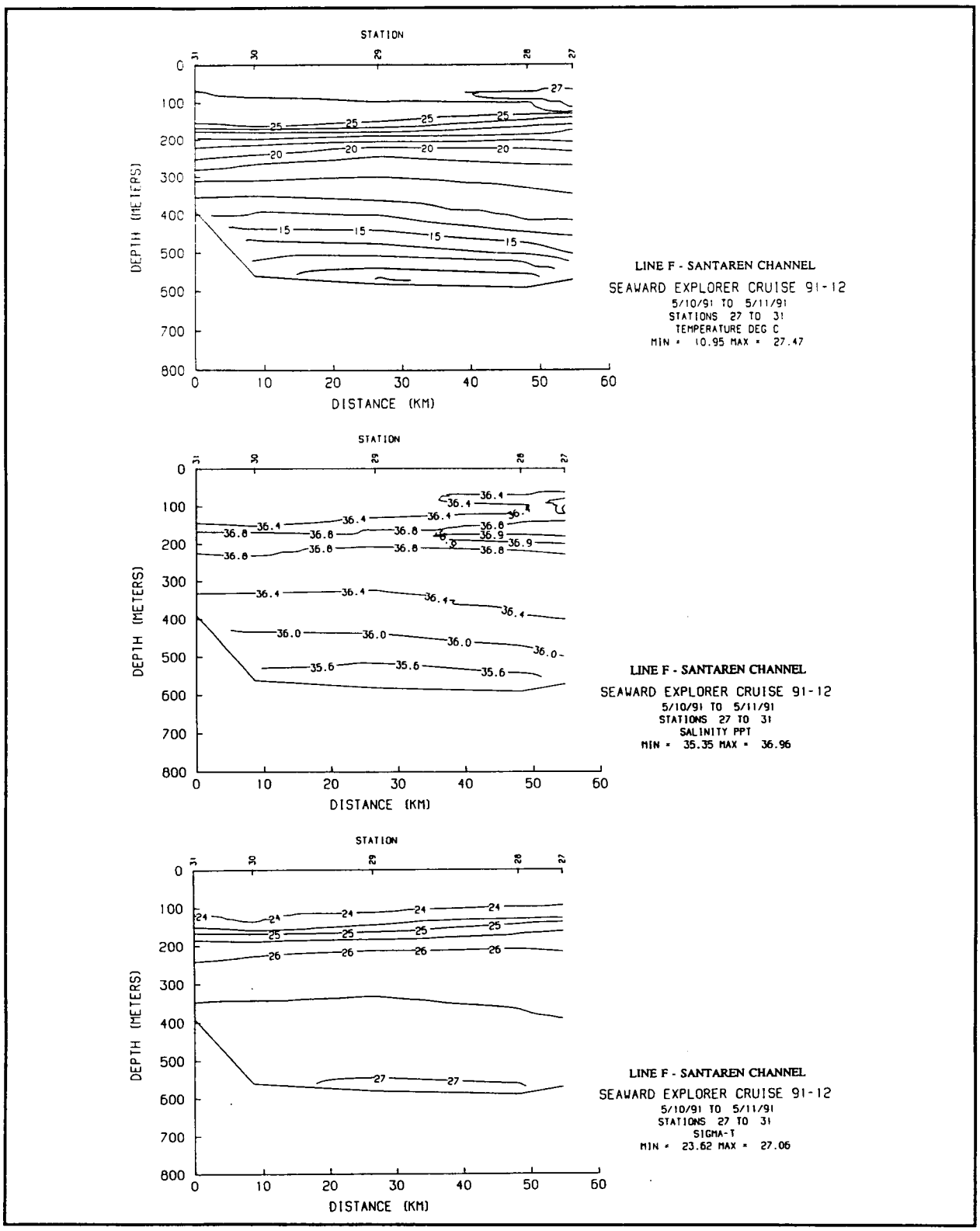

Figure 3.4-8. Temperature, salinity and density sections, Transect F.

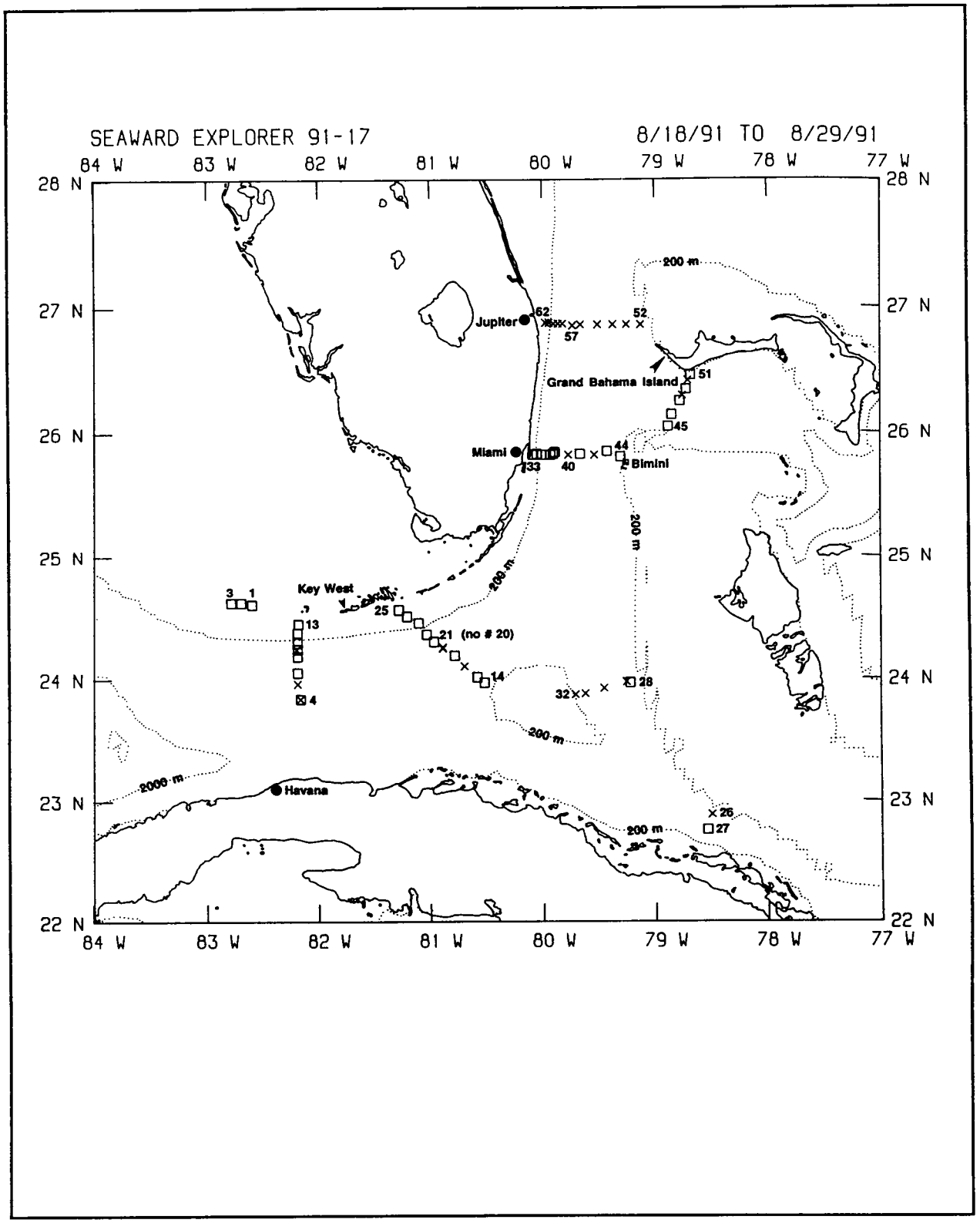

Figure 3.5-1. Location of stations for Cruise IV. Squares (□) indicate CTD stations, crosses (x) are XBT stations.

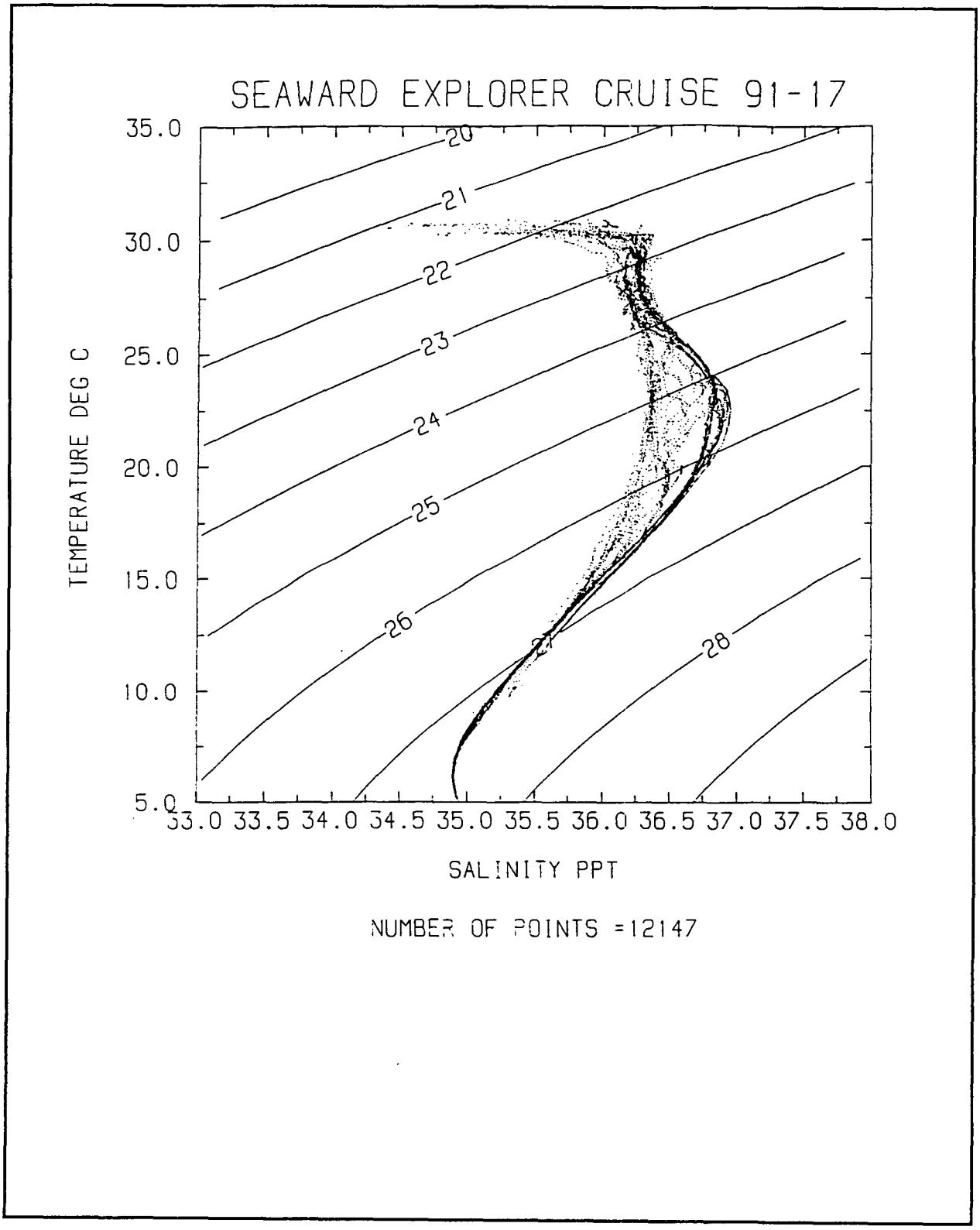

Figure 3.5-2. Composite T/S plot for Cruise IV.

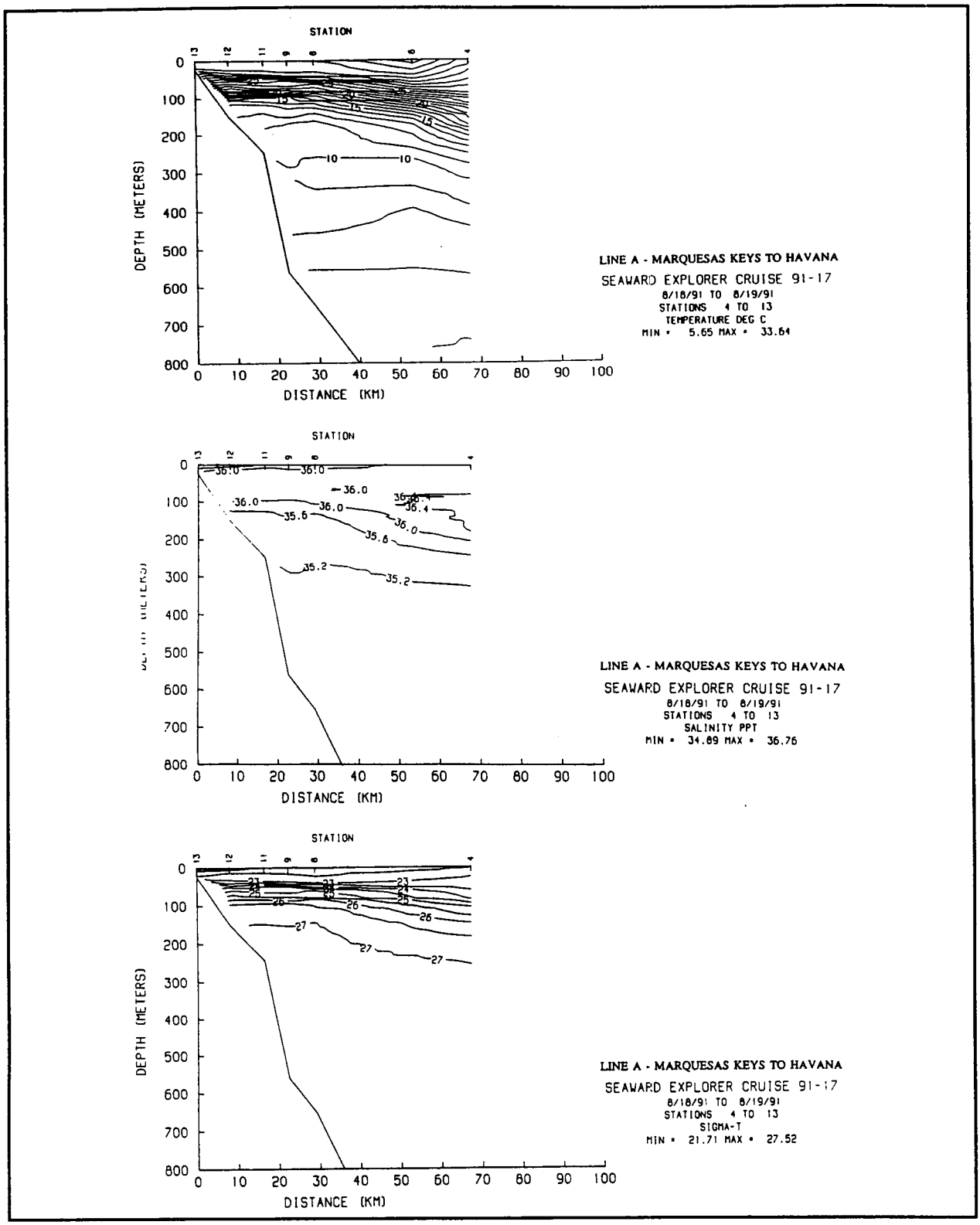

Figure 3.5-3. Temperature, salinity and density sections, Transect A.

salinity ranged from 34.89 to 36.76 psu (Figure 3.5-3b). The salinity maximum was on the Havana side of the Channel and was lower than the salinity maximum found on the previous cruise (36.89 psu). The lower salinities (35.12) were found on the Marquesas Keys side and probably resulted from drainage from Florida Bay. The density section showed a slope change across the channel at Station 8 (Figure 3.5-3c). This could have been related to the station spacing.

Transect B - Temperature ranged from 5.78 to 30.89°C (Figure 3.5-4a). The thermocline over the Portales Terrace was intense. There was a thermostad in the 17 to 18°C range and a second one between the seasonal thermocline and the layer of warm summer water. There was no evidence of dome structures. Salinity ranged from 34.89 to 36.91 psu (Figure 3.5-4b). The high value was in the Subtropical Underwater on the Bahamas side. A low salinity layer was located over the Portales Bank. The density section showed no doming, yet there appeared to be some structure over the outer Portales Bank (Figure 3.5-4c).

Transect C - The temperature section showed a strong thermocline over the terrace on the western end (Figure 3.5-5a). Thermostads occurred in the middle and eastern part of the channel. They were in the 16 to 19°C range and between the seasonal and summer thermocline. Temperatures ranged from 6.35 to 30.74°C. Salinity ranged from 34.89 to 36.93 psu. The high salinity core extended across the section with the 36.9 psu core on the Bahama side (Figure 3.5-5b). A low salinity layer (34.8 psu) was on the western (Miami) side. The density section revealed steepening isopycnals with depth and a slight dome at depth over the terrace on the west side of the channel (Figure 3.5-5c).

Transect D - Temperature ranged from 6.78 to 30.37°C (Figure 3.5-6). Thermostads were present in the 16 to 19°C range.

Transect E - Temperatures ranged from 9.89 to 29.70°C (Figure 3.5-7a). Thermostads were identified at 14°C and in the 17 to 19°C layer. Salinity ranged from 35.31 to 36.87 psu (Figure 3.5-7b). The high salinity layer extended across the channel. Isopyncals were flat across the channel with slight doming in the center of the channel at 50 and 300 meter depths (Figure 3.5-7c).

Transect F - The XBT section across the Santaren Channel shows a seasonal thermocline between 100 and 200 meters (Figure 3.5-8).

Transect G - The strength of density stratification was much less than observed during Cruise Three. The salinity maximum was centered on 200m, slightly below the normal depth farther north.

3.6 Hydrographic Conditions - Cruise Five (91-20)

The stations occupied on the fifth cruise are shown in Figure 3.6-1. Complete CTD sections were made on Transects A, B, C, E, F, G and H. The composite T/S plot (Figure 3.6-2) shows the standard Gulf Stream pattern. Note that the tight T/S lines vary below 12°C as they did in the previous cruise. There was an

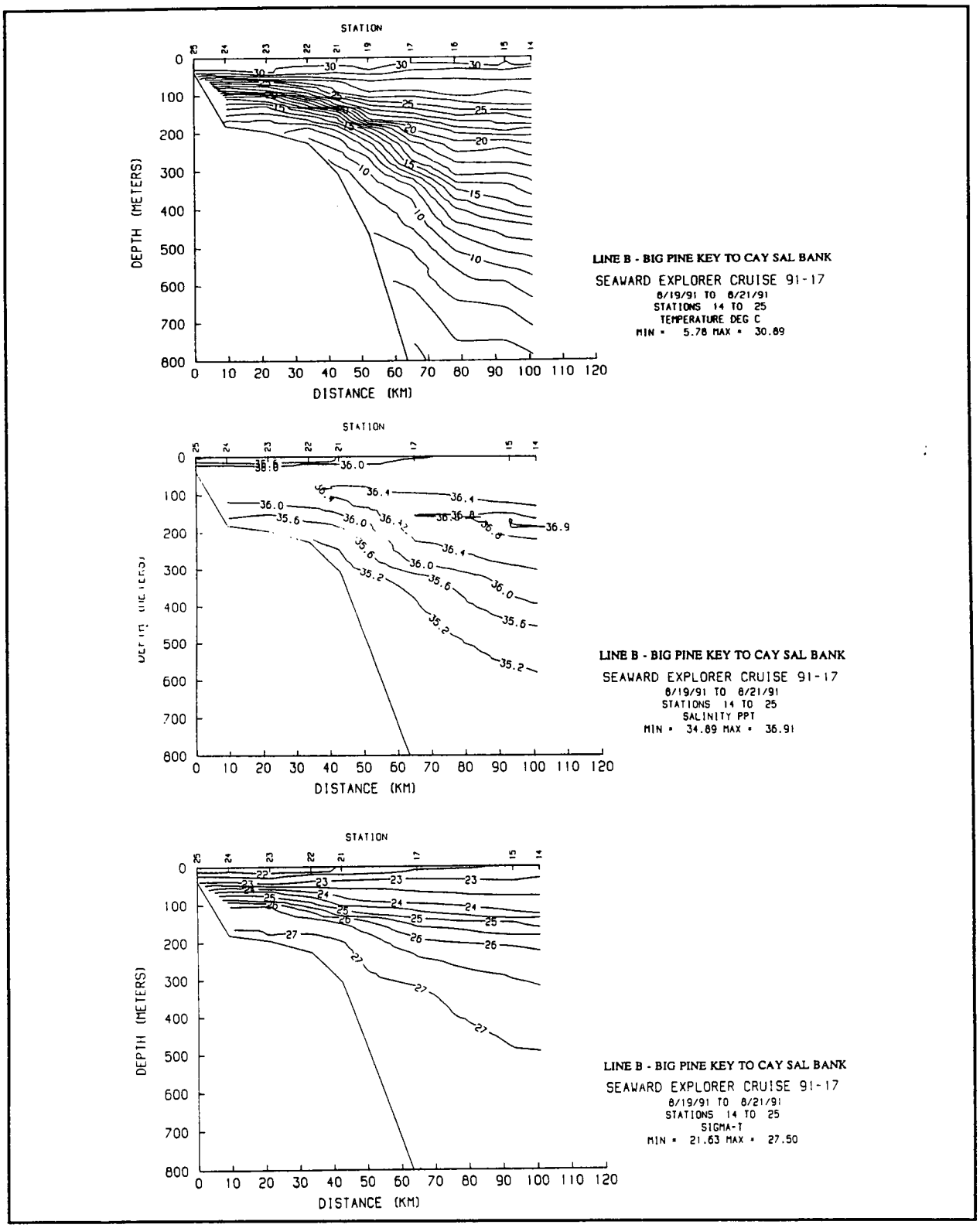

Figure 3.5-4. Temperature, salinity and density sections, Transect B.

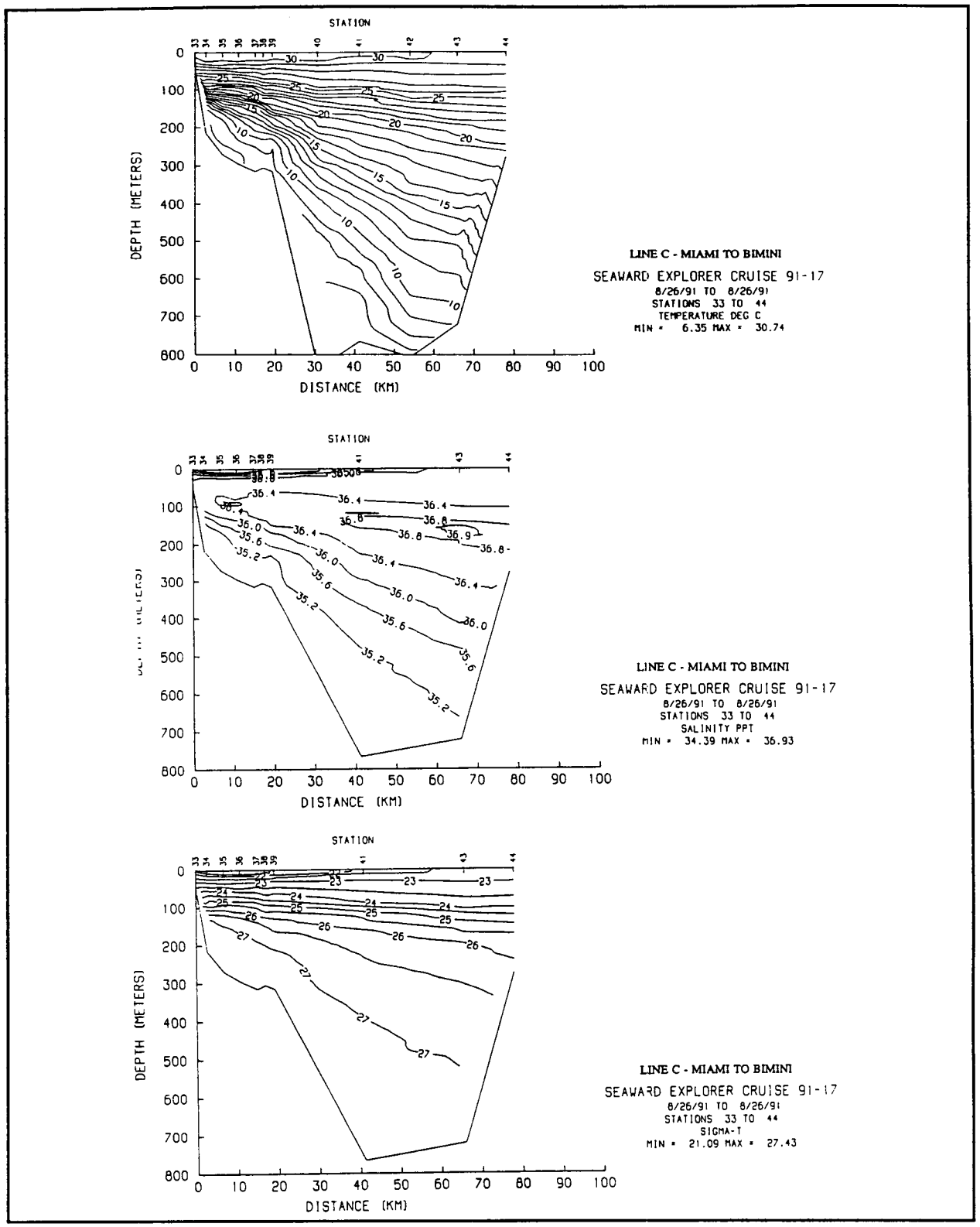

Figure 3.5-5. Temperature, salinity and density sections, Transect C.

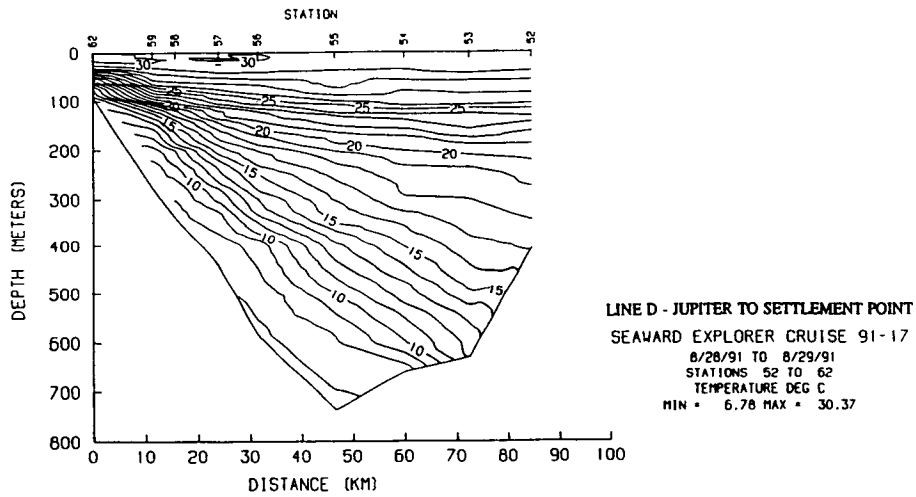

Figure 3.5-6. Temperature section, Transect D.

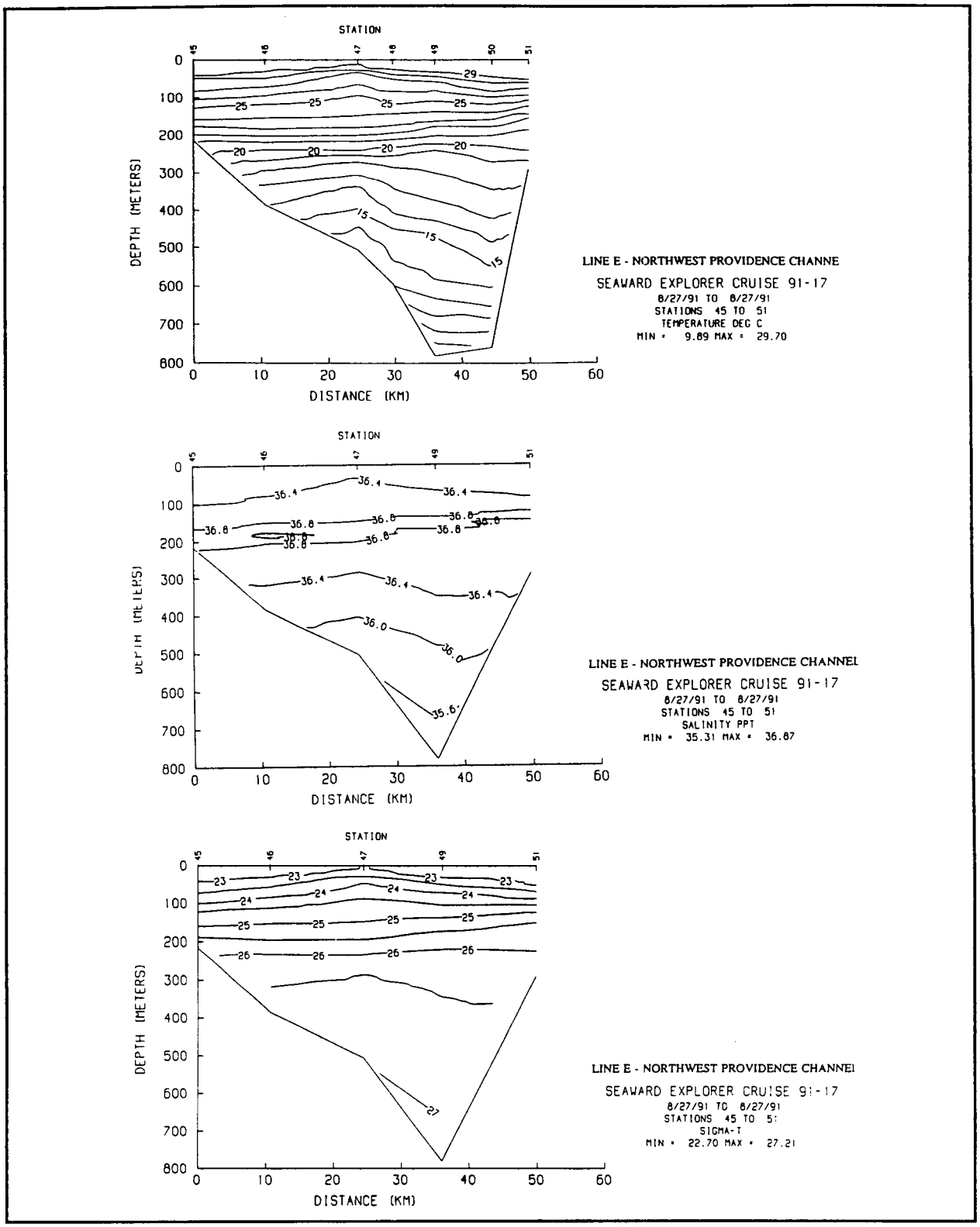

Figure 3.5-7. Temperature, salinity and density sections, Transect E.

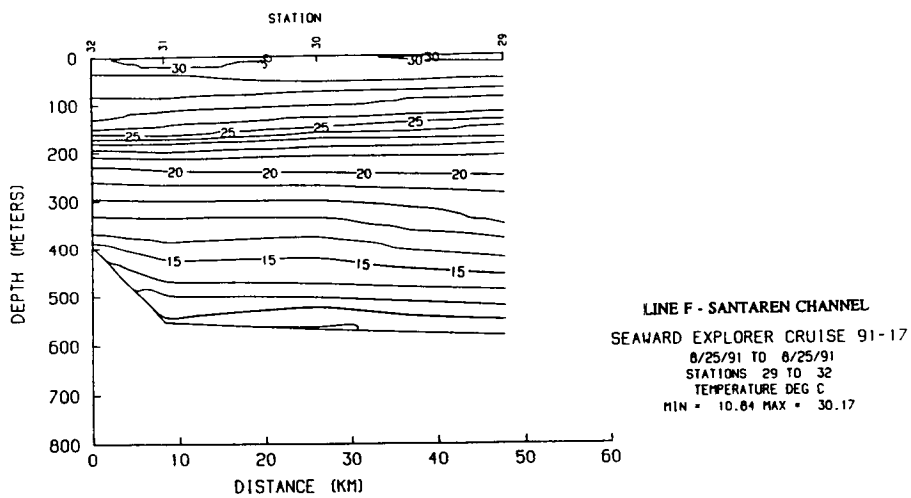

Figure 3.5-8. Temperature section, Transect F.

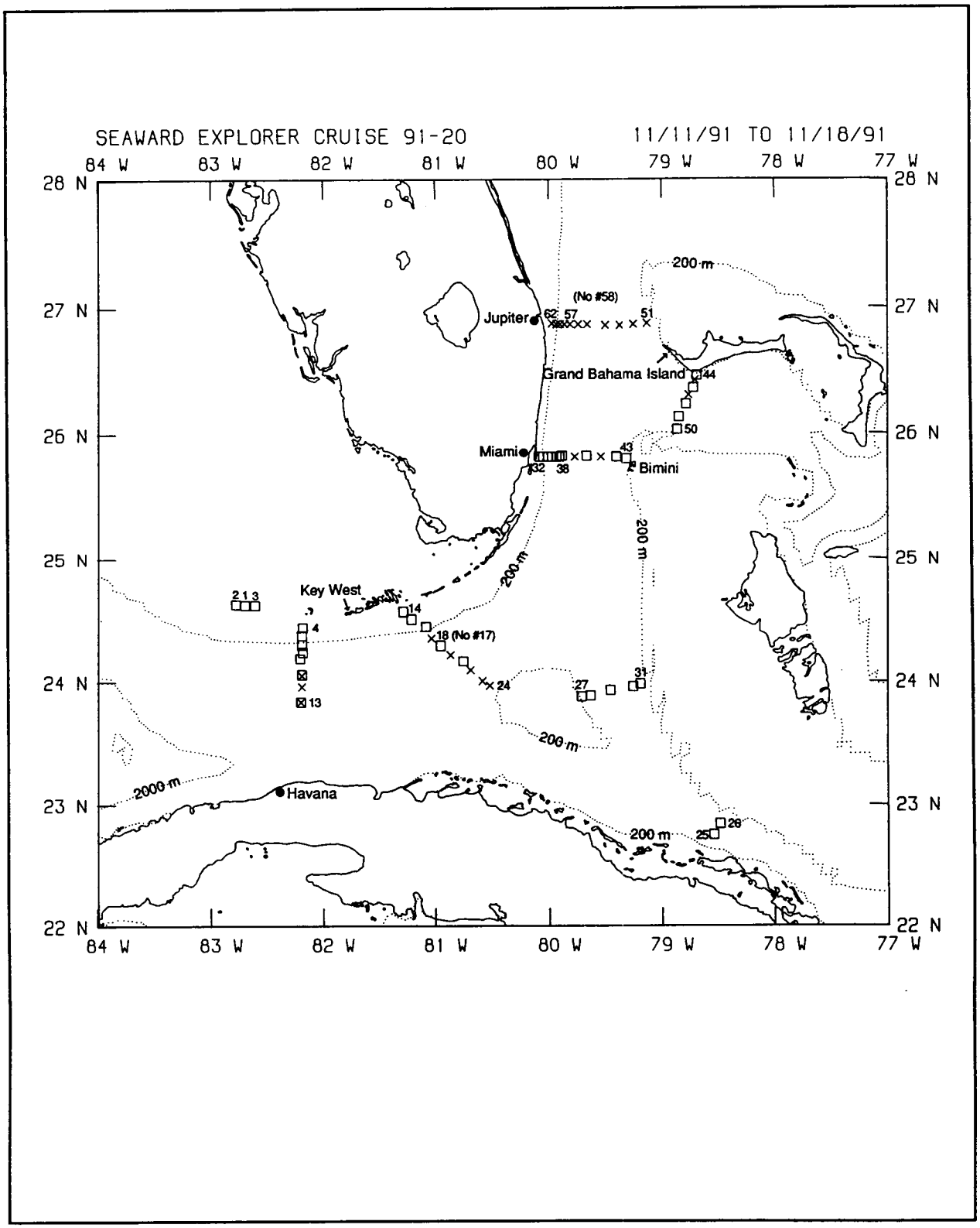

Figure 3.6-1. Location of stations for Cruise V. Squares (□) indicate CTD stations, crosses (x) are XBT stations.

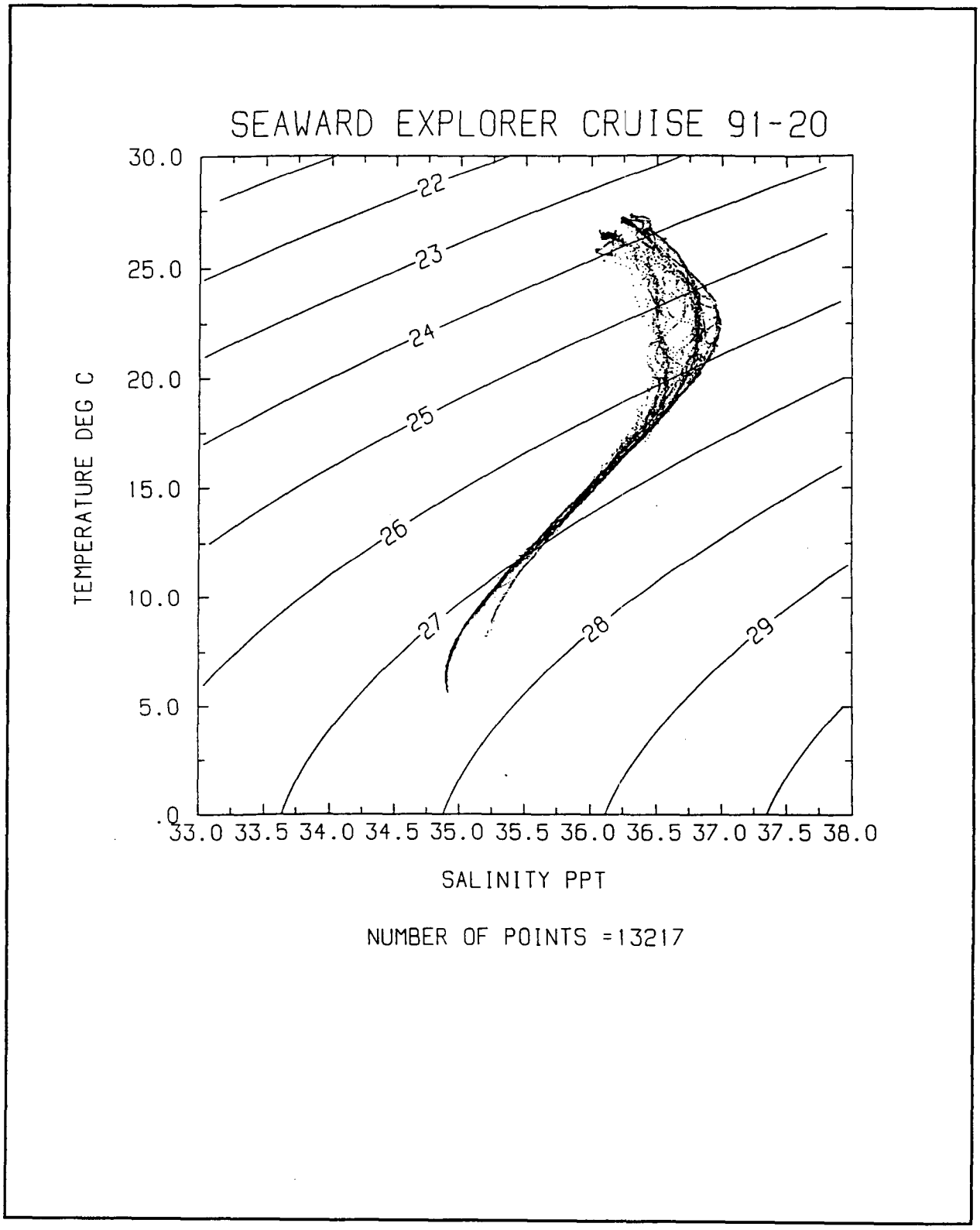

Figure 3.6-2. Composite T/S plot for Cruise V.

apparent bimodal distribution between 18 and 23°C. In the composite plot there are no obvious erratic high salinity layers.

3.6.1 Temperature, Salinity and Density Sections

Following are discussions of each section.

Transect A - Temperature on this section ranged from 6.04 to 26.90°C (Figure 3.6-3a). The upper layer was about 75m thick with little structure other than a dome structure centered at station 9. No thermostad was present above 15°C. Salinity ranged from 34.89 to 36.79 psu (Figure 3.6-3b). Since fewer CTD stations were made, the structure is difficult to observe. Density showed a noticeable lack of Gulf Stream structure; it presumably was toward the Havana side (Figure 3.6-3c). The dome structure is present, suggesting a westward current on the Marquesas Keys side of the Straits.

Transect B - Temperature ranged from 5.93 to 30.50°C with the upper layer extending down to 100m (Figure 3.6-4a). A stronger thermocline exists over Portales Terrace. There is a slight thermostad between 17 and 19°C. Salinity ranged from 34.89 to 36.85 psu (Figure 3.6-4b). The high salinity layer was restricted to the Cay Sal Bank side of the Straits. Density suggests a very weak Gulf Stream with a slight dome over the terrace (Figure 3.6-4c).

Transect C - Temperature ranged from 5.90 to 27.08°C (Figure 3.6-5a). The thermocline was strongest over the terrace. Thermostads appeared at various temperatures. A slight dome structure appeared over the terrace on the western end of the section. Salinity ranged from 34.90 to 36.94 psu with the high salinity layer along the Bimini side (Figure 3.6-5b). There was little evidence of low salinity water over the terrace. Density gradients were steeper with depth, and a small dome structure was present over the terrace (Figure 3.6-5c).

Transect D - Temperature ranged from 6.58 to 28.03°C (Figure 3.6-6). Strong Gulf Stream signals were present below 150m. The strongest thermocline was over the slope off Jupiter. A thermostad structure was apparent between 18 and 19°C on the west side.

Transect E - Temperature ranged from 8.20 to 27.01°C, and salinity ranged from 35.2 to 36.97 psu (Figure 3.6-7). The high salinity layer appeared to extend across the entire channel. Density shows little cross-shelf structure, although some deviations are indicated.

Transect F - Temperature ranged from 9.88 to 27.20°C (Figure 3.6-8).

Transect G - Salinity (and thus density) was slightly higher at Station 26. Again the salinity maximum was located deeper. The strength of the pycnocline was less than previously observed.

3.7 Mean Temperatures

Mean temperatures based on temperatures measured by current meters on Transects A, B, C, D, E and F are shown and discussed further in Chapter IV. Transects A, B, C and D all reveal the normal Gulf Stream structure. These sections are

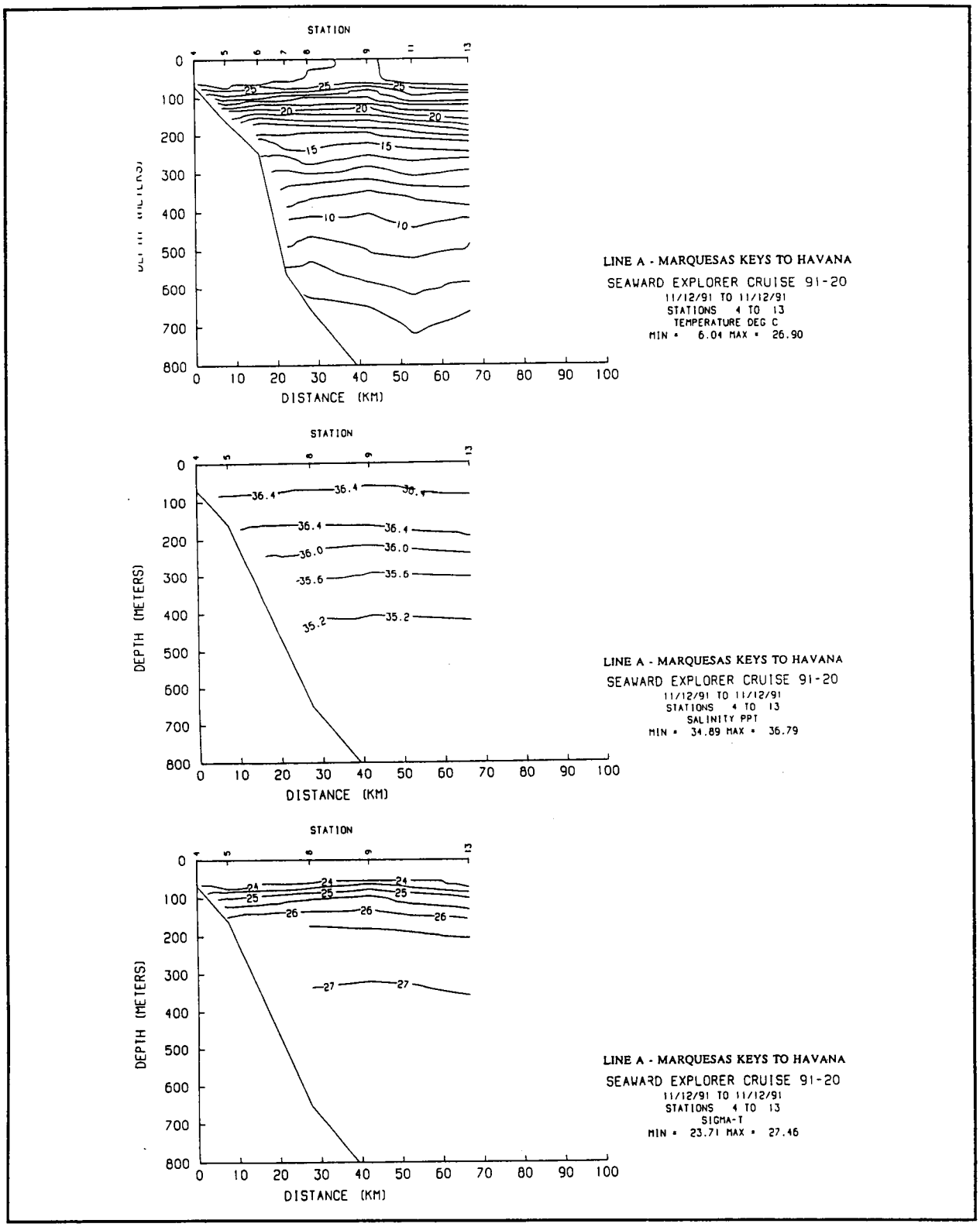

Figure 3.6-3. Temperature, salinity, and density sections, Transect A.

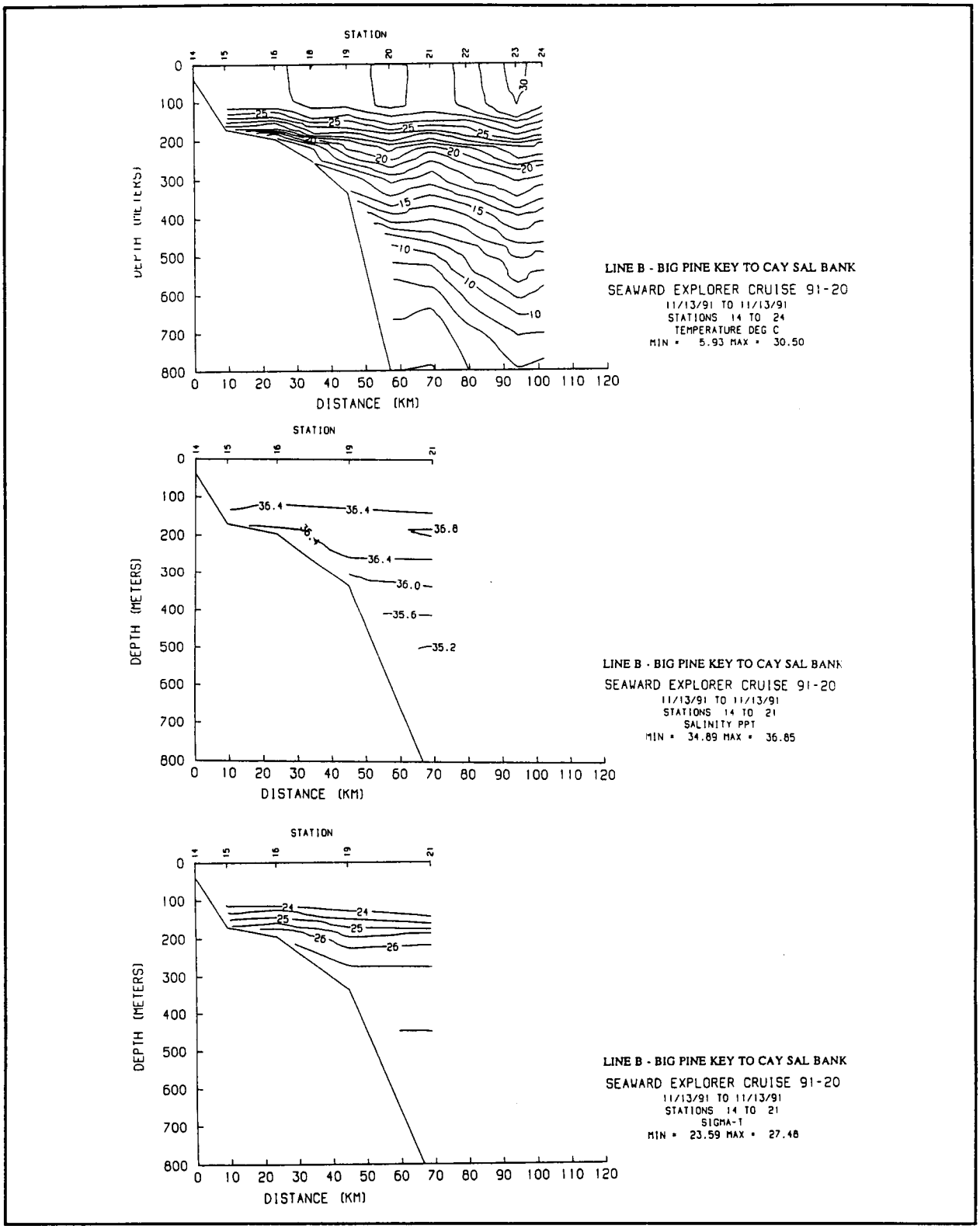

Figure 3.6-4. Temperature, salinity, and density sections, Transect B.

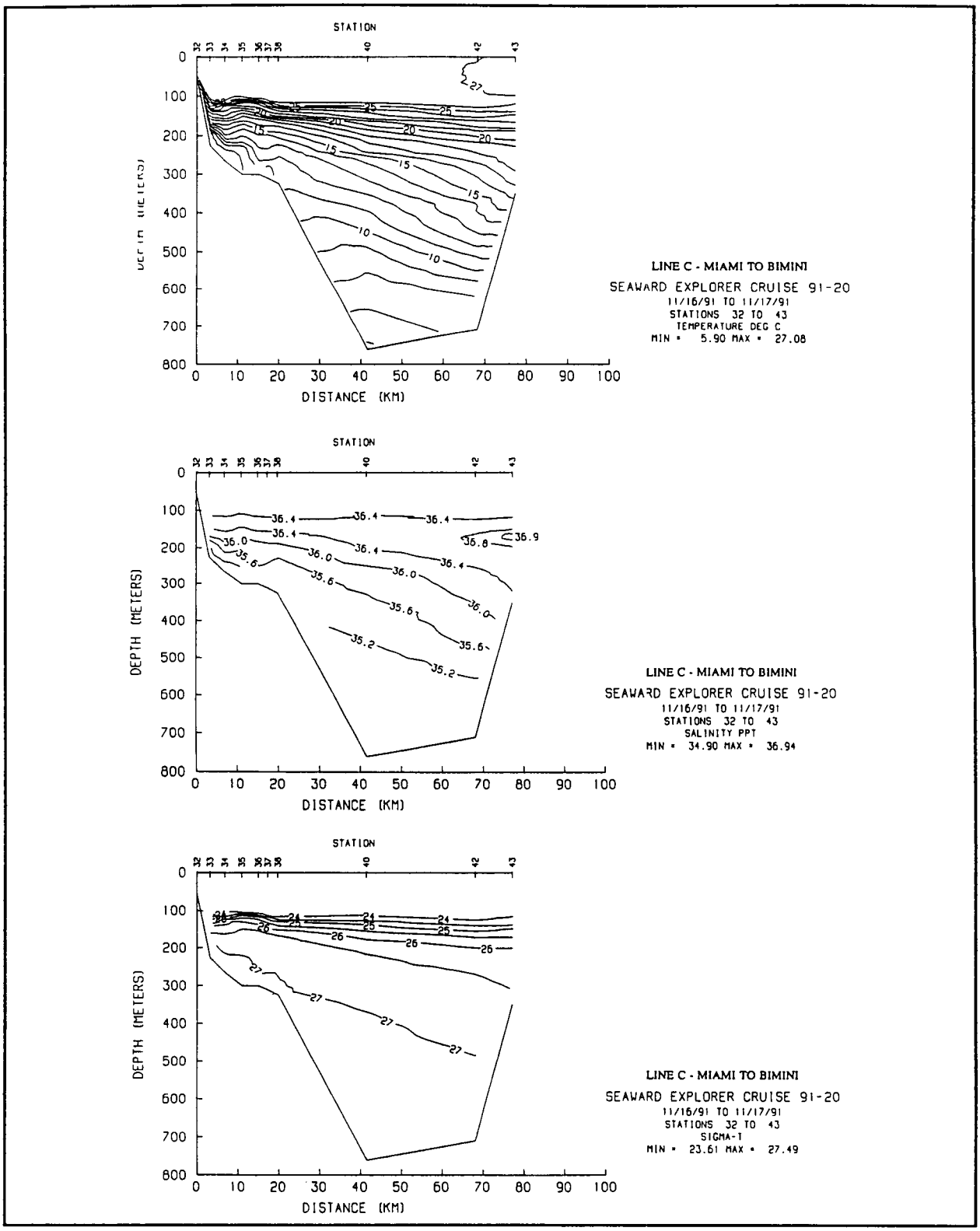

Figure 3.6-5. Temperature, salinity, and density sections, Transect C.

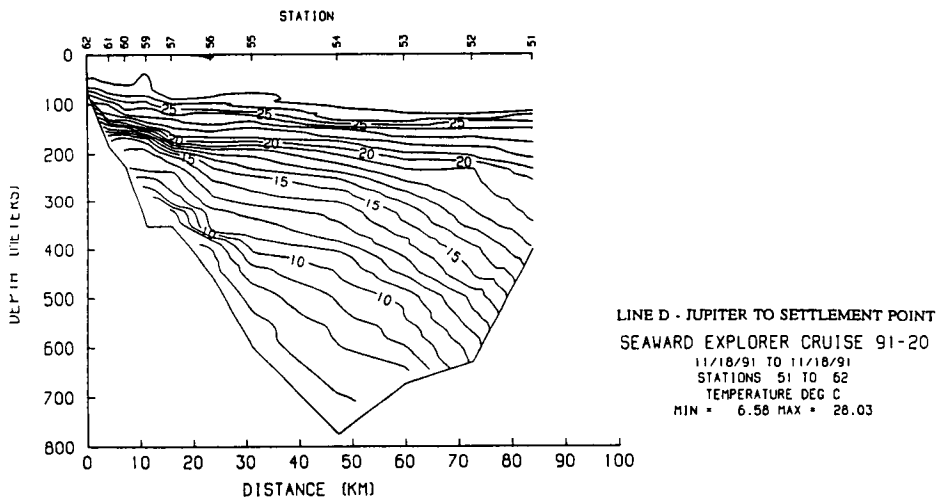

Figure 3.6-6. Temperature section, Transect D.

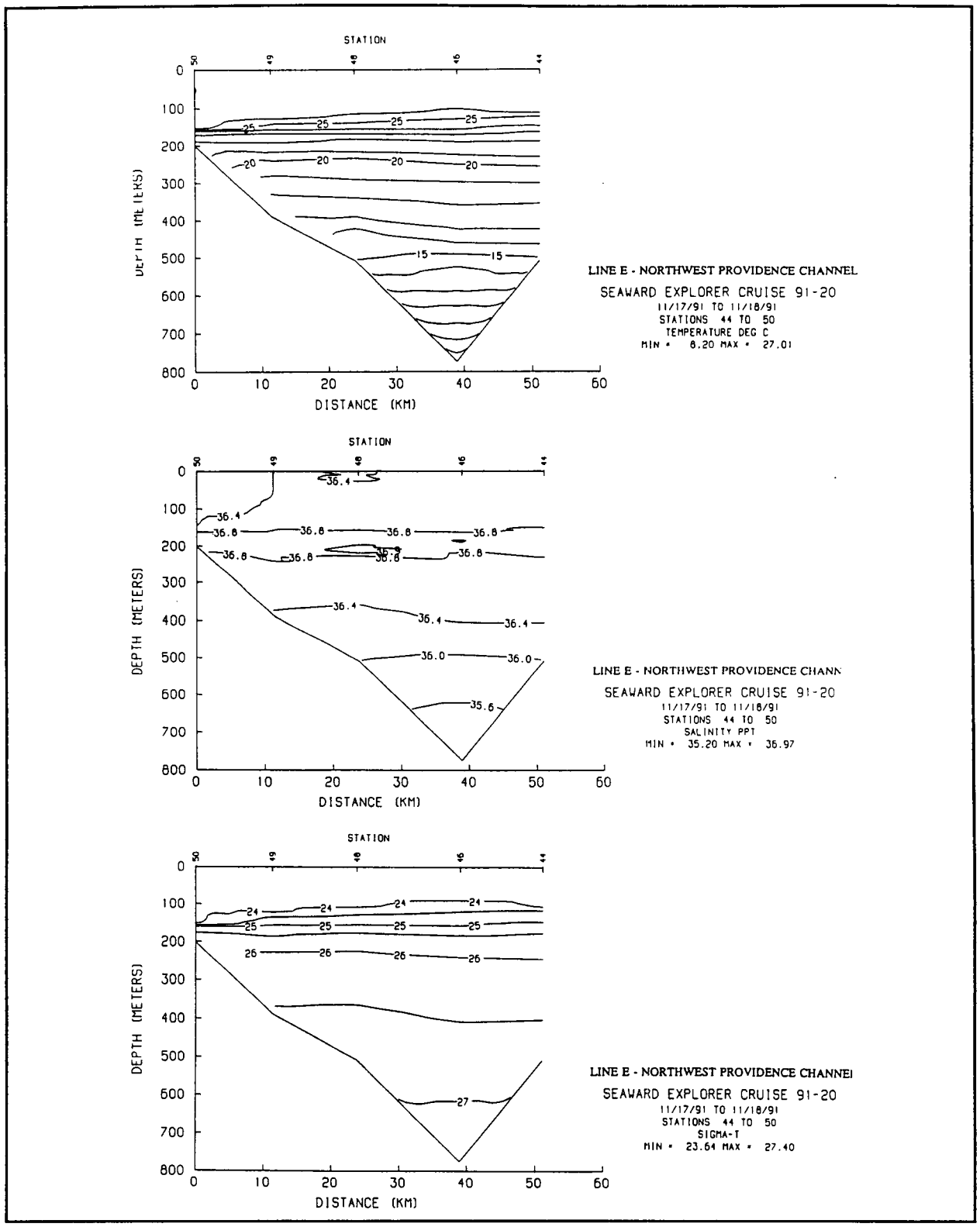

Figure 3.6-7. Temperature, salinity and density sections, Transect E.

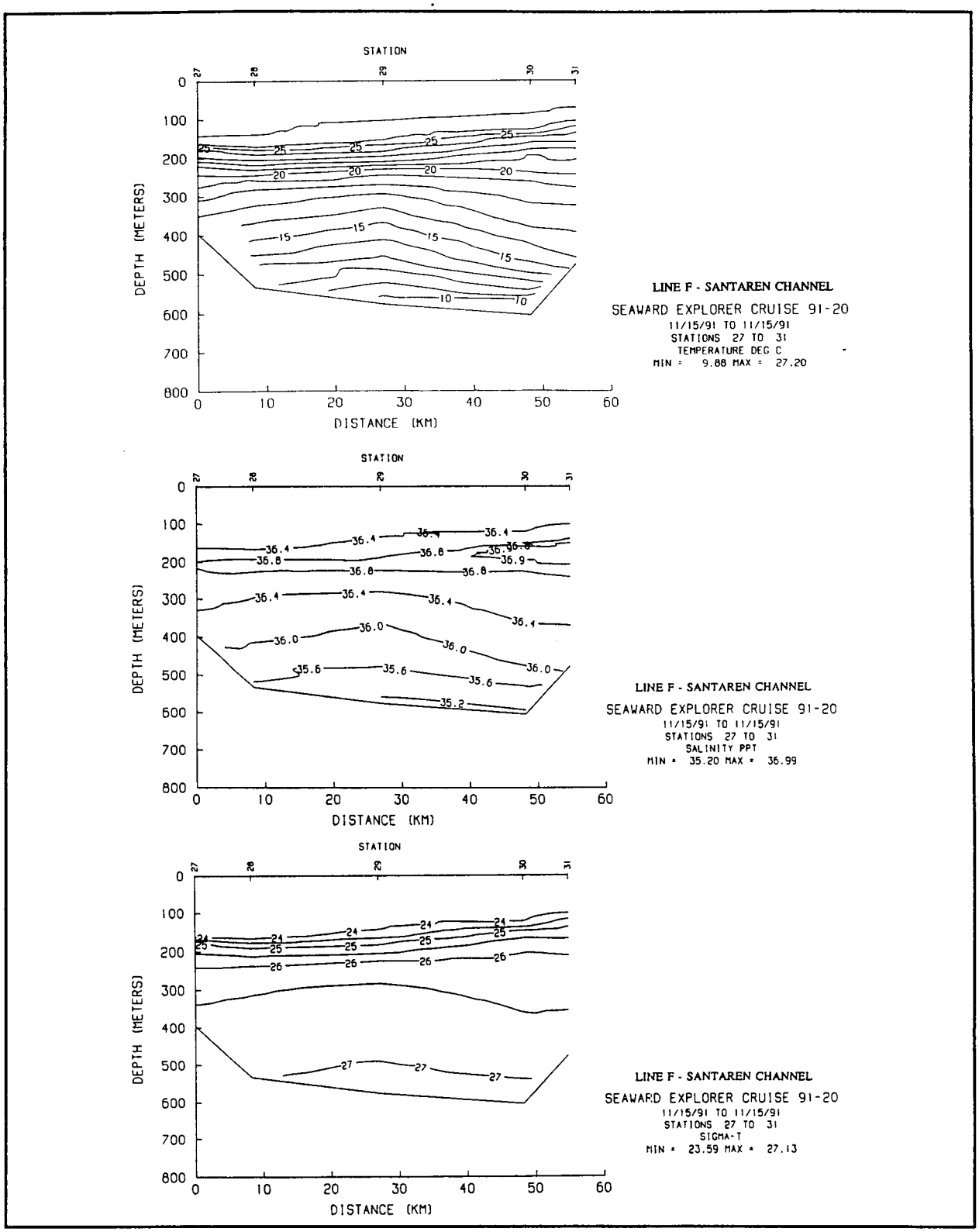

Figure 3.6-8. Temperature, salinity and density sections, Transect F.

progressively farther downstream in the Straits, and there is a suggestion of steepening isotherms between Transects B and C. The dome structures shown in the individual sections were not observed in the mean, although temperatures from XBT's were not included in these data.

Table 3.7-1 presents the mean high salinity values and the variance of the mean high salinity values from each section. The variance within channels is small, and all means are significantly different. The mean values suggest that the highest salinity water is coming from the OBC via SC and entering the FC into the upstream of Transect B. Note that the mean high salinity increases from Transect A (36.813) to Transect B (36.87) and Transect C (36.908). The low value in Transect A could result from not sampling the Cuban waters where higher salinities might be expected. Nevertheless, salinity in OBC and SC is consistently higher than in the SoF. Even NWPC is lower by 0.06 psu, but it is higher than other Straits samples. This could suggest that high salinity water from SC is moving into NWPC with the attendant salinity increase. The low mean high salinity at the Dry Tortugas (Mooring H) clearly indicated the influx of low salinity water from the north.

Table 3.7-1 Mean Maximum Salinity by Section

Section (Transect	Mean High Salinity (Var)
Old Bahama Channel (G)	36.99 (.0005)
Santaren Channel (F)	36.98 (.0006)
Marquesas to Havana (A)	36.813 (.005)
Big Pine Key to Cay Sal Bank (B)	36.87 (.001)
Miami to Bimini (C)	36.908 (.0008)
Northwest Providence Channel (E)	36.9225 (.004)
Dry Tortugas (H)	36.3275 (.056)

The above observations of high salinity sources form a consistent argument when combined with the transport charts data (Chapter 6). The observed flow was consistently into the Straits from the OBC and the SC. Thus if high salinity water was coming into the Straits from those channels, it would not appear until the Miami section. The observation of higher salinities in the NWPC is consistent with the observations of flow from the Straits eastward into this channel on the southern side. This high salinity water is then possibly mixed into the westward moving water in the northern part of NWPC Channel.

3.8 Seasonal Patterns

Seasonal variability in the study area should be observable in surface temperature and salinity. The five cruises over the one-year period provided minimal information about seasonal changes. However, the data do show a

variability that is definitely seasonal, thus adding to the existing database, which allows assessment of these patterns.

The seasonal change in maximum temperature on Transects B, C and F is shown in Figure 3.8-1. This plot represents the maximum temperature measured at CTD and XBT stations in the section. The value for December has been replicated at "month zero" to permit the creation of a cyclic plot. The pattern shows that minimum temperatures are in February and maximums in July with the obvious uncertainty. Note that Transect F, (SC) is consistently colder than the Straits stations. The reason for this is not obvious. The range in maximum temperature is about 5°C.

The seasonal change in maximum salinity is shown in Figure 3.8-2. The maximum salinity represents the maximum value in the SUW. The plot shows that maximum salinity was observed in December in the SC and in August and November in the Straits. The trend for higher salinity in the fall may reflect corresponding greater evaporation. However, since the SUW originates farther south, an in-phase relation with local evaporation would not be expected. It could be that the specific maximum salinity is related to local processes while the general salinity maximum is related to remote processes. Note that the SC salinity is consistently about 0.1 psu higher than the Straits salinity. This suggests a previously unmentioned source of salt to the Gulf Stream.

3.8.1 Comments

Water types in the SoF are classic and have been well described. However, as will be noted later, while the types are described, there is little published about the seasonal variations.

The first paper on the subject of water masses in the Straits was published by Wennekins (1959), who noted that the hydrography of the Straits is "greatly influenced by a flow of water originating in the Caribbean-Gulf of Mexico region and to a lesser extent by waters of the western North Atlantic." The water coming from the Caribbean is identified by its distinctive salinity maximum. This is what we now call SUW. Wennekins identified a water mass he called "Continental Edge Water." This is lower salinity water, modified in the Gulf of Mexico, and found along the continental margin in the Straits. Wennikens also noted that "The influx of Western Atlantic Water is frequently observed in the northern Straits of Florida off Bimini, being detected by its higher oxygen content; it is restricted to a narrow band along the Bahama Banks."

At this time, it will be useful to show the exact characteristics of the waters in the Straits. The key relationships for this purpose are T/S and density/oxygen plots. Since oxygen was not measured during the study, this relationship will not be further utilized. This is unfortunate since oxygen is the key to discriminating North and South Atlantic water.

It has been noted for many years that waters in the Straits are predictably segregated. Wennekins (1959) and Schmitz and Richardson (1991) noted that lower salinity water lies on the Florida side of the Straits while higher salinity water lies on the Bahamian side. Although we do not have oxygen data, lower oxygen water also generally lies on the Bahamian side. The low oxygen water is a positive indicator of a tropical source. The low salinity water was identified by Wennikens as a dilution of water flowing into the Gulf from the Yucatan; the

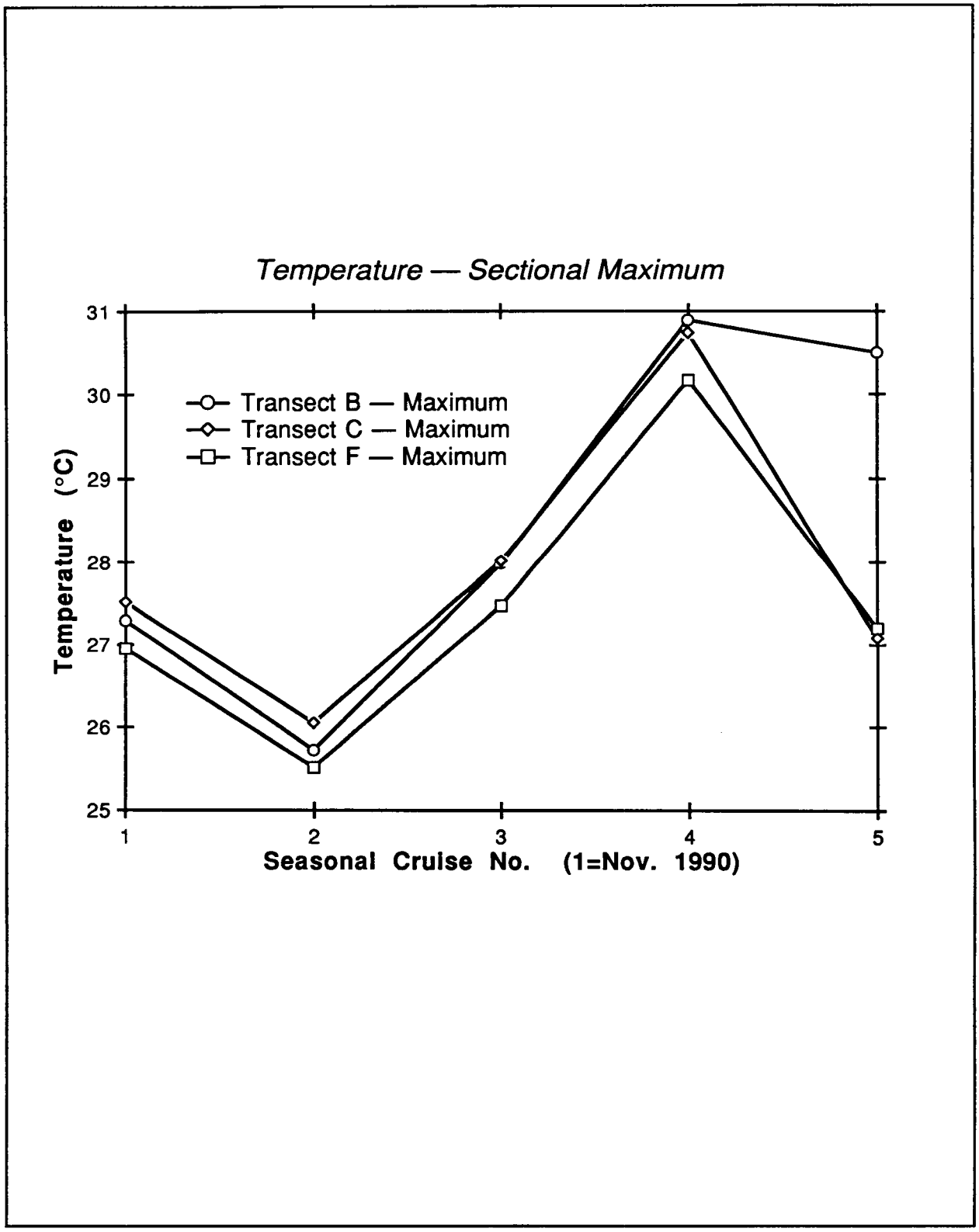

Figure 3.8-1. Maximum temperature at Transects B, C, and F.

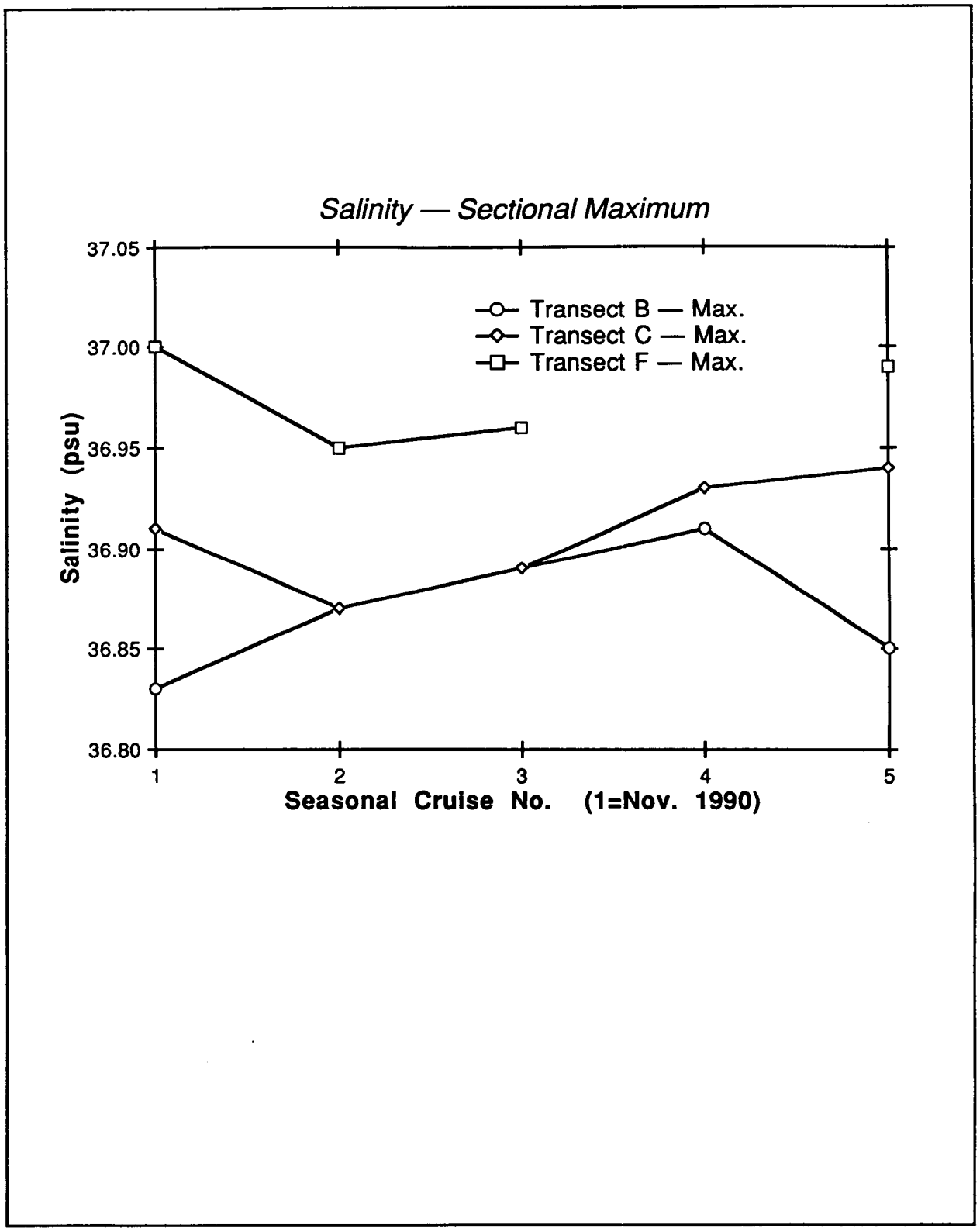

Figure 3.8-2. Maximum salinity at Transects B, C, and F.

water resides in the Gulf of Mexico for a time and is diluted with the resident river runoff.

IV. FLORIDA CURRENT VARIABILITY AND CIRCULATION

4.1 Introduction

Confined within the SoF is the strong, northward flowing FC, the portion of the Gulf Stream system which connects the Loop Current in the eastern Gulf of Mexico to the Gulf Stream off the southeast U. S. (Figure 1.1-1). The main SoF Channel is oriented in an east-west direction in the southern region below 25°N and turns cyclonically to a north-south orientation above 25°N. A shallow coral bank, the Cay Sal Bank, is located in the center of the channel where the northward turn occurs the bank separates the SoF from the SC. Water depths in the SoF decrease from about 2000m at the western entrance to less than 800m in the north. The Florida Straits are directly connected to the Atlantic through both the narrow OBC, which is located southeast of Cay Sal Bank and has a minimum depth of about 500m off central Cuba, and the NWPC, which has a control depth of about 600m at the western opening to the SoF.

Schmitz and Richardson (1991) estimate that roughly 45% of the water flowing through the SoF originates in the South Atlantic. They report that upper-layer FC waters, with temperatures greater than 24°C, are derived primarily from the tropical South Atlantic. Waters in the temperature range of 12-24°C consist mostly of Subtropical Underwater (SUW) of North Atlantic origin, which has a distinct salinity maximum. Waters in the temperature range of 7-12°C are associated with a distinct salinity minimum, the dominant source of which is Antarctic Intermediate Water (AIW) acquired from the South Atlantic. These water masses combine in the Caribbean due to the convergence of the North Brazil Current and the wind-driven, subtropical gyre to form the intense Yucatan Current/Loop Current/Florida Current in the eastern Gulf of Mexico and SoF. The shallow depths of the northern SoF inhibit most water colder than 8°C. However, geostrophic uplifting of isotherms on the western side of the FC allows water with temperatures as low as 6°C to be transported through the deeper sections of the Straits.

A considerable background of information exists on the Loop Current in the eastern Gulf of Mexico and on the FC in the northern part of the study area. However, few studies have been conducted on the flow behavior in the southern region off the lower and middle Florida Keys.

4.1.1 Northern Straits of Florida

The FC is an intense, baroclinic flow in approximate downstream geostrophic balance. The axial current is sheared both vertically and horizontally. The current axis is located about 25 km offshore of Miami in the mean and 80 km offshore of Key West. A mean westward countercurrent was observed on the northern side offshore of Key West (Brooks and Niiler, 1975), but no mean countercurrent occurs off Miami (Lee and Mayer, 1977). Düing (1975) reported the transient occurrence of deep counterflow beneath the current axis off Miami with speeds as high as 90 cm s^{-1} to the south. Volume transport fluctuations of the FC have been observed within the SoF on time scales ranging from tidal to annual. Tidal transport variations are typically on the order $\pm 1.5 \times 10^6$ m^3 s^{-1} (Sv) (Mayer, Leaman and Lee, 1984). Seasonal changes are estimated at ± 4 Sv and are asymmetrically distributed about a mean northward transport of about 32 Sv, i.e., maximum values occur in summer and minimum in fall (Niiler and Richardson, 1973; Molinari, Wilson and Leaman, 1985; Larsen and Sanford, 1985; Leaman, Molinari and

Vertes, 1987). Between the tidal and annual periods, a near continuum of transport fluctuations exists with amplitudes as large or greater than the seasonal signal (Lee, Schott and Zantopp, 1985). Many past studies have been concerned with FC variations in the 2- to 15-day period band, where current variability was explained by east-west meanders of the FC axis (Düing, 1975; Brooks, 1979) and atmospheric forcing (Düing, Mooers and Lee, 1977). Within the northern SoF, meandering motions have been associated with the generation of wind-forced continental shelf waves (Schott and Düing, 1976; Brooks and Mooers, 1977a and 1977b) and baroclinic instabilities (Boudra, Bleck and Schott, 1987 and 1988).

Statistical and dynamical analysis of FC variability at 27°N using STACS current-meter array data has shown that approximately 25% of the combined velocity and temperature variance is explained by meandering of the current core, with dominant time scales in the 1- to 2-week period band (Johns and Schott, 1987). Meanders were found to be characterized by an asymmetric or skewed wave form, with fluctuations leading on the eastern side of the SoF (Leaman and Molinari, 1987). Meander amplitudes at 27°N were found to be approximately 5 km r.m.s., and propagation speeds were downstream (northward) at 20-40 km day^{-1} with associated wavelengths of 150-350 km (Brooks, 1979; Johns and Schott, 1987).

Analyses of moored and cable-derived transports at 27°N by Lee et al. (1985), Johns and Schott (1987), and Schott et al., (1988), have shown significant coherence between FC volume transport and local meridional wind stress in several period bands. Highest coherence is found in the 4- through 10-day period band in winter, and near 20 days in summer, which is consistent with the dominant time scales of wind forcing in these seasons. In both seasons transport fluctuations are found to lag the wind fluctuations by approximately one day. Lee and Williams (1988) and Schott et al., (1988) developed simple barotropic models of the wind-forced response and concluded that frictional effects in the Straits were probably insufficient to account for deviations in the observed amplitude and phase of the response relative to linear, wind-driven theory. Lee and Williams (1988) hypothesized that the finite residence time of water parcels in the Straits, due to rapid advection by the FC, may be important in limiting the response. Persistent upwelling (downwelling) has been found to occur over the western shelf and slope of the northern SoF in association with northward (southward) wind fluctuations (Johns and Schott, 1987; Lee and Williams, 1988). Furthermore, the wind-driven velocity response was found to be strongly trapped over the continental shelf and upper slope.

The annual cycle of FC volume transport has been shown to be forced partly by a maximum in wind forcing fields over the northwestern region of the subtropical gyre (Anderson and Corry, 1985) and partly by local along-channel wind forcing (Lee and Williams, 1988; Schott et al., 1988).

In addition to horizontal meanders, the FC frequently forms cyclonic, cold-core frontal eddies in the slope and terrace waters. These disturbances were described by Lee (1975) and Lee and Mayer (1977) as small diameter (10-30 km) "spin-off" eddies, which form along the western (cyclonic) edge of the FC and travel northward along the continental margin at speeds ranging from 20 to 50 cm s^{-1}. At these rates it usually takes one to two days for an eddy to pass a fixed point. Frontal eddies occur on the average of once per week and they have been observed to disturb the temperature field down to a depth of 200m. They are recognized in the surface waters as warm, southward-oriented, tongue-like

extrusions of the FC coupled to a trailing band of shelf or slope water. Frontal eddies evolve commensurate with enlarging offshore meanders of the FC front and appear to be part of the final growth stage of baroclinically unstable meanders (Boudra, Bleck and Schott, 1988).

4.1.2 Eastern Gulf of Mexico

Circulation in the eastern Gulf of Mexico is dominated by the Loop Current, the portion of the Gulf Stream which connects the Yucatan Current to the FC (Cochrane, 1972; Nowlin and Hubertz, 1972). After penetrating the Gulf, the current pattern arcs anticyclonically to the east and southeast, forming a current "loop" which subsequently exits through the SoF. The western and eastern boundaries of the Loop are fixed by the topography of the basin, the Campeche Bank and the west Florida shelf (Cochrane, 1972; Molinari and Cochrane, 1972).

Interior flow in the Loop Current is also anticyclonic. The flow pattern is elongated along an axis parallel to the shelf regions on either side and centered over the deep basin (Cochrane, 1972). Some portion of the southern Loop Current flow may exit back through the Straits of Yucatan rather than the FS (Nowlin, 1971). This portion varies, depending upon the degree of arc in the Loop pattern. The Loop Current influences flow to a depth greater than 1000m (Nowlin, 1971). As would be expected, current velocities decrease with increasing depth from a maximum greater than 100 cm s^{-1} at the surface. Numerous estimates of transport in the Loop Current have been made from hydrographic observations. An average value of 30 Sv has been determined by Nowlin and Hubertz (1972), Nowlin and McLellan (1967), Schmitz and Richardson (1968), and Morrison and Nowlin (1977), although their reference levels are not necessarily directly analogous.

A comparison of the extent of the northward intrusion of the Loop as observed by different investigators indicates spatial extremes of 1) direct flow from the Yucatan Straits to the SoF and 2) intrusion of the loop as far north as 28.5°N. Leipper (1970) proposed an annual cycle of growth and decay of the Loop Current, beginning with the formation of a small loop near Cuba in January-February and subsequent growth into the Gulf through August. He termed this sequence the "spring intrusion." The decay phase follows with a general weakening of the Loop and splitting of the flow, either in detached eddies, current rings, or extensions to the west. Maul (1977) studied the annual cycle of the Loop Current between August 1972 and September 1973 and concluded that, although the pattern is cyclic, year-to-year variability is significant and that the "intrusion" is not necessarily a spring phenomenon. Maul (1977) showed a maximum penetration of the Loop to 28°45′N in August 1973 and a minimum to 24°15′N in December 1972. As the Loop penetrated deeper into the Gulf, it also moved further to the west (Maul, 1977).

Growth of the Loop in the Gulf has been related to an excess of inflow through the Yucatan Straits over outflow through Florida Straits (Leipper, 1970; Maul, 1977). Maul (1977) calculated that a net flow increase of 4 Sv was required to induce growth. The flow increase through the Yucatan area is probably associated with seasonal increases in transport of the FC. Hurlburt and Thompson (1980) studied Loop Current growth and eddy shedding with nonlinear numerical models. They found that the Loop Current can penetrate into the Gulf, bend westward and shed realistic anticyclonic eddies at near annual frequency with no time variation in the inflow. They concluded that the Loop Current growth and eddy shedding resulted from a mixed instability of the basic flow field. Sturges

(1992) used time series of satellite derived estimates of the northward penetration of the Loop Current to conclude that the primary period of Loop Current penetration was 8.5 months, which is believed to be the primary rate at which rings would be shed with constant inflow.

The detachment of large, anticyclonic eddies from the Loop Current is well documented (Nowlin, Hubertz and Reid, 1968; Leipper, 1970; Leipper, Cochrane and Hewitt, 1972; Morrison and Nowlin, 1977; Cochrane, 1972). These features exhibit a range of surface current speeds up to a maximum that is comparable to that observed within the main Loop Current (about 100 cm s^{-1}). The formation of these eddies is believed to occur on an average of about 8.5 months, normally following the intrusion of the Loop north into the Gulf. After formation, the eddies drift westward into the western Gulf of Mexico (SAIC, 1989; Hamilton, 1990; Sturges, 1992).

Flow variability on the west Florida shelf is primarily driven by the local wind at middle to inner shelf locations and by Loop Current intrusions in the outer shelf (SAIC, 1987; Mitchum and Sturges, 1982). The wind response produces cross-shelf flows in the upper and lower Ekman layers and a downwind geostrophic interior flow on the 2- to 10-day wind forcing time scale. Loop Current forcing of the outer shelf region can occur in the form of cyclonic frontal eddies that travel southward along the Loop Current's eastward boundary on a time scale of 2 to 14 days (Paluszkiewiez et al., 1983), similar to those observed in the northern SoF and southeast U.S. shelf (Lee and Mayer, 1977; Lee and Atkinson, 1983; Zantopp, Leaman and Lee, 1987), and large-scale onshore/offshore penetrations of the Loop Current over the shelf on time scales of greater than 2 weeks.

4.1.3 Southern Straits of Florida

Little is known about flow variability in the southern SoF. The few studies that are available indicate the presence of cold, cyclonic gyres offshore of the middle to lower Keys (Niiler and Richardson, 1973; Chew, 1974), and off the Dry Tortugas, where the Loop Current abruptly turns to the east and enters the southern SoF (Vukovich, 1988). Recent moored current meter measurements and hydrographic surveys made off the Florida Keys as part of the SEFCAR (Southeast Florida and Caribbean Recruitment) study have provided more detailed descriptions of gyre formation over the Pourtales Terrace between Key Largo and Key West and on the influence of the FC and local wind forcing on coastal water motions (Lee, et al., 1992).

Year-long current records from the shelf edge in the Florida Keys, seasonal hydrographic surveys and ADCP profiles from the Pourtales Terrace reveal the structure of a cold, cyclonic gyre that forms over the Pourtales Terrace between Key Largo and Key West with a period of 1-2 months. Because the gyre appears to have a preference for formation over the Terrace, it was named the Pourtales gyre (Lee et al., 1992). Spatial dimensions of the gyre are on the order of 100 km in the alongshore direction and 40 km cross-shore. Circulation velocities range from 20 to 50 cm s^{-1}. Upwelling velocities in the center of the gyre are estimated at 2m day^{-1} and appear to cause a 50 to 75m uplifting of cold, fresh waters onto the Terrace from deeper strata of the FC. Indications are that formation of the gyre is dependent on onshore/offshore meandering of the FC and on cyclonic flow curvature as the FC is forced to change direction from eastward to northward flow at this location due to the change in orientation of the bathymetry. When the FC

is in an onshore position, strong northeastward flow is observed over the Terrace. Westward flow develops as the FC front meanders offshore to a location near or offshore of the Terrace break. The flow curvature can account for approximately 20% of the cross shore momentum balance, causing an ageostrophic condition that increases the cross-shore pressure gradient and drives an onshore flow in the bottom boundary layer over the Terrace and upwelling.

Lee et al. (1992) observed a locally forced, wind-driven response in alongshore currents at the 30m depth off the lower Keys (Looe Reef) at a period of 10 days in winter/spring and 5 days in summer with lags of 14 and 5 hours, respectively. This response is typical of other shallow coastal seas with straight coastlines. Alongshore current variability at the 30m depth in the middle and upper Keys was found to be not as strongly influenced by local winds due to the curving coastline, which results in mostly cross shore winds at these sites. Also the nearness of the FC front to the northern site (Carysfort) results in meandering and eddy shedding processes having the dominant influence there.

Lee et al. (1992) found that the combination of strong eastward flow of the FC off the lower Keys and westward flow over the Pourtales Terrace when the gyre is "spunup" has a pronounced influence on the prevailing westward wind stress and can produce a doubling of the stress for typical wind strengths. This results in a convergence of surface Ekman transports into the gyre and Terrace that can transport and concentrate surface materials, such as passive plankton drifters, in the northwest portion of the gyre and along its northern side i.e., along the middle to lower Keys coastal zone. Thus, the lower Keys are a preferred region for onshore surface transport due to the prevailing westward winds and the Pourtales gyre circulation. North of the lower Keys, locally trapped gyres do not occur, and the prevailing southeast winds no longer cause onshore Ekman transports due to the change in orientation of the SoF from east/west to north/south.

4.2 Low-Frequency Variability

Low-frequency variability of the FC within the confines of the Straits of Florida is discussed using representative 40-hour, low-pass filtered current and temperature records from mooring Transects A - G, together with their energy, coherence and phase spectra, and large-scale surface thermal patterns derived from satellite AVHRR images.

4.2.1 Southern Straits of Florida

4.2.1.1 Spatial and Temporal Variability

The spatial and temporal variability of the FC in the southern Florida Straits is discussed with the aid of moored observations from Transect A that extends off Marquesas Keys to approximately half way across the Florida Straits to Cuba, Transect B off Big Pine Key that extends from near the Looe Reef Marine Sanctuary to the Cay Sal Bank, and Transect F that extends east from the Cay Sal Bank, across the SC to the Bahama Bank. Data from the single mooring, G, located in the center of the OBC between Cuba and the Bahama Bank, are also included in this analysis.

For March and April 1991, low-frequency current and temperature time series from inshore moorings located at the 245m isobath on Transects A and B and obser-

vations from the offshore sites and Transect F and G provide a basis for discussing spatial variability of meander and eddy processes (Figures 4.2-1 through 4.2-4). Subtidal-current and temperature records from Transect A show the influence of large, onshore-offshore shifts or meanders of the Florida Current (Figure 4.2-1). When the FC is in an onshore position, the northern front, with strong cyclonic shear and offshore increasing temperatures, will be located near Mooring A1, which will result in strong eastward currents and increased temperatures at this site, as occurred for the month of December. Surface temperature patterns derived from weekly composites of warmest pixels from satellite AVHRR imagery verify that the warm FC surface front was in an onshore position (relative to the Florida Keys) at Transects A and B for December (Figure 4.2-5).

In general, satellite-derived surface temperature patterns are in excellent agreement with the measured flow fields in the upper layer. Maximum current speeds tend to occur at maximum temperature gradients and in the warmest waters. Also current directions are parallel to the temperature gradients as in a thermal wind-type balance i.e., warmer water to the right of the downstream vector. At this time, currents at site A1 were strongly sheared over depth and reached speeds greater than 100 cm s^{-1} toward the east at the 75m depth. This onshore position appears to coincide with the absence of a Loop Current and a sharp eastward turning of the Yucatan Current into the southern Florida Straits with little penetration into the Gulf of Mexico. Eastward current speeds began to decrease at A1 in the latter part of December, becoming 30 cm s^{-1} or less toward the east for January 15 to February 18, then reversing toward the west until about April 10, when the flow abruptly shifted back toward the east and increased in speed to greater than 100 cm s^{-1} (Figures 4.2-1). The westward flow was slightly stronger at 150m than at 75m, reaching speeds of about 50 cm s^{-1}, and was accompanied by a 4°C drop in temperature at both measurement levels, suggesting an offshore shift of the FC and the set-up of a cold, cyclonic circulation.

A time sequence of satellite AVHRR imagery shows that the FC was moving offshore at this site from December 30 to February 18 as the Loop Current was growing northward into the Gulf of Mexico. Figure 4.2-6 shows that by the week of February 17 the Loop Current had penetrated into the eastern Gulf to about the latitude of Tampa Bay (27.5°N). As the Loop Current turns southward and flows along the seaward edge of the southwest Florida shelf, it appears to overshoot the entrance to the southern Florida Straits before turning eastward at about mid-channel between the Keys and Cuba. This pattern suggests that the offshore shift of the FC in the region from the Tortugas Keys to Marquesas Keys may be related to the growth of the Loop Current into the eastern Gulf of Mexico.

The offshore shift of the FC and the strong cyclonic curvature of the front at the entrance to the southern Florida Straits provides a mechanism for the generation of a cyclonic gyre. Weekly composite satellite AVHRR imagery shows that the spin-up and evolution of this gyre had a dramatic influence on the spatial and temporal variability of currents and temperature in the southern SoF (Figure 4.2-7a through 7g). The gyre appears to form initially in the region off the Tortugas, so for convenience this feature is called the Tortugas Gyre. The extension of this cold gyre into the region off the Marquesas appears to have caused the current reversals and temperature drops at stations A1 - A3 between February 18 and April 10 (Figures 4.2-1, and 4.2-2).

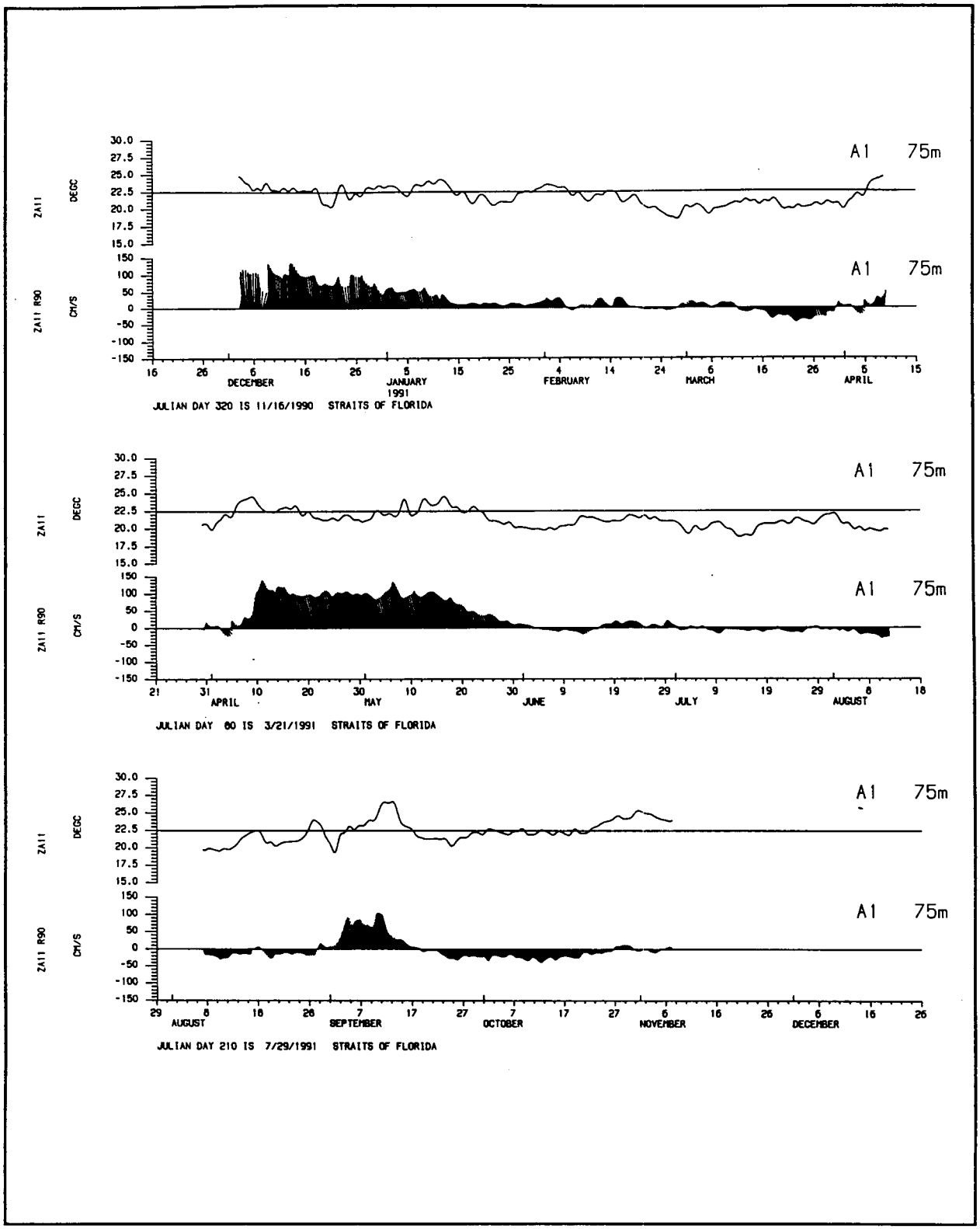

Figure 4.2-1 40-HLP filtered temperature and velocity for the entire measurement period at Mooring A1, instrument at 145 m below the surface. Data from the beginning of the study period is at the top and the end at the bottom.

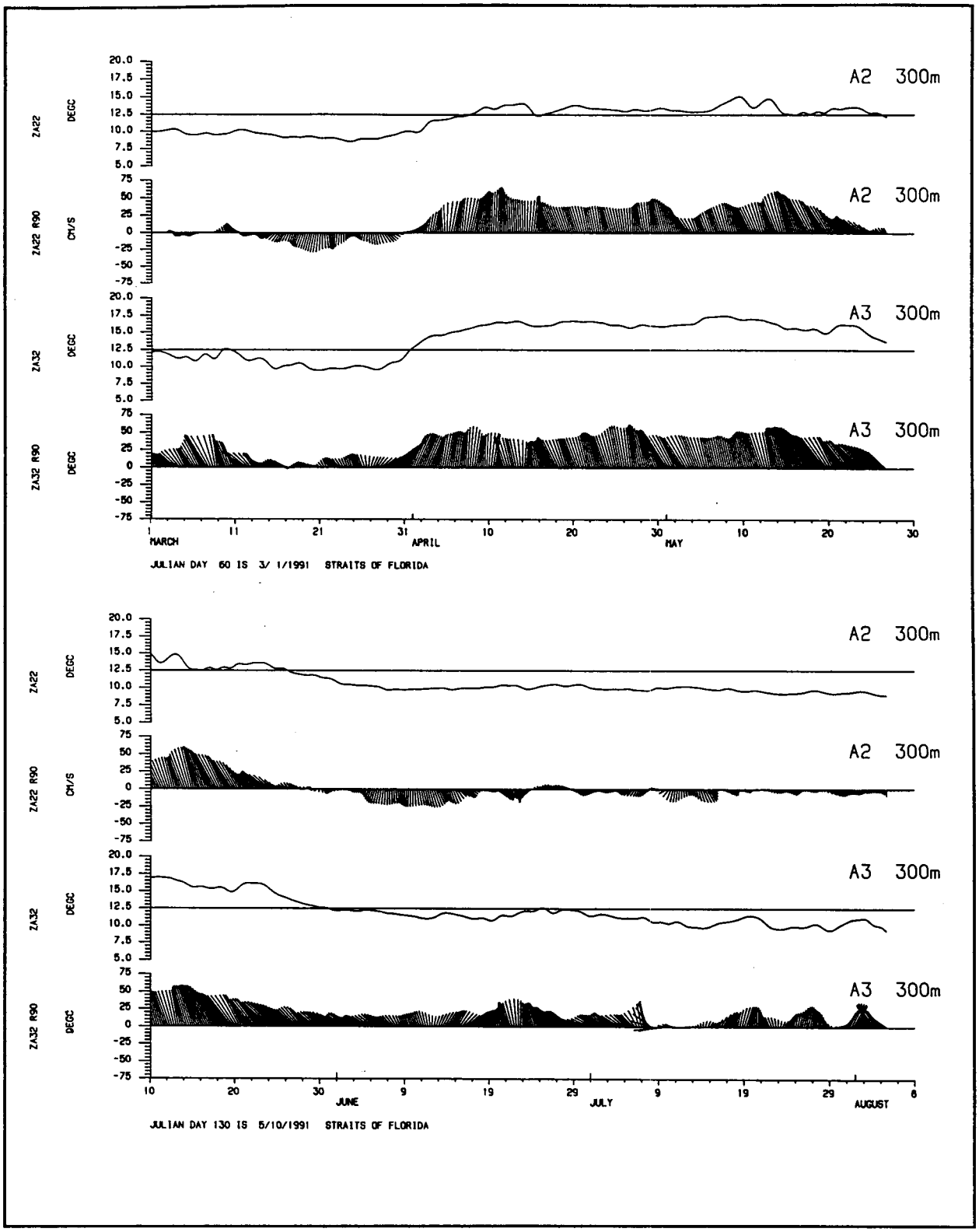

Figure 4.2-2 40-HLP filtered temperature and velocity for the period March 1991 through August 1991 for instruments at 300 m on Moorings A2 and A3. The first half of the record is at the top and the second half on the bottom.

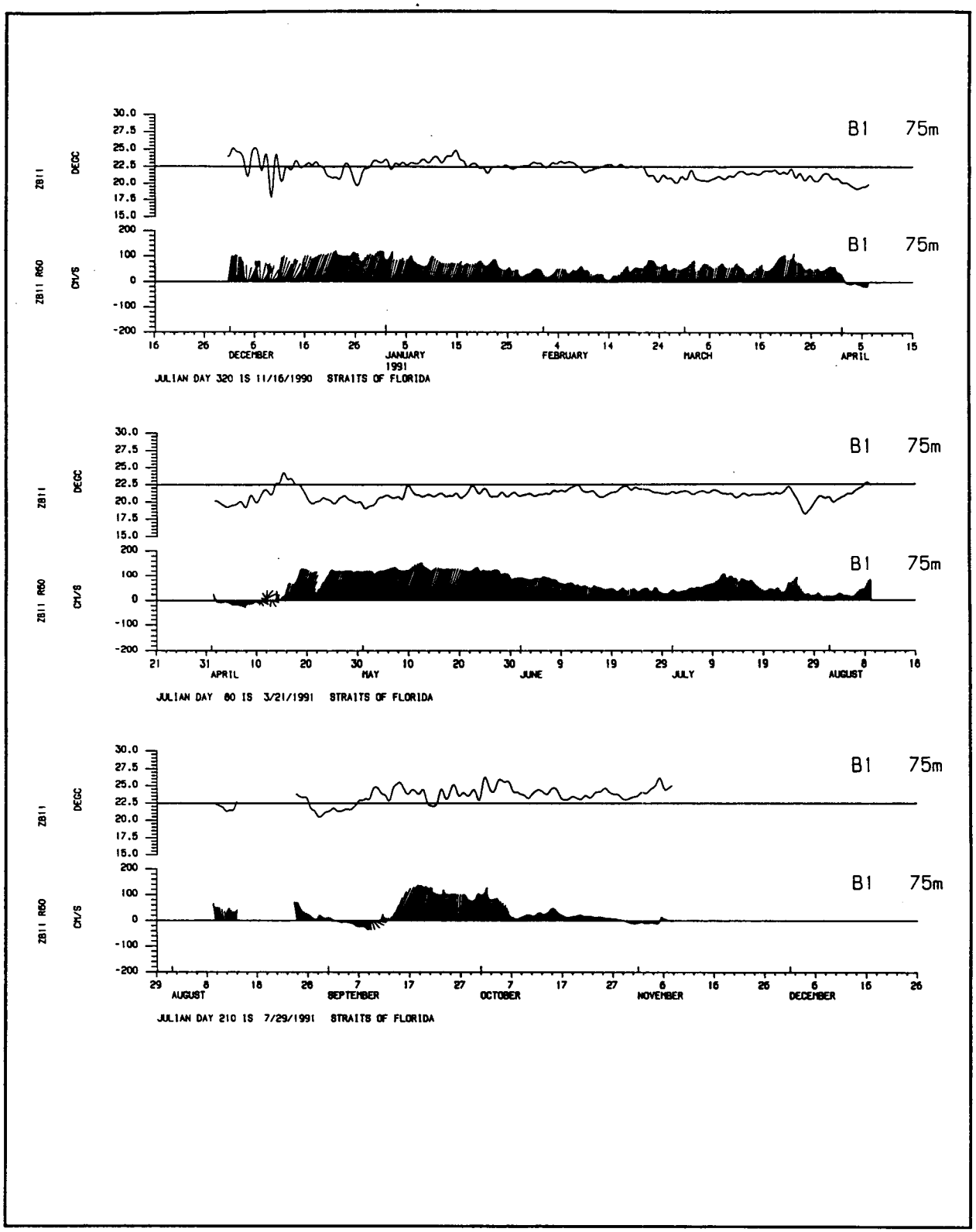

Figure 4.2-3 40-HLP filtered temperature and velocity data for the entire measurement period at 75 m on Mooring B1. The total record is divided into three periods and presented. See the axis just below each stick plot for time.

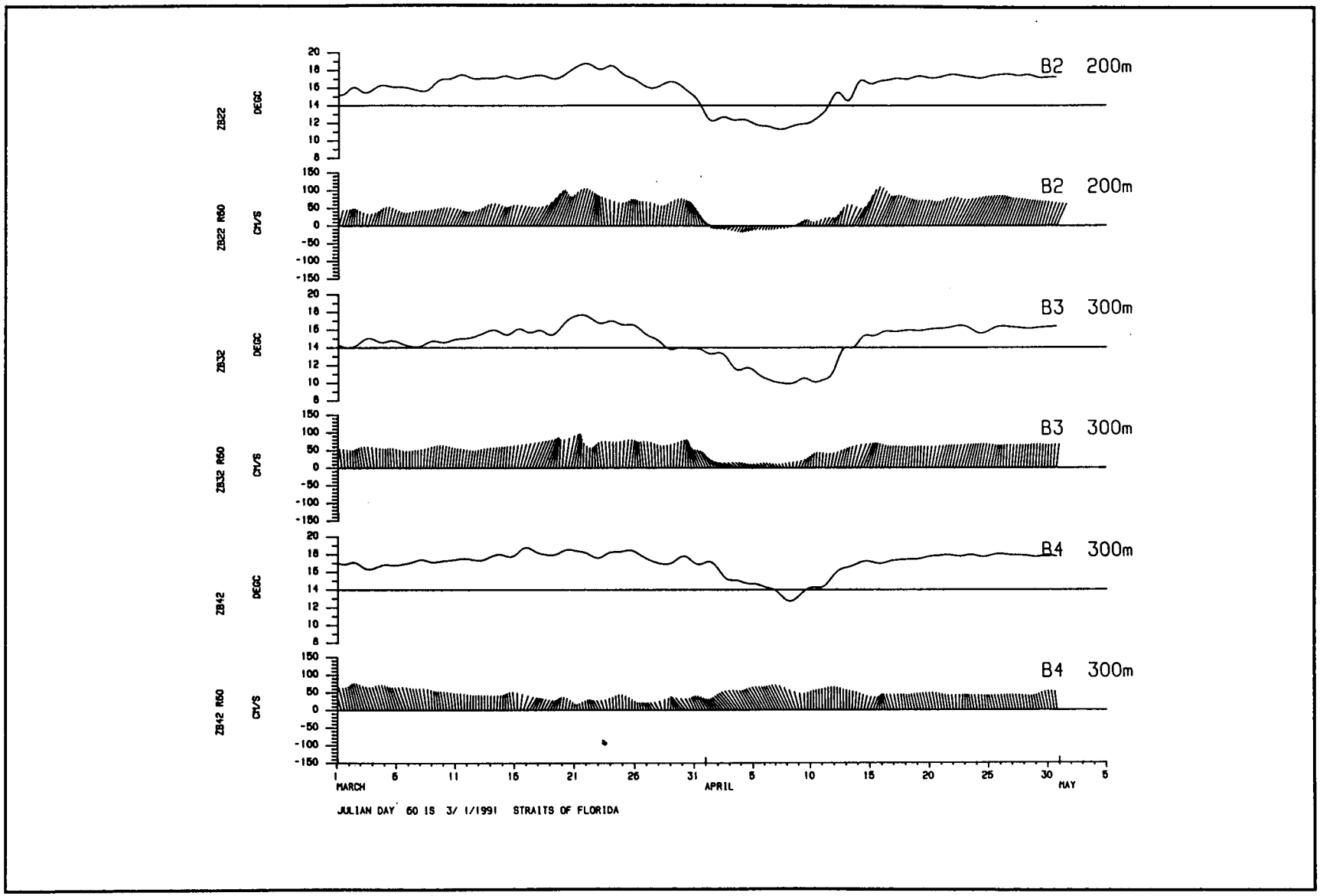

Figure 4.2-4 40-HLP velocity for the indicated moorings and depths. Time interval presented is from March through April 1991.

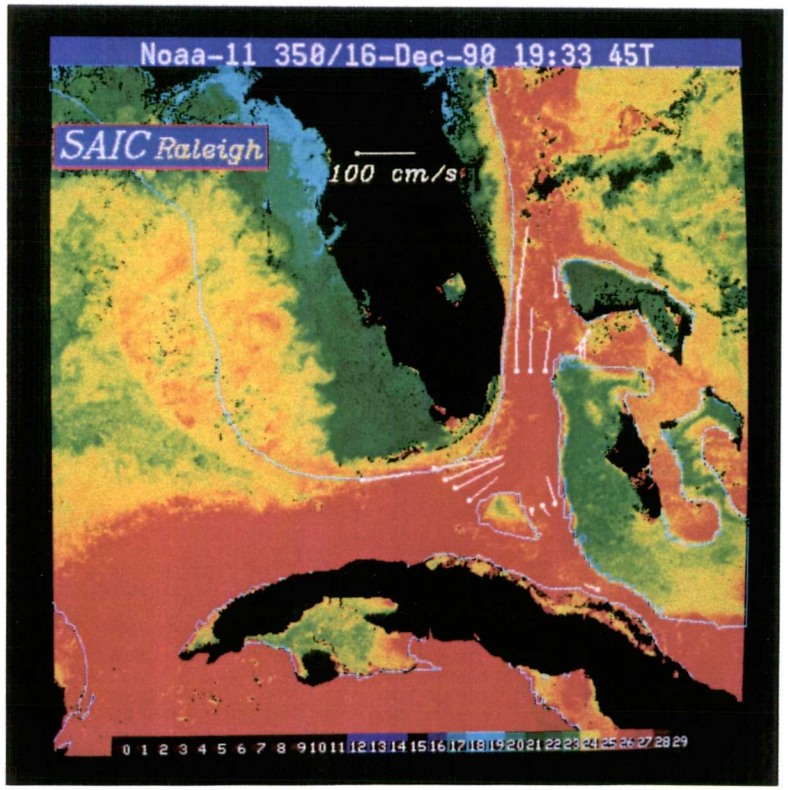

Figure 4.2-5 Composite thermal image for week of Dec. 16-22, 1991. Vectors are as of noon GMT, December 19, 1991. The scale at the bottom of the image shows the relation of color to temperature (°C).

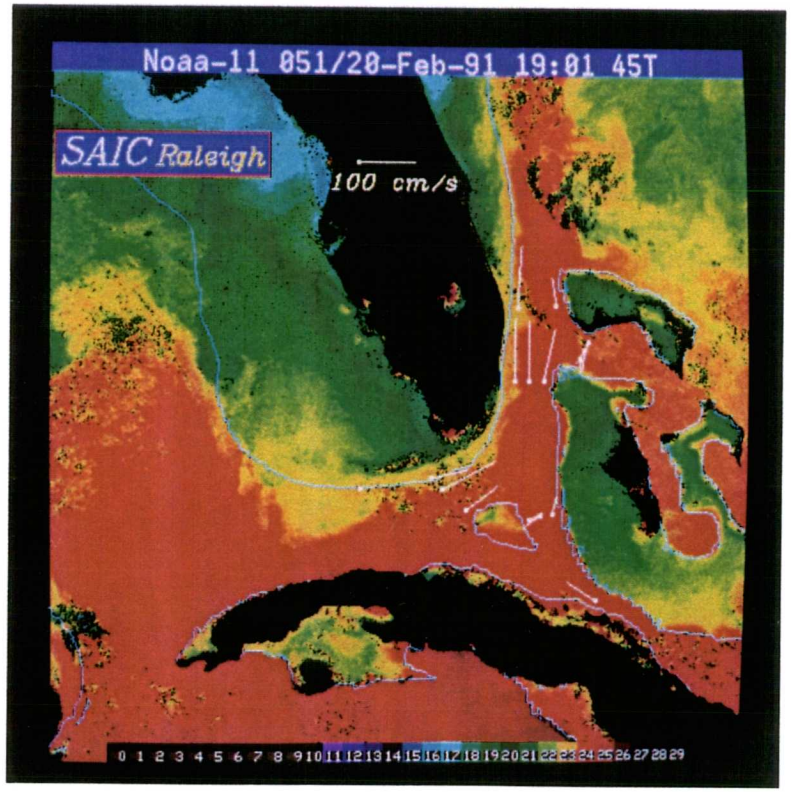

Figure 4.2-6 Composite thermal image for week of Feb. 17-23, 1991. Vectors are as of noon GMT, February 20, 1991. The scale at the bottom of the image shows the relation of color to temperature (°C).

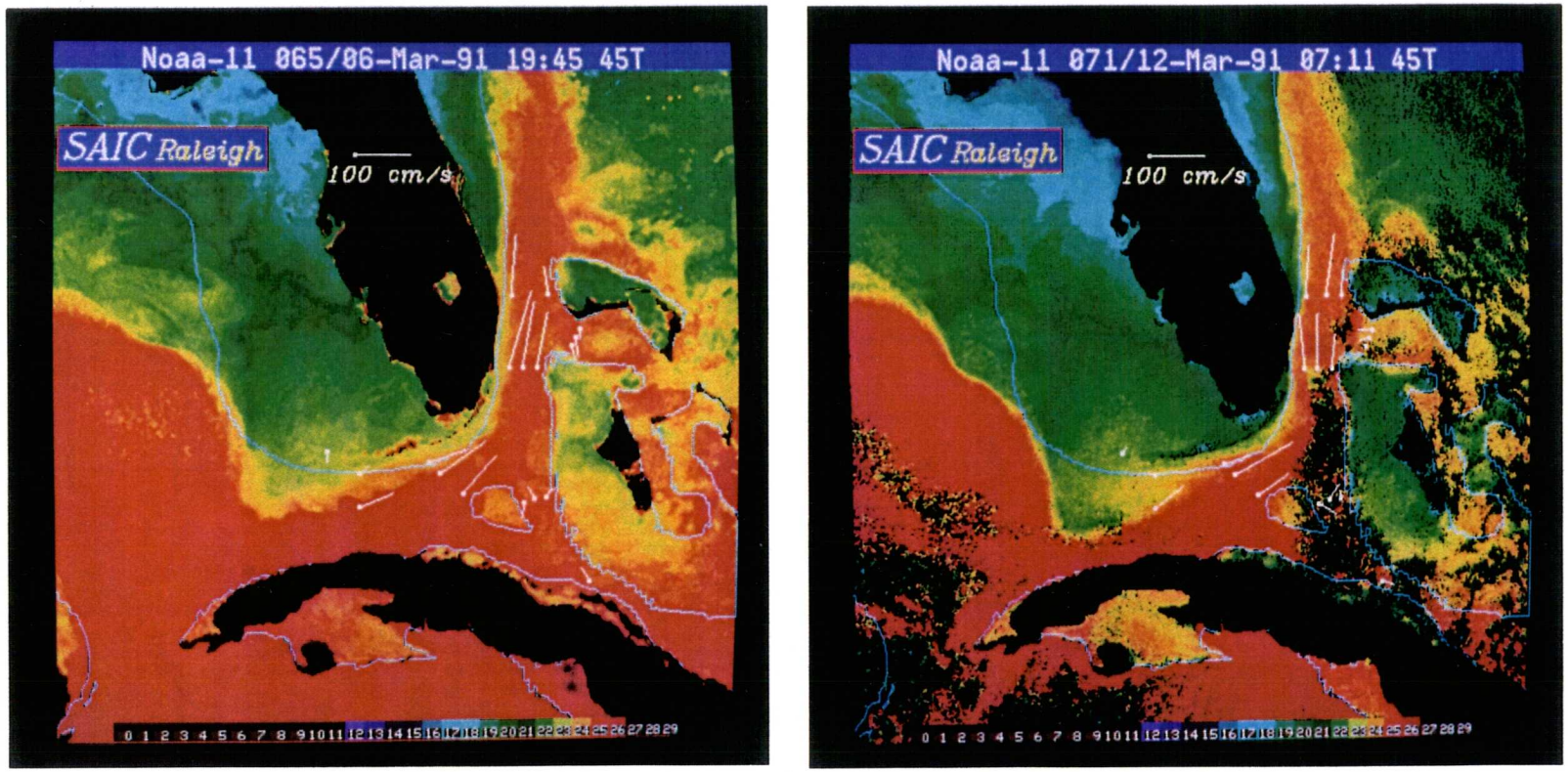

Figure 4.2-7a,b Composite thermal images a) week of March 3-9, 1991, vectors as of noon GMT, March 5, 1991; b) week of March 10-16, 1991, vectors as of noon GMT, March 12, 1991. The scale at the bottom of each image shows the relation of color to temperature (°C).

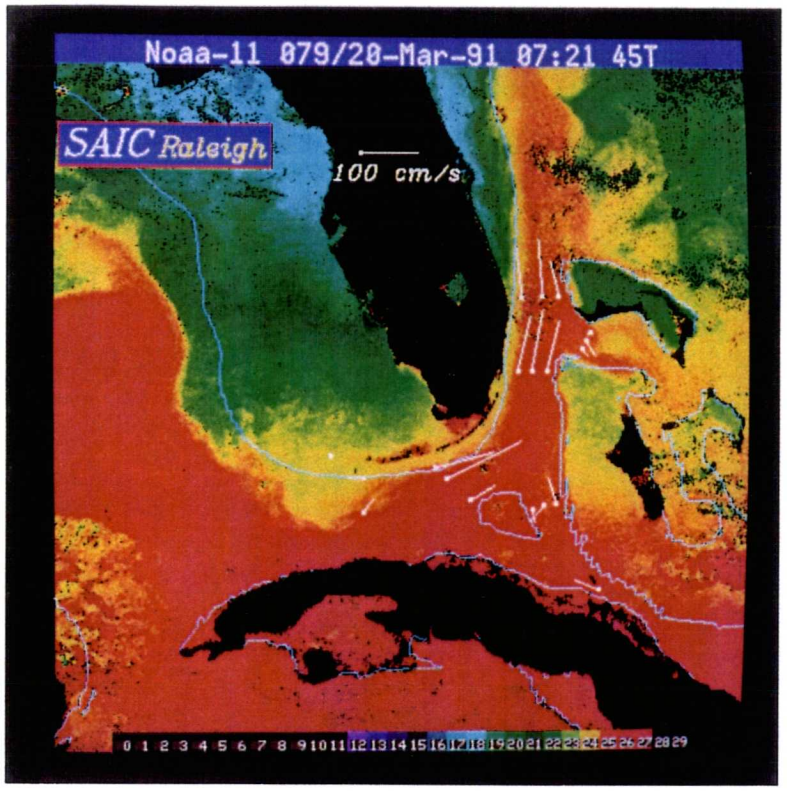

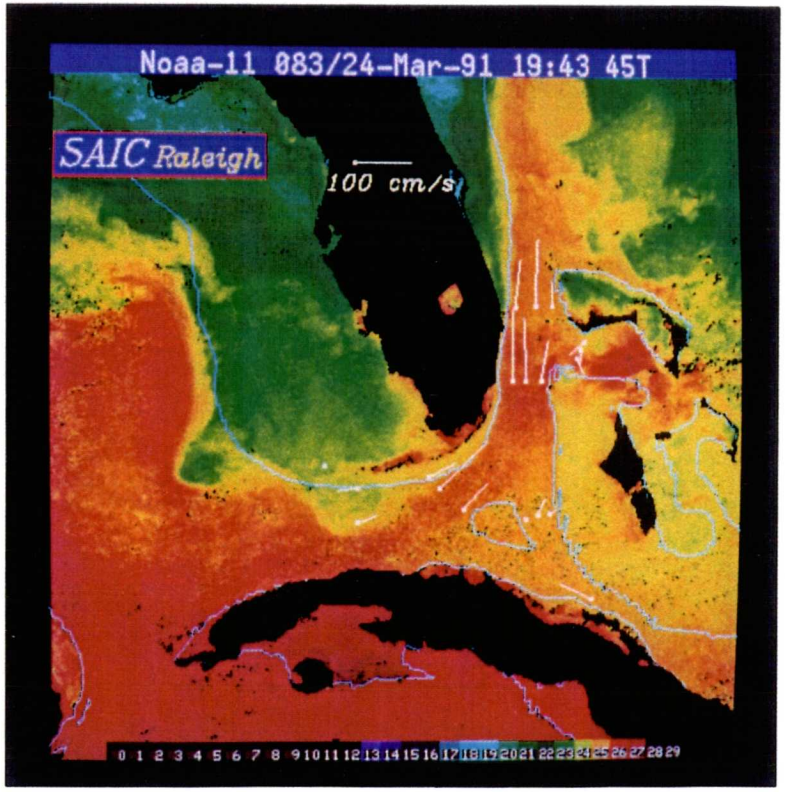

Figure 4.2-7c,d Composite thermal images c) week of March 17-23, 1991, vectors as of noon GMT, March 19, 1991; d) week of March 24-30, 1991, vectors as of noon GMT, March 26, 1991. The scale at the bottom of each image shows the relation of color to temperature (°C).

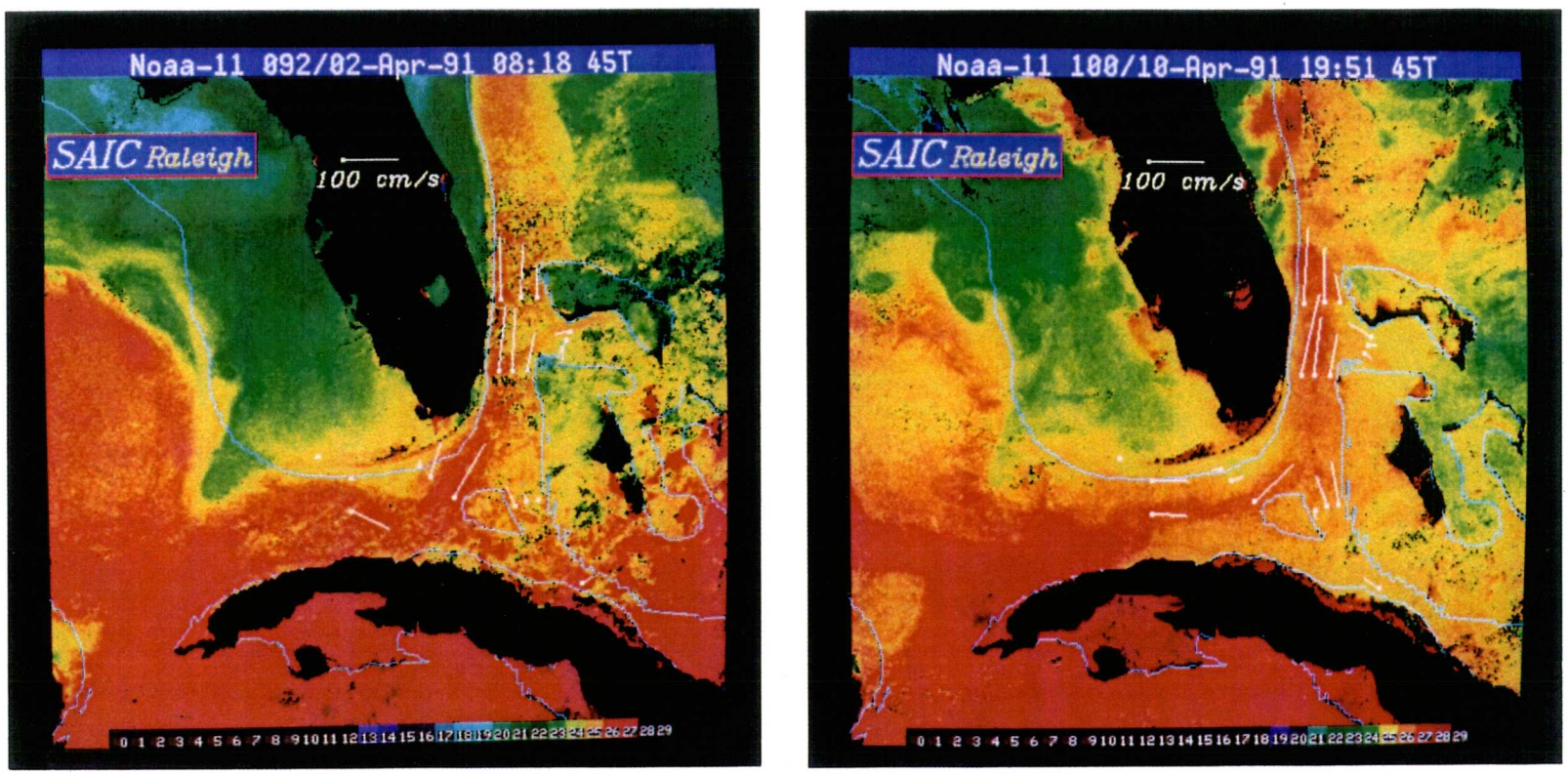

Figure 4.2-7e,f Composite thermal images e) week of March 31-April 6, 1991, vectors as of noon GMT, April 2, 1991; f) week of April 7-13, 1991, vectors as of noon GMT, April 9, 1991. The scale at the bottom of each image shows the relation of color to temperature (°C).

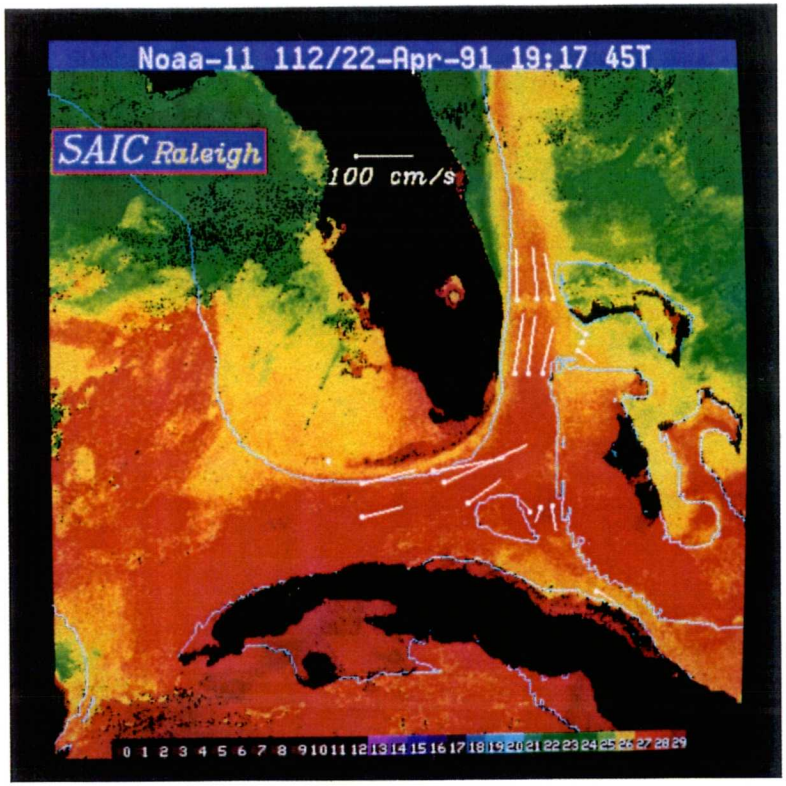

Figure 4.2-7g Composite thermal image for week of April 21-27, 1991. Vectors are as of noon GMT, April 23, 1991. The scale at the bottom of the image shows the relation of color to temperature (°C).

Uplifting of the thermocline from upwelling in the center of the gyre can also be seen in the temperature section made off Marquesas Keys on February 17 and 18, when the gyre was just beginning to influence the flow and water properties at this section (Figure 4.2-8). The gyre appeared to move east of Transect A by about April 10 and was replaced by the following wave crest (onshore meander of the FC front), which resulted in an abrupt current reversal, with strong eastward flow and increasing temperatures at all sites on A (Figures 4.2-1, -2, and -7f). The increasing currents and temperatures occurred first at the offshore locations, resulting in a time lag between sites that gives an average onshore movement of the FC front of about 5 km day^{-1}. The signature of the gyre in satellite-derived surface temperature patterns consists of an offshore, cyclonic curvature of the FC front, with colder/upwelled waters in the gyre center and entrainment of a warm streamer from the leading wave crest (onshore meander of the FC front downstream of the gyre) that is wrapped around the northern or onshore portion of the gyre by the cyclonic flow field (Figures 4.2-7b through 4.2-7d). This signature is similar to that found previously for GS frontal eddies and meanders in the northern Florida Straits (Lee, 1975; Lee and Mayer, 1977) and in the South Atlantic Bight (Lee and Atkinson, 1983) and along the Loop Current front (Paluszkiewiez et al., 1983).

Whereas GS frontal eddies were found to move swiftly downstream at a mean speed of about 35 km day^{-1}, the Tortugas Gyre moved slowly toward the east between Transect A and B at a speed of about 5 km day^{-1} as determined from the moored current and temperature variations at these sections and from the movement of the vortex shown in the satellite imagery. The gyre appeared to influence the flow and temperature fields at Transect B from about April 1 - 18 (Figure 4.2-3, -4, -7e and -7f). As the gyre moved past this section, it caused an offshore shift of the FC axis, in-phase cyclonic current reversals and temperature drops at stations B1, B2 and B3 on the cyclonic side of the current axis (Figures 4.2-3 and -4), and an increase in downstream current speeds coupled to a decrease in temperature on the anticyclonic side of the axis at station B4 (Figure 4.2-4). A current reversal was also observed at the 30m isobath on Transect B that was coherent and in-phase with the reversal observed offshore. This inshore measurement was made as part of a NOAA-supported recruitment project (Williams and Lee, 1992).

The end of the gyre at Transect B was similar to that observed at Transect A and consisted of an onshore shift of the FC as the trailing wave crest approached, which caused a reversal from westward to eastward flow and caused increasing temperature at sites shoreward of the axis. The speed of the onshore movement of the FC front, as determined from the onshore phase lag of either increasing eastward currents or temperature, was also similar to that found for Transect A and for the downstream movement of the gyre, at about 5 km day^{-1}.

This meandering current jet, coupled to an inshore cyclonic gyre, causes an out-of-phase relationship of downstream currents measured with fixed moorings on either side of the jet. The in-phase temperature variations result because the cross channel temperature gradient, which geostropically balances the jet in a thermal wind sense, does not change sign so that an offshore (onshore) shift of the current will cause a decrease (increase) in moored temperature measurements at all points on the section. A similar moored current and temperature response to Gulf Stream meanders was previously observed in the northern SoF (Lee, Schott and Zantopp, 1985; Johns and Schott, 1987) and in the South Atlantic Bight (Lee and Waddell, 1983; Lee, 1975).

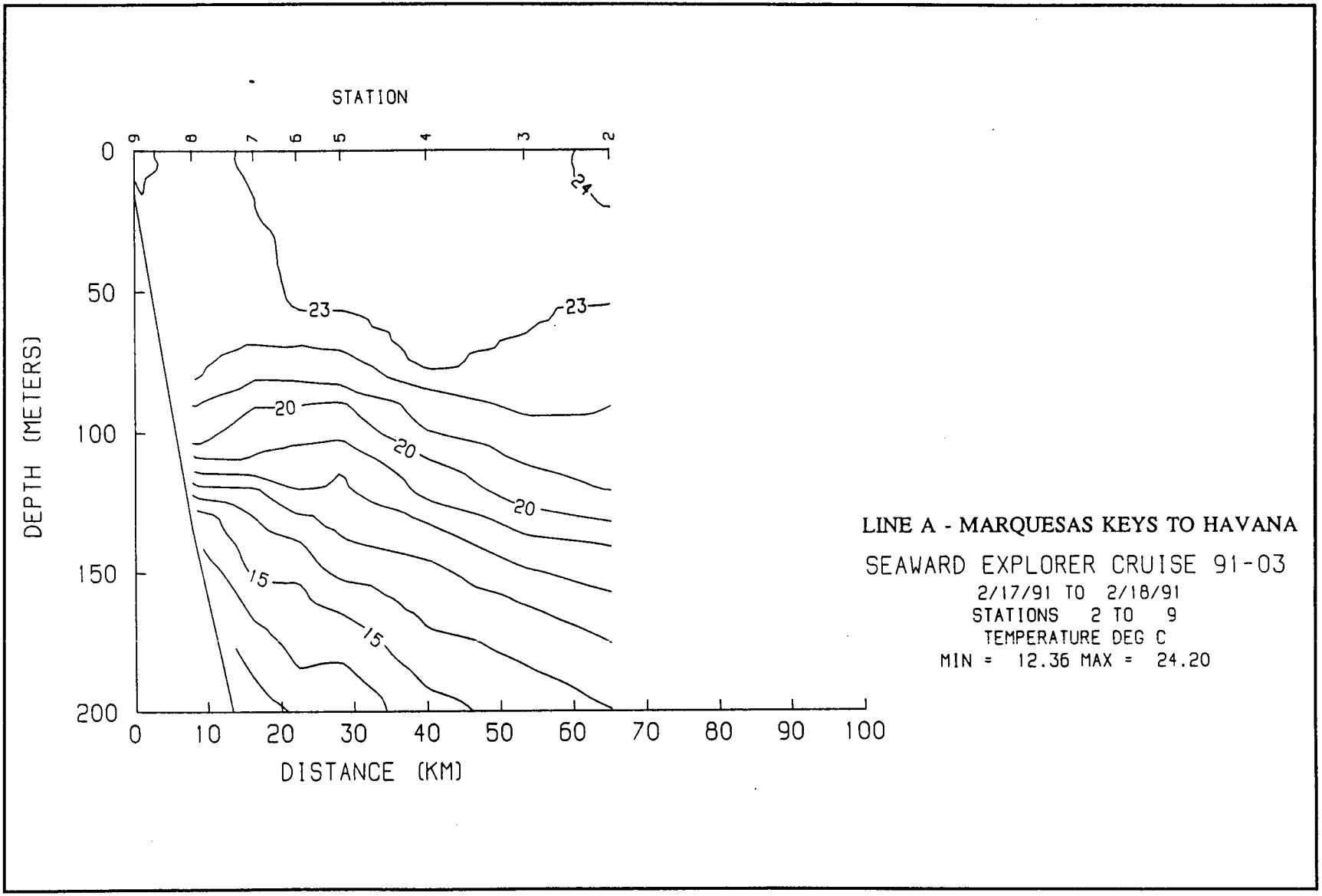

Figure 4.2-8 Cross section of temperatures in the upper 200 m on Line A.

The movement of the gyre through Transect B and the offshore shift of the FC axis appear to have a strong influence on the current and temperature variability in Transect F, which is east of Cay Sal Bank. When the FC shifted offshore at Transect B in early April, there followed, with about a four-day lag, a sudden increase in northward flow and a decrease in temperature on the east side of Transect F (F3) throughout the water column (Figure 4.2-9). Currents on the west side of Transect F (F1) were out-of-phase with the flow on the east, but showed a similar temperature change, indicative of the set-up of a cyclonic eddy within this channel (Figure 4.2-9). Satellite imagery often shows eddy-like thermal patterns suggestive of current reversals across this channel (Figures 4.2-5, -6 and -7).

Currents at the center of Transect F appear to be a mixture of the reversing current patterns on either side (Figure 4.2-9), but the temperature variations are coherent and in-phase across the entire section. The temperature minimum at 300m during this event was about 15°C across Transect F and appears to match the temperature at 300m on the east side of Transect B. This indicates that, as the FC shifted offshore, there was a diversion of part of the flow counterclockwise around Cay Sal Bank and northward through the east side of Transect F. It is not clear if part of the FC flow forced around Cay Sal Bank also entered the OBC, for there was only a single mooring (G1) placed in this channel, and current and temperature variability there appear to be uncorrelated to fluctuations observed at other sites (Figure 4.2-10). Temperatures at 300m at G1 were typically about 2°C or more higher than at the same depth at any other sites. Currents at 250 and 435m showed persistent flow into the Florida Straits throughout the one-year measurement period, with temperature and salinity values indicative of a Subtropical North Atlantic source. Currents at 50m were highly variable, with flows either into or out of the SoF that sometimes persisted for several months at a time.

Low-frequency current and temperature time series for the total one year of measurements at the inshore locations on Transects A and B are shown in Figures 4.2-1 for A1 and 4.2-3 for B1. Two additional gyres off the Tortugas caused cold flow reversals off Marquesas from about May 24 to September 5 and again from September 13 to October 29. These gyres moved downstream at approximately the same speed as before, 5 km day^{-1}, and then caused cold flow reversals on the shoreward side of Transect B from about August 28 to September 17 and October 27 to about November 6. The reversals were coupled to flow increases (decreases) on the eastern (western) side of Transect F and to a temperature drop throughout Transect F, similar to the April event. The duration of the Tortugas gyre as observed at the Marquesas section was 52, 105 and 47 days for the three events, respectively.

An inshore current meter mooring deployed on the 30m isobath offshore of the Dry Tortugas as part of the SEFCAR Project also showed a westward flow event that persisted from about May 8 to August 24 (Williams and Lee, 1992). The SEFCAR Project also conducted several hydrographic surveys in the Tortugas/Marquesas region between May and July that revealed the presence of a cold, cyclonic gyre centered about 40 km off the Dry Tortugas. The dimensions of the gyre remained relatively constant over the one-month interval between surveys at approximately 180 km in alongshore length and 100 km cross-shore, although the eastern portion of the gyre extended further to the east and across the Marquesas section in the July survey. The cyclonic circulation of the gyre produced an upwelling of the

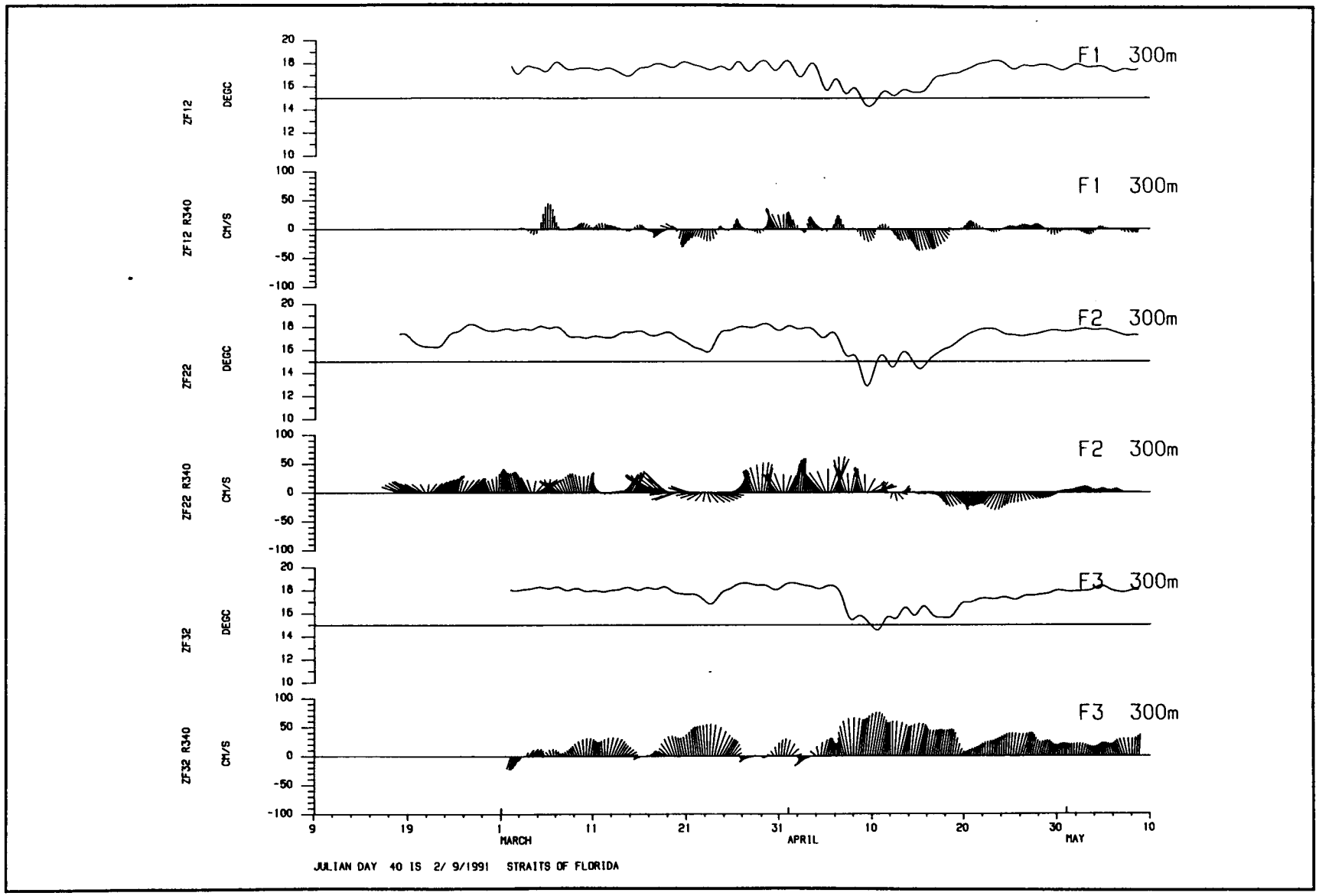

Figure 4.2-9 40-HLP velocity and temperature records for Moorings F1, F2 and F3 at 300 m for the period March-May 1991.

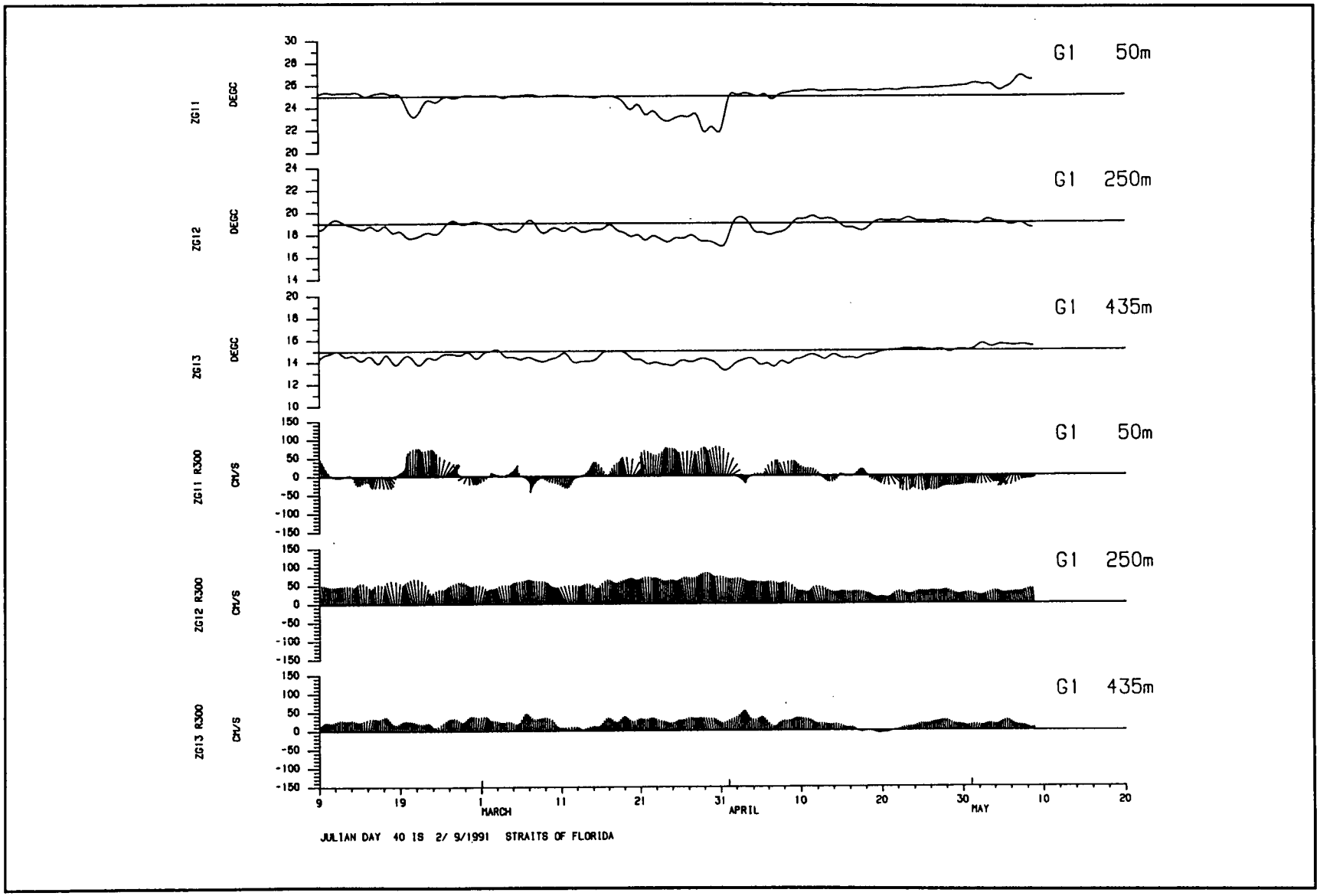

Figure 4.2-10 40-HLP velocity and temperature records for Mooring G1 at 50, 250 and 450 m depths over the period from March-May, 1991.

thermocline of about 25m in the center of the feature. The duration of this event off the Tortugas was 108 days, which matches the duration observed at the Marquesas section. At Transect B (off Looe Reef) the durations of the three gyres were 19, 21 and 11 days, respectively. The shorter durations at Transect B indicate that the gyre is becoming smaller as it approaches the northward turn of the SoF, where the channel width decreases by about a factor of two due to the presence of the Cay Sal Bank. Indeed, satellite thermal imagery shows that for the April event, gyre dimensions decreased from about 90 x 150 km (cross-shore x alongshore distance) off the Tortugas to 70 x 120 km off Marquesas and approximately 60 x 100 km at Transect B (Figures 4.2-7b, 7d and 7e, respectively).

4.2.1.2 Energy Distribution and Coherence Scales

The energy associated with low-frequency current and temperature fluctuations in the southern SoF and OBC is primarily grouped in a 30- to 70-day period band, with the peak energy centered at a period of 60 days (Figures 4.2-11 and 12). Fluctuations in this period band appear to be associated with the observed onshore/offshore meanders of the FC and the formation of the Tortugas gyre. The motions are more energetic in the downstream direction because downstream currents tend to be much stronger than cross-stream. Velocity component and temperature fluctuations were highly coherent in the 30- to 70-day band over the upper 1000m water depths or total water column for shallower sites at all measurement locations. The 30- to 70-day meanders of the FC axis produced large-amplitude fluctuations in downstream currents and temperatures that were coherent across the entire channel at Transect B. Downstream currents tend to be in-phase on the cyclonic shear side of the axis (Figure 4.2-13) and out-of-phase at stations located on different sides of the axis (Figure 4.2-13), as was originally observed in the vector time series (Figures 4.2-3 and 4.2-4). In contrast, temperature, which increases uniformly across the FC, shows a coherent and near in-phase relationship across the entire Straits at these long periods (Figures 4.2-3 and -4).

As a consequence of the offshore meandering at Transect B, where the channel narrows abruptly, some of the offshore portion of the flow is forced around Cay Sal Bank and flows north in SC (Figures 4.2-4 and 4.2-9), resulting in high coherence between downstream currents at the east side of Transects B and F in the 30- to 70-day period band, with fluctuations at Transect B leading by about 10 to 15 days (Figure 4.2-14). At the same time, a countercurrent is set up on the west side of Santeren Channel that results in a coherent, out-of-phase relationship between downstream current at the sides of Transect F (Figure 4.2-14). Downstream current fluctuations in the 30- to 60-day band were also highly coherent in the downstream direction between Transects A and B for stations on the cyclonic shear side of the axis, with current variations at the upstream sites leading in phase by about 100°, or approximately 17 days for an average 60-day period meander. Since the distance between stations A1 and B1 is about 107 km, the average phase speed for the 60-day period meanders is about 6 km day^{-1}. This average phase speed is close to the 5 km day^{-1} previously estimated for individual events. The average wave length determined for the 60-day period meanders with 6 km day^{-1} phase speed is 360 km.

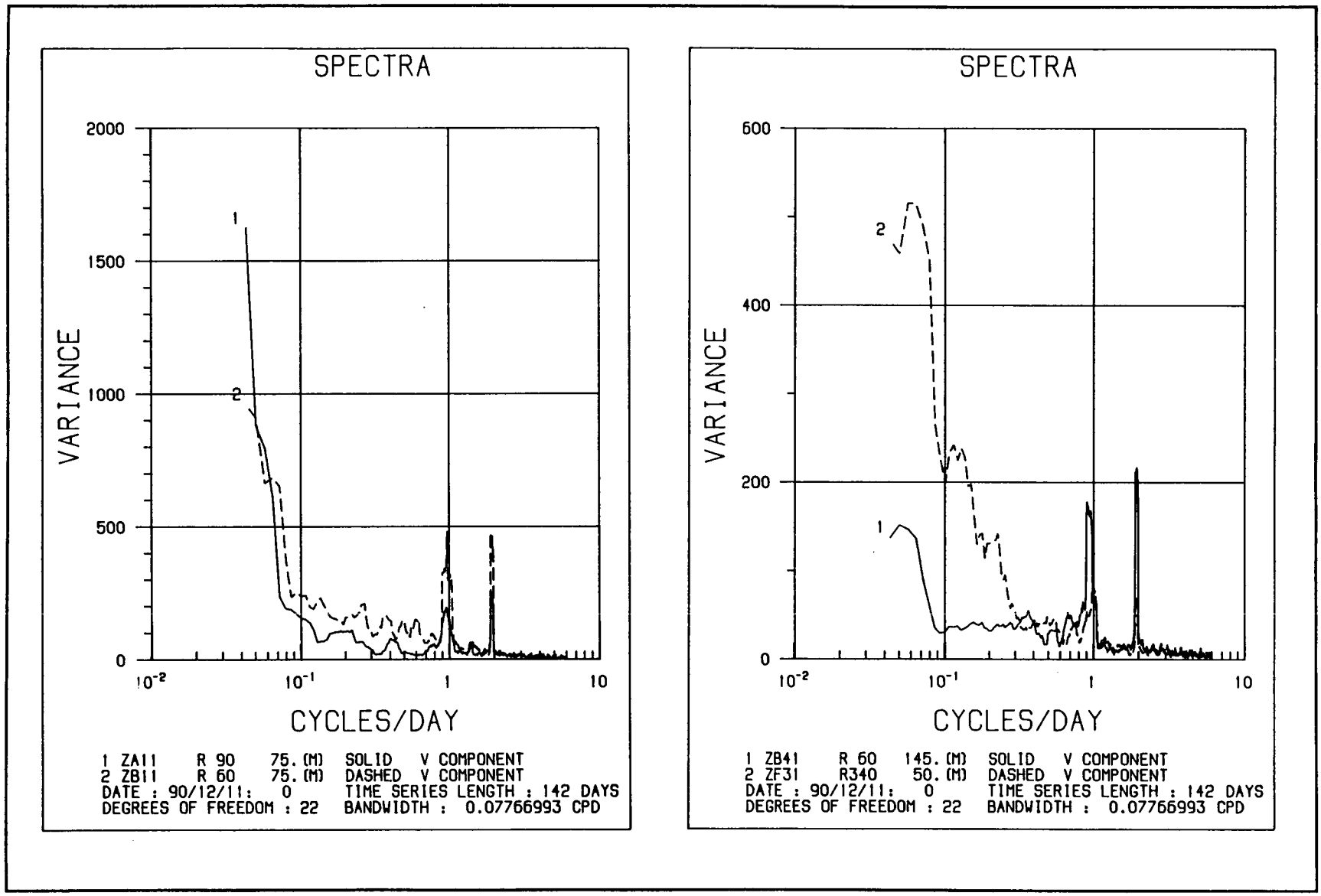

Figure 4.2-11a Spectra of 3-HLP normal velocity components. Records analyzed were made by the uppermost instrument on Moorings A1, B1, B4, and F4 as noted in the figure.

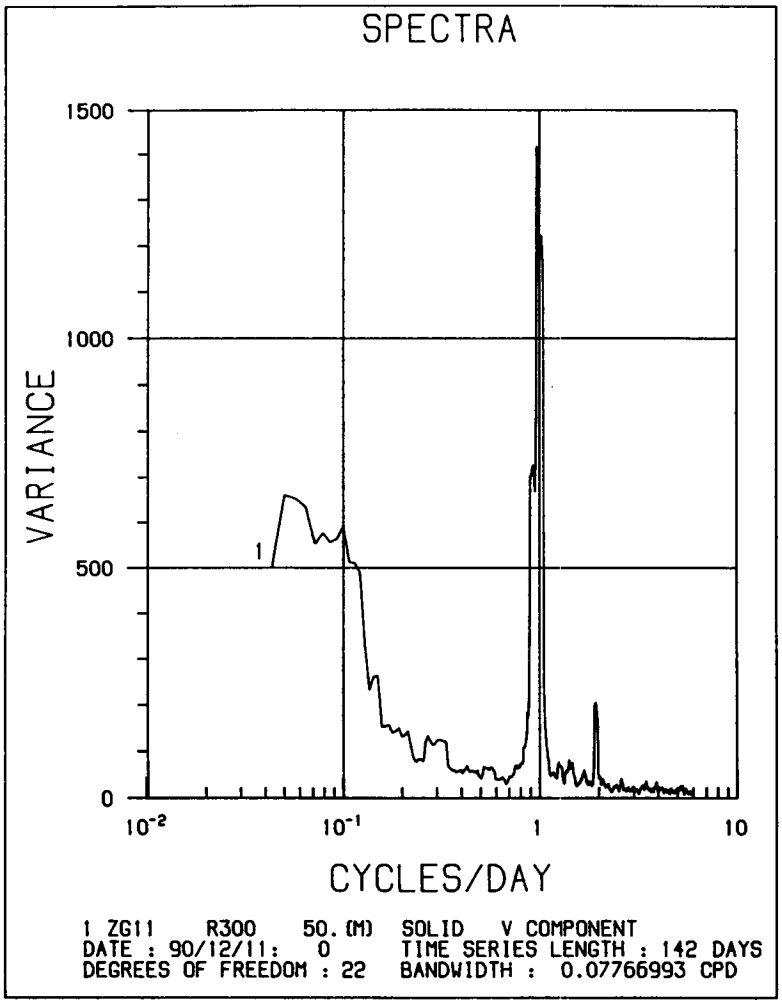

Figure 4.2-11b Spectra for 3-HLP normal velocity components. Record analyzed was made by the uppermost instrument on Mooring G1. The time interval analyzed is the same as in Figure 4.2-11a.

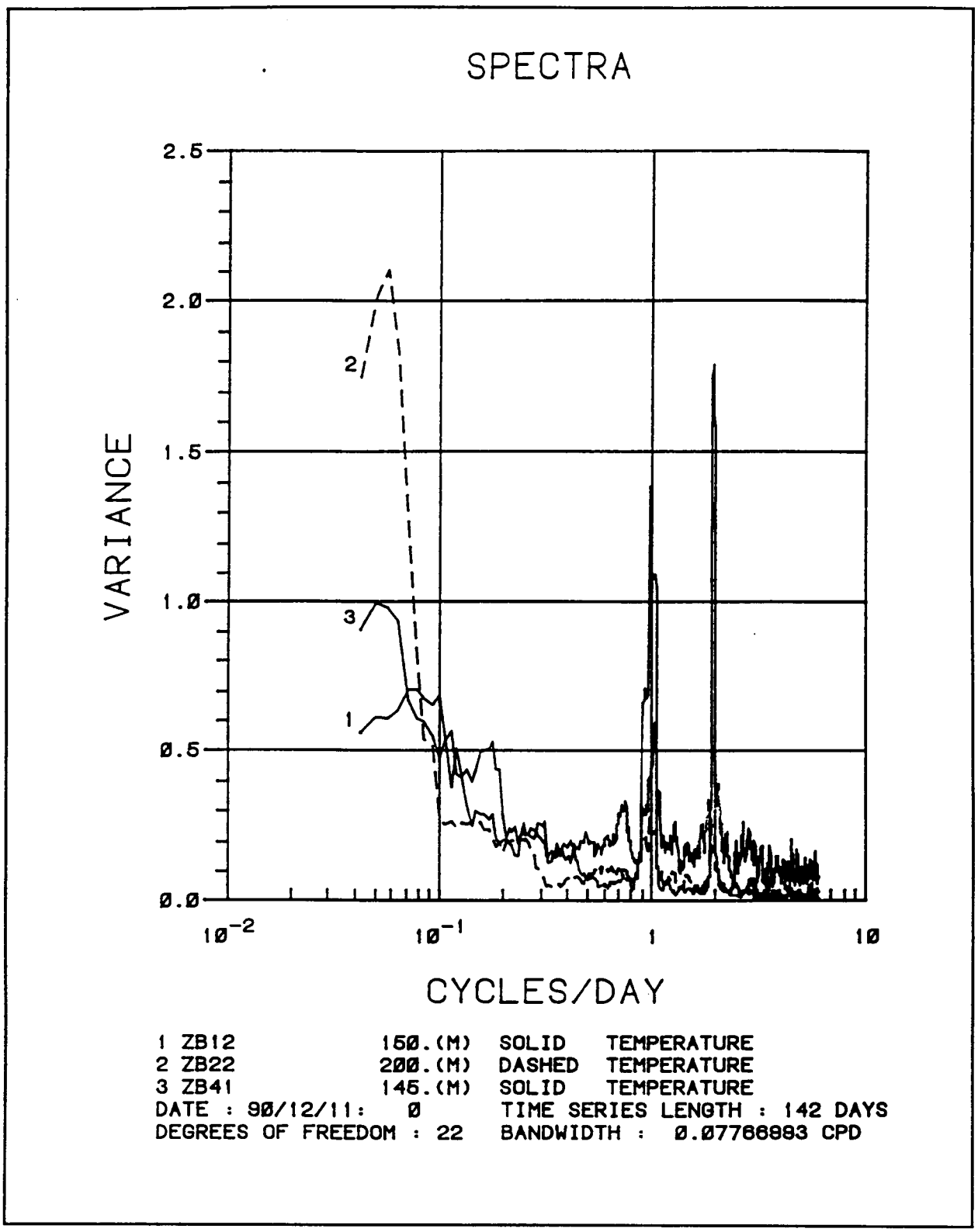

Figure 4.2-12 Spectra for 3-HLP temperature records as measured on Moorings B1, B2 and B3. The time period analyzed is the same as in Figure 4.2-11.

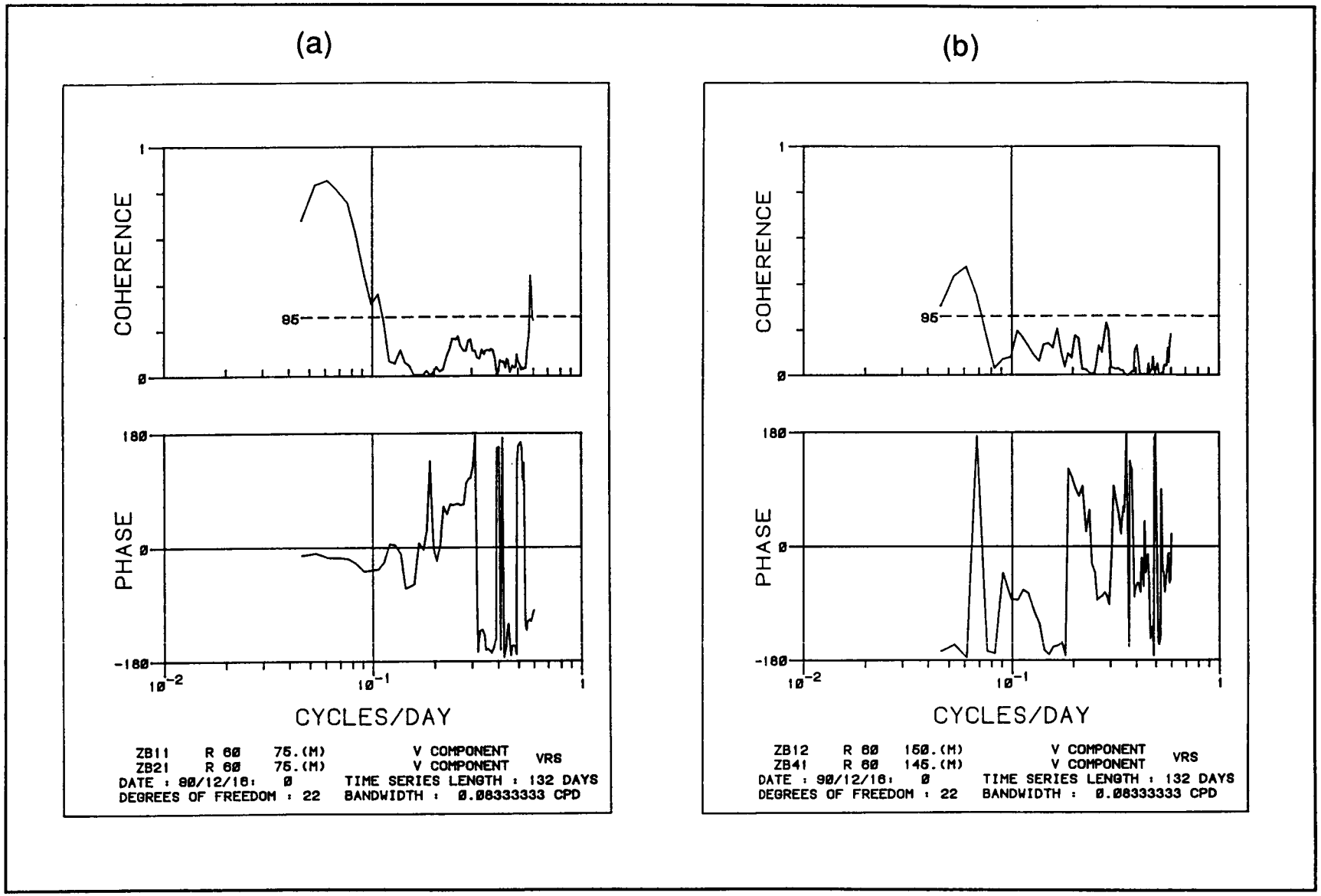

Figure 4.2-13 Phase and coherence plots for a) normal velocity components at the upper instrument (75m) on B1 and B2, and b) the normal velocity components as measured by the instrument on Moorings B1 (150 m) and B4 (145 m).

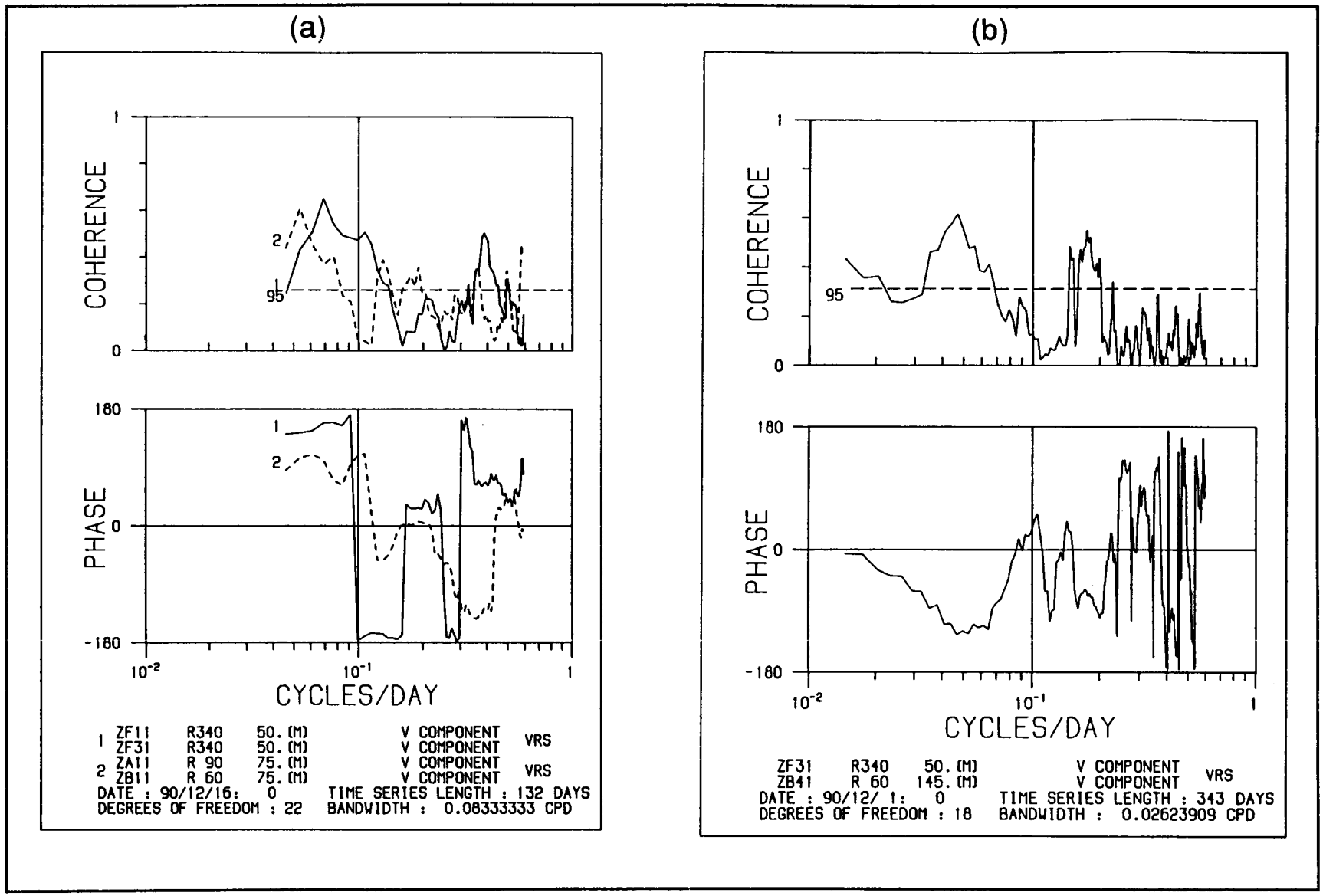

Figure 4.2-14a,b Phase and coherence for a) uppermost instrument on 1) Mooring F1 and F3 and 2) A1 and B1, and b) uppermost instruments on Moorings F1 and B4.

4.2.2 Northern Straits of Florida

4.2.2.1 Spatial and Temporal Variability

The spatial and temporal variability of the FC in the northern Florida Straits is discussed with the aid of moored observations from Transects C and D across the FC at Miami and Palm Beach, respectively, and at Transect E across the western end of the NWPC. Past observations have shown that in the northern Florida Straits, low-frequency current and temperature variability results primarily from a mix of northward propagating wave-like meanders of the axis (Brooks, 1979; Johns and Schott, 1987) coupled to cold, cyclonic frontal eddies along the western boundary (Lee, 1975: Lee and Mayer, 1977; Lee, Yoder and Atkinson, 1991), from evolving baroclinic instabilities of the background flow and density fields (Boudra, Bleck and Schott, 1988), and from a local wind driven response to along-channel wind forcing (Lee and Williams, 1988; Schott, Lee and Zantopp, 1988). Each of these processes can produce energetic current and temperature fluctuations in a period band of several days to several weeks. Fluctuations of this type are clearly evident as the dominant mode of variability in the low-frequency current and temperature records from Transects C and D for the winter deployment period (Figure 4.2-15 and 4.2-16). Currents at all sites were strong toward the north, reflecting the narrow confines of the northern Straits. Current speeds were persistently greater than 100 cm s^{-1} at the upper current meters, with large vertical shear on the mean due to the baroclinic structure of the mean FC. Current reversals are uncommon except near the bottom on the east side of the channel at Transect D.

4.2.2.2 Energy Distribution and Coherence Scales

Energy of the low-frequency current and temperature variations is concentrated in a 6- to 20-day period band at all sites and at the longer 50- to 60-day periods (Figure 4.2-17). Fluctuations with these periods are highly coherent over the vertical instrument separations and between adjacent stations on a transect (Figure 4.2-18). The out-of-phase meandering mode for downstream currents measured on either side of the current axis is also quite obvious (Figure 4.2-19). There was significant along-channel coherence between Transects C and D for downstream current fluctuations in a broad band of about 8- to 60-day periods with the upstream locations leading in phase (Figure 4.2-19). However, between Transects B and C the only significant coherence in downstream currents was near the center of the channel in a 9- to 20-day period band. For the longer 60-day meander period there was high coherence between downstream currents on the eastern side of SC and the eastern side of Transect C for the total year-long records with the southern section leading (Figure 4.2-19).

4.2.2.3 Northwest Providence Channel

Low-frequency current and temperature records from the Northwest Providence Channel show a persistent pattern of inflow to the Florida Straits on the northern side of the channel at all depths and outflow from the Straits on the southern side, again at all depths (Figure 4.2-20). Satellite-derived surface temperature patterns clearly show that this counterflow is associated with a cold, cyclonic gyre that conforms to the shape of the NWPC (Figures 4.2-5, -6 and 7a through 7g). This gyre pattern is particularly clear in the week of March 3 to 9 (Figure 4.2-7a) and is also indicated in across channel temperature sections as a cold uplifting in the center of the channel supporting the cyclonic

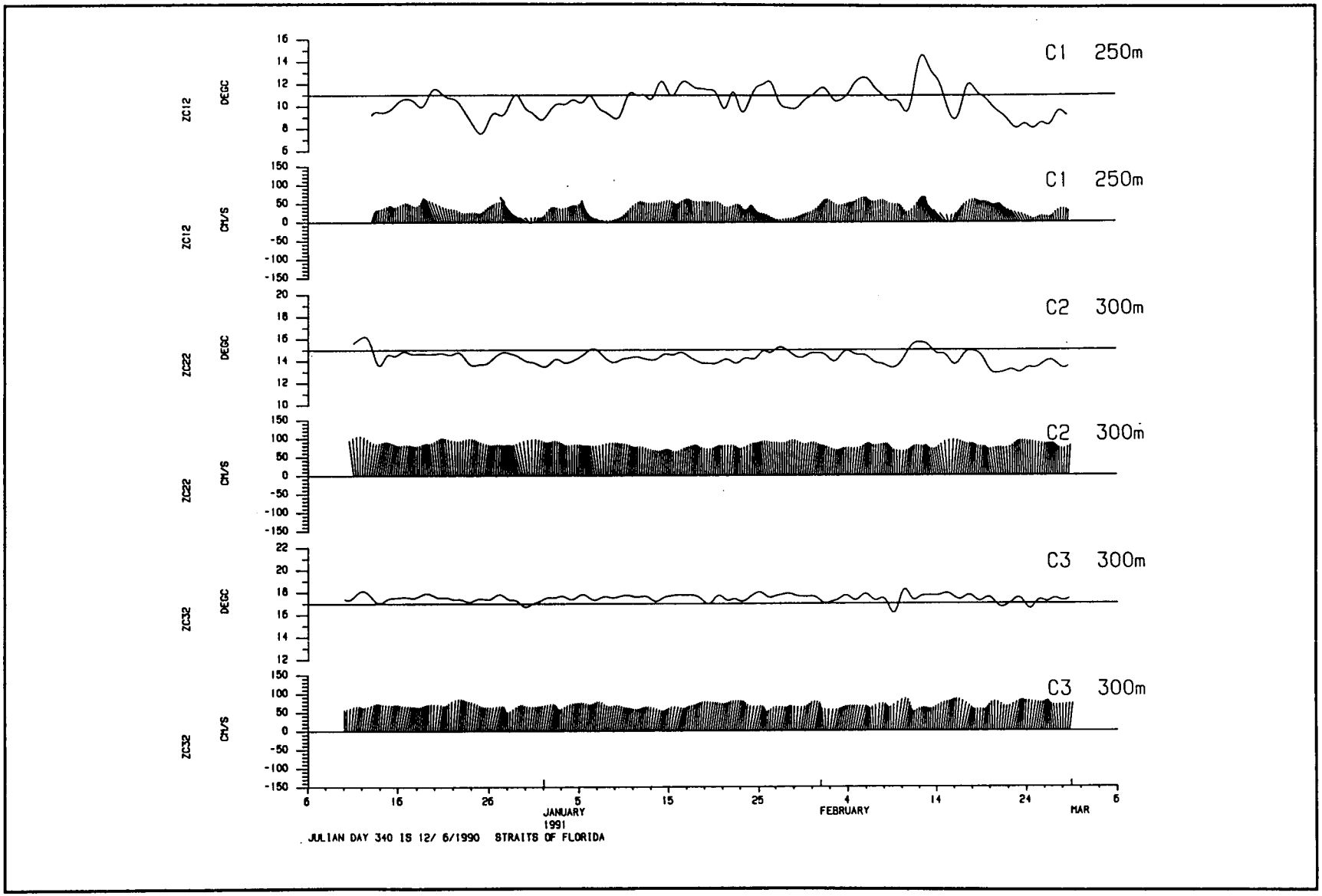

Figure 4.2-15 40-HLP filtered temperature and velocity records for the upper instruments on Moorings C1, C2 and C3 for the period from December 1990 - March 1991.

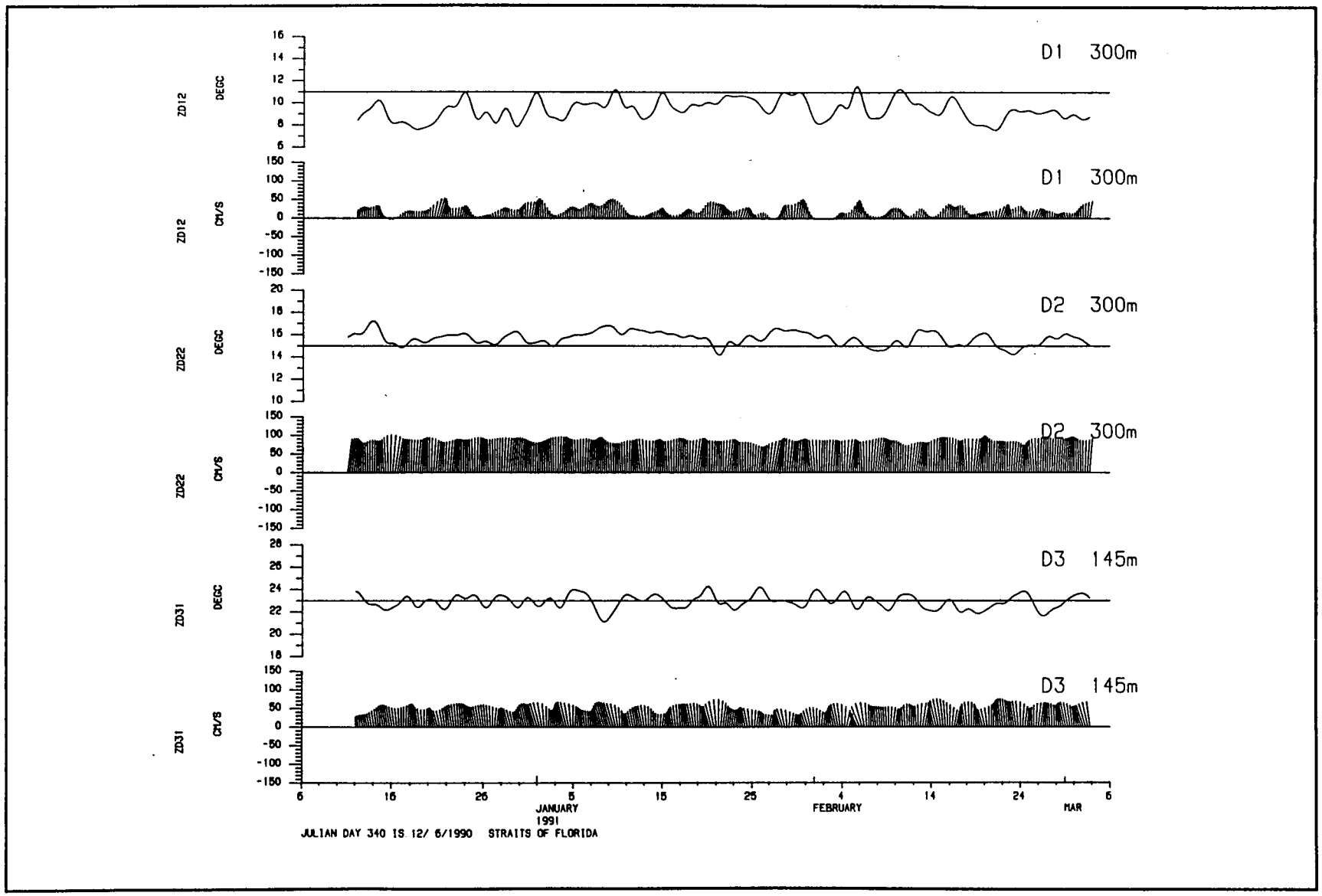

Figure 4.2-16 40-HLP filtered temperature and velocity records for the upper instruments on Moorings D1, D2 and D3 for the period from December 1990 - March 1991.

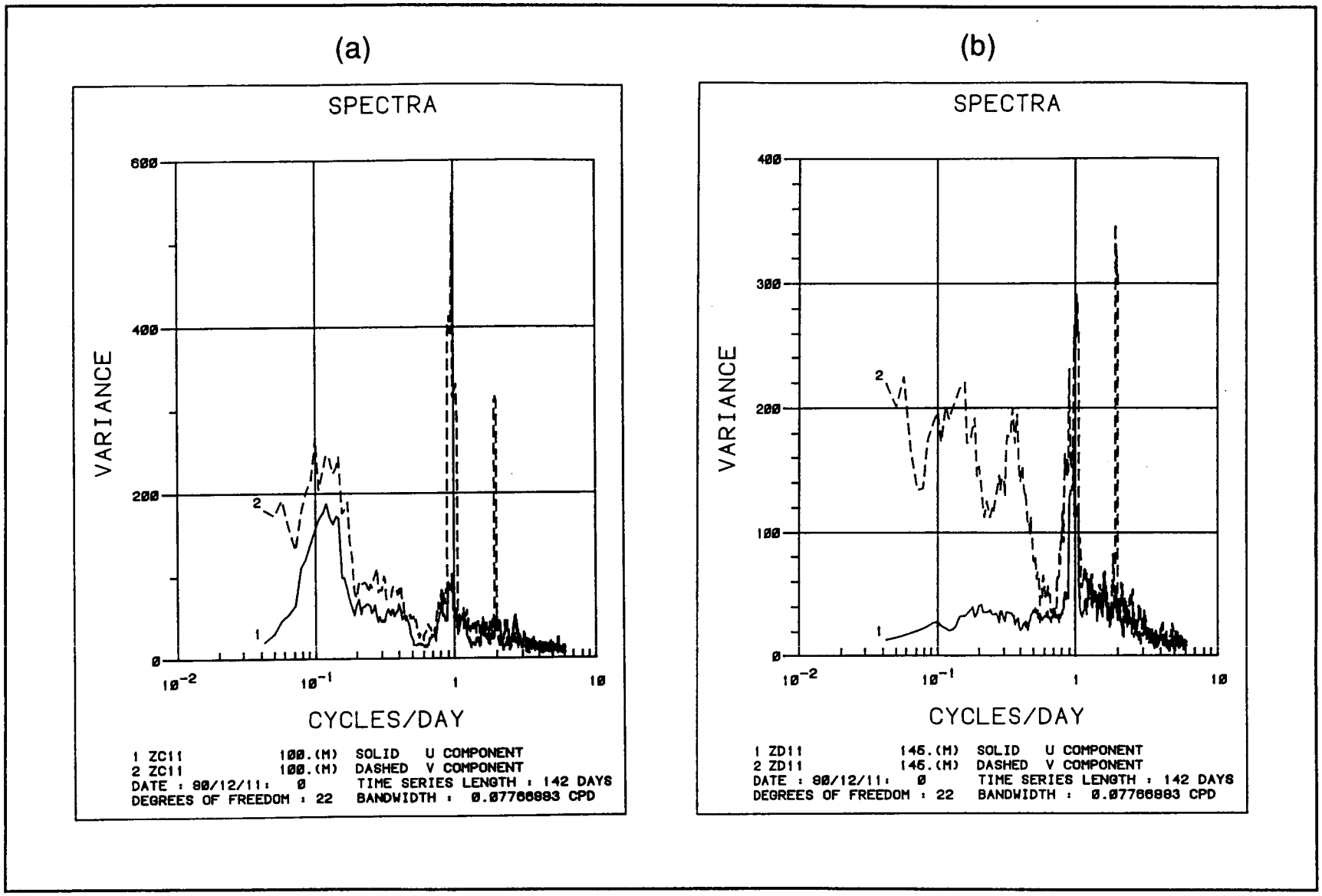

Figure 4.2-17 Spectra of 3-HLP velocity components for instruments at a) 100 m on Mooring C1 and b) 145 m on Mooring D1.

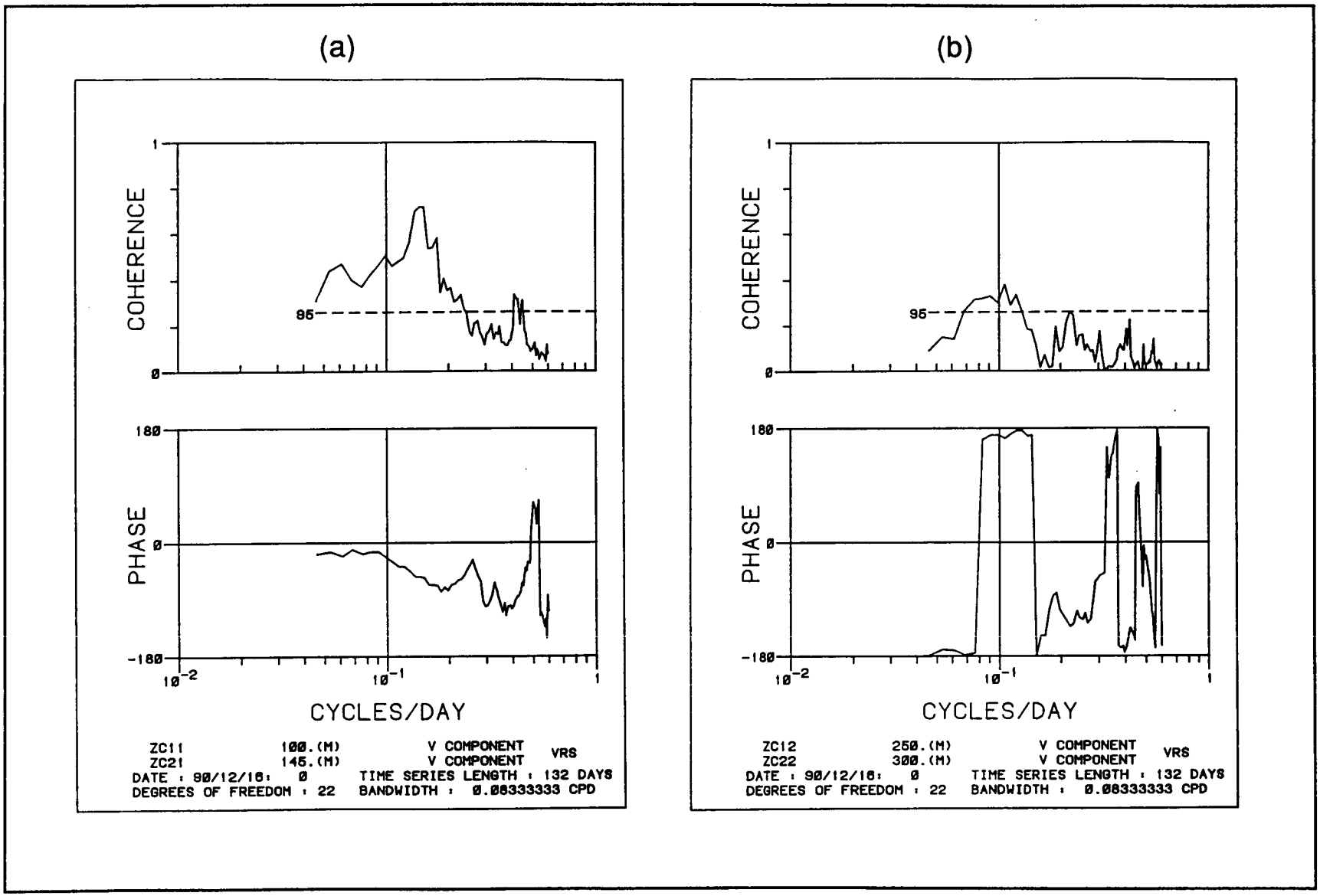

Figure 4.2-18 Phase and coherence for 40-HLP filtered normal (v) components of velocity between a) the upper instruments on Moorings C1 and C2, and b) the instruments at 250 m and 300 m on Moorings C1 and C2, respectively.

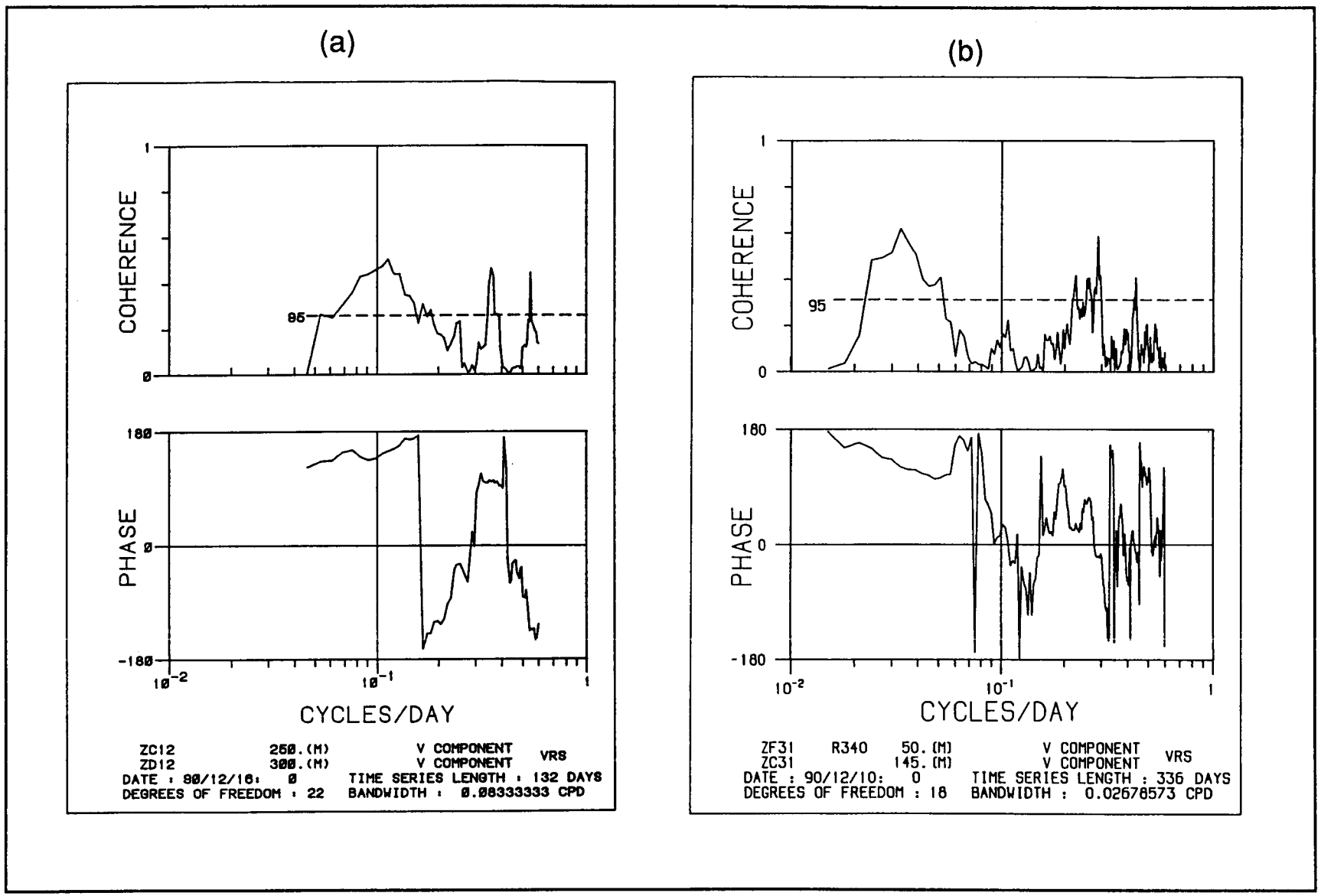

Figure 4.2-19 Phase and coherence for 40-HLP filtered transect normal (v) velocity components between a) instruments on C1 at 250 m and D1 at 300 m, and b) instruments on F3 at 50 m and C3 at 145 m.

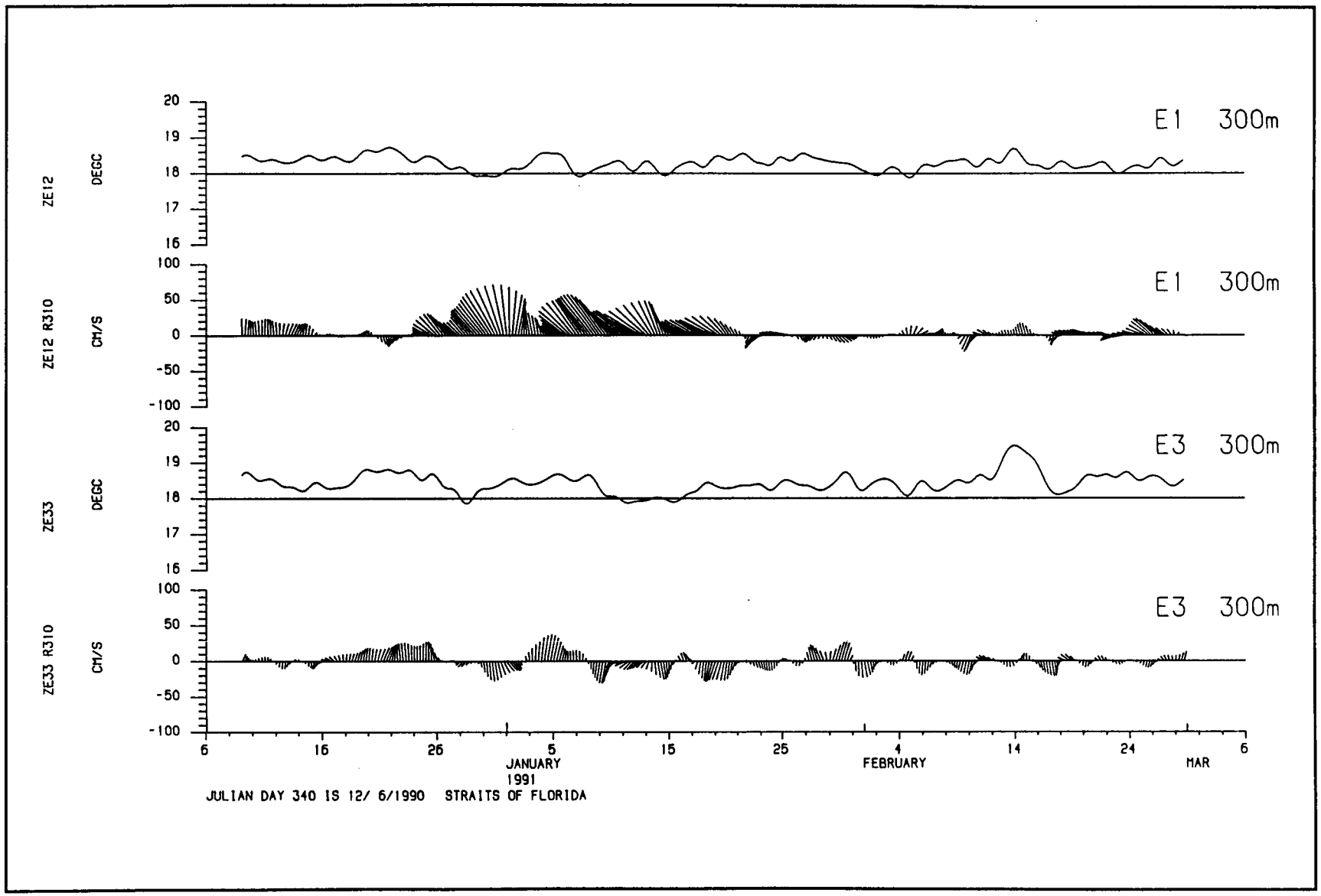

Figure 4.2-20 40-HLP temperature and velocity records from Mooring E1 (300 m) and E3 (300 m) for the period from January to March 1991.

circulation. The gyre may serve to exchange some waters between the FC and the Atlantic east of the Bahamas, with inflow to the FC on the north side of the NWPC and outflow on the southern side. Downstream currents from stations on either side of the NWPC are highly coherent at periods of 7- to 30-days and near 60 days with variations at the southern side leading in phase for 7- to 10- day motions and a near out-of-phase relationship for the longer period motions (Figure 4.2-21). There was also significant coherence between downstream currents on the east side of Transect C with the flow events on the south side of Transect E, and between currents on the north side of Transect E with the east side of Transect D for periods of about 9 days.

4.3 First Order Statistics of Moored Current and Temperature Fields

4.3.1 Mean Properties

The spatial distributions of mean current vectors for depths of 145, 300 and 600m averaged over the total record lengths are shown in Figure 4.3-1 through 4.3-3. Most of the means were computed over record lengths of about one year and are reasonably stable. This is particularly true for flows in the northern Straits, where the most energetic motions occurred on time scales less than several weeks so that even a six month average should be stable. However, in the southern Straits the dominant time scale is on the order of two months, so averages of records over less than one year are probably not reliable.

The spatial pattern of mean current vectors shows the effect of the mean downstream FC baroclinic jet flowing through the deeper parts of the sections. In the mean the axis of the jet appears to be further offshore in the southern Straits due to the overshooting of the Loop Current as it turns eastward and enters the southern Straits and the set-up of the Tortugas gyre. This results in weak eastward mean currents over the slope off Marquesas Keys and a mean current reversal in the lower layer over the slope that is supported by uplifting of mean isotherms (Figure 4.3-4). The mean axis of the current appears to be south of A3 and probably closer to Cuba than to the Keys. On Transect B the mean axis appears to be located near the center of the channel (Figure 4.3-5). In Transects C (Figure 4.3-6) and D (Figure 4.3-7) the mean axis is shown near the center of the channel, but this position is not well resolved with three current meter moorings. High vertical and horizontal resolution from PEGASUS current profiling shows the mean axis to be shifted toward the west in those sections with maximum currents of about 180 cm s^{-1} at the surface (Leaman, Molinari and Vertes, 1987).

Mean flow fields in the NWPC show the influence of a mean clockwise rotating eddy with net inflow to the FC on the northern side of the channel and net outflow on the southern side (Figures 4.3-1 through -3). The mean inflow appears to be strongest at the 300m level on the northern side of the channel (Figure 4.3-8) and will likely contribute to a net transport addition to the FC. A mean clockwise gyre is also evident in the average currents and temperature from the SC, with inflow to the FC on the eastern side of the channel and outflow on the western side (Figures 4.3-1 through -3 and 4.3-9). The inflow also appears to be stronger at the 300m level on the eastern side of the channel, similar to that for the NWPC, and may also account for a mean addition to the FC transport through this channel. The source of this inflow at 300m may be through the OBC, where a maximum mean flow of about 50 cm s^{-1} into the SoF occurred near the 300m level (Figures 4.3-1 and -2).

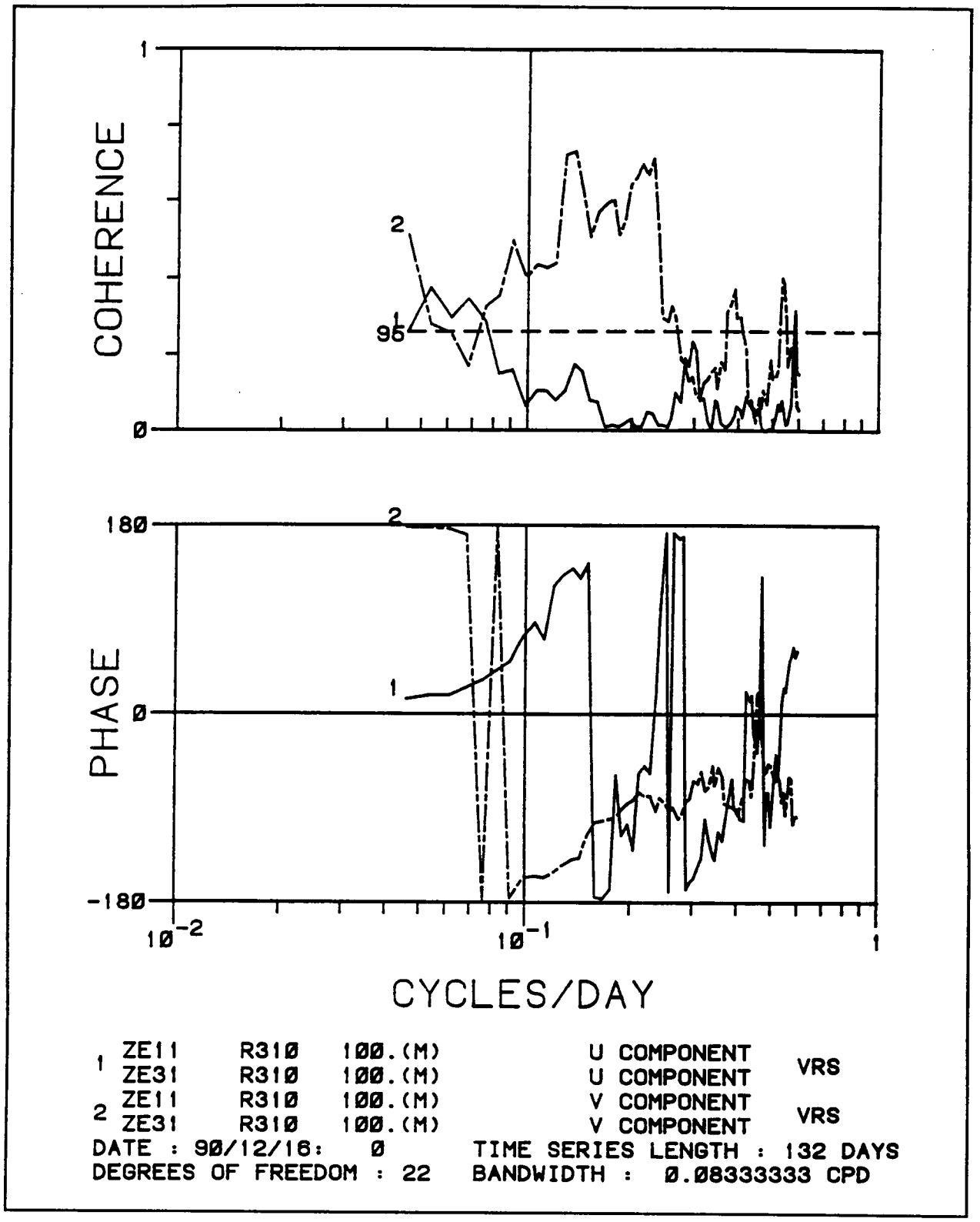

Figure 4.2-21 Phase and coherence between like components at 100 m on Moorings E1 and E3.

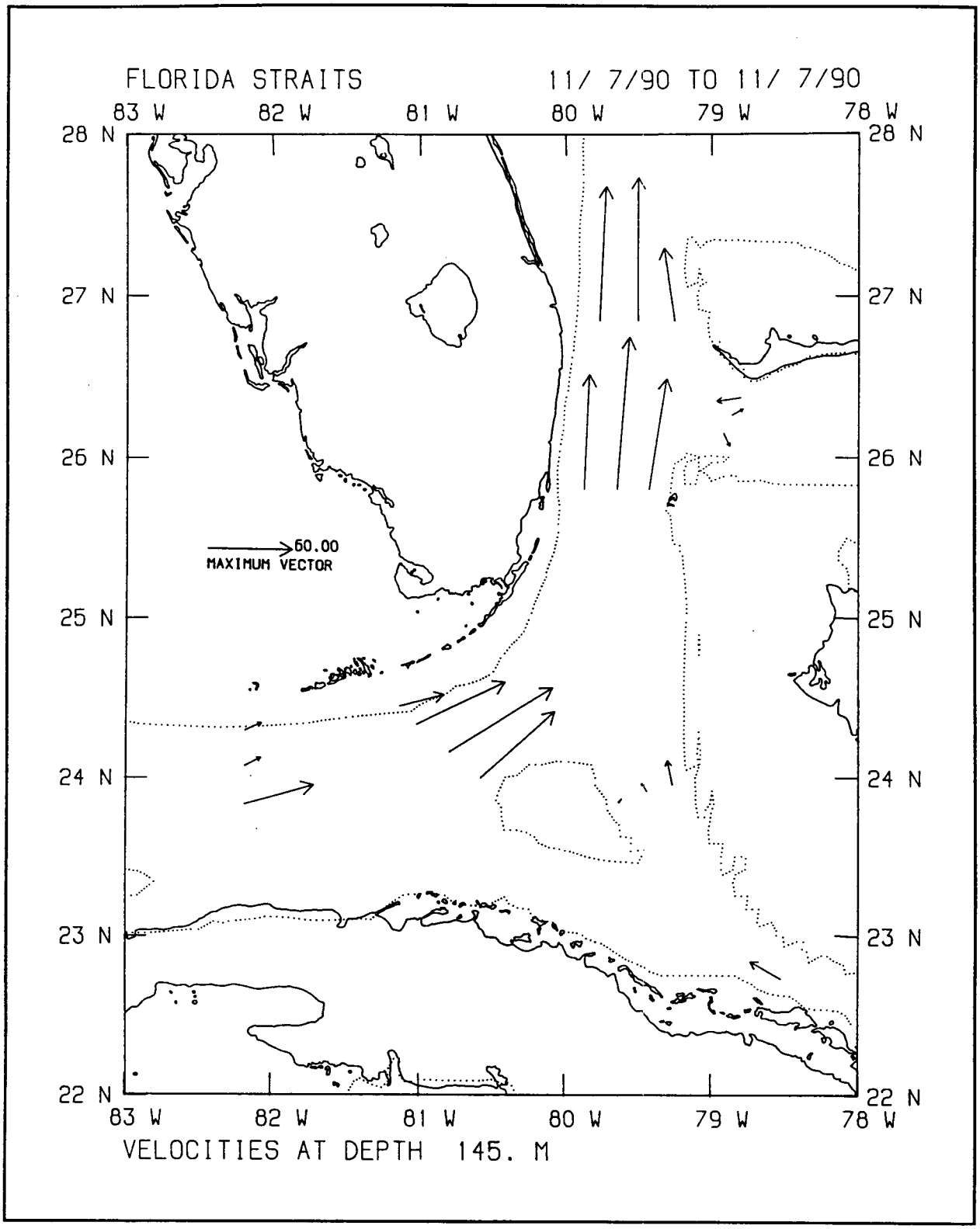

Figure 4.3-1 Plot of the mean vector for current velocities measured at the upper instrument on each mooring. The notation for 145 m is provided since that is the upper instrument depth for many of the moorings. Note the scale vector drawn on the west Florida shelf.

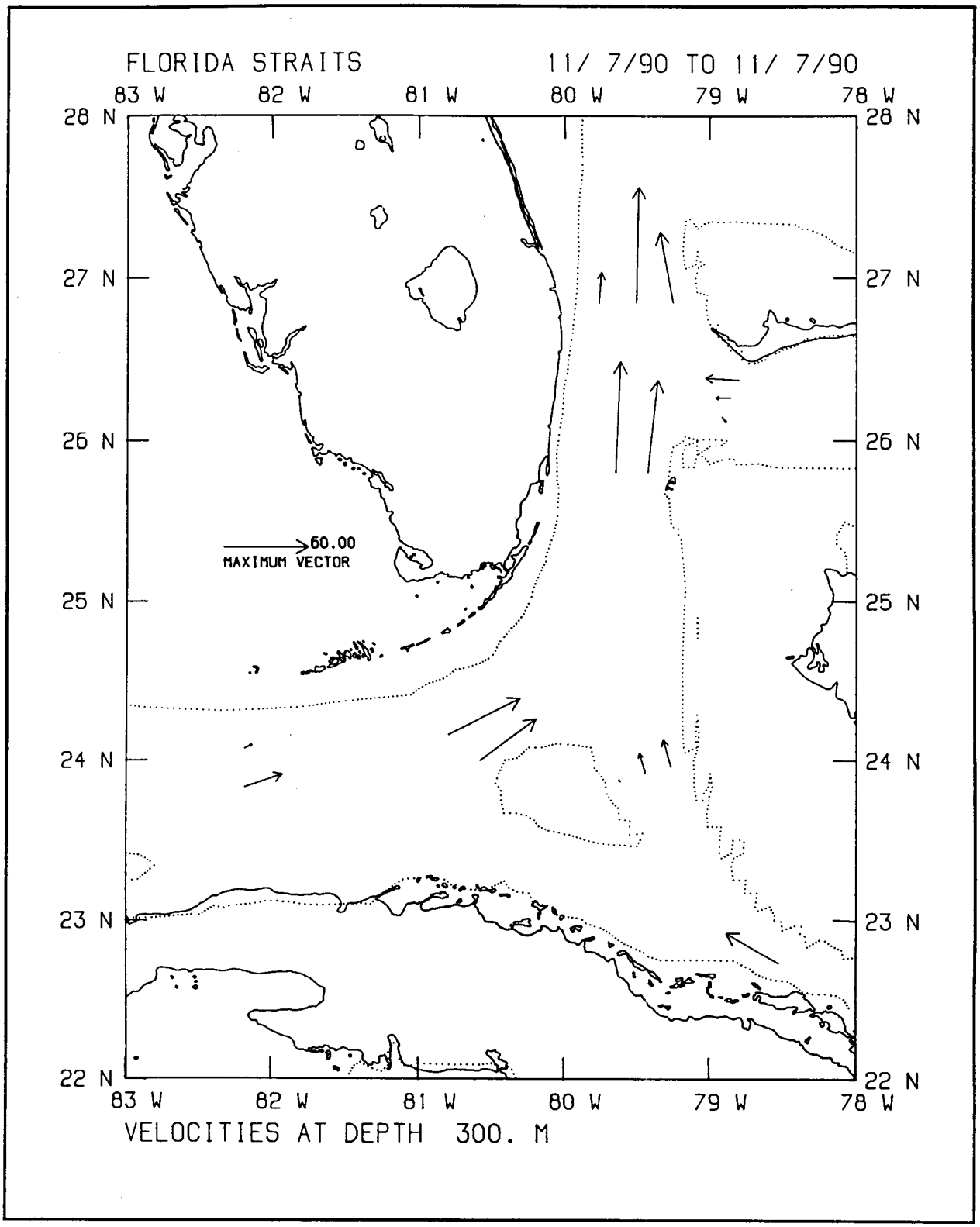

Figure 4.3-2 Plot of the mean vector for current velocities measured at approximately 300 m. below the surface. Note the scale vector drawn on the west Florida shelf.

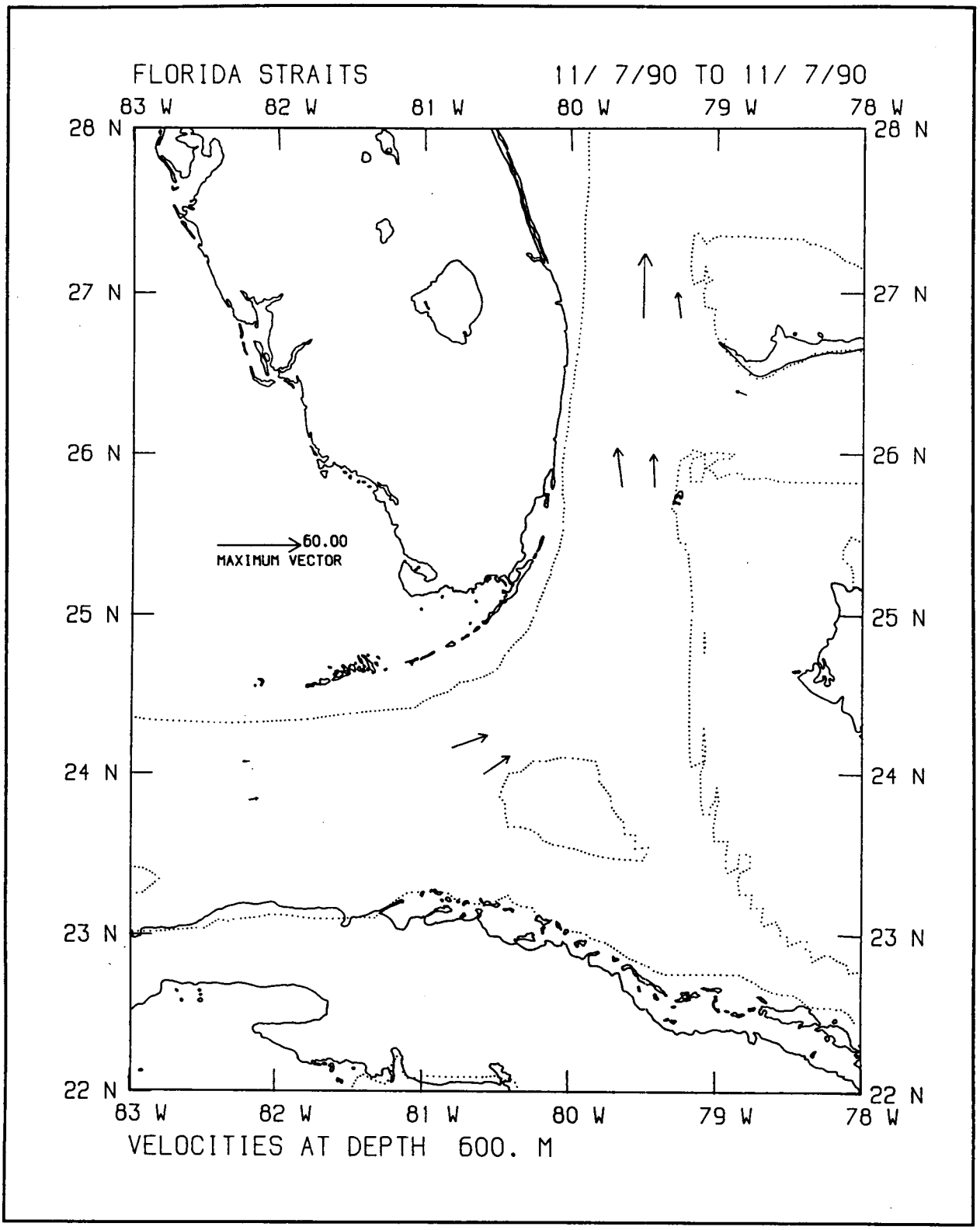

Figure 4.3-3 Plot of the mean vector for current velocities measured at approximately 600 m. below the surface. For those moorings having no instrument that deep, no vector is drawn. Note the scale vector drawn on the west Florida shelf.

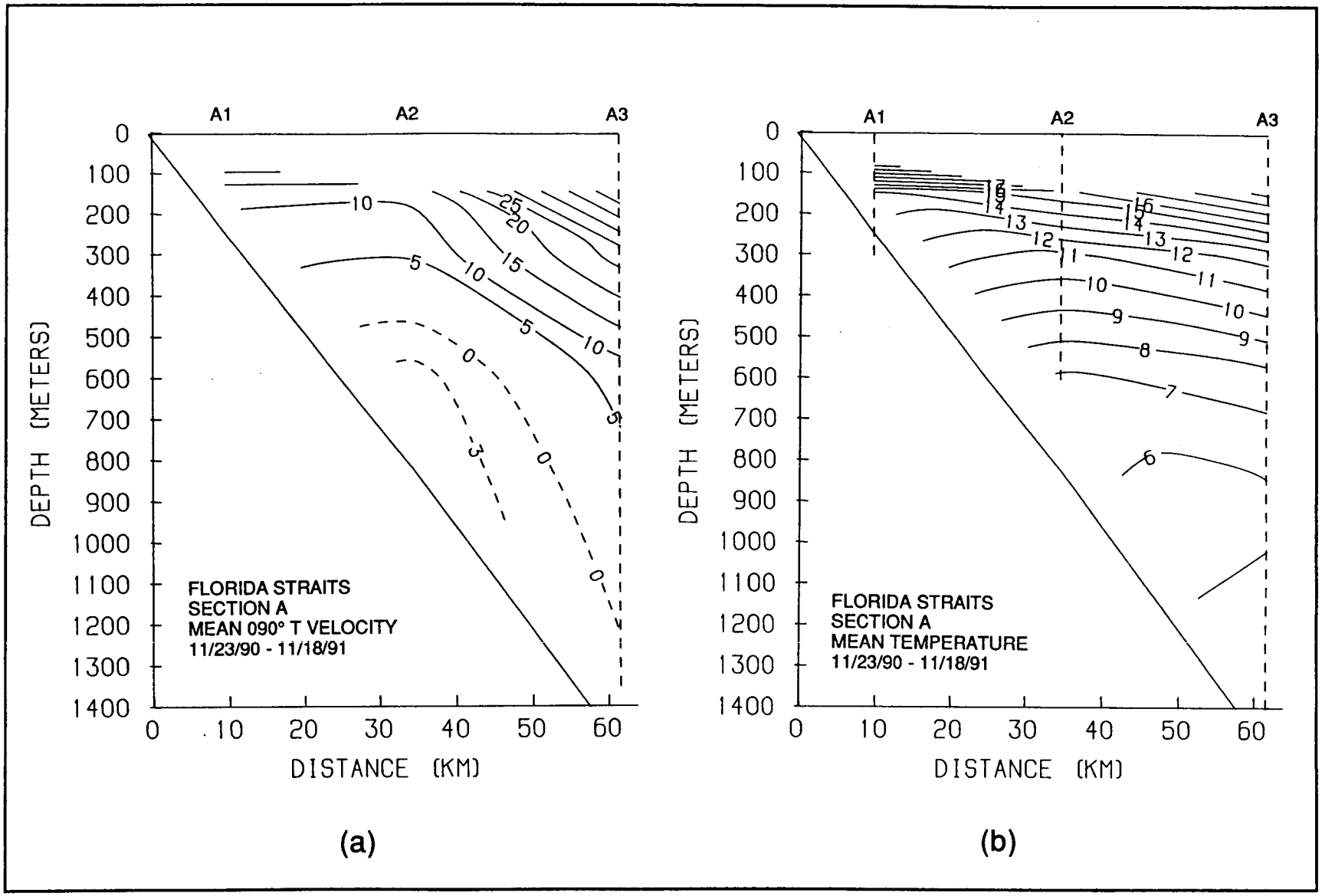

Figure 4.3-4 Contours of means for a) transect-normal velocity and b) temperature. Mean values were computed using the complete available time series on Transect A.

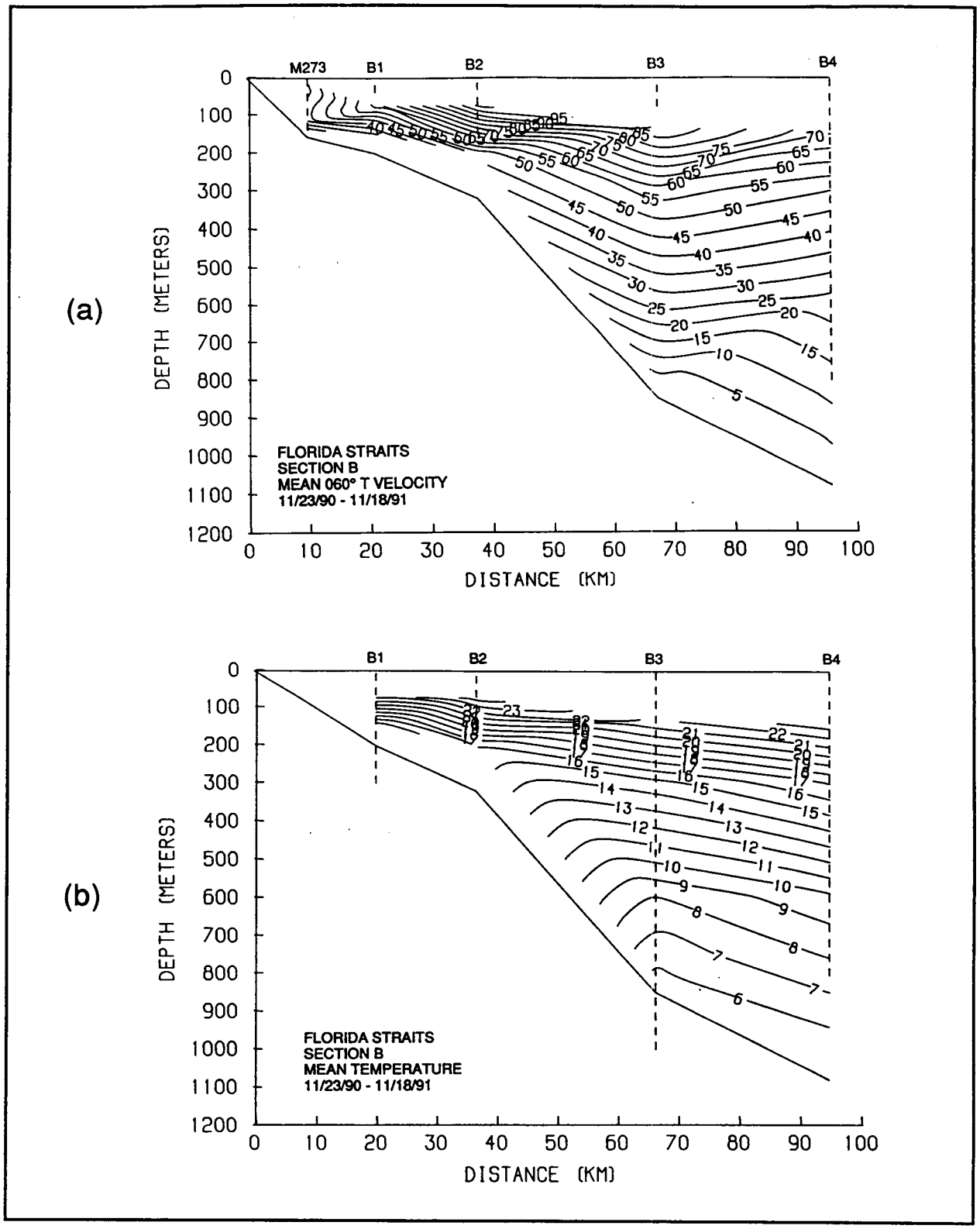

Figure 4.3-5 Contours of means for a) transect-normal velocity and b) temperature. Mean values were computed using the complete available time series on Transect B.

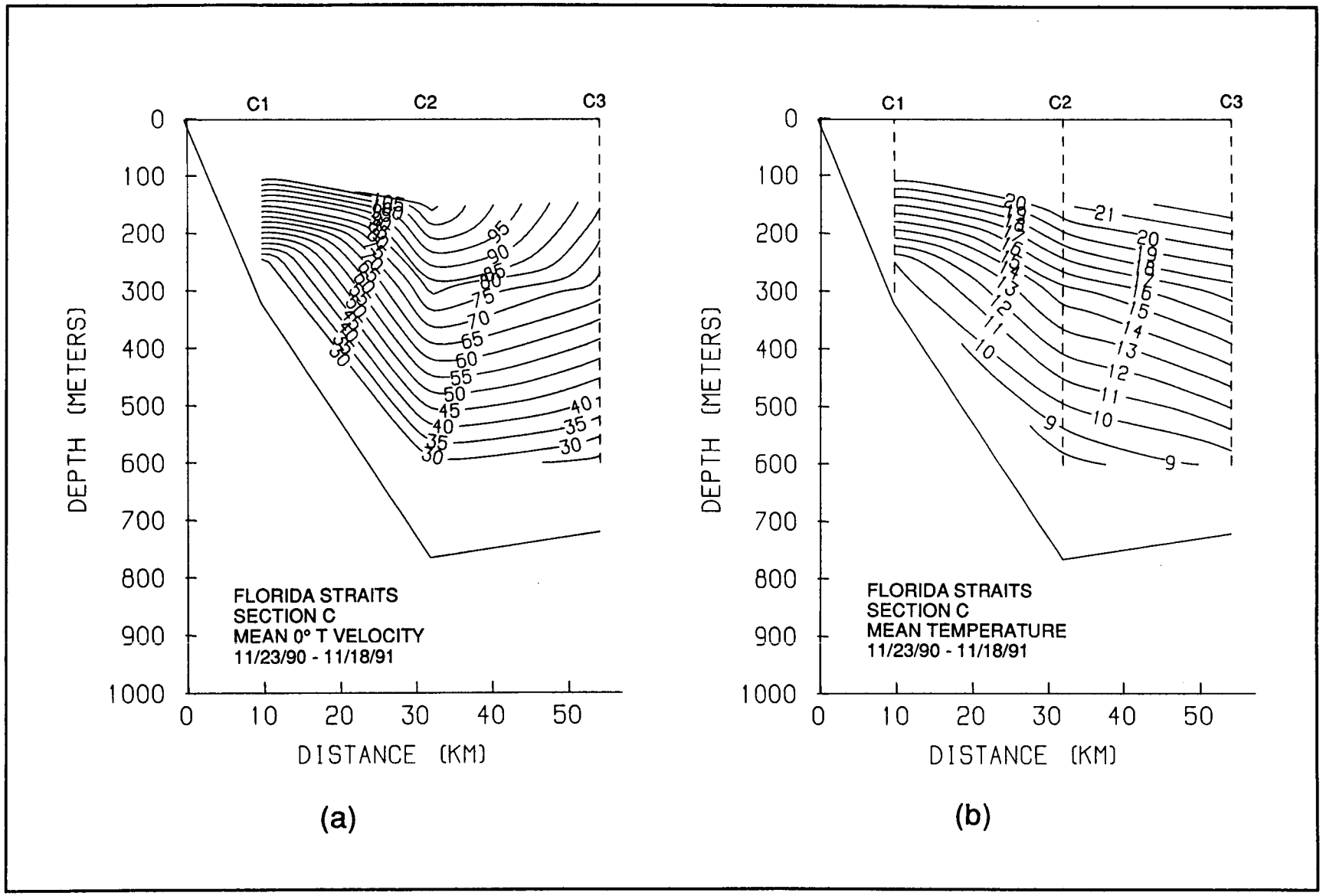

Figure 4.3-6 Contours of means for a) transect-normal velocity and b) temperature. Mean values were computed using the complete available time series on Transect C.

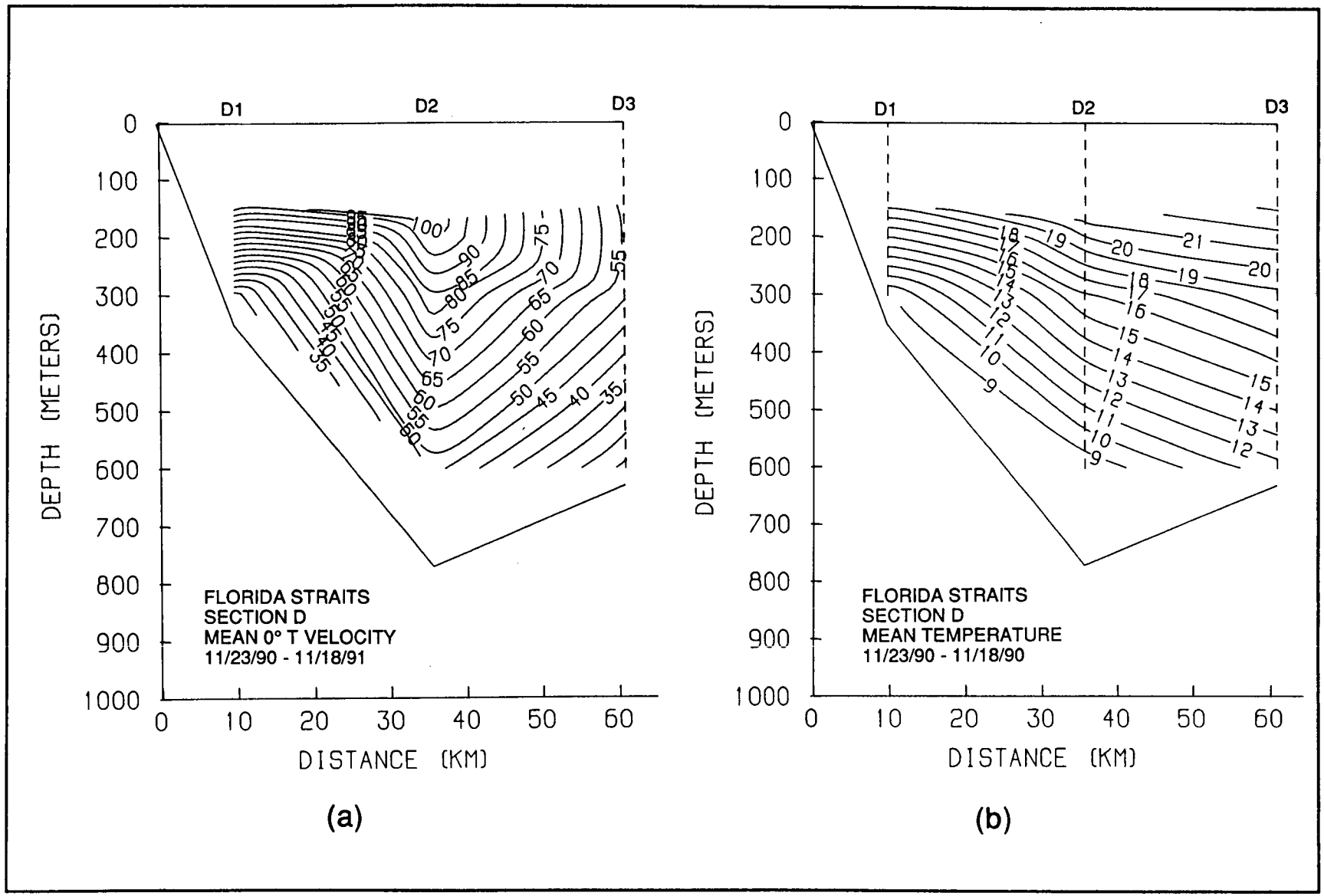

Figure 4.3-7 Contours of means for a) transect-normal velocity and b) temperature. Mean values were computed using the complete available time series on Transect D.

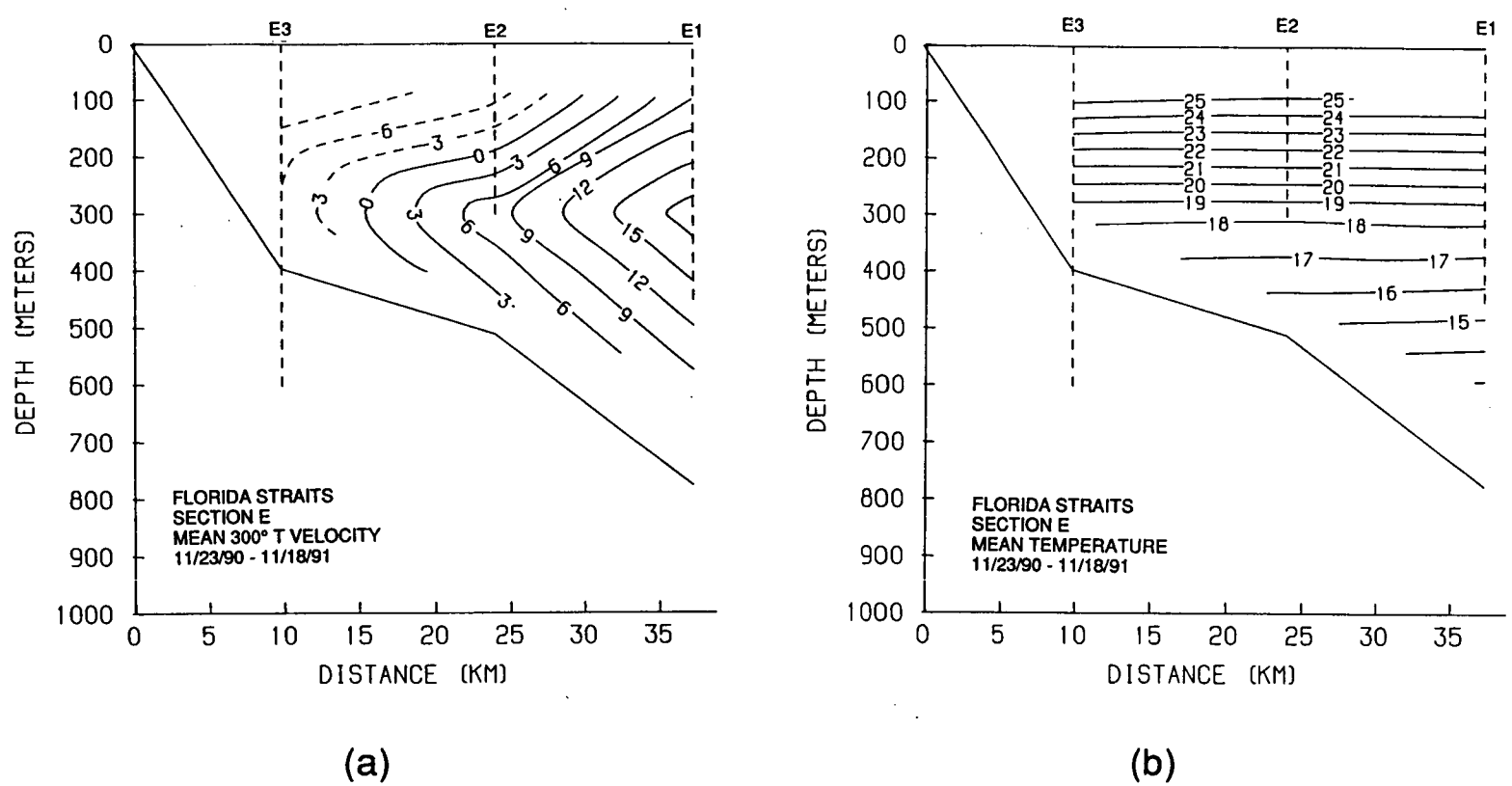

Figure 4.3-8 Contours of means for a) transect-normal velocity and b) temperature. Mean values were computed using the complete available time series on Transect E.

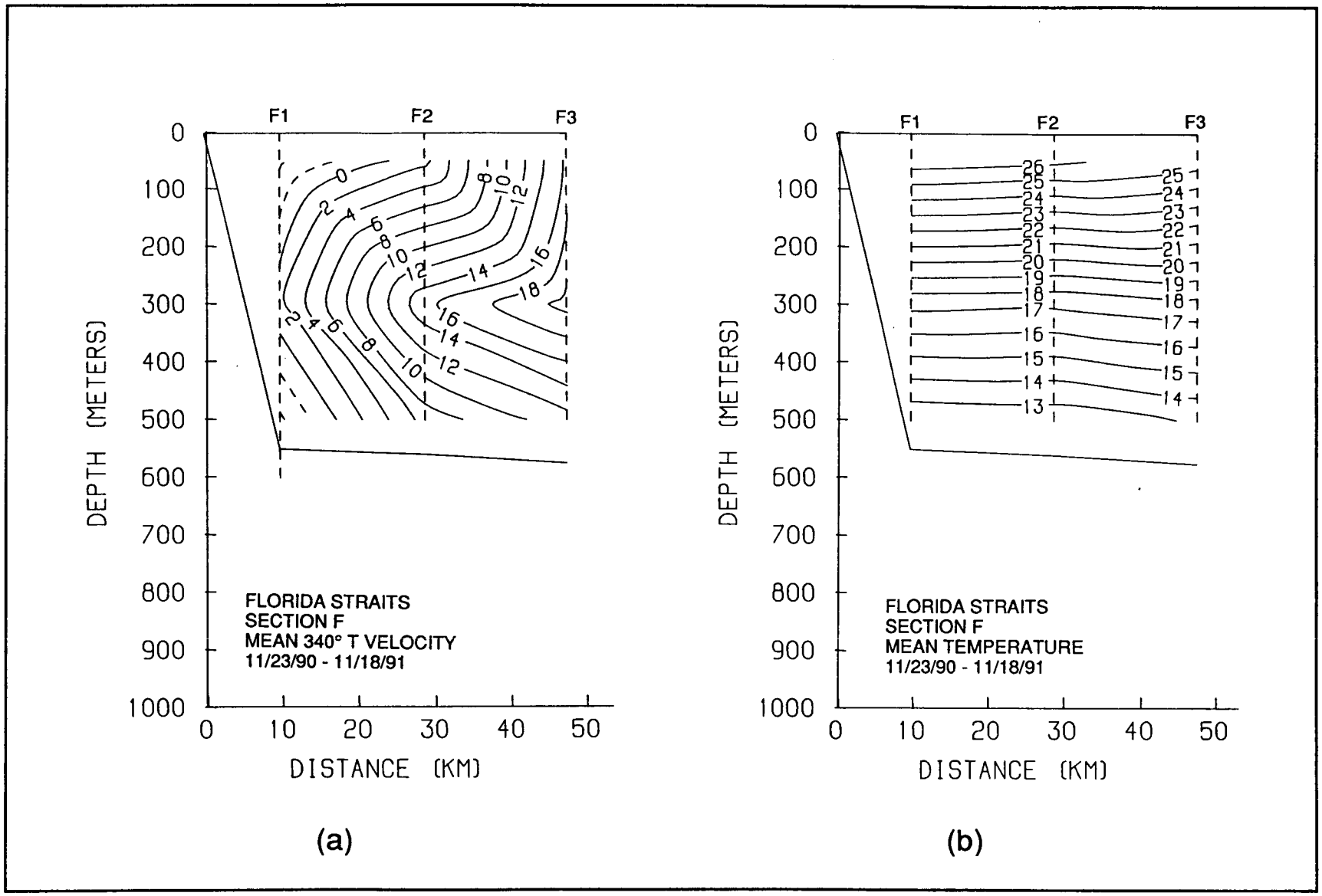

Figure 4.3-9 Contours of means for a) transect-normal velocity and b) temperature. Mean values were computed using the complete available time series on Transect F.

4.3.2 Standard Deviation Fields

Cross-channel distributions of downstream current standard deviations are presented in Figures 4.3-10 through -12. Downstream current variations were greatest in the southern Florida Straits on Transects A and B, where largest variations occurred near the surface on the shoreward side of the sections. Standard deviations were about twice the mean flow on the shoreward side of the Marquesas section and about the same order as the mean on the shoreward side of Transect B. This pattern generally reflects the strong flow variations that occur during large-scale FC meandering and gyre formation in this region. Standard deviations of downstream currents in Transects C and D were much weaker than the mean flows and were generally distributed with a minimum in the center of the channel where the mean flow was largest. Standard deviations across the NWPC were about the same magnitude as the mean flow and were slightly more variable on the northern side of the channel. Standard deviations across the SC were also about the same magnitude as the mean flow on the eastern side of the channel but were greater than the mean flow on the western side, where the mean flow was weak.

4.4 Forcing Mechanisms

4.4.1 Florida Current Meanders, Eddies and Gyres

The primary mode of subtidal current and temperature variability within the SoF appears to be associated with cross channel shifts of the FC. This meandering mode produces an out-of-phase relationship in downstream currents on either side of the axis and in-phase temperature change across the FC. The dominant period of the meandering mode in the northern Straits falls within a 3-day to 3-week band and can be due to inherent barotropic or baroclinic instabilities of the flow and density fields (Boudra, Bleck and Schott, 1987 and 1988), flow over topographic features such as the Miami Terrace (Lee and Mayer, 1977), and along-channel wind forcing (Brooks and Mooers, 1977a and 1977b). Cold, cyclonic, frontal eddies are formed together with growing offshore meanders as part of the baroclinic instability process (Lee, 1975; Lee and Mayer, 1977; Lee, Yoder and Atkinson, 1991). These features have dimensions of 10's of km and travel downstream at a mean speed of about 30 km day^{-1}. The passage of a frontal eddy can produce large current variations and even current reversals on the shoreward side of the FC, coupled to cold anomalies which result from upwelling in the cores of the features.

In the southern Florida Straits the dominant period of FC meanders occurs in a 30- to 70-day band, which can cause the FC front to be displaced up to 100 km offshore. The cross channel position of the axis appears to be strongly influenced by the manner in which the FC enters the southern Straits from the eastern Gulf of Mexico, as well as by the disturbances that propagate downstream along the cyclonic (northern) front. Satellite-derived surface temperature patterns show that in December 1990 the Loop Current was not extended northward into the Gulf of Mexico, so the warm flow through the Yucatan Channel turned abruptly to the east and entered the southern Florida Straits (Figure 4.2-5). This anticyclonic turning of the flow caused the northern boundary of the FC to extend close to the lower Florida Keys, resulting in strong downstream currents at the inshore moorings A1 and B1. As the Loop Current grew northward into the eastern Gulf of Mexico, the southward flow along the seaward edge of the

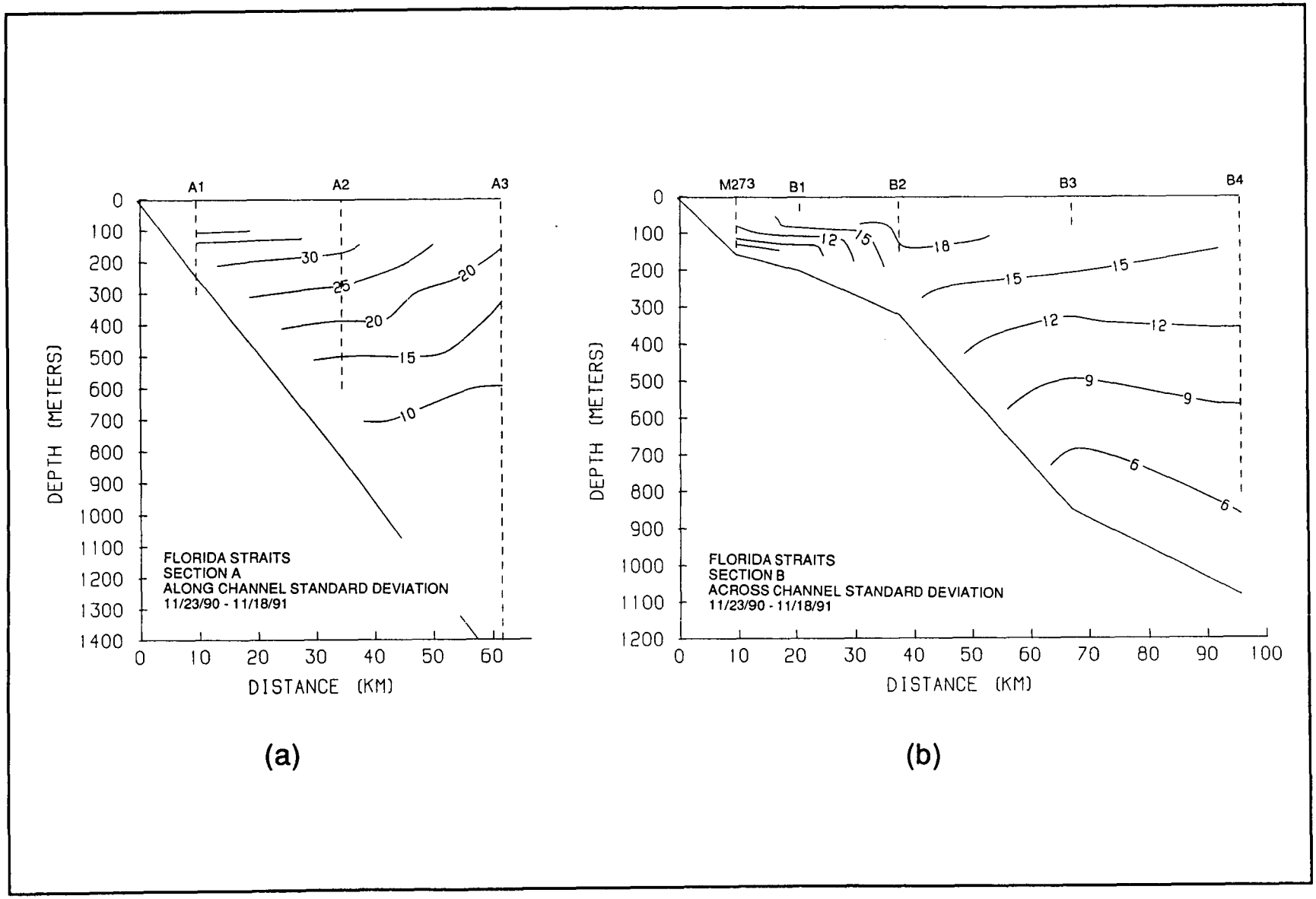

Figure 4.3-10 Contours of standard deviations of transect-normal velocity for a) Transect A and b) Transect B.

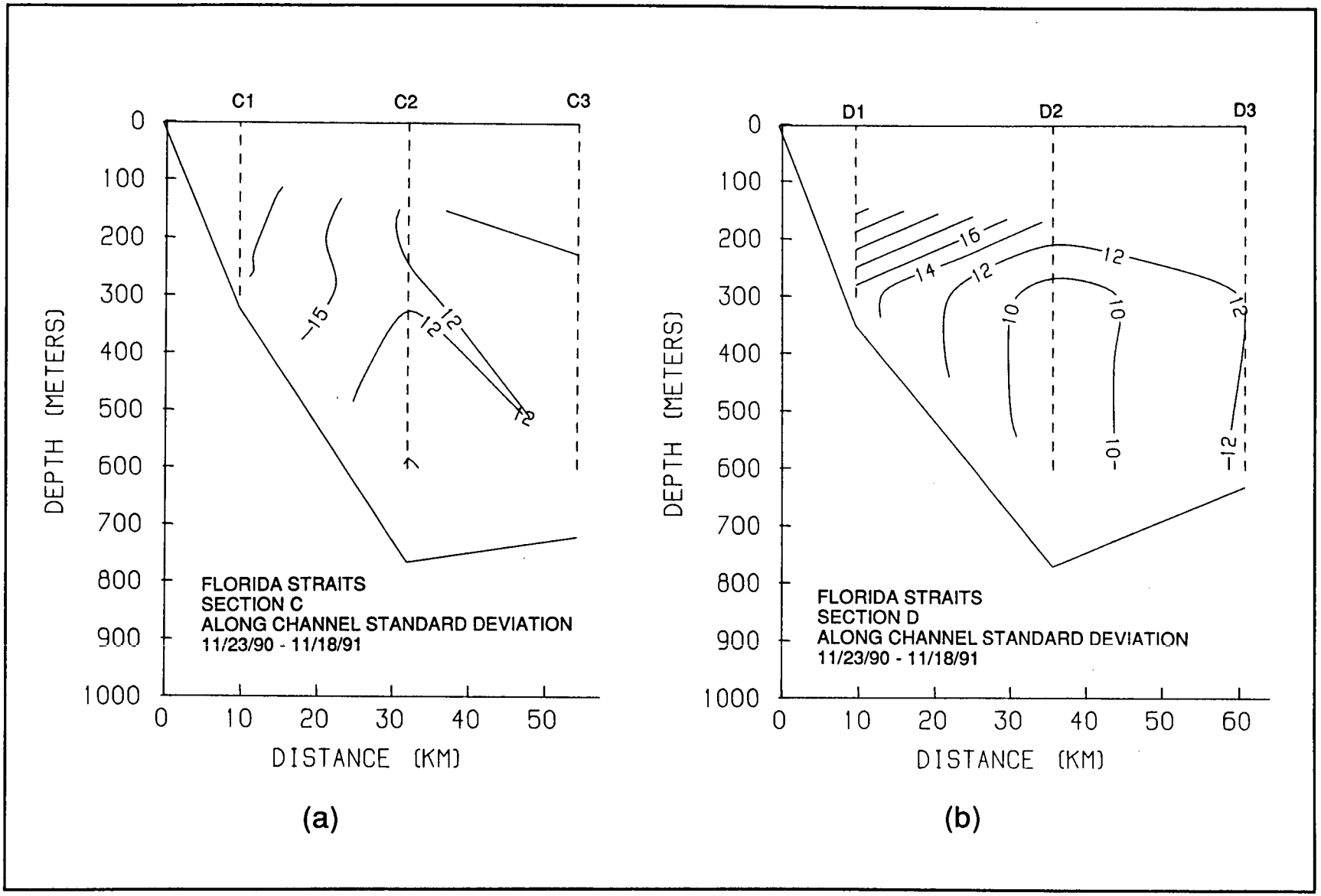

Figure 4.3-11 Contours of standard deviations of transect-normal velocity for a) Transect C and b) Transect D.

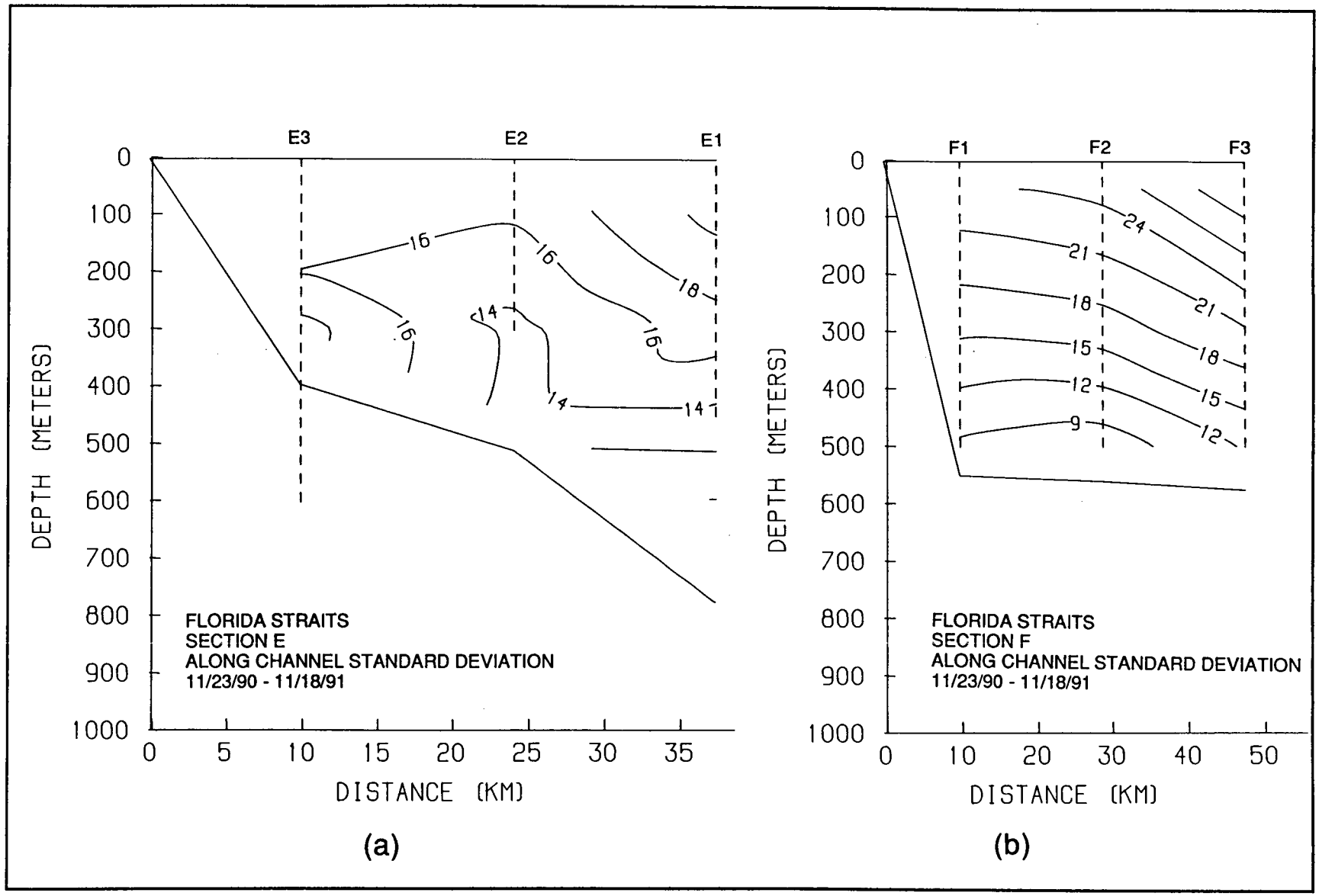

Figure 4.3-12 Contours of standard deviations of transect-normal velocity for a) Transect E and b) Transect F.

southwest Florida shelf appeared to "overshoot" the western entrance to SoF before turning abruptly to the east.

The southward "overshooting" of the Loop Current, combined with the strong cyclonic curvature vorticity from the sharp eastward turning, appears to spinup a cold cyclonic gyre offshore of the Dry Tortugas that we have called the Tortugas gyre (Figure 4.2-7b). Further enhancement of this gyre appears to occur with encounters of Loop Current frontal eddies that sometimes propagate into the region. The duration of the gyre off the Tortugas is on the order of 100 days, and its spatial scale is about 100 by 180 km. The demise of the gyre occurs with the approach of an onshore FC meander crest that sends the gyre toward the east at about 5 km day^{-1} and causes a rapid decrease in size. By the time the Spring 1991 gyre event reached Transect B (in the region of the Pourtales Terrace), it had decreased in size to about 60 by 100 km (Figure 4.2-7e). Presumably the decrease in size results from the narrowing of the channel due to the presence of the Cay Sal Bank. Oey (1988) showed that the growth of finite-amplitude disturbances in the Gulf Stream front off the southeast U. S. is dependent on the cross-stream distance from the slope to the Gulf Stream axis. This distance decreases as the gyre approaches Transect B, which may account for the gyre decay. Previous SEFCAR studies of gyre formation off the middle and lower Keys found a preference for gyre formation on the Pourtales Terrace (Lee et al., 1992). With the aid of time series of satellite thermal imagery and the large-scale moored array that covered the entire Florida Straits, we now have clearly established that the previously studied Pourtales gyre is a later stage in the evolution of the Tortugas gyre.

Offshore meandering and gyre formation in the Pourtales Terrace region has a significant influence on the flow in the SC. When the FC axis shifts offshore in this region, part of the flow interacts with Cay Sal Bank and forces a counter-clockwise circulation around the Bank and toward the north on the east side of the SC (Figure 4.2-7f). Flow in the SC appears to respond in eddy-like fashion, and a southward flow reversal occurs along the western side of the channel as a cold, cyclonic eddy is set-up.

Eddy motions are also common in the NWPC, where inflow to the FC occurs on the north side of the channel and outflow occurs on the south side (Figures 4.2-7a through d). It is unclear what the forcing mechanism is for this eddy feature, but there is some indication that increases in downstream flow on the east sides of SC and Transect C off Miami are correlated to the countercurrent flow in NWPC and subsequent flow increases on the east side of Transect D off Palm Beach. If this were true, then the gyre/offshore meander over the Pourtales Terrace could be directly responsible for the eddy motions in Santeren and Northwest Providence Channels and accelerations in the flow on the east side of the northern Florida Straits. This indicates that the ultimate forcing mechanism would be the large-scale meanders off the Tortugas, or in other words, the position and orientation of the Loop Current as it enters the southern Florida Straits.

4.4.2 Wind Forcing

Recent time series measurements of FC transport fluctuations at 27°N indicate a strong connection between transport variations in the 2- to 10-day period band and local meridional wind stress (Lee, Schott and Zantopp, 1985). Lee and Williams (1988) applied a simple, wind-forced, coastal response model to the SoF to show that local along-channel winds from synoptic weather events can generate

significant fluctuations in FC volume transport. A northward wind (over the northern Straits) can cause an increase in transport, and a southward wind, a decrease. Eastward/westward winds over the southern Straits would have a similar effect. This is a barotropic process in which uniform along-channel flow is accelerated due to cross-channel interior flows adjusting to surface Ekman transports in a channel where there is a two-sided coastal constraint (U = 0 near the coasts) which causes simultaneous divergence and convergence at the channel boundaries. The sea surface then adjusts geostrophically to the developing along-channel transport. Bottom friction appears to be insignificant so that the transport response will continue until the wind forcing changes. However, the finite length of the north-south (or east-west) domain of the Straits appears to have an effect similar to that of bottom friction in shallow shelf regions, for the fluid has no memory of the wind forcing that occurred on time scales longer than the mean advection time of the north-south or east-west portions of the channel. Because of the strong mean downstream transport, this memory is approximately 2 days for either channel segment.

The annual cycle of FC volume transport, with a maximum in summer and minimum in fall, appears to result from a combination of local and remote wind forcing. Numerical model studies of the North Atlantic show that wind stress curl over the topography of the NW Atlantic makes a significant contribution to the annual cycle (Anderson and Corry, 1985). Lee and Williams (1988) used their simple, local wind-forced model to show significant contribution to the annual transport cycle. Apparently, seasonal differences in along-channel winds over the SoF, from summer winds with a northward component to fall winds with a southward component, are partly responsible for the seasonal volume transport changes.

Local winds over the SoF are primarily from the southeast because of the persistence of the Azores-Bermuda atmospheric high. The southeast winds are most persistent in the summer months of June - August, when the atmospheric high is strongest. During fall (September - November) a high pressure system develops over the southeastern coastal states that can produce strong southward wind events that are coherent over the SoF on time scales of 5 to 10 days. These fall wind events are primarily responsible for the seasonal minimum of FC transport observed in the northern Straits (Lee and Williams, 1988). During winter (December - February) and spring (March - May) cold fronts extend southward across the southern Straits with a period of about 10 days, causing an increase in wind speeds and a clockwise rotation in direction.

Along-channel winds observed at coastal sites from Palm Beach to Key West during the one year of moored observations were most energetic in a period band of 7 to 10 days (Figure 4.4-1). Variance of downstream volume transports derived from moored current meters and submarine cable voltages was mostly associated with the long-period meander time scale of 30 to 80 days for transects in the southern Florida Straits (Figures 4.4-2 and -3), whereas in the northern Straits energetic transport fluctuations occurred at periods of about 10 days and greater than 30 days. Transport fluctuations were highly coherent with along-channel winds in the 7 to 10 day period band at all transects, with transport lagging by about 2 days for the northern sections (Figures 4.4-4 and -5) and about 0.5 days for the southern sections (Figure 4.4-6). There was also significant coherence between transport fluctuations in the NWPC and the along-channel winds at periods of 7 to 8 days.

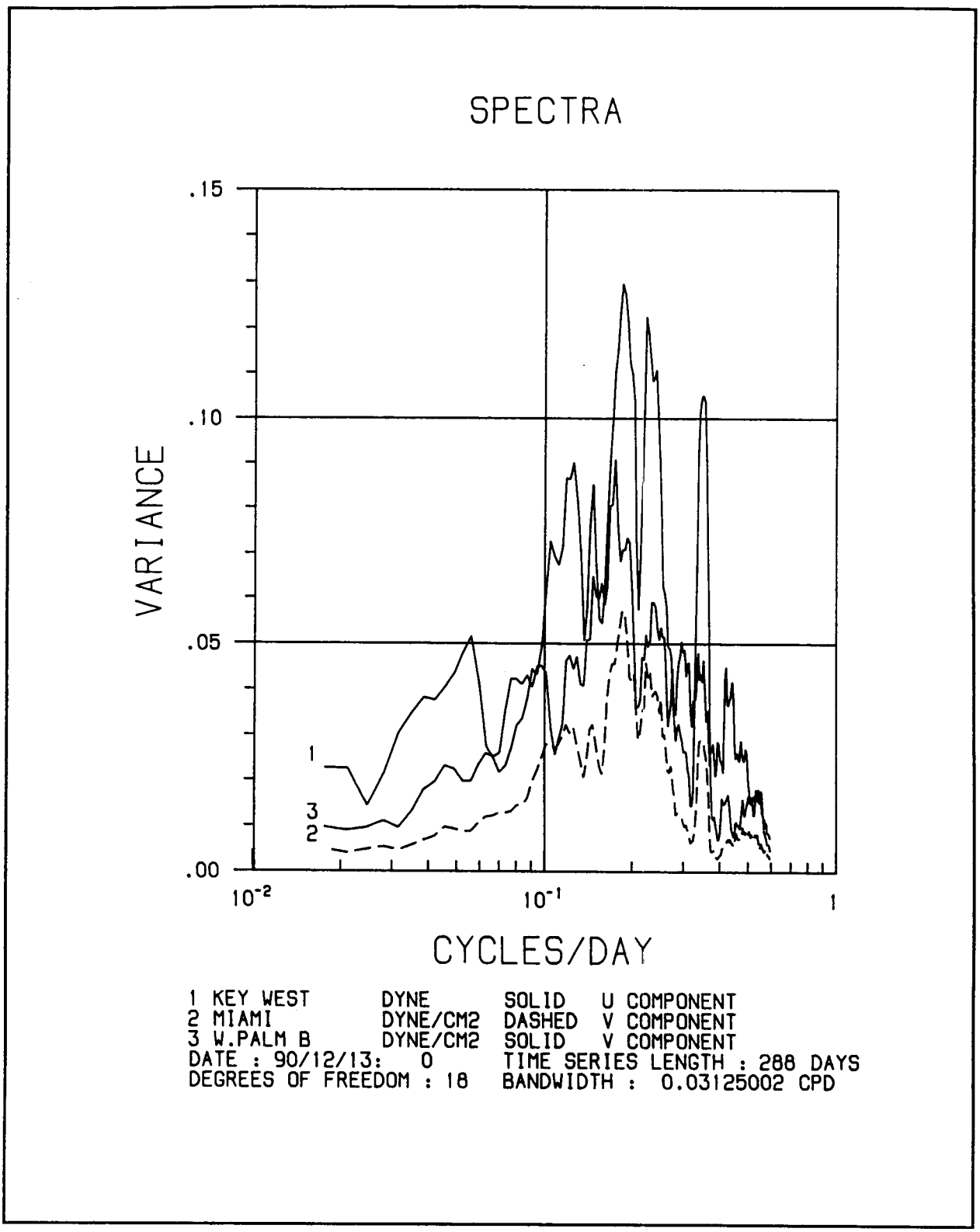

Figure 4.4-1 Spectra for the indicated components of 40-HLP filtered wind stress at Key West, Miami and W. Palm Beach FL. All units are dyne cm^{-2}.

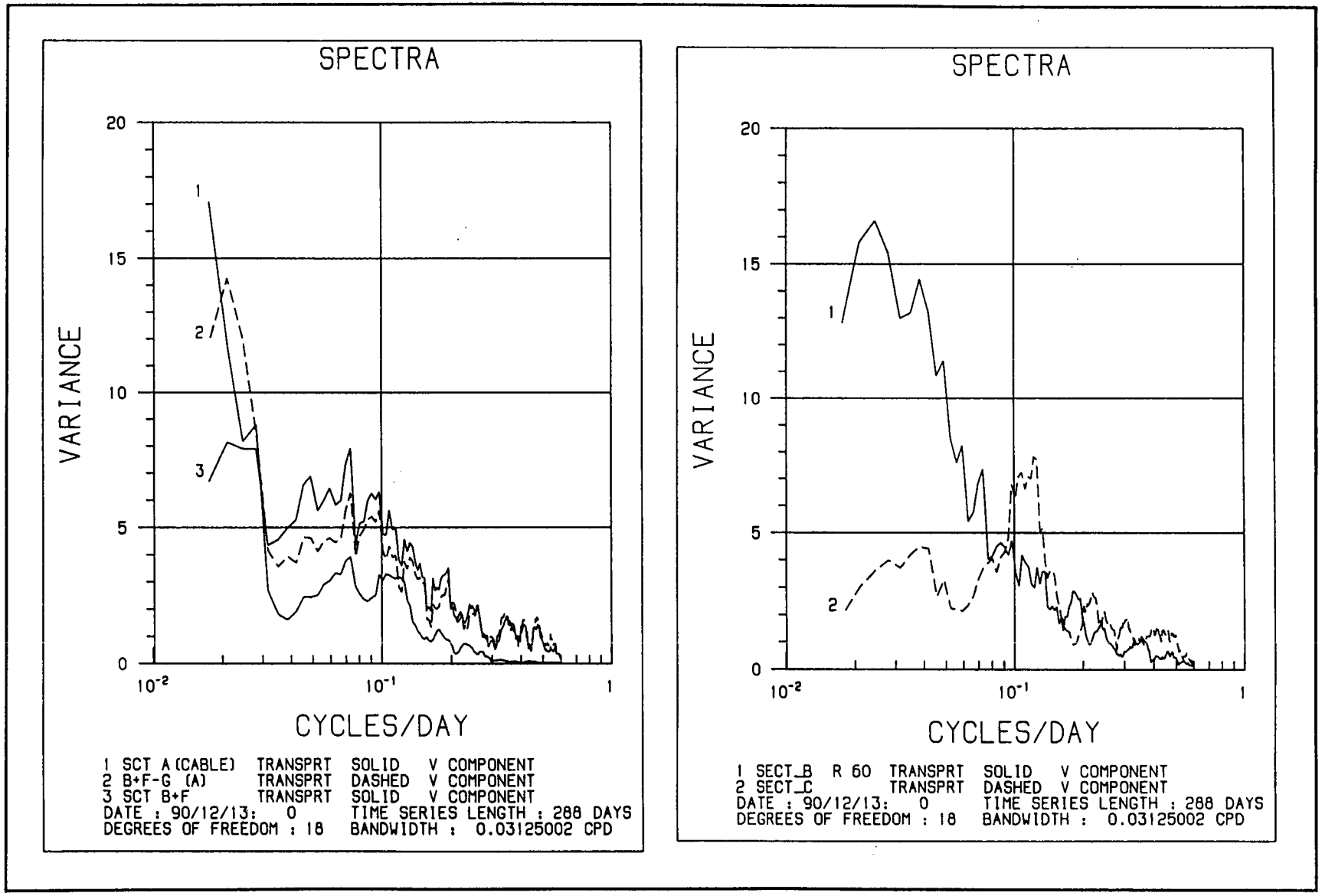

Figure 4.4-2 Spectra of transport over the indicated transects.

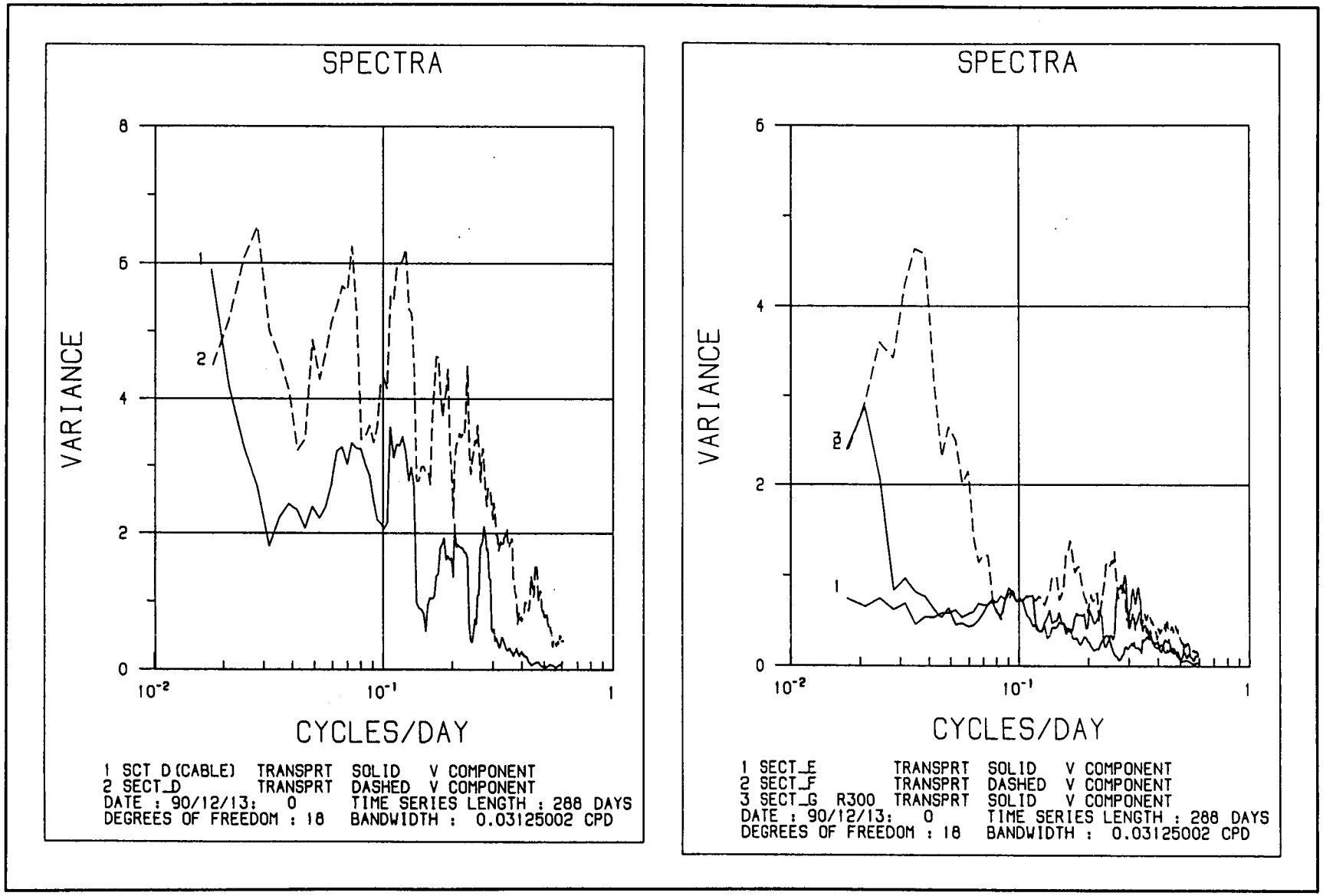

Figure 4.4-3 Spectra of transport over the indicated transects.

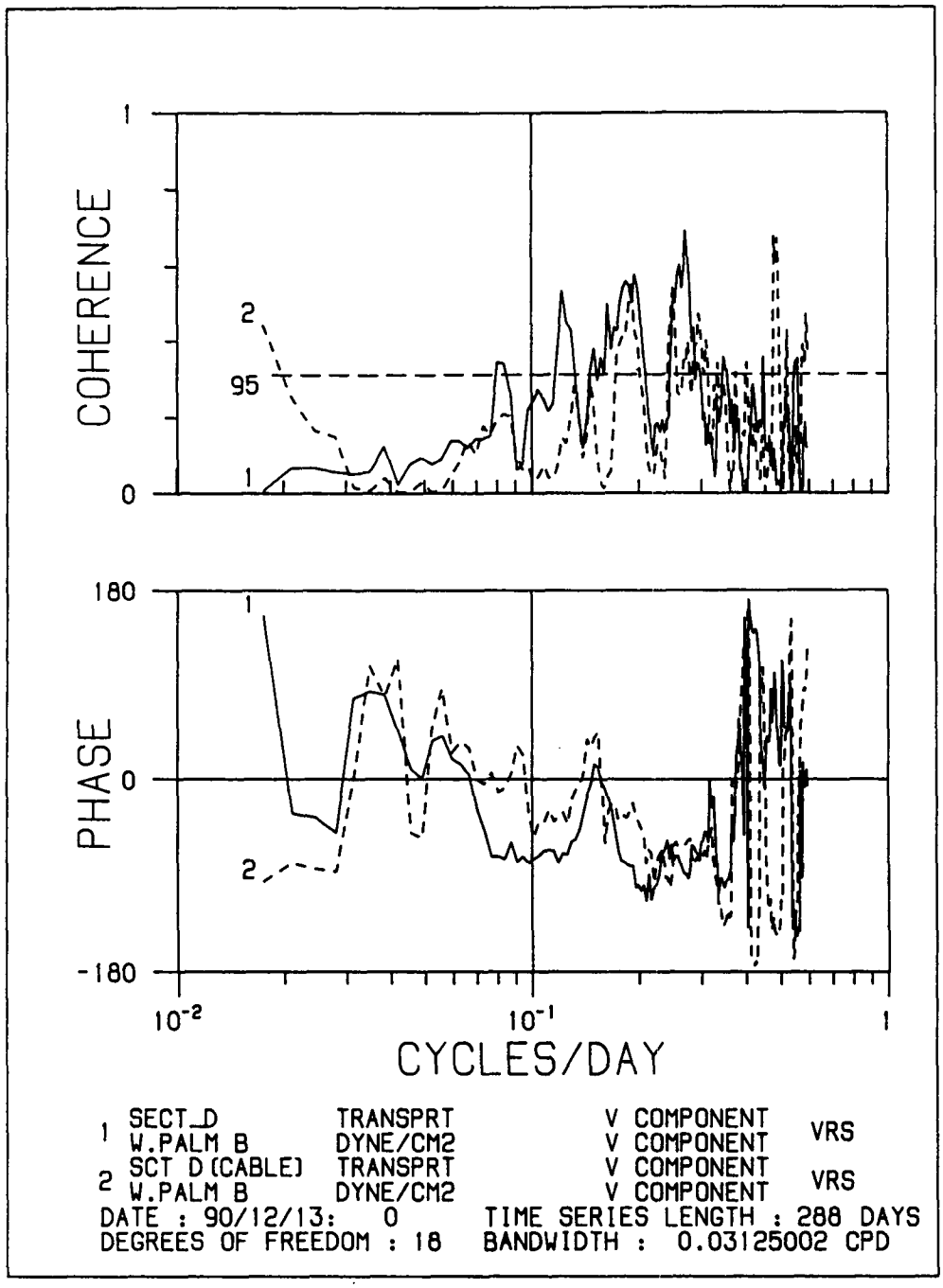

Figure 4.4-4 Phase and coherence between 1) Section D transport as computed from current meter data and along channel component of wind stress at W. Palm Beach, and 2) Section D transport as estimated from cable voltages and along channel component of wind stress at W. Palm Beach.

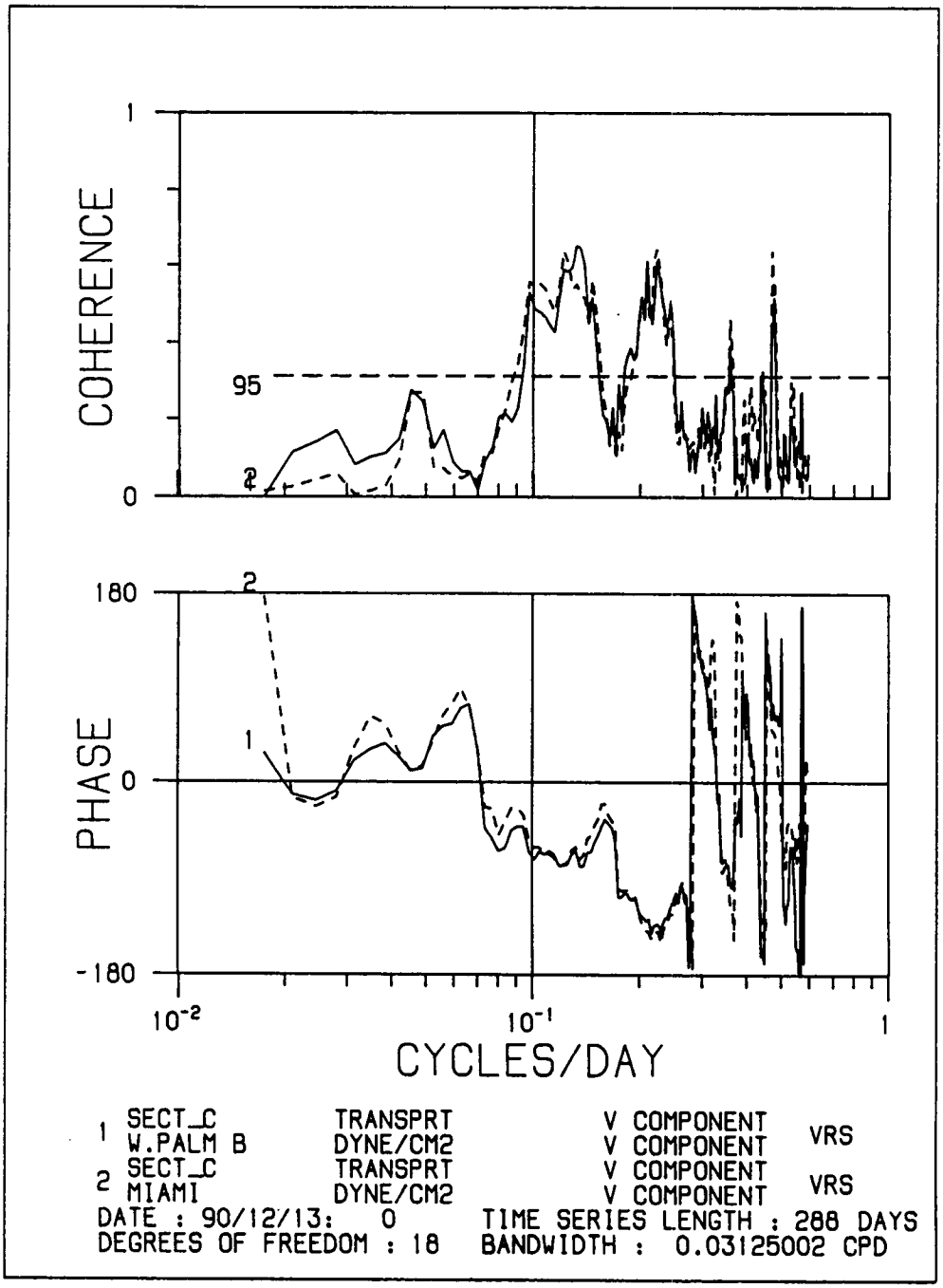

Figure 4.4-5 Phase and coherence between transport over Transect C and the along channel component of wind stress from 1) W. Palm Beach and 2) Miami.

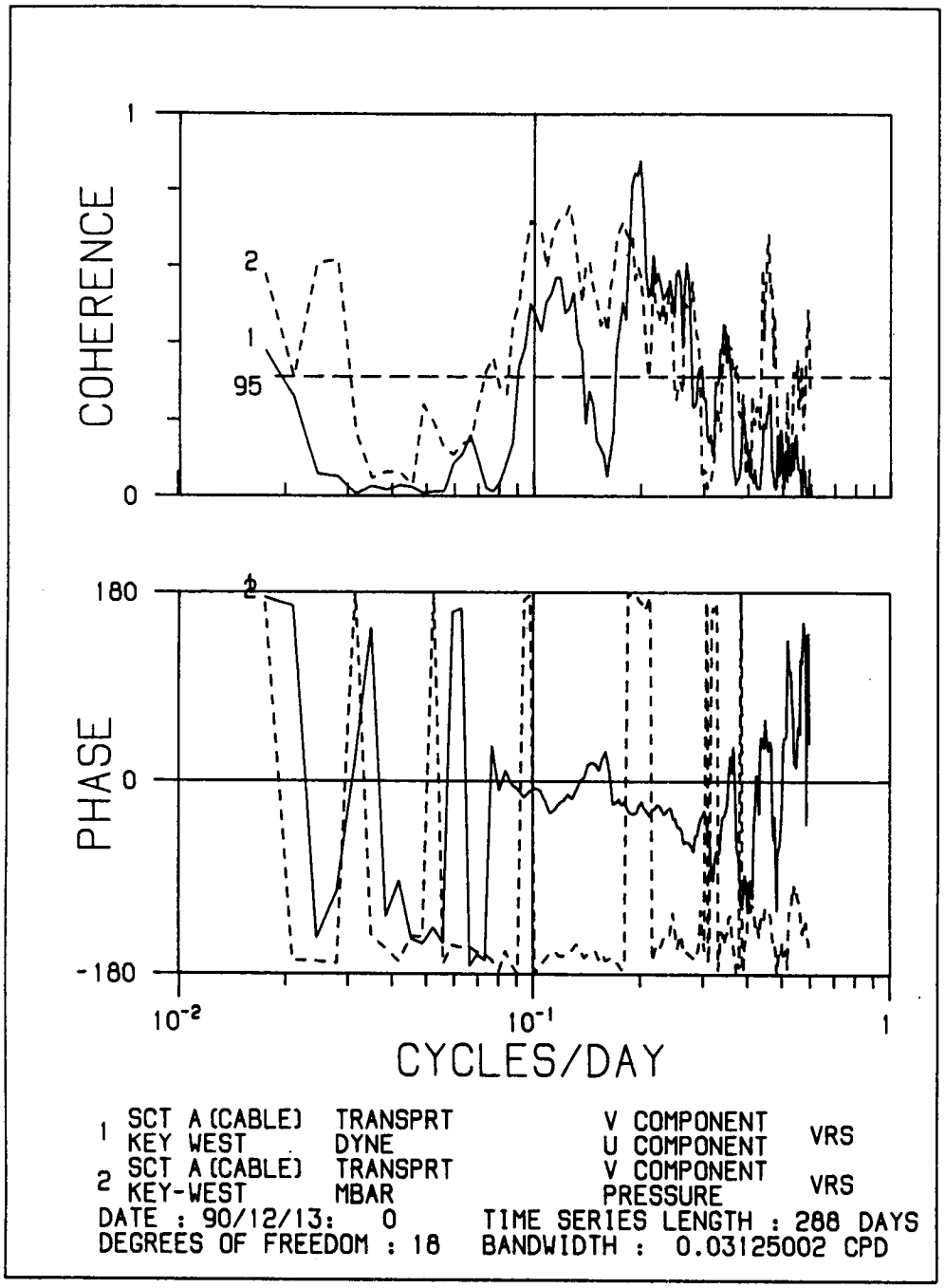

Figure 4.4-6 Phase and coherence between transport as estimated by the cable at Transect A and 1) along channel component of wind stress and 2) water level at Key West.

Lee et al. (1992) observed a locally forced, wind-driven response in alongshore coastal currents at the 30m depth off the lower Keys (Looe Reef) that occurred within a 10-day period in winter/spring and a 5-day period in summer with lags of 14 and 5 hours, respectively. This response is typical of other shallow coastal seas with straight coastlines (Csanady, 1982). Alongshore current variability at the 30m depth in the middle and upper Keys was not strongly influenced by local winds due to the curving coastline, which resulted in mostly cross-shore winds at these sites. Also the nearness of the FC front to the northern site (Carysfort) resulted in meandering and eddy shedding processes having the dominant influence there.

Lee et al. (1992) estimated that the combined effect of the eastward flowing FC in the southern Straits, with westward flow nearshore when the Pourtales gyre is spun up, can have a profound influence on wind stress and Ekman transports for the prevailing westward winds. This can be seen by comparing the magnitude of the east-west component of the wind stress given by

$$\tau_x = P_a C_d (U - u)^2$$

where P_a is the density of air, $C_d = 1.5 \times 10^{-3}$ is the drag coefficient, U and u are the east-west components of the wind and current velocities (respectively). For a typical westward wind speed of 6m s^{-1} against the FC eastward speed of 1.5m s^{-1} gives $\tau_x = -60$ m^2 s^{-2}, whereas on the northern side of the Pourtales gyre, or the Tortugas gyre, the current is in the same direction as the wind at a speed of about 0.5m s^{-1}, which gives a wind stress of $\tau_x = -30$ m^2 s^{-2}. Thus, for the same wind, the wind stress is a factor two times larger near the FC axis compared to the region of westward flow on the northern side of the gyres. Therefore, Ekman transport, $T_E = t/f$, is also two times greater at the FC axis as compared to the westward flow region of the gyre. This will result in a northward convergence of surface Ekman transport into the gyre and coastal boundary, where downwelling should occur over the steep continental slope. This leads to the conclusion that the lower Keys region is a preferred area for onshore surface transport due to the prevailing westward winds and coastal gyre circulations. North of the lower Keys, coastal gyres do not occur due to the narrowing of the channel, and orientation of the prevailing southeast winds relative to the change in orientation of the SoF from east/west to north/south no longer causes onshore Ekman transports.

4.4.3 Circulation in the Old Bahama Channel

Mooring G in the OBC produced good velocity and temperature records throughout the yearlong field measurement program. These data showed unexpectedly high currents in the lower two-thirds of the water column that were usually directed towards the SC and the Florida Current. The upper layer currents were generally weaker and had flows both into and out of the Caribbean. Of particular note also is the occurrence of a highly saline layer between 100 and 300m (Figure 4.4-7). The salinity maximum reaches 36.98 psu at about 180-220m depth, which is deeper and more saline than the salinity maximum on the east side of the northern part of the FC. The maximum salinity layer occurs at about 100m in the FC with salinities typically between 36.6 and 36.8. In the OBC, this maximum salinity layer is present throughout the year (Figure 4.4-7).

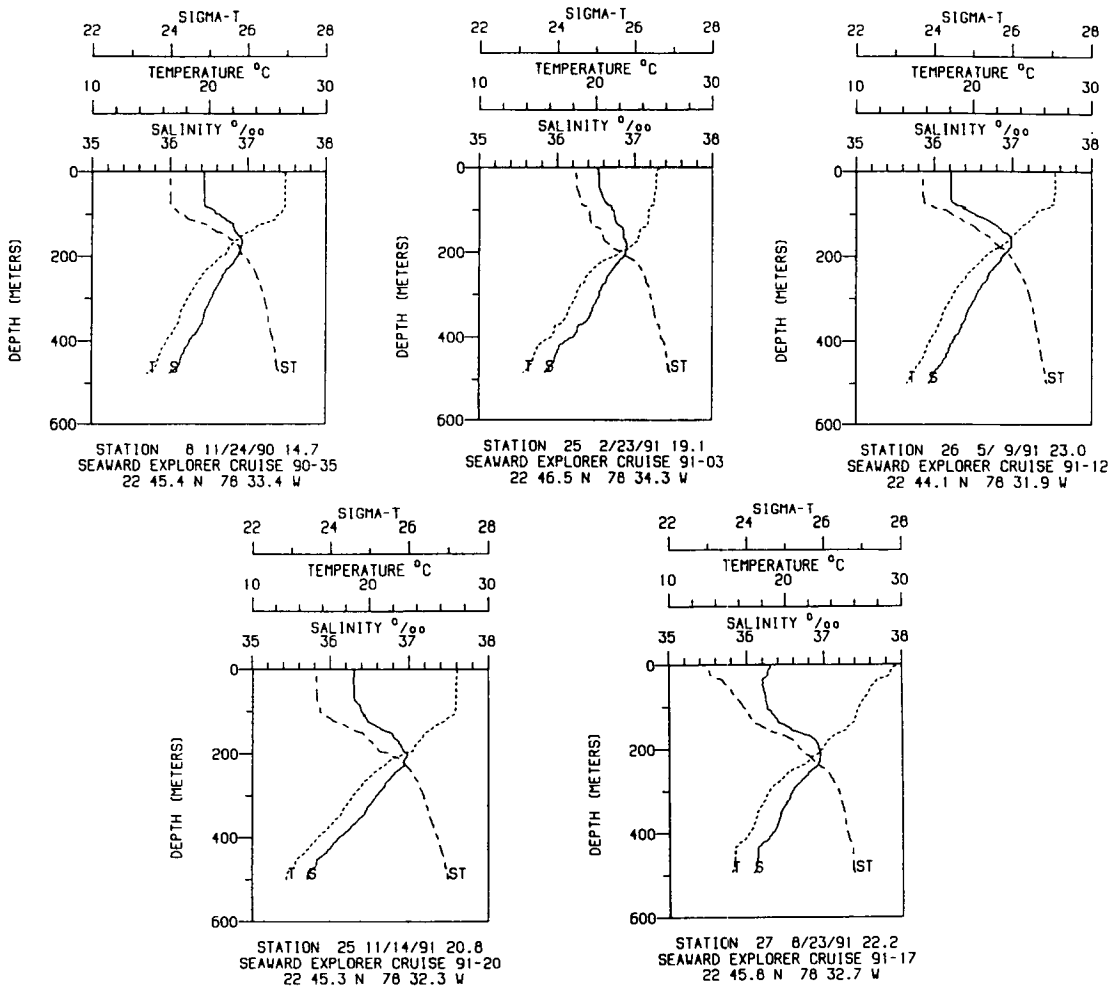

Figure 4.4-7 Profiles of temperature, salinity and density taken at Mooring G in Old Bahama Channel. One set of profiles is given for each cruise. Note the mid-depth (100-300 m) salinity maximum which is commonly found.

The time series plots of along-channel (V) current velocity, temperature and the depth of the upper level instrument are given in Figure 4.4-8 for Mooring G. In June and July 1991, the mooring underwent a long period of substantial "draw downs" at a predominantly diurnal tidal period. The upper current meter is being moved across a shear layer with outflow (-ve V) above about 75m and inflow towards the Florida Straits below that depth. This produces large apparent diurnal oscillations in temperature and velocity at G1. Figure 4.4-9 shows the spectrum of the complete 12-month record from G1 and shows prominent K_1+P_1 and O_1 peaks in the diurnal frequency band. The deeper velocities have about 40-60 cm of inflow with relatively small diurnal oscillations (amplitude $\approx$ 10 cm s^{-1}). These currents are not large enough to produce the more than 100m draw down of the subsurface float. The diurnal oscillation would indicate that there are large diurnal internal tidal currents at some level in the water column that are affecting the inclination of the mooring. The events of June and July are not unique; similar events occurred during the first six months of the record at irregular intervals.

In the last three-month deployment, beginning on August 26, 1991, the mooring was stiffened by increasing the amount of flotation. The success of this modification can be seen from the lack of large depth excursions in the pressure record from G1 (Figure 4.4-8). The tidal current oscillation in the records between August and November is much more regular with outflow in the mean at 50m and the inflow in the lower half of the water column. However, during the first 20 days of October, large pulses of inflow current occurred at G2 at the 250m level. Speeds approached 200 cm s^{-1}. Since the current record is quite regular and well behaved both prior to and after this episode, there is no reason to believe that the G2 instrument malfunctioned. Thus, there appears to be some direct evidence that large internal diurnal tidal current shears are being generated intermittently, presumably when mean vertical shear and stratification produce a critical condition. Mooring G is situated on a broad sill in the OBC, which may contribute to the topographic generation of diurnal internal waves. Diurnal internal waves are supported at latitudes below about 28°30′N. In the OBC, the period (f^{-1}) at which internal waves are not supported is about 30 hours.

There is evidence that there is intermittent generation of large internal diurnal tidal currents. Further investigations are needed to confirm their existence and determine their dynamics. The existence of two-layer flow, with predominantly outflow above 75 to 100m and strong inflow below this depth with the largest inflows apparently occurring at the depth of the salinity maximum, indicates that density driven circulations may be an important part of the large-scale dynamics of the OBC. The mean volume and salt flux towards the FC are important components of the overall volume transport and salt balances for the Gulf Steam north of Miami.

4.5 Summary

Low-frequency current and temperature variability in the SoF results primarily from a mix of onshore/offshore meandering of the FC axis, formation and evolution of gyres and eddies, and response to local and remote wind forcing. In the southern Florida Straits, below 25°N latitude, the dominant mode of variability consists of a large-scale meander of the FC coupled to the formation of a cold, cyclonic gyre off the Dry Tortugas. The offshore position of the FC in this region appears to be strongly dependent upon the development of the Loop Current

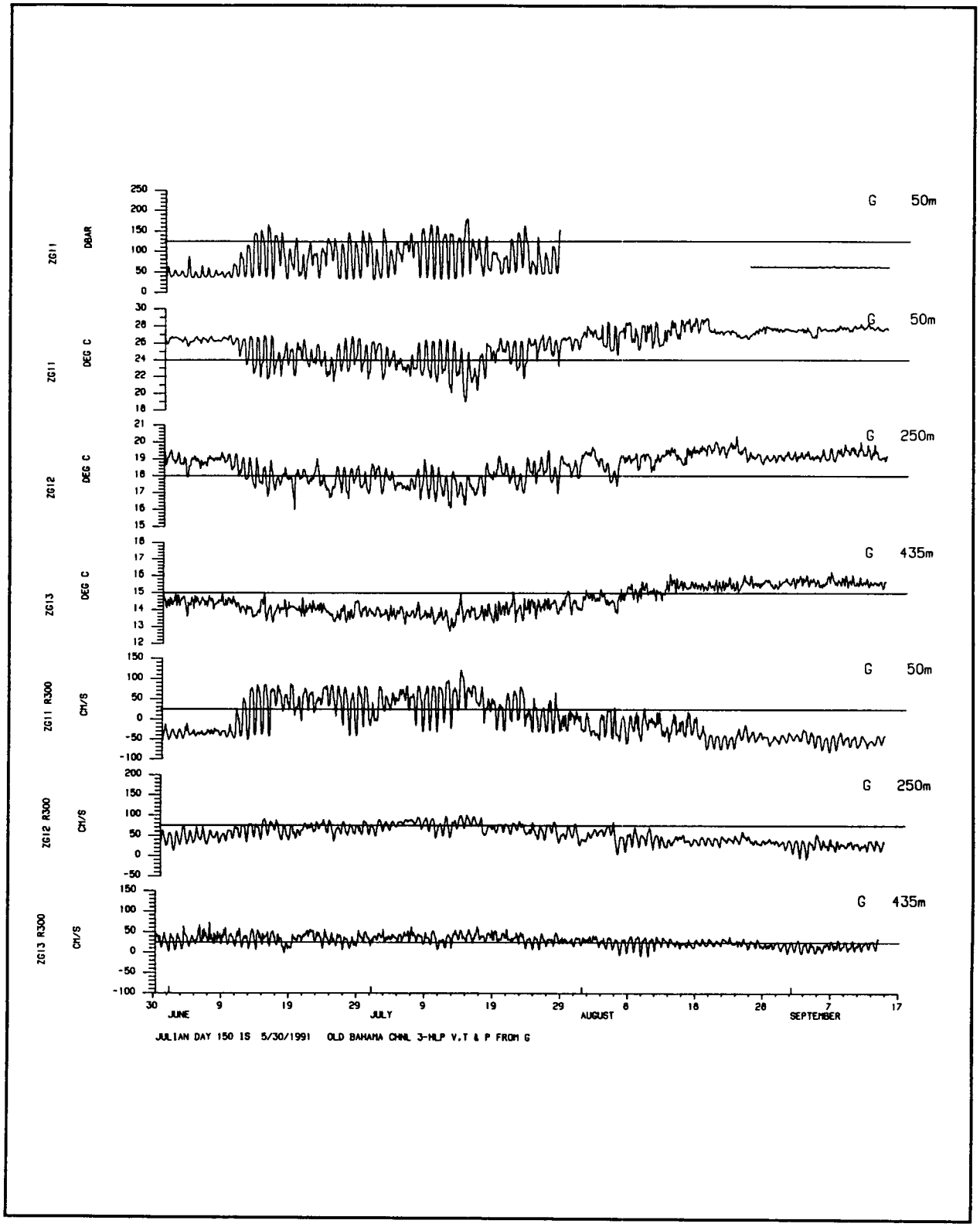

Figure 4.4-8a Time series (3-HLP) of pressure, temperature and along channel current speed at the indicated depths. The time interval presented is from June to September 1991. Note the large pressure changes in June and July as strong currents caused the top of the mooring to be drawn down.

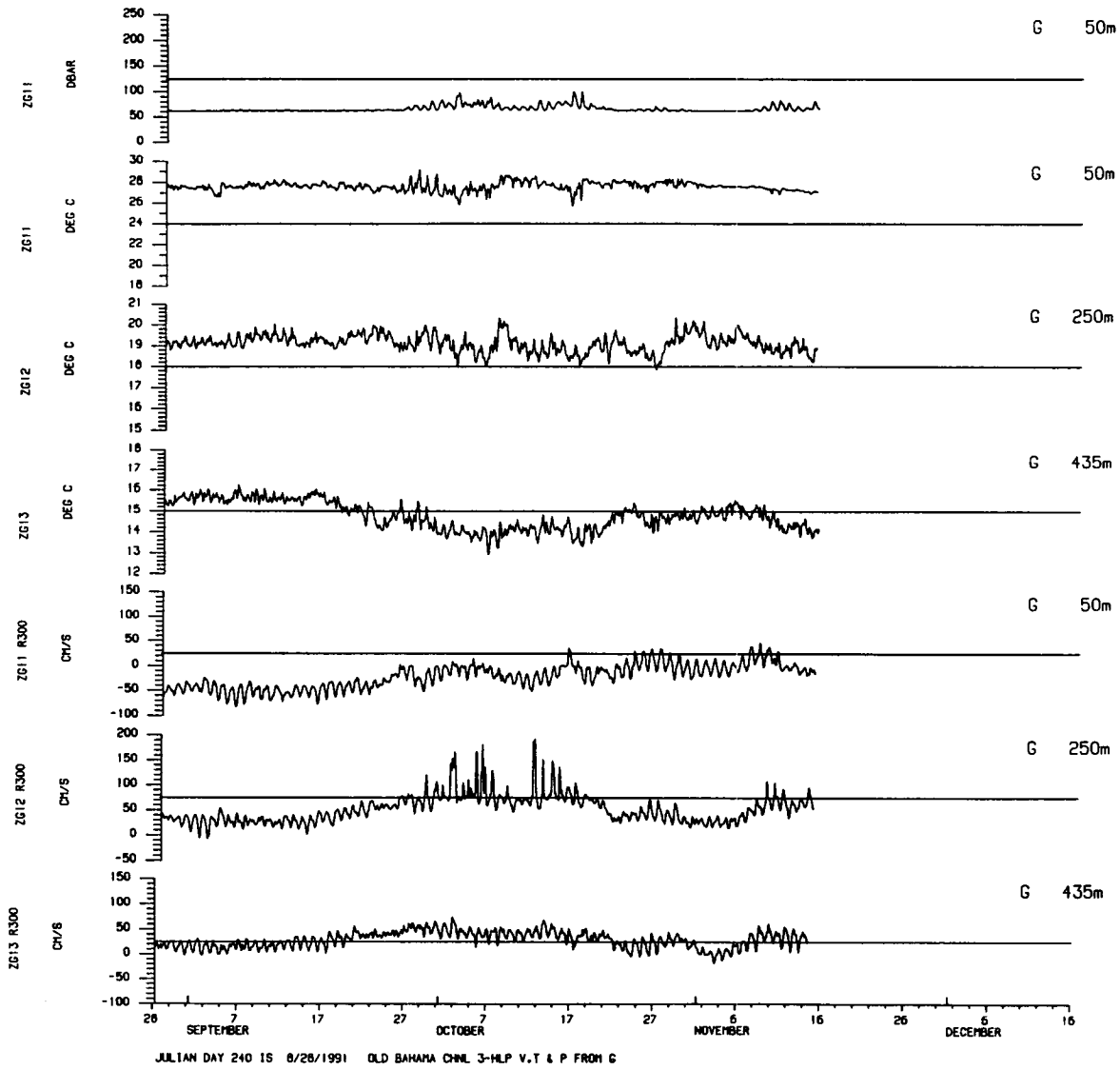

Figure 4.4-8b The same time series presented in Figure 4.4-8a but for the period from September to November 1991. Note the absence of large pressure fluctuations after the mooring was stiffened. Note the episodes of very high currents at mid-depth in October.

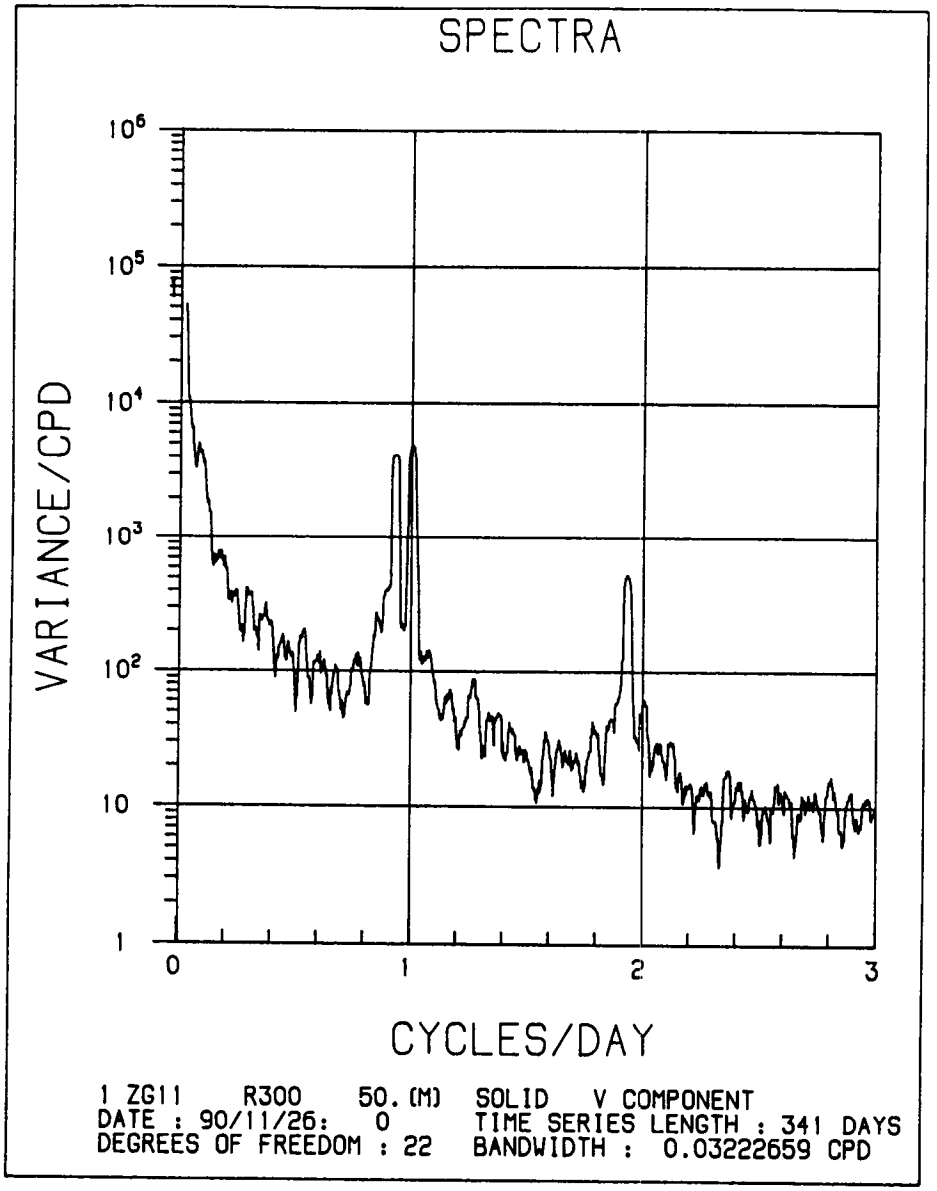

Figure 4.4-9 Spectra of 3-HLP along channel velocity component showing the strong tidal and inertial signals.

in the eastern Gulf of Mexico and the occurrence of frontal eddies that propagate along the Loop Current eastern boundary.

The absence of a Loop Current coincides with strong eastward flow in the coastal boundary zone off the western Keys of the Dry Tortugas and Marquesas whereas, with a well developed Loop Current, southward flow along the shelf edge of the southwest Florida shelf will "overshoot" the entrance to the southern Florida Straits before abruptly turning to the east off the Tortugas. This offshore displacement of the flow, coupled to strong cyclonic curvature vorticity, appears to spin up a cold, cyclonic gyre off the Dry Tortugas, the Tortugas gyre. This gyre can be further enhanced or temporarily displaced by the occurrence of smaller scale frontal eddies and meanders. Onshore/offshore shifts of the FC front in this region can be up to 100 km with a mean period of 60 days. Duration of the Tortugas gyre is on the order of 100 days, and spatial scales can be approximately 180 km alongshore and 100 km cross shore. The demise of the gyre can occur with the approach of an onshore meander crest from a propagating frontal disturbance or the pinch-off of a Loop Current ring that enables the Yucatan Current to "short-circuit" the eastern Gulf and turn directly into the southern Florida Straits. The time scale for ring formation is approximately 8.5 months (Sturges, 1992). With the approach of a meander crest, the Tortugas gyre is forced to the east at a speed of about 5 km day^{-1} and decreases in size, presumably due to the narrowing of the channel caused by the presence of the Cay Sal Bank. When the gyre reaches the Pourtales Terrace region offshore of Big Pine Key and Marathon, it has decreased to about half its (original) size off the Tortugas. It is not observable off the northern Keys, where the distance from the slope to the FC axis has greatly decreased. With the aid of time series of satellite thermal imagery and observations from the large-scale moored array that covered the entire Florida Straits, we now have clearly established that the previously studied Pourtales gyre (Lee et al., 1992) is a later stage in the evolution of the Tortugas gyre.

Offshore meandering and gyre formation in the Pourtales Terrace region has a significant influence on the flow in the SC. When the FC axis shifts offshore in this region, part of the flow interacts with the Cay Sal Bank and forces a counter-clockwise circulation around the Bank and toward the north on the east side of the SC. Flow in the SC appears to respond in eddy-like fashion, and a southward flow reversal occurs along the western side of the channel as a cold, cyclonic eddy is set-up.

Eddy motions are also common in the NWPC, where inflow to the FC occurs on the north side of the channel and outflow occurs on the south side. It is unclear what the forcing mechanism is for this eddy feature, but there is some indication that increases in downstream flow on the east sides of SC and Transect C (off Miami) are correlated to the countercurrent flow in NWPC and subsequent flow increases on the east side of Transect D off Palm Beach. If this were true, then the gyre/offshore meander over the Pourtales Terrace could be directly responsible for the eddy motions in SC and NWPC and accelerations in the flow on the east side of the northern Florida Straits. This indicates that the ultimate forcing mechanism would be the large-scale meanders off the Tortugas, or in other words, the position and orientation of the Loop Current as it enters the southern Florida Straits.

The dominant period of the meandering mode in the northern Straits falls within a 3-day to 3-week band and can be due to inherent barotropic or baroclinic

instabilities of the flow and density fields (Boudra, Bleck and Schott, 1987 and 1988), flow over topographic features such as the Miami Terrace (Lee and Mayer, 1977), and along-channel wind forcing (Brooks and Mooers, 1977a and 1977b). This meandering mode produces an out-of-phase relationship in downstream currents on either side of the axis and in-phase temperature change across the flow. Cold, cyclonic frontal eddies are formed together with growing offshore meanders as part of the baroclinic instability process (Lee, 1975; Lee and Mayer, 1977; Lee, Yoder and Atkinson, 1991). These features have dimensions of 10's of km and travel downstream at a mean speed of about 30 km day^{-1}. The passage of a frontal eddy can produce large current variations and even current reversals on the shoreward side of the FC, coupled to cold anomalies from upwelling in the cores of the features.

Local along-channel winds from synoptic weather events can generate significant fluctuations in FC volume transport. A northward wind over the northern Straits can cause an increase in transport and a southward wind a decrease. Eastward/westward winds over the southern Straits have a similar effect. This is a barotropic process in which uniform along-channel flow is accelerated due to cross channel interior flows adjusting to surface Ekman transports in a channel where there is a two-sided coastal constraint ($U = 0$ near the coasts). This process causes simultaneous divergence and convergence at the channel boundaries (Lee and Williams, 1988). The sea surface then adjusts geostrophically to the developing along-channel transport. Bottom friction appears to be insignificant so that the transport response will continue until the wind forcing changes. Along-channel winds observed at coastal sites from Palm Beach to Key West during the one year of moored observations were most energetic in a period band of 7 to 10 days. Variance of downstream volume transports derived from moored current meters and submarine cable voltages was mostly associated with the long-period meander time scale of 30 to 80 days for transects in the southern Florida Straits, whereas in the northern Straits energetic transport fluctuations occurred at periods of about 10 days and greater than 30 days. Transport fluctuations were highly coherent with along-channel winds in the 7- to 10-day period band at all transects, with transport lagging by about 2 days for the northern sections and about 0.5 days for the southern sections. There was also significant coherence between transport fluctuations in the Northwest Providence Channel and the along-channel winds at periods of 7 to 8 days.

The lower Keys region appears to be a preferred area for onshore surface flows due to the prevailing westward winds and coastal gyre circulations. The combination of the offshore eastward jet, coastal gyres and prevailing westward winds in the lower Keys can enhance onshore Ekman transports. North of the lower Keys, coastal gyres do not occur due to the narrowing of the channel, and the prevailing southeast winds no longer cause onshore Ekman transports due to the change in orientation of the SoF from east/west to north/south.

V. SECTIONAL VELOCITIES AND TRANSPORT

5.1 Introduction

An important component of the present study was to develop estimates of transports across key sections in the study area, in particular Transects A and D. These data are also to be used to understand better the dynamics of the region and identify some of the conditions which result from various forcing mechanisms that directly affect transport.

The material below presents sectional velocity and transport data obtained by three different methods:

- PEGASUS profiling
- Subsurface, moored current meters
- Cable voltages

Data obtained from each method is presented and discussed.

From this chapter it should be apparent that the program objectives of documenting and understanding transport patterns have been accomplished.

5.2 Velocity and Transport Based on PEGASUS Technology

5.2.1 Velocity Cross Sections

As part of the Straits of Florida Physical Oceanography Study, PEGASUS acoustic ocean current/temperature profiler stations were occupied along each of three sections (Transects B, E and F in Figure 1.1-1; Stations X1-X17 in Figure 5.2-1) during four seasonal cruises. Although a number of previous experiments have obtained data in the FC proper, such as along Transect B (Leaman et al., 1987), only one previous experiment by Richardson and Finlen (1967) reported transports in the NWPC (Transect E). Virtually no significant amount of data had been collected in SC (Transect F) prior to this experiment.

Discussed below are "average" cross sections of temperature and velocity components normal and parallel to the section. The order of presentation is by section (NWPC or Transect E, SC or Transect F, and Transect B), by cruise (Cruise I-IV) within each section, and velocity normal, velocity parallel and temperature for each cruise. Cruises spanned the following dates:

Cruise I:	November 19-29, 1990
Cruise II:	February 23 - March 2, 1991
Cruise III:	May 28 - June 2, 1991
Cruise IV:	September 6-12, 15-21, 1991

The following points are relevant to this discussion of sectional transports:

- Observations in NWPC were not made during Cruise 3 because of vessel problems.

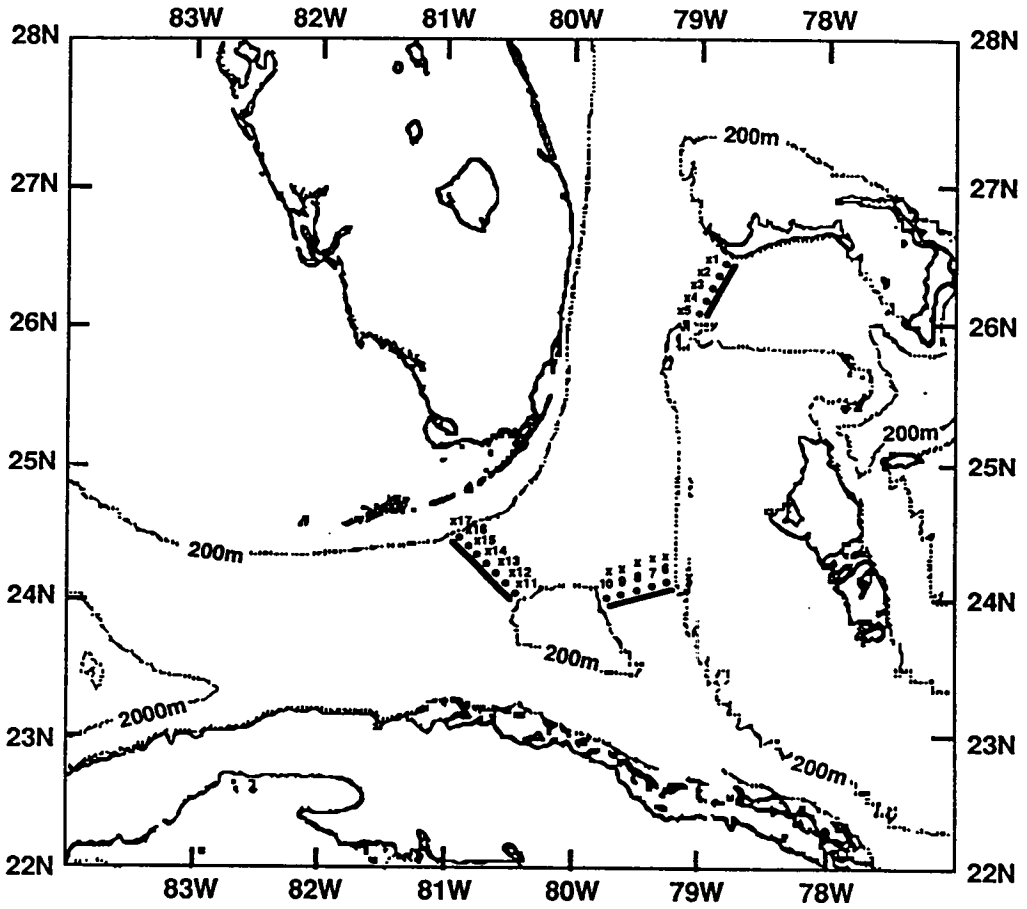

Figure 5.2-1 Area maps showing PEGASUS station locations and identifiers.

- During Cruise II, Station no. 17 was deployed (Note the change in horizontal scale from Cruise I to Cruise II on Transect B).

- Positive velocities normal to the sections are directed downstream in the FC (Transect B) or toward the FC in the subsidiary channels (NWPC, SC). Positive velocities parallel to the sections are 90° to the right of the directions given above for the normal velocity components.

- The type of averaging used is section dependent. On NWPC, where the semidiurnal tide dominates, samples were obtained over one (Cruises I, II) or two (Cruise IV) semidiurnal cycles and averaged. This procedure tends to eliminate or substantially attenuate the tidal component of transport. In SC, where diurnal tides predominate, such samples were taken over two semidiurnal (one diurnal) cycles at each station and averaged, thus tending to remove the diurnal tidal energy. (Note, however, that because of the time required to deploy transponders on Cruise I, only a single section could be made on SC). This type of averaging was not feasible on Transect B because of the greater depths (longer profile durations) of the southeastern stations. Therefore, it was decided simply to make as many crossings of the section as possible in a "zig-zag" pattern and average the results. On Cruises I, II, III, and IV a total of 2, 4, 2 and 4 such crossings, respectively, were made. These field procedures are discussed further in the Program Data Report (SAIC, 1992).

5.2.2 Average Velocity/Temperature Cross Sections

5.2.2.1 Northwest Providence Channel (Figures 5.2-2 through -4).

In general, considerable variability is observed in the current structure on these sections, and the total downstream transport is small relative to the total of the GS/FC. The most clearly defined features of the normal velocity component are the strong (35 cm s^{-1}) core of flow into the FC at depths of 200-300m during Cruise IV and the strong flow to the southeast in the upper 150m, which was observed during Cruise II. The latter is of particular interest in that it is confined to the northern part of NWPC (south of Grand Bahama Island). This feature may be similar to previous observations (Leaman and Molinari, 1987), which showed that during certain periods a westward shift of the FC core could actually induce a southward (i.e. against the FC) current in the upper 100-200m within 20-30 km of Little Bahama Bank. This phenomenon was attributed to the reverse baroclinicity commonly found on the eastern side of the FC and was traced (using shipboard ADCP's) part-way around the island and into NWPC. During these periods large (≈20 km) vortices, which break away from the island and propagate into NWPC, were clearly visible in sea-surface SAR images.

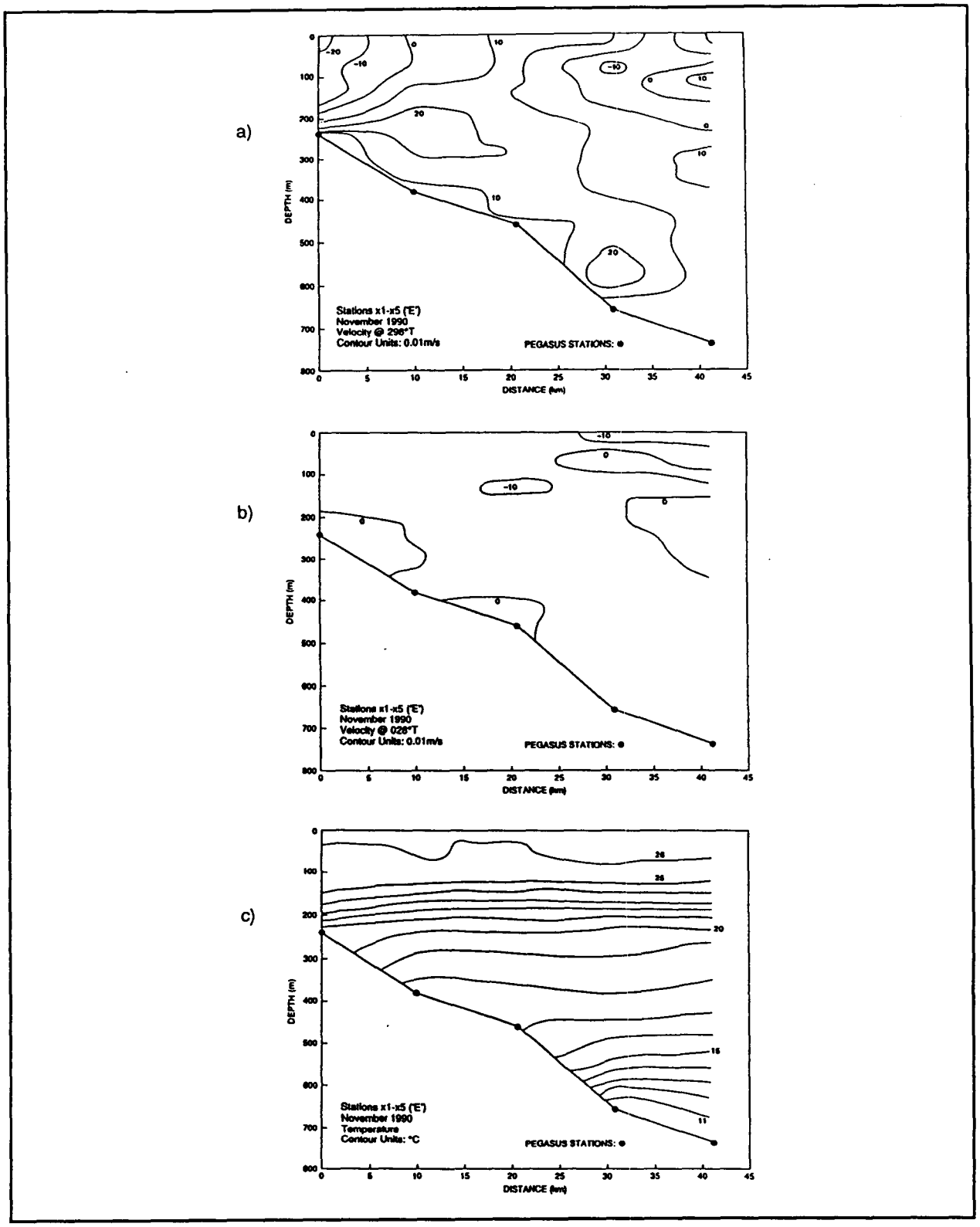

Figure 5.2-2 Average velocity component normal (a) and parallel (b) to Section E, and temperature (c): November 1990.

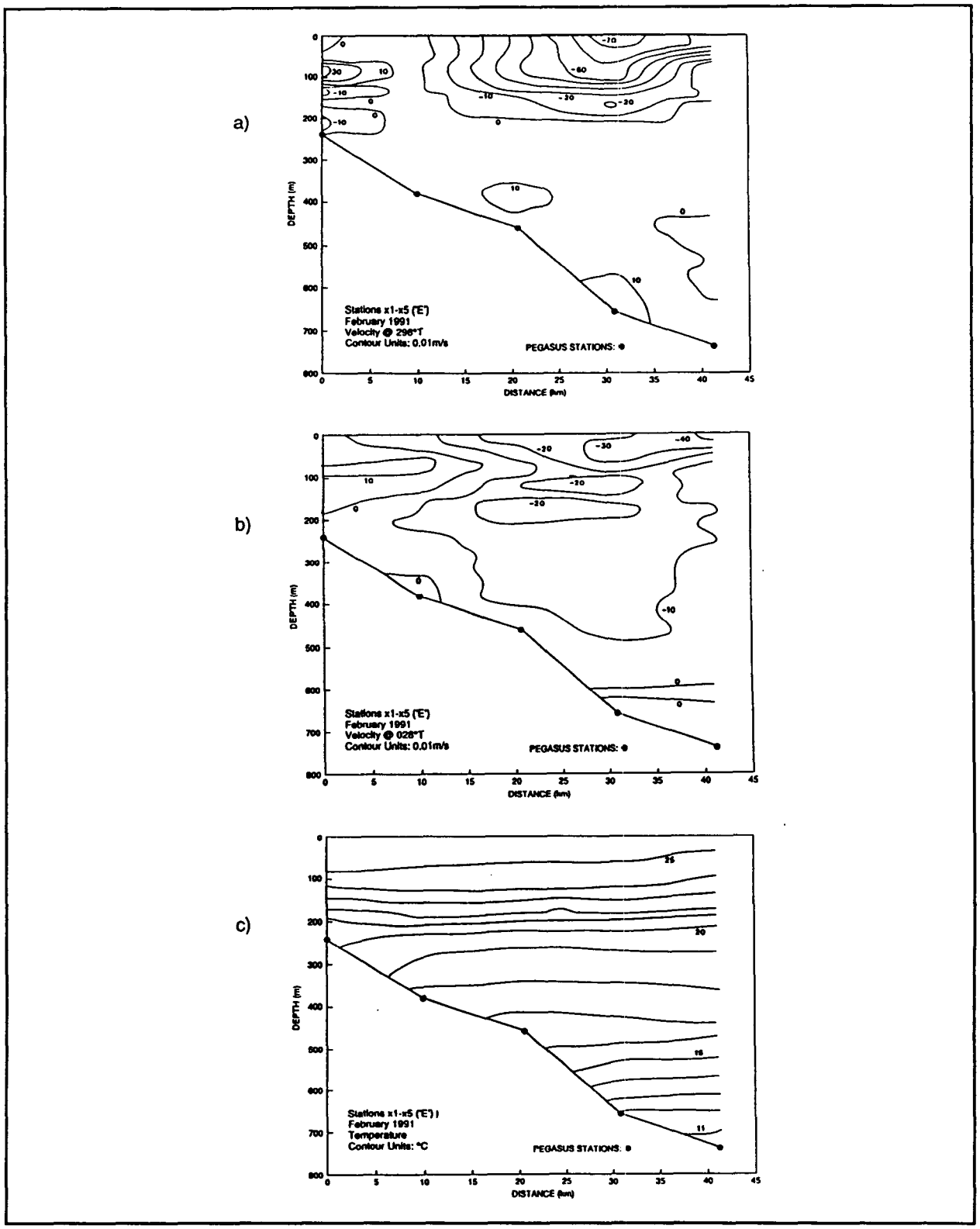

Figure 5.2-3 Average velocity component normal (a) and parallel (b) to Section E, and temperature (c): February 1991.

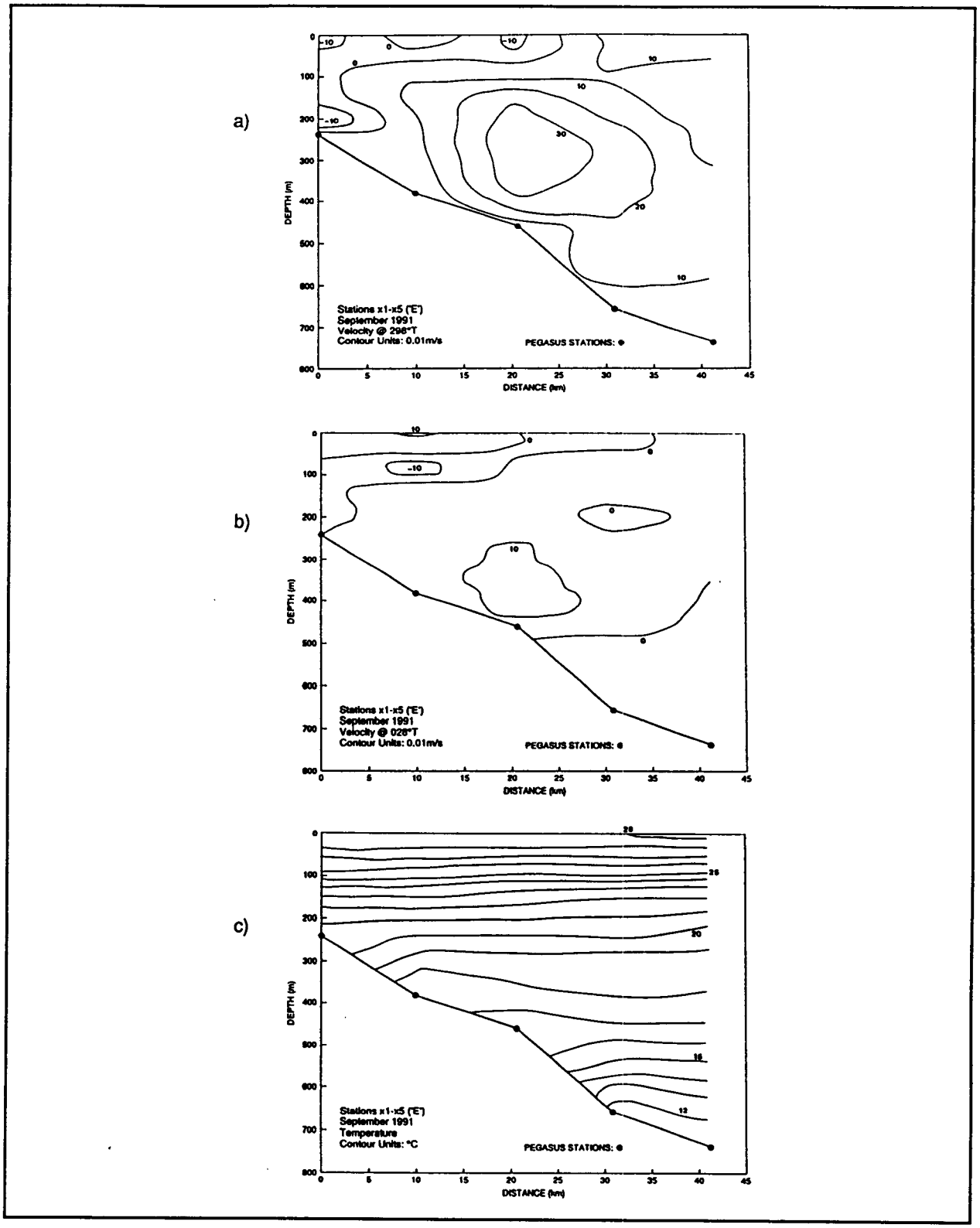

Figure 5.2-4 Average velocity component normal (a) and parallel (b) to Section E, and temperature (c): September 1991.

The lack of strongly tilted isotherms in these sections nevertheless suggests that the baroclinicity of the geostrophic current is not pronounced. At the northern (deepest) side of the channel, bottom temperatures are >11°C at depths of 750m, which is warmer than the bottom temperatures (≈7°C) observed at similar depths in the FC to the west (Leaman, et al., 1987). In all sections a fairly clearly defined thermostad is present in the 18°C water, suggesting a westward transport of this water, on average, from the North Atlantic. Water with this low potential vorticity (f/thickness, where f = Coriolis parameter) is typically found only on the extreme eastward side of the Florida Current (Leaman et al., 1989).

5.2.2.2 <u>Santaren Channel</u> (Figures 5.2-5 through 8).

Compared to the FC, relatively striking changes were observed in the low-frequency current and temperature structure in SC. These are mirrored as well in large transport variations. Cruise I (Figures 5.2-5a-c) is somewhat difficult to interpret since as a single section, tidal velocities have probably not been completely removed. These observations show a relatively large (≈4 Sv) transport into the FC; this transport is confined to the eastern side of the channel. Of particular interest is the bottom layer, which is significantly colder (2-3°C) than the other SC sections, with a bottom inversion at stations X7, X8 and X9. Given the large flow to the northwest near the bottom (Figure 5.2-5a), it is probable that this colder water has been advected "uphill" into the area from deeper regions of OBC. In comparison, the average depth of 8°C water in the FC is about 600m. (Leaman et al., 1987).

During each cruise, section-normal velocities showed a bimodal structure so that some flow was into the FC and some was to the southeast. During Cruise I, this separation occurs in approximately mid-channel and extends from the surface to the bottom (note zero velocity isotach). The substantially larger currents directed into the FC (on the right or east side) dominate the magnitude and sign of transport. These velocities in combination with section-parallel velocities tend to show a rotational sense.

During Cruise II (February, 1991), the partition of section-normal velocities were of substantially lower magnitude (Figure 5.2-6). The higher speed core was to the east of the channel center and subsurface (≈ 150-250m). Section-parallel velocities show a somewhat similar pattern with westward currents above 200m in the western two thirds of the channel and eastward currents below 200m or on the eastern side of the channel.

Section-normal currents reversed during Cruise III (Figure 5.2-7a). The northward currents are again subsurface but on the western side of the channel. Southward currents are predominantly above 100-125m. The zero isotach is nearly horizontal. On the west side of the channel the section-parallel velocities are directed to the west with the core maximum at about 250m. Note that westward currents occurred at almost all locations. These velocity components combine to produce generally southwestward currents in the upper layer and generally northwestward currents below approximately 125m.

During the final cruise (Figure 5.2-8) most locations experienced flow to the south away from the FC. These negative, normal velocities dominated the section. The maximum along-channel velocity descended from near-surface (≈ 50m) in the east to 200-300m approximately 10 to 20 km from the western margin. The

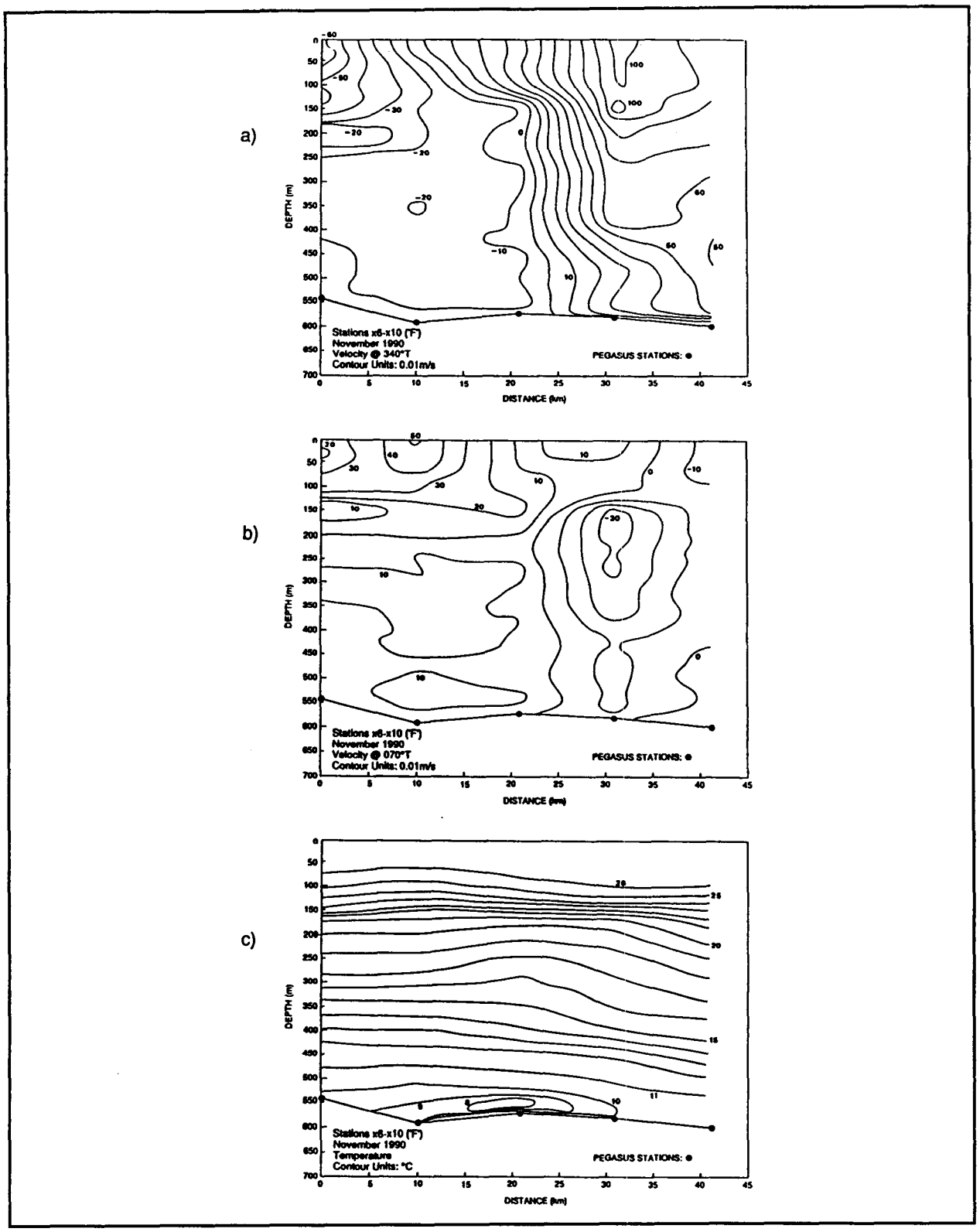

Figure 5.2-5 Average velocity component normal (a) and parallel (b) to Section F, and temperature (c): November 1990.

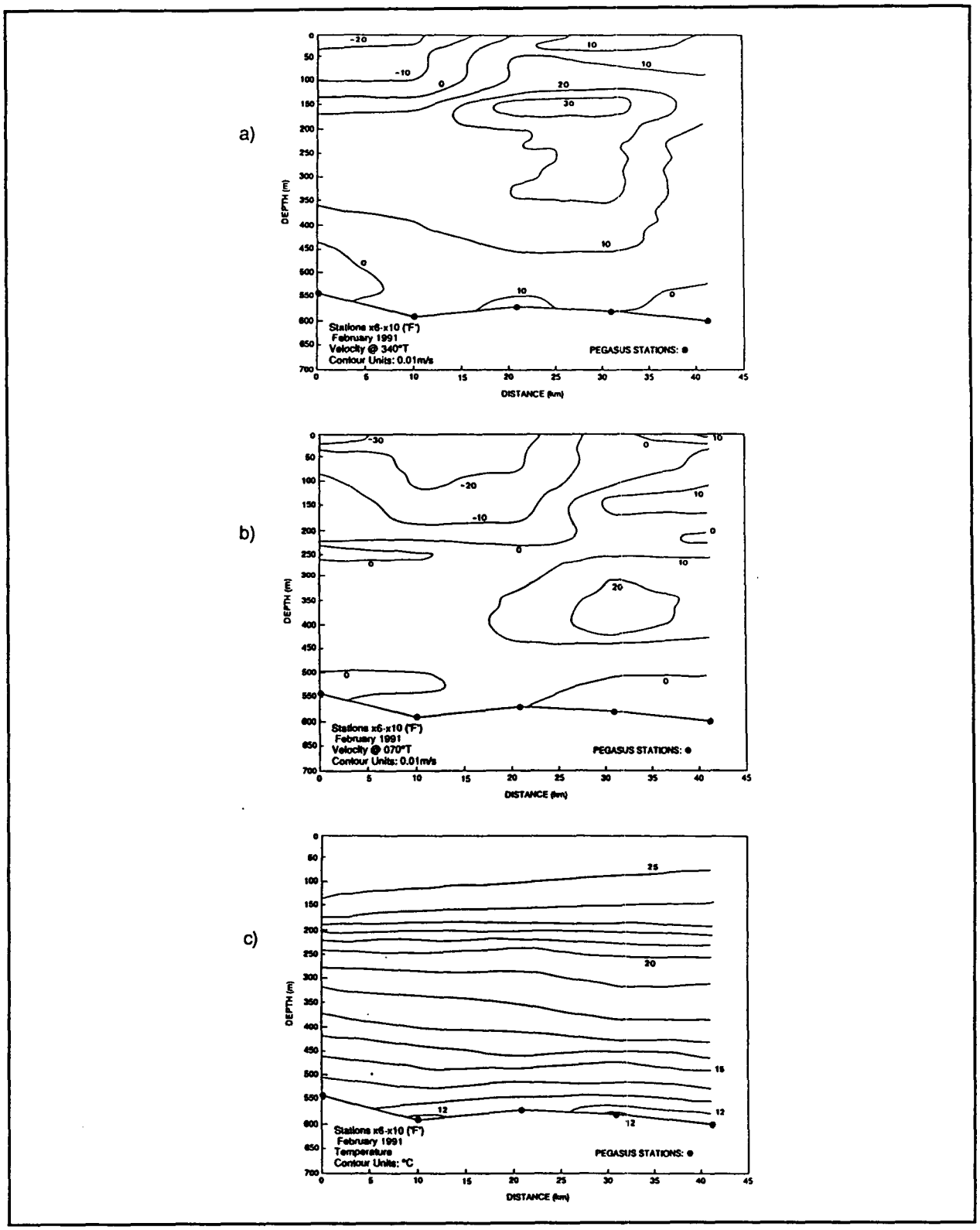

Figure 5.2-6 Average velocity component normal (a) and parallel (b) to Section F, and temperature (c): February 1991.

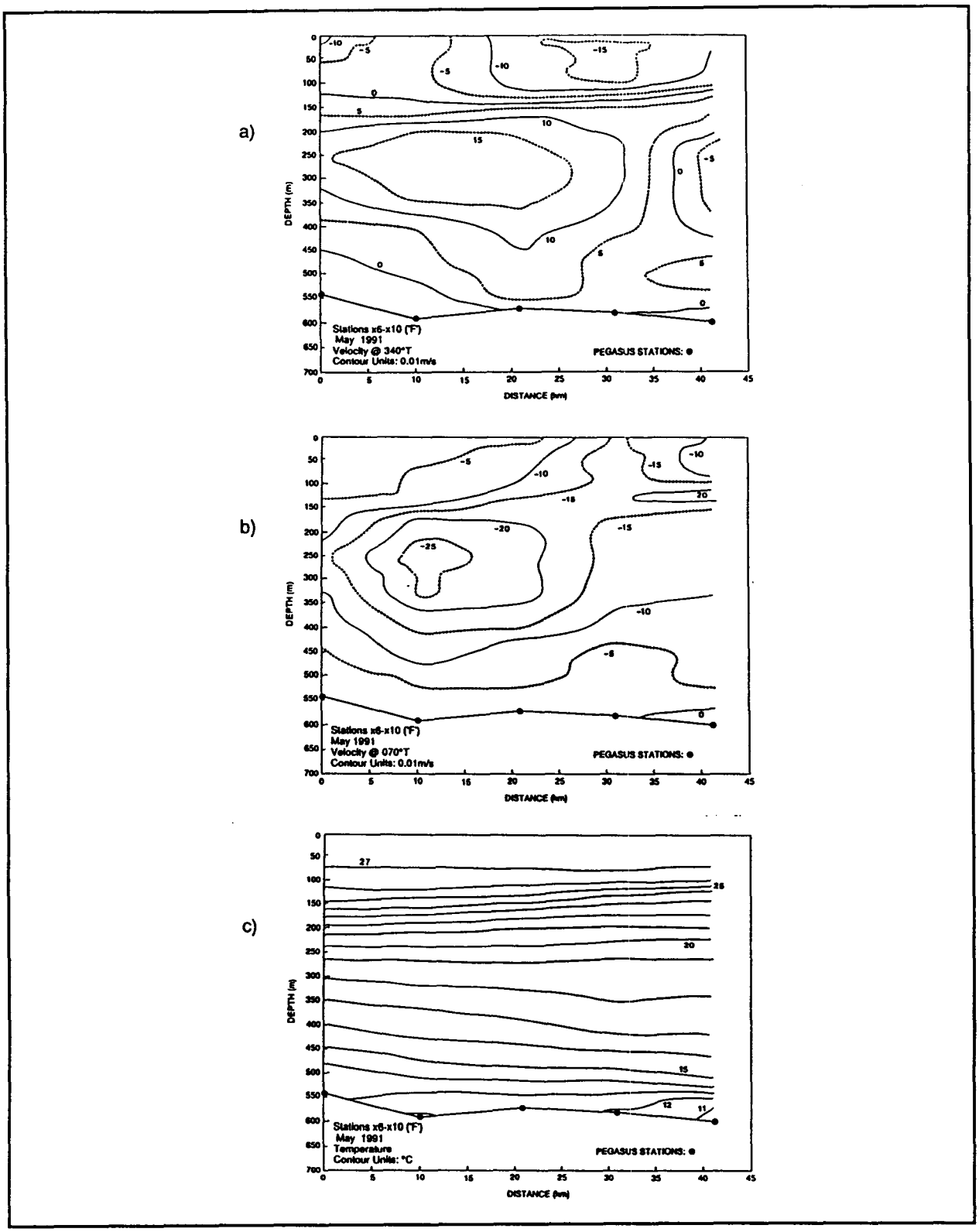

Figure 5.2-7 Average velocity component normal (a) and parallel (b) to Section F, and temperature (c): May 1991.

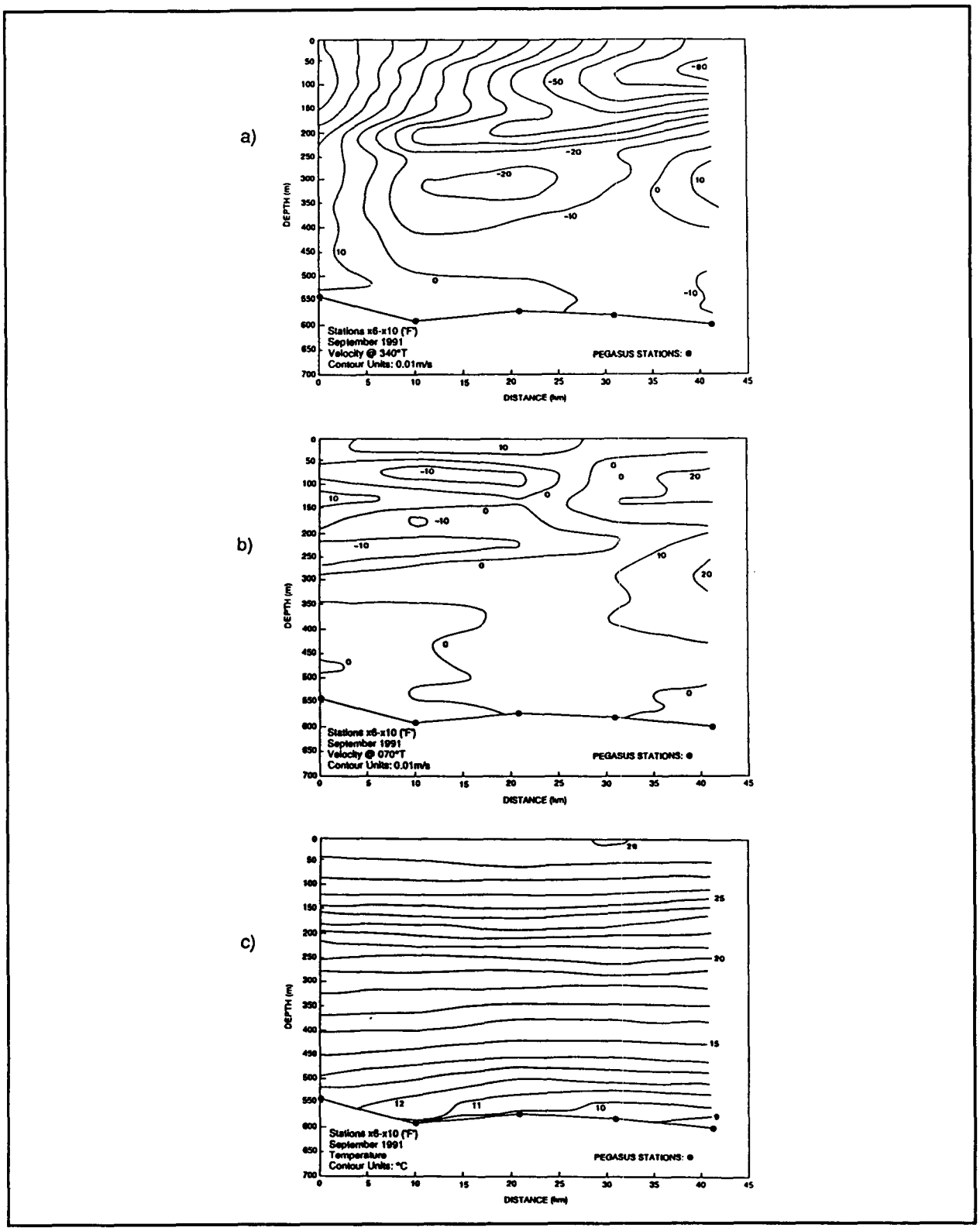

Figure 5.2-8 Average velocity component normal (a) and parallel (b) to Section F, and temperature (c): September 1991.

magnitude of northward currents (toward the FC) were generally weaker and occupied considerably less sectional area. The section parallel velocities were weak and showed no consistent spatial pattern.

Large variations in the amount of 18°C water could also be observed in this section. During the winter and spring cruises (II, III) a relatively thick 18°C layer (low potential vorticity or f/thickness values) could be seen extending almost the whole width of the section. In contrast, the late summer (Cruise IV) section showed virtually no excess 18°C water. The section taken during the fall (Cruise 1) was more difficult to interpret since it appeared that the isotherm (density) contours were strongly distorted by the large current shears observed at that time. However, there did appear to be a distinct spreading of the 17°C through 19°C isotherms in the eastern half of the channel.

An explanation for this variability may be associated with the downstream flow patterns at this level (roughly 300m) if it is assumed that a pool of 18°C water is present to the southeast in OBC. During Cruises II and IV flow of this level was generally to the northwest except for a small region near Great Bahama Bank during Cruise III; this would suggest that advection there was bringing in 18°C water from the southeast. In contrast, during Cruise IV, advection at this level was southeastward, and no 18°C water was observed. Cruise I may be an intermediate case.

5.2.2.3 Transect B (Figures 5.2-9 through 12).

Maximum section-normal velocities of 130-140 cm s^{-1} consistently occurred at or near the surface during three of the cruises. During Cruise II (Figure 5.2-10) maximum currents were approximately 170 cm s^{-1}. Essentially all velocities were directed downstream with no evidence of counter currents at any depth.

Large lateral shifts in the position of the near-surface (upper 200m) downstream velocity core are a major feature of these sections. In late fall (Cruise I; Figure 5.2-9a) this core is far to the southeast and appears to contact Cay Sal Bank. Through the winter and spring (Cruises II, III; Figures 5.2-10, and 5.2-11a) the core shifts northwestward into the center of the channel, and by late summer (Cruise IV; Figure 5.2-12a) the core is up against Pourtales Terrace. During the winter months, warm core temperatures at the surface tend to follow the velocity core, but by late summer there is little contrast in surface temperatures across the FC. The thin layer of surface water with temperatures >29°C at the southeastern end in September (Figure 5.2-12c) may have been blown off Great Bahama Bank by the persistent southeast trades during this time. Deeper, the downstream velocity core also changes seasonally and is related to shifts in the surface core. Deep isotachs to the southeast are much "flatter" (horizontal velocity gradients are less) during periods when the surface core is near Cay Sal Bank.

It should be noted that significant positive velocities are present throughout all sections in the velocity component parallel to the section (Figures 5.2-9b through 12b). This results in part because the section is not strictly perpendicular to the bottom topographic contours (Figure 1.1-1), but also because the flow tends to "point" toward Cay Sal Bank, rather than following the bottom topographic contours precisely.

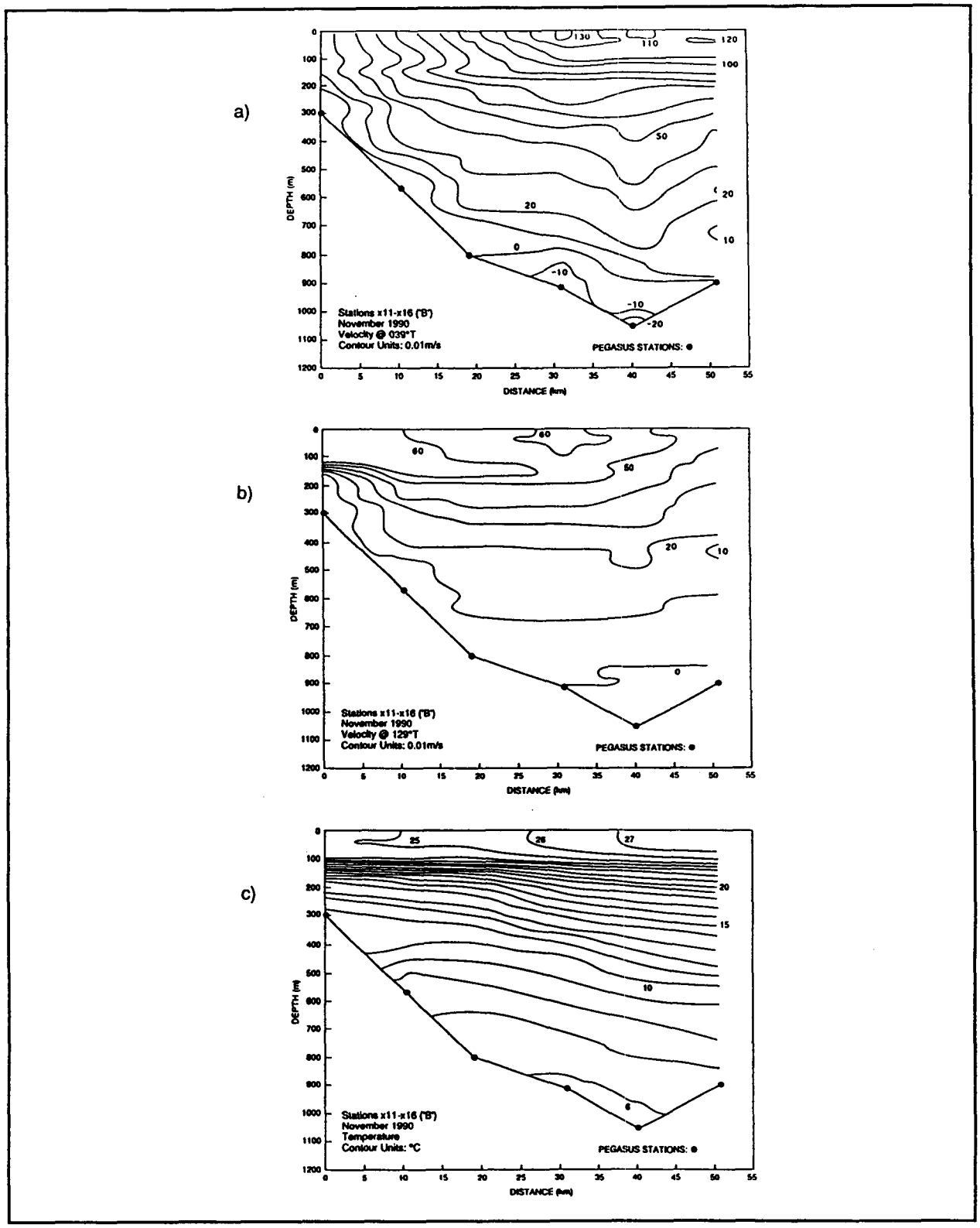

Figure 5.2-9 Average velocity component normal (a) and parallel (b) to Section B, and temperature (c): November 1990.

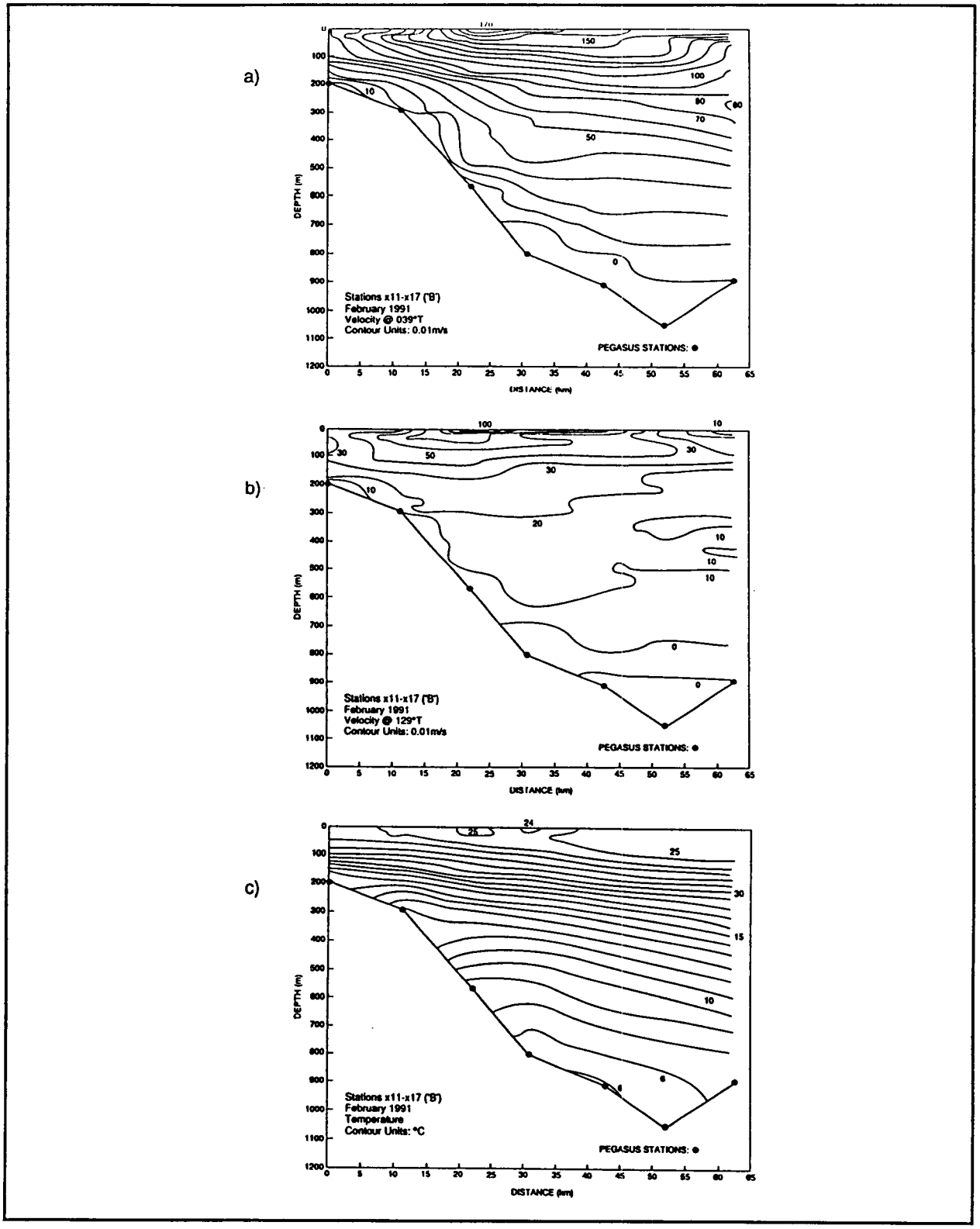

Figure 5.2-10 Average velocity component normal (a) and parallel (b) to section B, and temperature (c): February 1991.

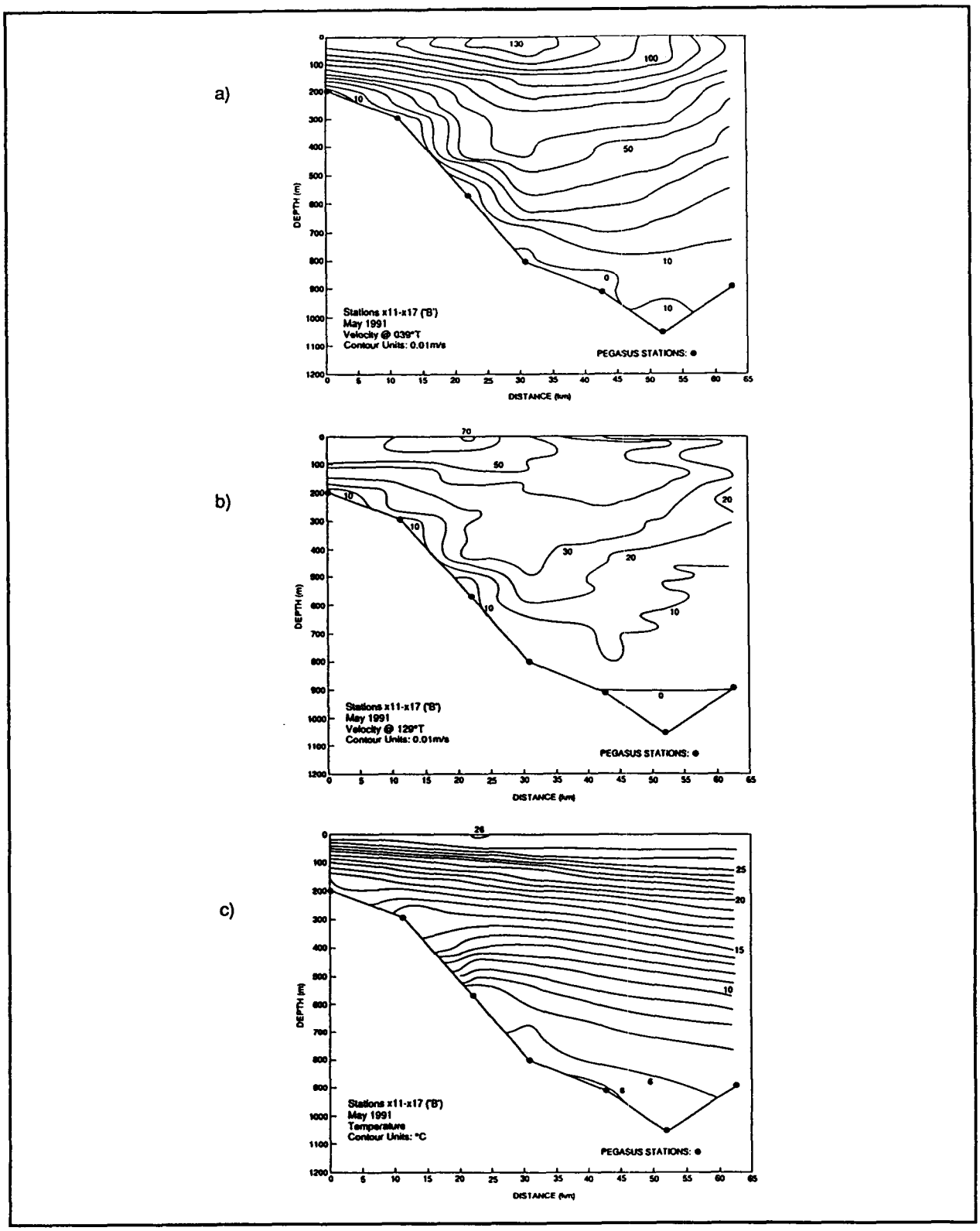

Figure 5.2-11 Average velocity component normal (a) and parallel (b) to Section B, and temperature (c): May 1991.

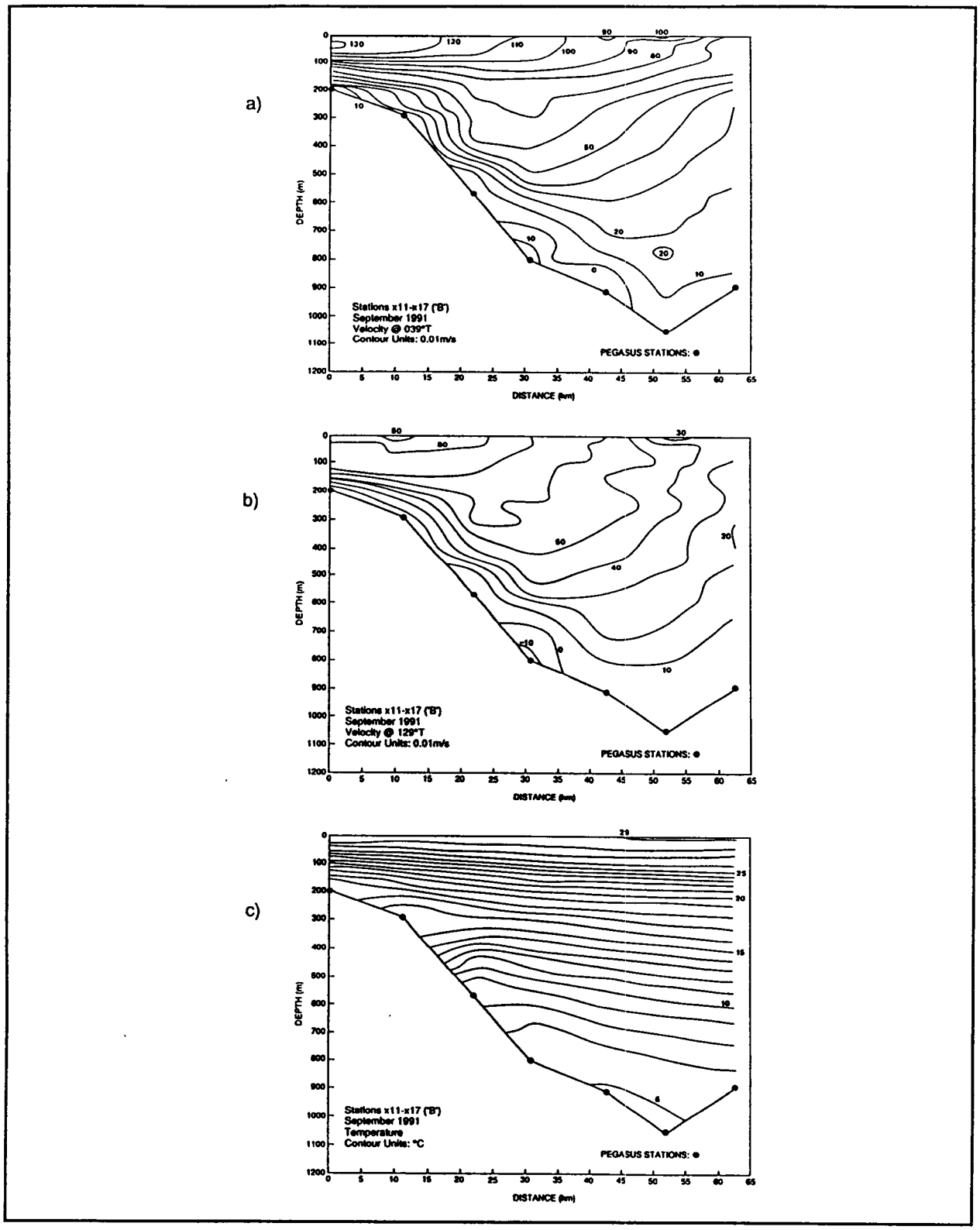

Figure 5.2-12 Average velocity component normal (a) and parallel (b) to Section B, and temperature (c): September 1991.

There is little indication of a thicker layer of 18°C water in any of these sections and in particular near the eastern boundary (Cay Sal Bank). This is in marked contrast to what is seen farther north (Leaman et al., 1989) where such a layer is clearly present and extends at least 20 km into the FC.

5.2.3 Transports

Section-normal average transports on each cruise for each section are given in Table 5.2-1.

Table 5.2-1 Average Sectional Transports

Cruise	Transect	Transport ($x10^6 m^3 sec^{-1*}$)
I	NWPC (E)	1.77
	SC (F)	4.88
	B	16.95
		23.20
	TOTAL	**[23.93]****
II	NWPC (E)	-0.76
	SC (F)	2.44
	B	22.44
	TOTAL	**24.12**
III	NWPC (E)	-----
	SC (F)	0.94
	B	23.10
	TOTAL	**24.10**
IV	NWPC (E)	2.72
	SC (F)	-3.86
	B	20.62
	TOTAL	**19.48**

* $10^6 m^3 sec^{-1}$ = 1 Sverdrup

** For Cruise I, the [] number includes the average transport increase (as determined from the other three cruises) due to inclusion of Station X17.

The average section transports are thus: NWPC = 1.24 Sv (three cruises); SC = 1.00 Sv; B = 20.96 Sv for a total of 23.2 Sv. Although this is significantly less than the total average transport of 31.7 Sv at 27°N (Leaman et al., 1987) in the FC it must be remembered that these transports are only computed between

the end-point stations of each section, whereas the STACS data were extrapolated to the boundaries. If each end-point station (X1, X5; X6, X10; X11, X17) is extrapolated to the nearest boundary using a simple "box" extrapolation the average total transport will be increased by about 8 Sv. Of this, the largest contribution (about 4 Sv) comes from X11, because of the large depth and depth-averaged velocity there, with smaller contributions from X17 (about 2.9 Sv) and X6 (about 0.8 Sv). The X17 "extrapolation" is clearly an estimate because of uncertainties as to the total transport over Pourtales Terrace. Nevertheless, the total average (extrapolated) transport for these sections is 31.2 Sv, which within the experimental limits agrees well with that seen previously at 27°N. (Projecting the Transect B velocities onto a "synthetic" section that is normal to the average downstream flow direction also results in a slight downstream transport increase).

5.2.4 Comparison To Other Observations

To gain a more complete picture of regional circulation patterns, it is useful to correlate these data with other observations obtained either previously or as part of this experiment.

Turning first to NWPC, the average total transport into the FC from these PEGASUS sections is in reasonable agreement with the values of 1.5-2.5 Sv obtained by Richardson and Finlen (1967). However, the actual current structures seen (Figures 5.2-2 through 4) can show a marked variance from the general comment made by these authors that "easterly flow was observed on the southern side of the channel and westerly flow on the northern side...". It is also clear that local features can dominate the current field on occasion. For example, the alternating velocity cells in the upper 80m seen during Cruise IV (Figure 5.2-4a) are strongly suggestive of the small-scale vortices (0 - 20 km) seen in previous data (Leaman and Molinari, 1987). Such vortices appear to originate from the southwestern tip of Grand Bahama Island and propagate southward across NWPC during periods when the FC is weak and/or displaced to the west.

Two useful hydrographic tracers in this area are the presence (or absence) of the 18°C thermostat and the layer of salty (S>36.9 psu) Subtropical Underwater (SUW) at depths of ≈150m. Both suggest waters of North Atlantic origin, the former formed in the northwestern North Atlantic and the latter in the subtropical North Atlantic to the east-northeast of the Lesser Antilles (Worthington, 1976). During this experiment (and discussed elsewhere), five hydrographic cruises were carried out: Cruise 90-35 (20 November - 7 December, 1990), Cruise 91-03 (15 February - 1 March, 1991); Cruise 91-12 (2 May - 17 May, 1991); Cruise 91-17 (18 August - 29 August 1991); Cruise 91-20 (11 November - 18 November, 1991). (The first two cruises are more-or-less simultaneous with PEGASUS cruises I and II.) All CTD and PEGASUS sections show the presence of a substantially thick layer of 18°C water in NWPC. Given the relatively weak 18°C layer usually found on the eastern side of the FC to the north (Leaman et al., 1989), this at least suggests there is no strong net inflow to the FC via NWPC, in agreement with the average transport obtained there.

Indications of SUW are perhaps more revealing. For those cruises where salinity data from NWPC were available, SUW was only weakly present during 91-03, corresponding to a period of upper layer flow away from the FC (Figure 5.2-3a). During two cruises (91-12, 91-20 - neither simultaneous with PEGASUS data) a parcel of SUW (S>36.9 psu) was present, but only in a small area in the center

of the channel, indicating that SUW was only intermittently carried this far west into NWPC.

In SC somewhat the reverse situation holds. Most cruises with salinity data showed a sharply defined SUW layer (S>36.9 psu) concentrated on the eastern side of the channel. The presence of a similar layer at the eastern end of Transect C would suggest either a) advection from Transect B to the northeast, or b) advection north from SC into the FC. During CTD Cruise 90-35 (PEGASUS Cruise I), for example, Transect B showed only a weak (S≤36.8 psu or less) salinity maximum whereas both SC and Transect C showed a strong SUW peak. This indicates advection of SC water into the FC and is consistent with the large downstream velocities observed in the eastern half of SC during the first PEGASUS cruise (Figure 5.2-5a). In contrast during the second simultaneous cruise pair (PEGASUS Cruise II; CTD cruise 91-03), Transects B and C both showed only a weak SUW layer whereas a strong SUW salinity peak was still present in SC. During this time northward flow in SC had appreciably weakened (Figure 5.2-6a). The 18°C layer, however, was quite variable, being present during CTD Cruises 91-03, 91-12 and 91-20 and weak or absent during Cruise 91-17. During the first CTD Cruise (90-35) the layer appeared mainly on the eastern half of SC. For the first two (simultaneous) cruises, these results were in agreement with the PEGASUS temperature sections (Figures 5.2-5c, and 6c).

All CTD sections along Transect B showed only a weak 18°C thermostad, if any (again in agreement with the PEGASUS sections). This, combined with the SC data, suggests that a primary source of the 18°C low-potential vorticity layer that appeared (intermittently) to the north on the eastern edge of the FC must have been SC inflow, although the amount was small given that the total SC transport into the FC appeared to be only 1-2 Sv. This is in agreement with previous studies (Leaman et al., 1989), wherein it is argued that the "excess" 18°C water appearing on the eastern side of the FC farther north (27°N) contributes only about 1 Sv to the total transport.

Finally, it is of interest to compare the relative amounts and intensities of SUW observed in these passages to the distribution of SUW in the tropical and subtropical North Atlantic Ocean. Worthington (1976) indicates that the 36.9 psu SUW contour intersects the Greater Antilles island arc near the eastern end of Hispaniola (i.e. the far eastern end of Old Bahama Channel). As one moves to the northwest along the Bahamas, salinities in this layer decrease until values of about 36.7 psu are reached in the NWPC. Keeping in mind that this is no doubt a highly smoothed contour map, the CTD and PEGASUS observations clearly are consistent with advection of SUW northwestward along Old Bahama Channel.

It appears that at irregular intervals (e.g. Cruise 91-17) high salinity SUW can also appear at the eastern end of Transect B. It is probably unlikely that this water arrived there after traversing the entire Gulf of Mexico Loop Current System, which leaves the possibility that it was advected to the west between Cay Sal Bank and Cuba and then was carried northeastward in the FC to Transect B, rather than flowing through SC. This type of alternation in transport between SC and Transect B may explain the negative correlations found in transport variations through these two sections.

The high (S>36.9 psu) SUW values infrequently found in NWPC are somewhat surprising since open ocean values at that latitude are typically 0.2 psu--0.3 psu lower. Either parcels of SUW are intermittently carried via the Antilles

Current northwestward towards NWPC or remnants of SUW are entrained in the small-scale vortices as the FC passes NWPC.

5.3 Transport Estimates Based on Current-Meter Data

5.3.1 Methods of Estimation

The subtidal volume transports for each section were calculated based on a general method developed for the STACS program. The 40-HLP records of the along-channel velocity component and depth of the instrument were obtained for all the current meters in a section. On most moorings, the near surface current meter on each string recorded pressure. However, on some deployments, the pressure sensor gauges may not have functioned properly or instruments without pressure sensors were used. The missing pressure records were synthesized for the near-surface instruments by using a linear regression of pressure against the square of the current speed. For the overlapping part of the records, the synthetic pressure correlated with measured record with $R^2>0.9$. Figure 5.3-1(d) shows a synthetic and measured pressure record for the 145m instrument on D1. The mid-depth instruments' pressure was estimated from the observed or synthetic records of the near surface instrument multiplied by a factor d_i/d_m, where d_i and d_m are the heights of the instrument and the near surface instrument above the bottom, respectively, with the mooring slack. Below 300m, the depth variations of the instruments caused by mooring tilt were less than 5m and were neglected. The design or nominal depth was used in these cases.

Once pressure records had been constructed for each instrument, the along-channel velocity (V) profile was interpolated through the water column for each mooring using splines under tension with a moderately strong tension factor. The bottom boundary condition was assumed to be V=0 and the surface velocity was found by extrapolation to the surface using the subsurface values. Where the near surface current meter was deeper than 145m, an additional constraint, $\partial V/\partial z = 0$, was assumed at the surface so as to give more realistic surface current values. The interpolated profiles were resampled at 10m intervals, and for each 10m level the cross sectional profile was horizontally interpolated using splines under tension at 5-km intervals (3 km for Transect E and G) assuming that V=0 at the sides of the channel. The resulting two-dimensional grid of velocity values was summed to generate the transport. The 10m x 5 km area of the grid cell was adjusted, if the cross section was not quite normal, to the along-channel flow direction (e.g. Transect B) by projecting onto the normal direction. Generally a minimum of two current meter velocity values on each string were required for vertical interpolation, and three vertical profiles were required for horizontal interpolation, to produce a transport value at a given time. If this criterion was not met, then a flag value was written to the time series.

Figure 5.3-1 shows the calculated transport (e) and individual 40-HLP along-channel velocity component records (a, b, c) for Transect D. Transports were calculated at six-hour intervals. The time lines for the velocity records obtained for all the sections may be found in the Program Data Report (SAIC, 1992) so that the relative quality of the transport calculations can be estimated by the number of current meters in each section which were operating at any given time.

Transports have been measured from voltages induced in submarine cables. The Jupiter-Settlement Point inactive submarine telephone cable was calibrated

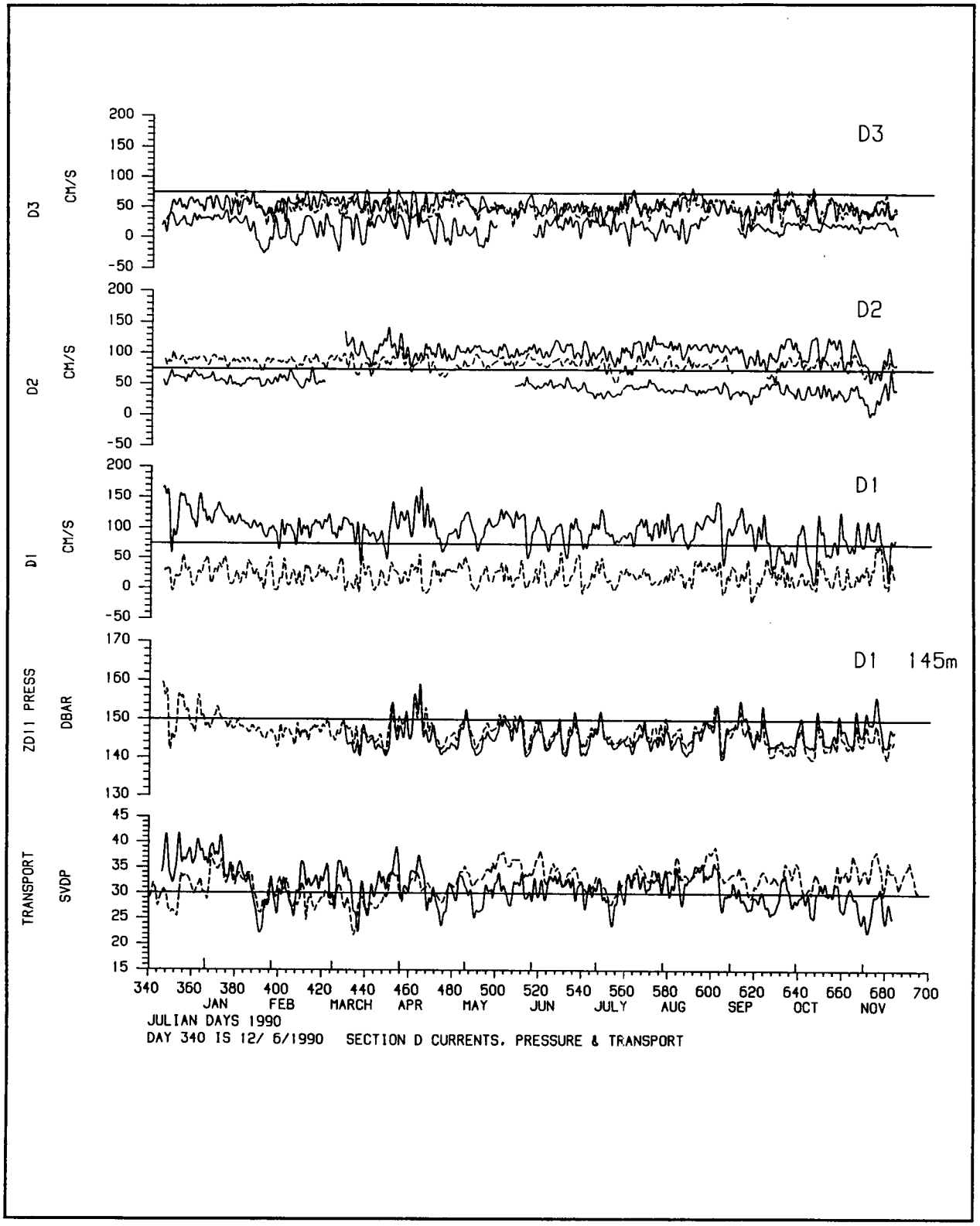

Figure 5.3-1 Time series of along channel velocity components at the indicated depths, the actual (solid line) and estimated (dashed line) pressure used in the transport computation scheme, and transport based on current meters (solid) and the cable (dashed).

against PEGASUS and current measurements on Transect D during the STACS program as described by Larsen and Sandford (1985). When transports derived from daily mean voltages were compared with transport derived from 137 days of PEGASUS profiles, the rms misfit was 0.75 Sv or 2.3% of the mean flow of 32.3 Sv derived from 9 years of daily observations. When the cable-derived transports were compared with current meter-derived transports using five moorings and a calculation scheme essentially the same as described above, the rms misfit was 1.4 Sv (Lee et al., 1985). Decreasing the number of moorings to three increased the rms misfit to about 10% or 3 Sv. Thus, the Transect D current meters cannot be expected to measure transport more accurately than this error estimated from the STACS arrays (Schott et al., 1988).

The Jupiter-Settlement Point cable ceased functioning November 30, 1990. Consequently, the voltage-derived transports for Transect D are based on the voltage from the in-service cable between West Palm Beach and Eight Mile Rock. These voltages were calibrated by comparison with the Jupiter-Settlement Point voltage when both systems were working. These comparisons are discussed in detail in Larsen (1992). He found that the correlation squared between the two transport estimates was 0.60 and the rms misfit 1.9 Sv. Since 1988, daily averaged transport values at the two cables differed by less than 5 Sv. Therefore, the accuracy of the active West Palm Beach - Eight Mile Rock cable is about the same as the current meter-derived transport. Figure 5.3-2 shows the daily transports from the active cable after November 30, 1990 and from the Jupiter-Settlement Point cable prior to this.

Transports for Transect D were obtained from profiling (dropsonde) cruises conducted by NOAA-AOML (Mark Bushnell, personal communication) and these are shown by dots on Figure 5.3-2. It can be seen that in 1990 the dropsonde-derived transports and the Jupiter-Settlement Point cable appear to agree very well. In October and November 1991, they do not agree with the WPB-EMR cable with the apparent decrease in transport at the beginning of November not being reproduced. The current meter-derived transport, however, does show this decrease and correlates better than the cable with the profile-derived transports. It is noted that all eight current meters in Transect D produced good velocity records in October and November, 1991 so that the current meter-derived transports are as good as they can be. The dropsonde cruises took approximately seven hours to make the transect and thus there will be biases caused by the tides of order 1 to 2 Sv (Mayer et al., 1985) in these measurements that are not part of the current meter or cable derived transports. The statistics of the eight cruises and the correlation with the current meter and cable transports extracted for the period of each cruise are given in Table 5.3-1.

An initial visual comparison of the current meter- and active cable-derived transports is given in the time series plots of transport shown in Figure 5.3-3. It can be seen that the higher frequency oscillations (periods less than about 10 days) correspond quite well, but some of the longer period shifts, such as that in November 1991, are not well reproduced. The consistency between current meter and dropsonde-based transports on Transect D would suggest that the cable may be providing the less representative transport estimates. These will be discussed in terms of spectral coherences in the next section.

The transport for Transect A was estimated from an inactive cable between Havana and Key West. This is presented in Figure 5.3-3 and shows considerable differences at times, both in fluctuations and magnitude, from Transect D. The

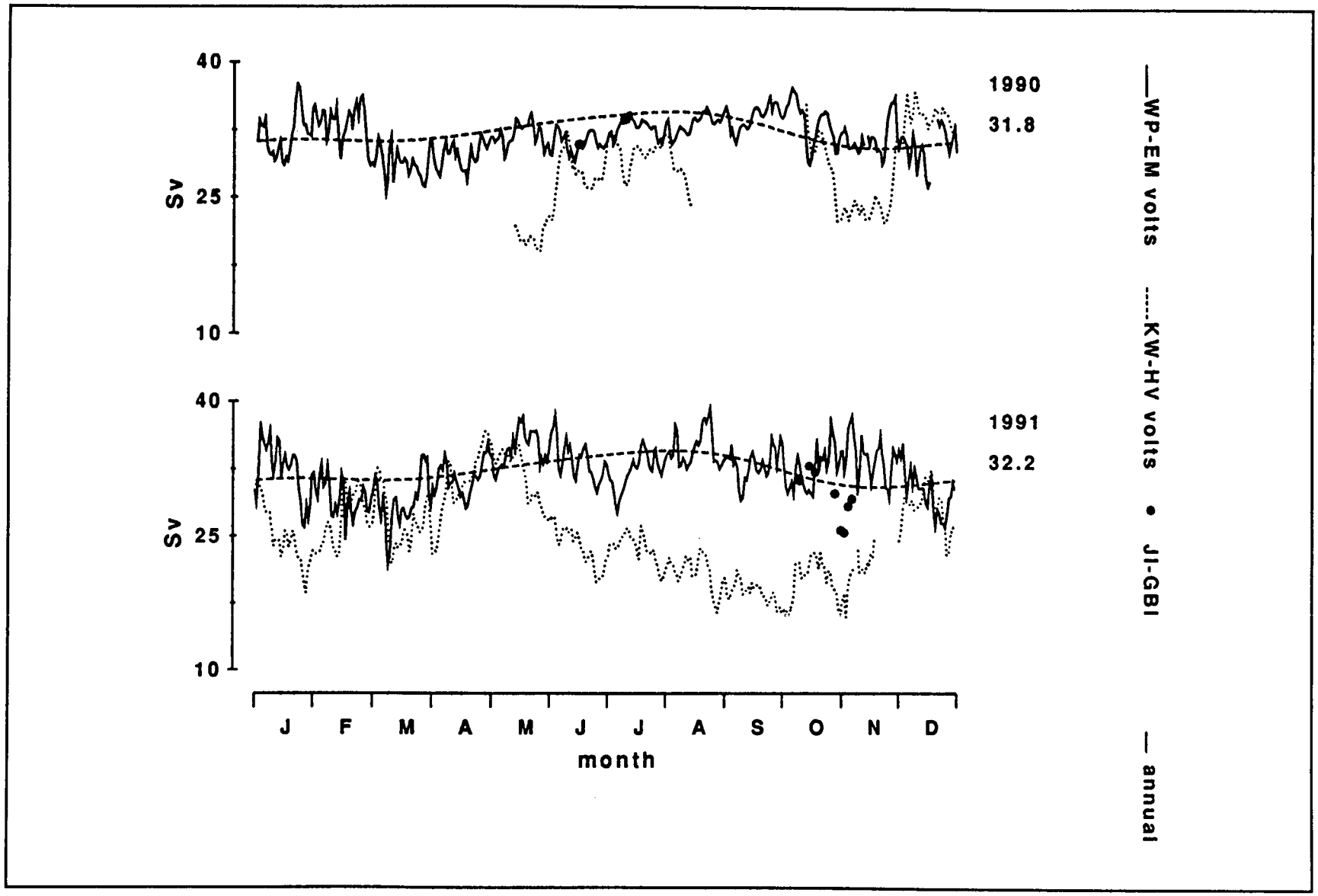

Figure 5.3-2 Time series of transport as based on cable voltages at the north end of the study area (solid line), the west end of the study area (dotted line/Key West to Havana) and the annual signal at the norther line. The larger dots show transports as estimated using Pegasus technology. See text for further information.

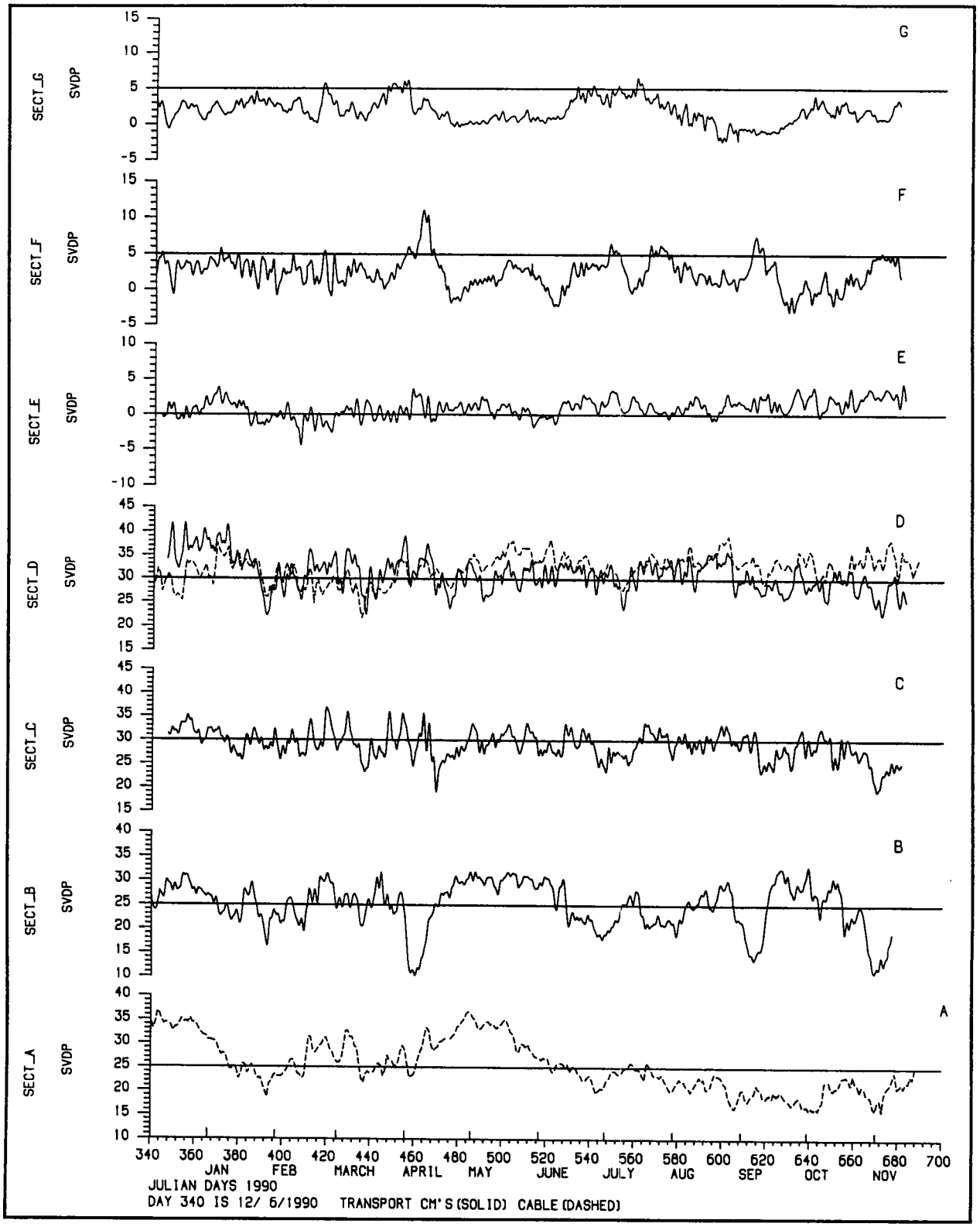

Figure 5.3-3 Time series plots of transport based on current meters (solid lines) and cables (dashed line) on the indicated transects for the period from December 1990 to November 1991.

Table 5.3-1 Comparison of 1991 Transport Measurements. October 10, 15, 18, 28, 31 and November 2, 4, 6 1991.

	TRANSPORTS		
	Profile	Current Meter	Cable
Mean	28.70	27.82	33.91
Standard Deviation	2.97	3.06	2.58
R^2 with Profile Cruises	——	0.69	0.33

calibration factor applied to the Key West Havana cable was 26.0 Sv/Volt. The base level was then adjusted so that the mean transport south of Key West was an arbitrary 5 Sv less than the mean transport east of Jupiter. Model studies show that the calibration factor could lie between 22.9 and 34.5 Sv/Volt (Larsen, personal communication). The arbitrary adjusted level and the best guess calibration factor turn out to produce reasonable agreement with transports calculated from continuity using the current-meter records at Transect B, F and G, and no further adjustments have been made to the transports derived from the Key West-Havana cable voltages. The current meter-derived transports at Transects B, F and G and the comparison with Transect A, derived from cable voltages, will be described in the following section.

5.3.2 Subtidal Transport

Subtidal transports for each instrumented section were calculated from the 40-HLP currents as described in the previous section. The results are given in Figure 5.3-3 which includes the cable-derived transports for Transect A (Key West-Havana) and D (Jupiter-Settlement Point). The time series are about 11 months long. Immediately apparent is the difference in character between the fluctuations in the southern part of the study area and the northern part. Variability on Transects C, D and E is mostly at shorter periods (< 10 days) whereas longer period fluctuations occur on Transects A, B, F and G. Transect B shows at least 3 abrupt decreases to less than 15 Sv, which have corresponding (or compensating) increases at Transect F but little effect on Transect C, implying that part of the transport is periodically diverted south of Cay Sal Bank and around into the SC.

Analysis of the first event at the end of March 1991, which is discussed in Chapter 4, showed, with aid of satellite imagery, that reduction of flow through Transect B was related to the slow eastward propagation of a large meander trough from the region of the Dry Tortugas (i.e. the "Tortugas Gyre"). The southward

movement of the FC core at Transect B as the gyre moved over the Pourtales Terrace has now been shown to produce a clear reduction in transport, which is not, however, observed in the northern part of the Straits. Therefore, the FC transport must be partially diverted into the SC and rejoin the FC at Transect C. There is no evidence in the time series (Figure 5.3-3) that these "diversion events" cause corresponding increases or decreases in flow through the OBC (Transect G). Neither is there any evidence of a foreshadowing of the abrupt decreases at Transect B by increases or decreases in transport south of Key West. This is not unexpected as meander motions of the FC do not cause corresponding fluctuations in transport (Johns and Schott, 1988).

The differences between the transport fluctuations at Transects A and D have already been noted. This implies that the Florida Straits cannot be considered to be a uniform channel as far as transport is concerned. There are substantial contributions from the OBC and NWPC. It also implies that cable measurements for the Jupiter-Settlement Point section are not a good substitute for the outflow of the Loop Current from the Gulf of Mexico. Thus contributions from the subsidiary channels (G and E) are sufficient to cancel out much of the very low frequency variability of the transport through Transect A that is not observed at Transects C and D.

A measure of the realism of the current meter-derived transports can be assessed by continuity checks. There are not sufficient sea level measurements to determine accurately the rates of change of volume caused by the average rise and fall of sea level integrated over the surface area of the Straits. Compared to errors in estimation of FC transports of ± 3 Sv, neglect of the sea level term in the continuity computation is justified if unavoidable. Larger errors are expected from the calculation of transport differences. The following sum and difference transports were calculated:

Transports at:

	B + F - G	corresponding to A
	B + F	corresponding to C
	C - B	corresponding to F
and	D - C	corresponding to E

They are given in Figure 5.3-4.

The correspondence of (B + F - G) to the cable-derived transport for Transect A is remarkably good except for deviations around the beginning of April and in September. These events are attributed to large decreases of transport at Transect B, which are not being entirely compensated by corresponding increases at Transect F. Since currents at F often show a bimodal, cross-channel structure, it is possible that the transport is less well resolved than for the unidirectional flows in the FC. A comparison of (B + F) with A is very similar to the complete simulation showing that fluctuations in OBC transports (G) have only a minor influence on the continuity calculation of transport through Transect A.

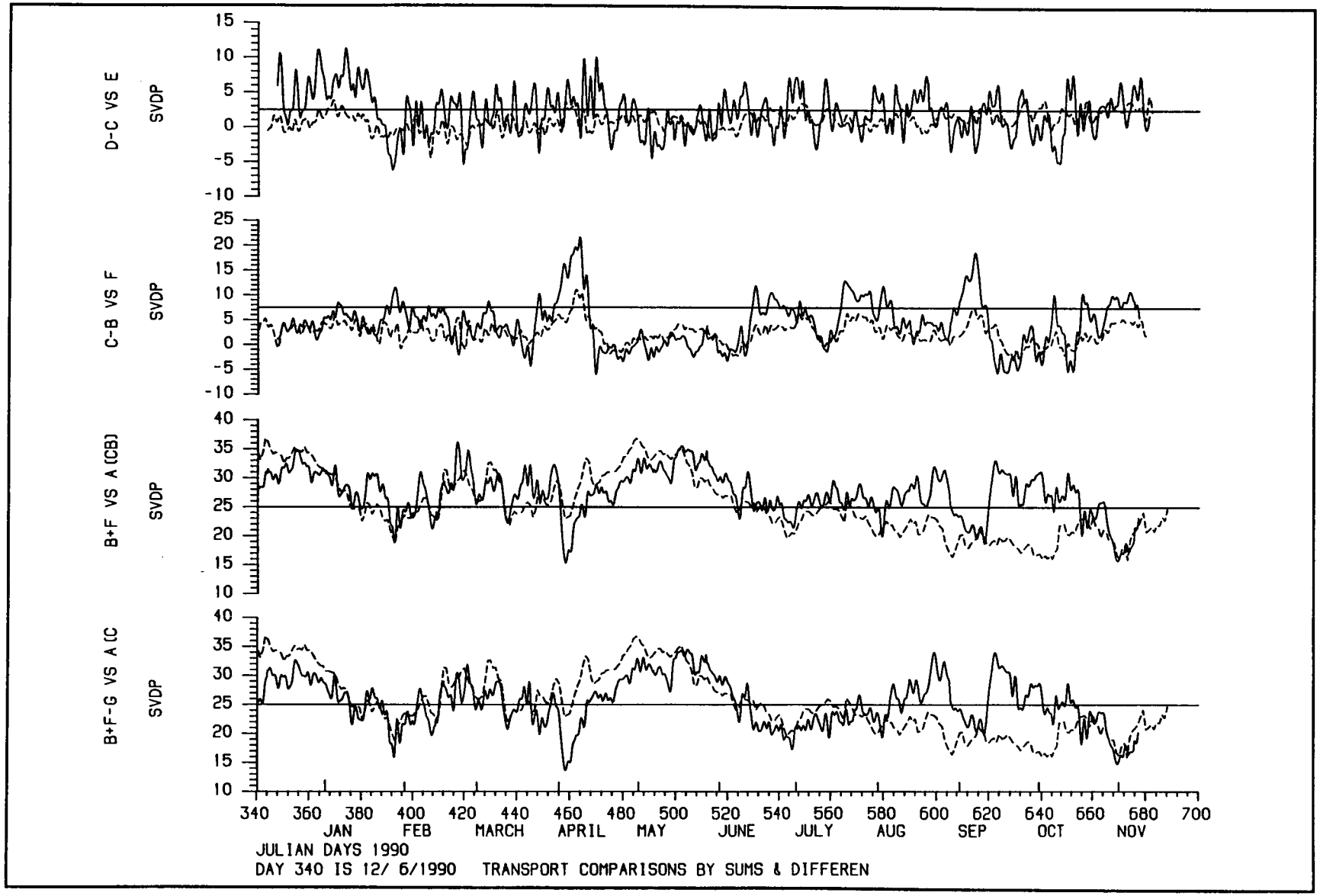

Figure 5.3-4 Transport time series estimated by sums or differences (solid line) and cable-based or current-meter based estimates on the indicated transect. The bottom plot shows the complete estimate of transport on Transect A using both cable and sums and differences of transport in other channels.

The difference of two large FC transports, (C-B) and (D-C) with their respective subsidiary channel directly estimated transports on Transects F and E, (Figure 5.3-4) tends to overestimate the magnitude of the fluctuations but, in general, the direction is reproduced. The difference calculation at Transect F is better than for E, because of the larger signal at F. The volume transports through E (± 3 Sv) are within the noise levels of the calculated transports through C and D. Therefore a good reproduction of E (from the difference calculation, D-C) is not to be expected.

The statistics of the current meter-and cable-derived transports are given in Table 5.3-2. The 11-month means for the FC show a general increase from 25 to 31 Sv from Key West to Jupiter. The standard deviations, however, show the opposite trend, decreasing from about 5 to 3 Sv. Subsidiary transports from OBC and NWPC account for half of this increase in the means by contributing 2 and 1 Sv, respectively. Therefore, the mean transport balances to within 3 Sv, which is the approximate margin of error in estimating the FC transport through Transects B, C or D. The agreement between the cable at 82°W and the continuity-derived transport, (B+F-G), is remarkably close for the means and extremes and thus is the basis of not adjusting the base calibration of 26 Sv/Volt, which was the initial (and independent) best guess. The statistics for the current meter- and cable-derived transports for Transect D agree similarly with means differing by ≃ 1 Sv.

Perhaps the most interesting aspect of these transport calculations is the importance of the OBC. Examination of the current meter records shows that flows at the lower two instruments, nominally at 250 and 435m depths, were always toward the Straits. The 50m instrument occasionally reversed with flows toward the Caribbean. High currents were measured at all depths with an extreme speed of 200 cm s^{-1} occurring at the mid-depth instrument. The mooring was often drawn down by more than 150m, which indicated that larger flows at depth may have been missed by the current meters. Because of these "draw downs", estimating the velocity profile was error prone at times for the upper water column and thus, despite the narrow channel, the transport estimates may not be capturing the larger volume flows. However, the transport estimates show that volume transport is toward the Florida Straits about 95% of the time with extremes greater than 5 Sv. The strongest inflow occurs at the depths of the salinity maximum (100-300m), which indicates that OBC may be an important source of highly saline water for the east side of the FC. Maximum salinities at 200m depth from the hydrographic cruises often reach 37 psu (see Chapter 4).

The correlation coefficients given in Table 5.3-2 confirm the comparisons discussed qualitatively above. Note the inverse correlations of transports over Transects B versus F and C versus E. Also note the correlations of transports over Transects (B+F-G) versus A (derived from the cable); (B+F) versus C; and C versus D. The correlations show that the fluctuations at Transect F are dominated by the diversions around Cay Sal Bank which "swamp" the contributions from OBC (Transect G). The inverse correlation of C and E shows that pulses from C may force NWPC transports and the cyclonic gyre in the entrance that is observed in the imagery (see Chapter 4). The correlation of the two measurements for Transect D is disappointing and results from the poor long-period correspondence of the fluctuations that is a combination of using the active cable and varying number of good current meter records in each of the 4 deployments.

Table 5.3-2 Transport Statistics and Correlations

Transport (11 Months 12/13/90 - 11/81/91)				
	Mean	Standard Deviation	Minimum	Maximum
Line A (Cable)	25.2	5.16	15.9	36.8
B+F-G	25.3	4.27	13.6	34.5
B+F	27.3	3.93	15.3	36.2
Line B	24.8	4.87	10.26	33.0
Line C	29.1	2.88	19.1	36.8
Line F	2.4	2.14	-3.1	11.1
Line C-B	4.2	4.73	-6.1	21.6
Line D	31.1	3.49	22.3	41.8
Line D (Cable)	32.2	2.90	21.8	39.2
Line E	0.9	1.33	-4.5	3.9
Line D-C	2.0	3.10	-6.3	11.4
Line G	1.9	1.67	-2.4	6.6

CORRELATIONS

B versus C	0.34
B+F versus C	0.48
B versus F	-0.62
G versus F	0.21*
C versus F	0.10*
C-B versus F	0.70
C versus D	0.55
C versus E	-0.31
E versus D	0.00*
D-C versus E	0.28
B+F-G versus A (cable)	0.52
B+F versus A (cable)	0.58
D versus D (cable)	0.22

* Not significant at 99% level.

5.3.3 Transport Spectra and Coherence

Variance preserving spectra for the transport time series are given in Figure 5.3-5. The cable- and current meter-derived transports for Transect D have similar energy peaks centered around 14, 7 and 5 days (Figure 5.3-5a). Energy levels are consistently lower for the cable except at very low frequencies. Transect C has similar energy levels with a marked 7 to 10-day period peak. The comparison of transports over Transects C with B (Figure 5.3-5b) shows the dominance of the low frequency energy at periods greater than 14 days from the latter. There is major peak at 40 days, which corresponds to the large meander periods in the southern Straits. This 40-day peak is prominent also in the spectra for transport at A derived from continuity (i.e. B+F-G) but is not resolved in the cable measurements where the energy is shifted to lower frequencies (Figure 5.3-5c). The 40-day peak in the (B+F-G) spectra is caused by an incomplete cancellation of the inversely correlated fluctuations at B and F caused by partial diversions of the FC flow south of Cay Sal Bank. The formation of the Tortugas Gyre is not likely to change the transport through Transect A unless part of the southward flowing Loop Current is diverted back through the Yucatan Straits. Drifters have exited the Gulf through the Cuban side of the Yucatan Straits, so this could be a possible mechanism for very low frequency variability of the transport. It is clear that low frequency shifts of the FC axis by the eastward movement of a large meander of gyre through Transect A will generate large changes in the distribution of downstream current across the section; however, this process does not necessarily imply a change in transport of the FC.

Finally, the spectra for the subsidiary channels (Transects E, F and G) are given in Figure 5.3-5d. Transects F and G show low-frequency energy; however, the peak at F is at 25-30 days rather than the 40 days at B. A 25 to 30-day peak with similar energy to that at F is observed at C (Figure 5.3-5d). Transect E has a very uniform distribution of energy with frequency.

Coherence squared and phase differences between the transports are given in Figure 5.3-6. The coherences between the cable- and continuity-derived transports at Transect A are quite good at periods greater than a week for those frequency bands that are energetic (Figure 5.3-6a). Comparisons of Transects B with C and C with D show moderate coherence at periods longer than a week (Figure 5.3-6b). At periods longer than 20 days, Transect B leads C by about 90° implying a wave-like response, though C has little energy at these frequencies. Figure 5.3-6c shows moderate coherence between Transects F and C where F lags C by 90° at low frequencies. Transport over Transects F and B are 180° out-of-phase at these frequencies, so contributions to Transect C from both B and F tend to cancel out, thus the lower coherence of (B+F) with C at periods longer than 20 days.

Comparisons of Transects C with E and E with D show coherence in the wind-forced band at periods shorter than 10 days (Figure 5.3-6d). The coherence squared between the current-meter and cable-derived transports (Figure 5.3-6e) at Transect D is quite high for the energetic peaks in the spectrum (Figure 5.3-5). Thus, except at very low frequencies (periods > 50 days) the coherence squared between the two signals is much better than the correlation coefficient in Table 5.3-2 would indicate. Figure 5.3-6e also shows the coherence between the transport over Transects A and D (both derived from cable voltages). This is barely or not significant at periods greater than 14 days and significant for

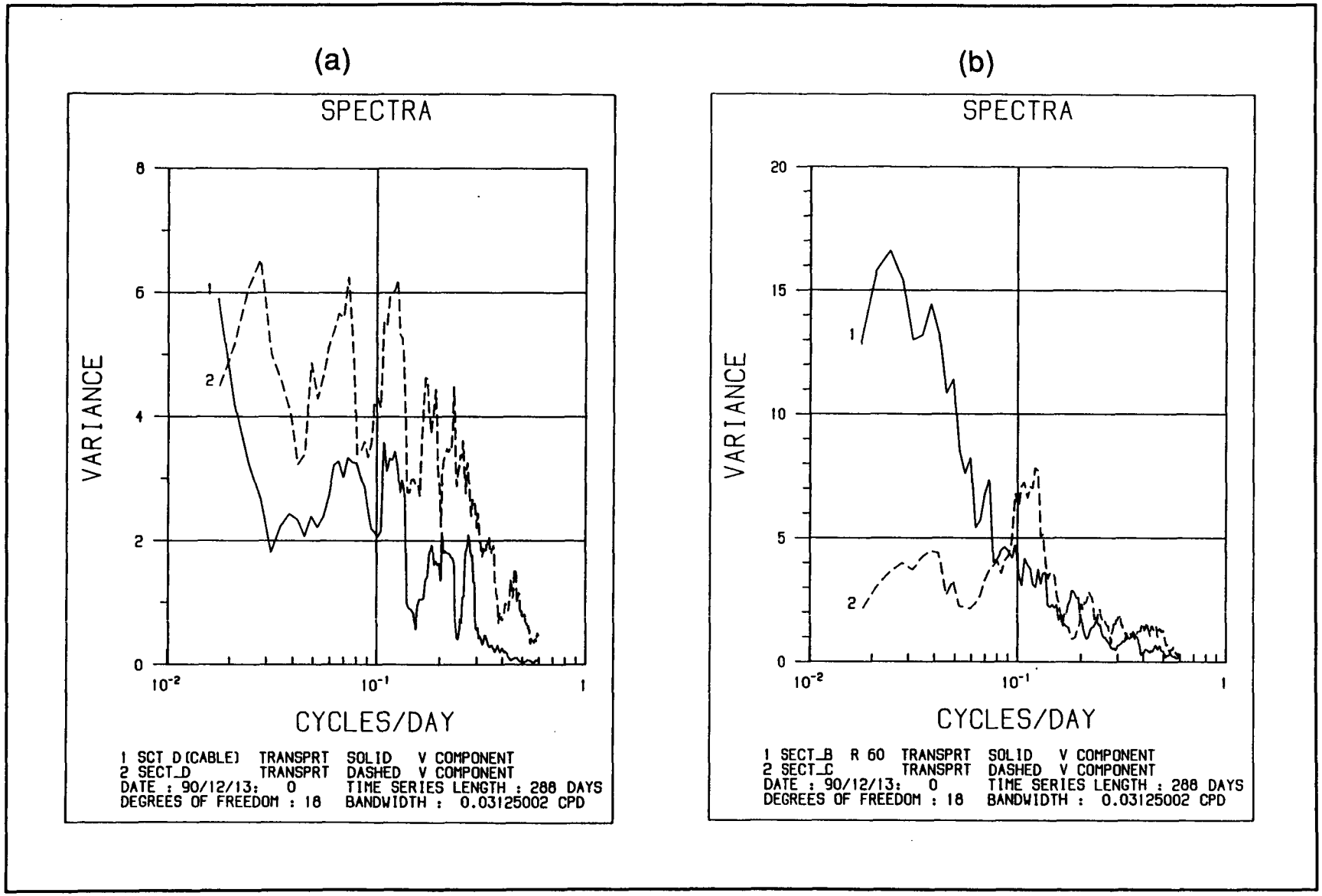

Figure 5.3-5a,b Spectra of 40-HLP transport over the indicated transects: a) transport over Transect D based on current meters and cable, b) transport over Transects B and C.

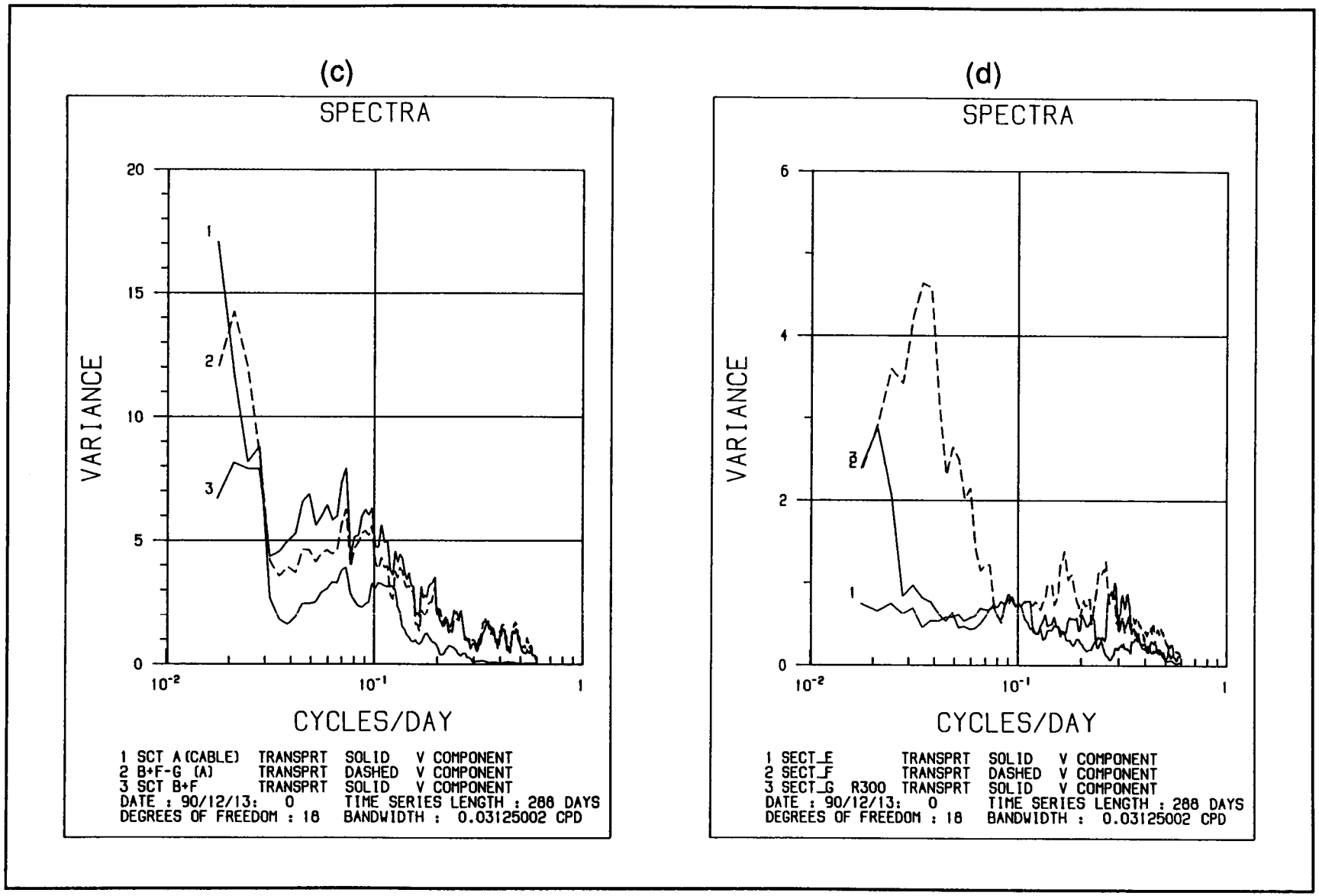

Figure 5.3-5c,d Spectra of 40-HLP transport over the indicated transects: c) transport over A with 1) cable, and 2) and 3) sums and differences, d) transport over Transects 1) E, 2) F and 3) G. Note that (B+F) estimates Transect A without consideration of input from OBC. B+F-G is the complete estimate of transport over Transect A.

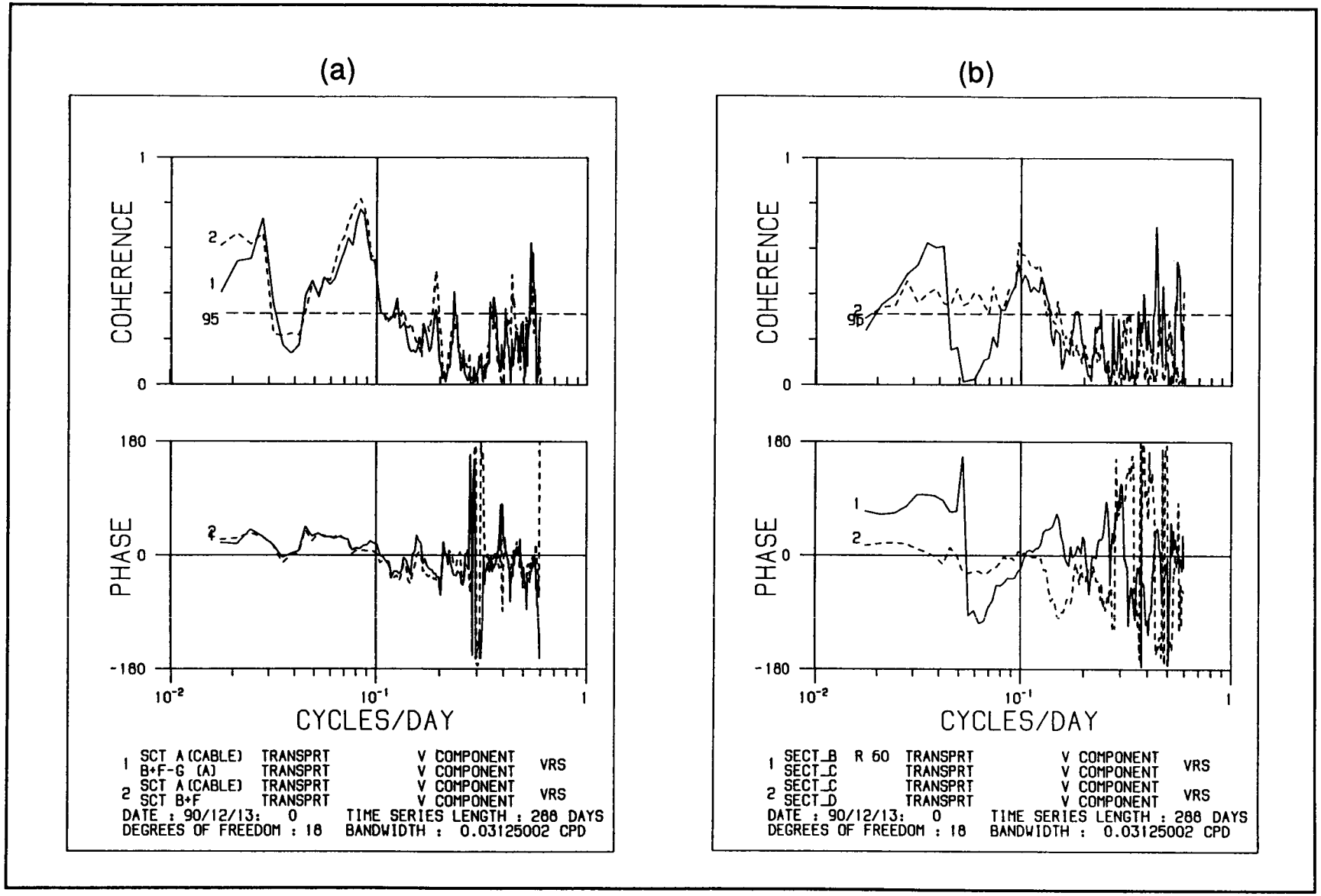

Figure 5.3-6a,b Phase and coherence between the indicated time series. (a) shows results for various methods of estimating transport on Transect A; (b) shows relation between 1) Transects B and C, and 2) Transects C and D.

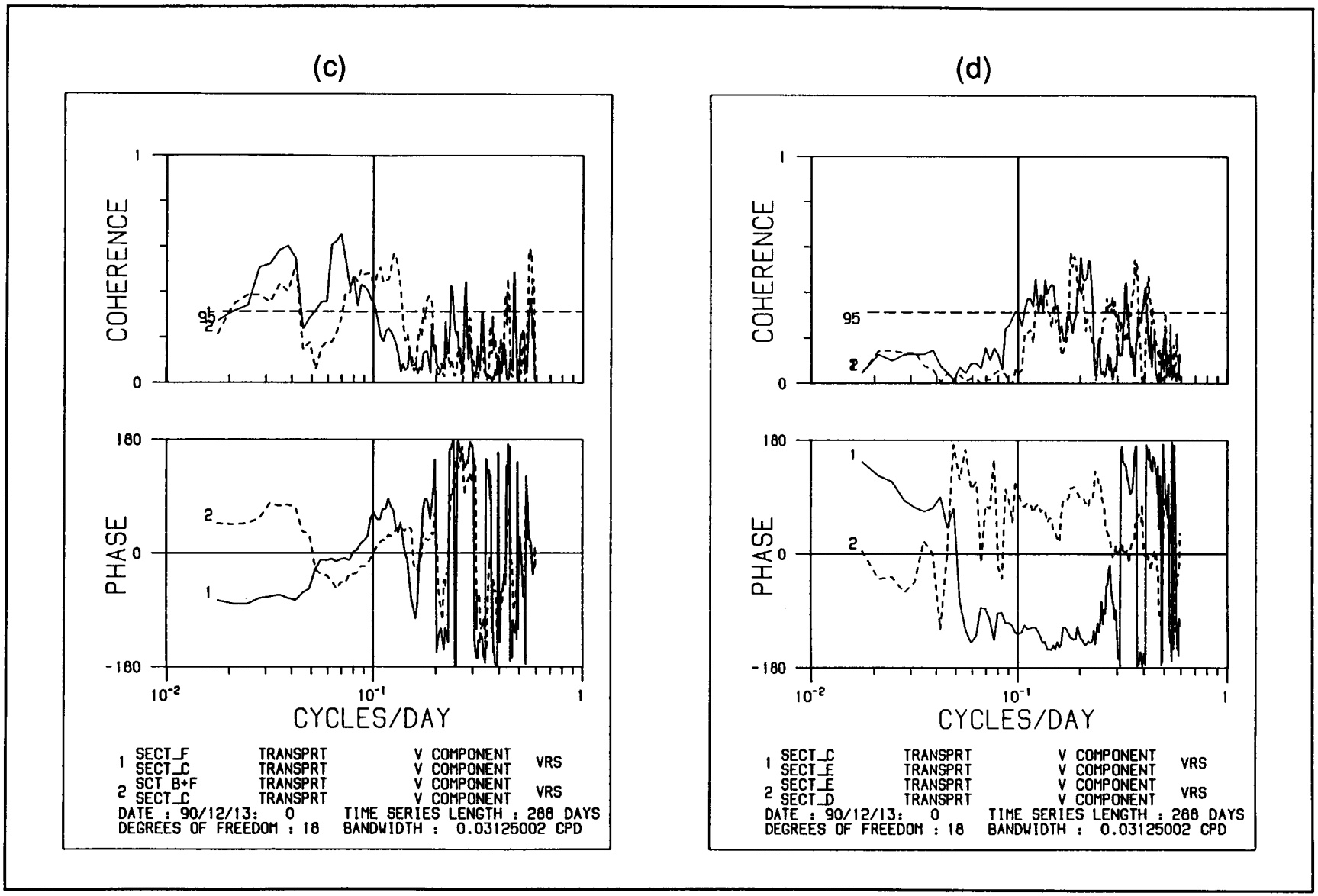

Figure 5.3-6c,d Phase and coherence between the indicated time series. (c) shows (1) Transects F vs. C and (2) sum of B+F vs. C; (b) shows (1) Transects C vs. E and (2) Transects E vs. D.

(e)

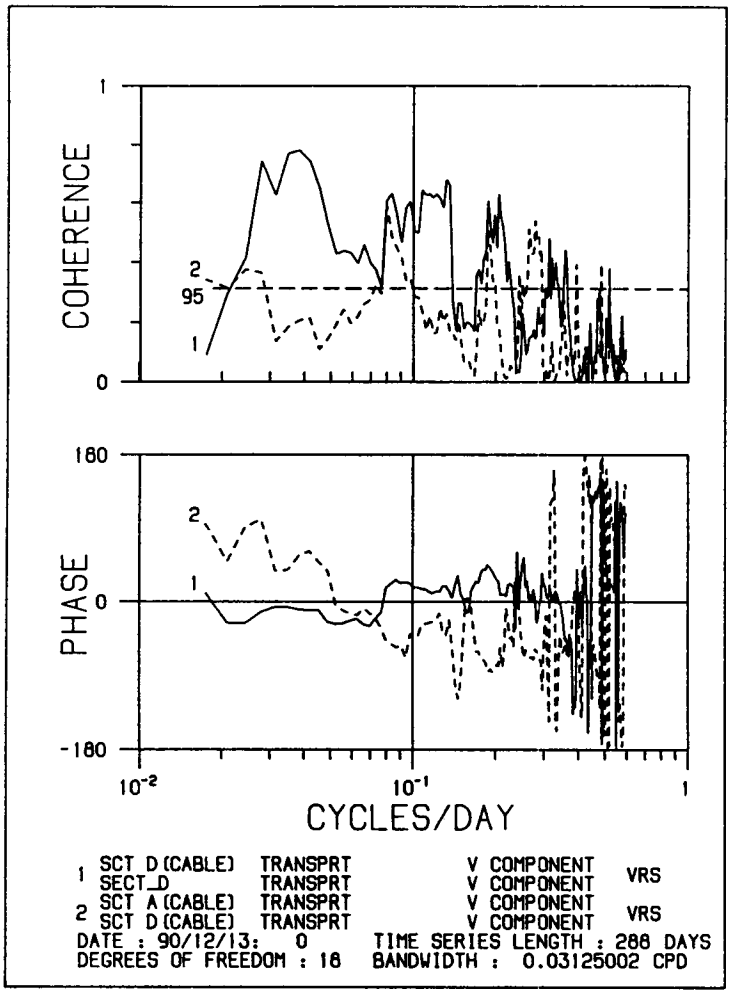

Figure 5.3-6e Phase and coherence between 1) transport on Transect D as estimated by the cable and current meters, and 2) transport as estimated by cables on Transects A and D.

three isolated frequency bands at shorter periods. This again confirms that transport measurements through Transect D are not a good measure of transport fluctuations south of Key West.

The coherence between Transects A and G, and G and F are not significant and not shown. This implies that transport through the OBC is only slightly influenced by flows in the FC and in particular by events that divert part of the transport south of Cay Sal Bank.

5.3.4 Wind Forcing

The variance preserving spectra of the along-channel components of wind stress are given in Figure 5.3-7a. Wind stress is calculated from the wind velocity components using the Large and Pond (1981) coefficients and the quadratic stress law. The majority of the energy is at periods less than 10 days, and most of the spectra have similar peaks. The strongest peak is centered at about 5 days. The east component of wind stress at Key West shows a prominent low frequency peak at a period of about 20 days that is not present in the northward components for Miami and West Palm Beach. The coherence squared between the along-channel components is shown in Figure 5.3-7b. Key West is not coherent with Miami at low frequencies and is only moderately coherent at periods less than 10 days except at the energetic five-day peak. Key West lags Miami by 90° (≈1 day) at this five-day period. In contrast, Miami and West Palm Beach wind-stress components are highly coherent as might be expected.

Lee and Williams (1988) discuss wind-forced transport fluctuations of the FC using the STACS data from 27°N. They found significant coherence between the transport and along-channel winds in the 4- to 10-day period band. They also showed that the finite north-south extent of the channel dampened the response of the transport to longer period wind fluctuations. This effect should be enhanced by the lack of any coherence between along-channel winds off Key West and the north-south part of the channel, which will tend to isolate longer period wind-forced flows in the two sections of the channel. The time to advect a water parcel through the east-west part of the channel is 2-3 days, which is similar to the 2 days for the north-south section (Lee and Williams, 1988).

Coherence squared and phase differences between along-channel wind stress and transport for the four FC sections are given in Figure 5.3-8. Transport from the cable at Transect A is quite strongly coherent with the wind between 12- and 3-day periods. Key West sea level is also coherent at the same frequencies, but is also coherent at periods longer than 30 days, which corresponds to the low frequency peak in the transport spectrum (Figures 5.3-8a). The 180° phase difference between sea level and transport in the 3- to 12-day period band also indicates an Ekman response to coastal sea level consistent with the Lee and Williams model of wind-forced flows in a channel. Transect B transports are only moderately coherent with along-channel winds and along-channel pressure gradients as measured by sea level differences between Miami (Haulover Pier) and Key West (Figure 5.3-8b). This may be an effect of the complex behavior of the FC at Transect B as well as the constriction and turning of the channel. At Miami, Transect C, where the channel is again straight and less constricted, the 4- to 12- day period shows good coherence squared (0.6) with the along channel wind stress (Figure 5.3-8c). Similar results are found for Transect D using both the cable- and current meter-derived transports (Figure 5.3-8d). The latter produce slightly better results. The transport lags the wind by ≈1 day at Transects C

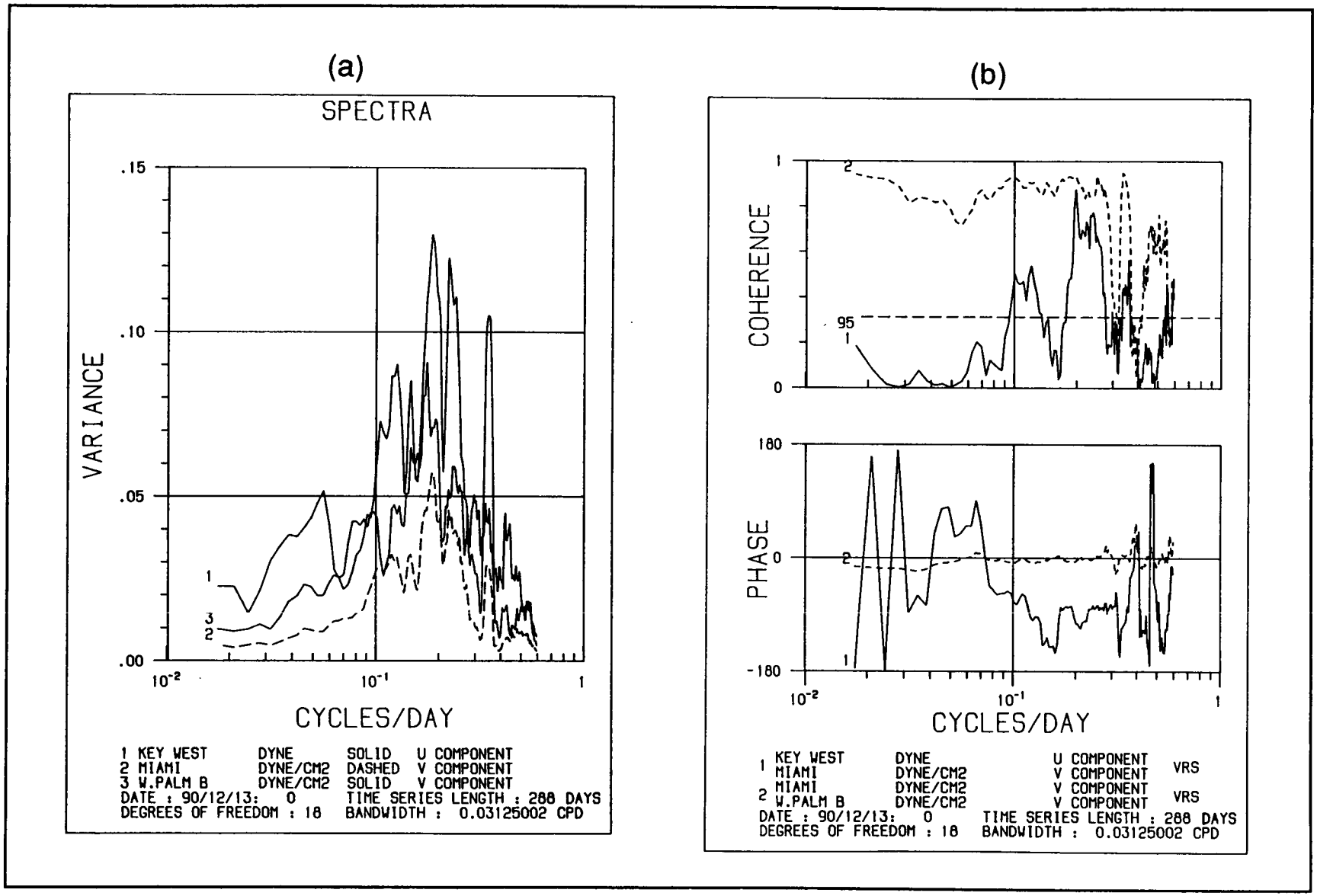

Figure 5.3-7 a) Spectra of along channel wind stress for the indicated locations, b) Phase and coherence between 1) along channel components at Key West and Miami and 2) N-S (along channel) components at Miami and West Palm Beach.

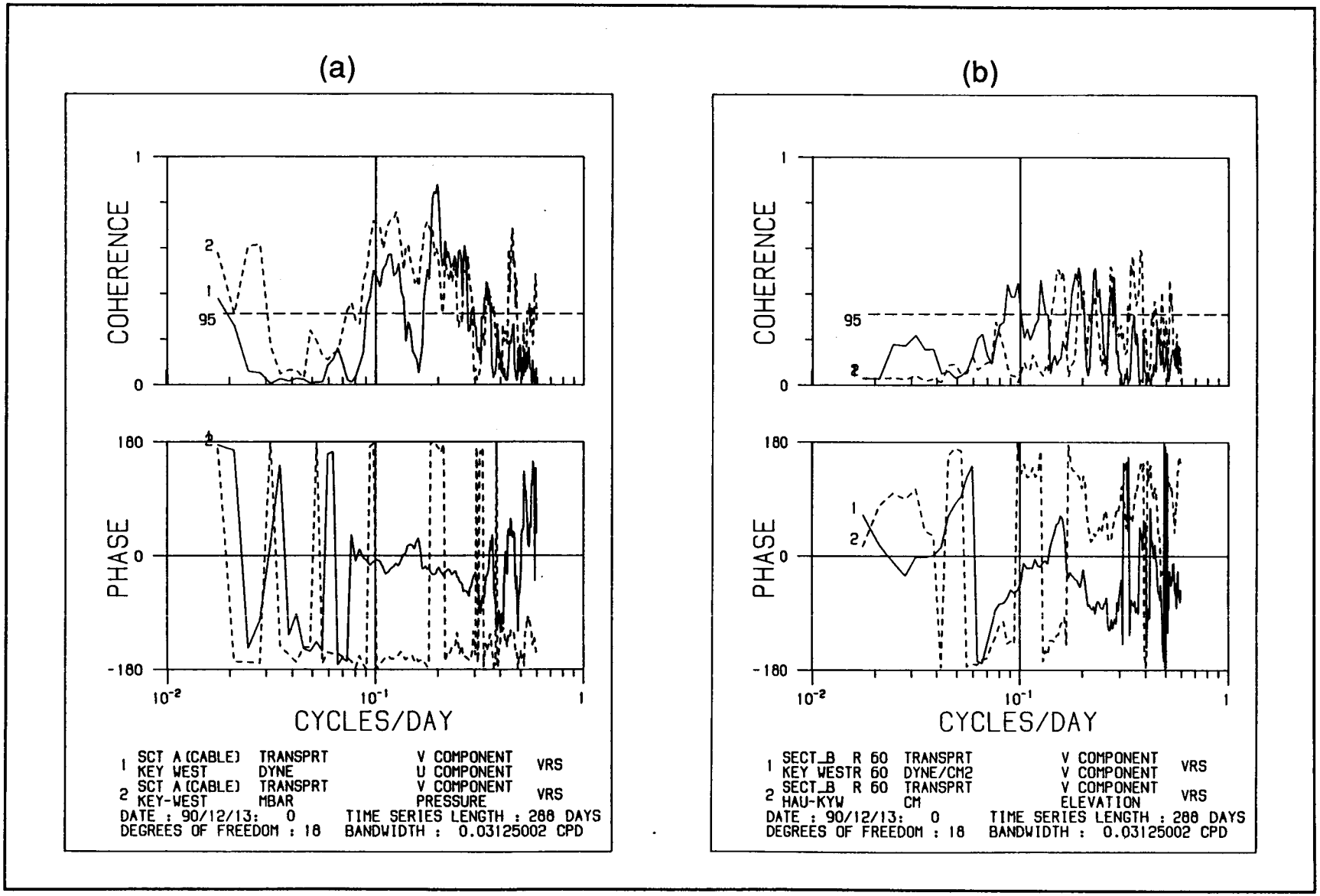

Figure 5.3-8a,b Phase and coherence for: a) transport over Transect A (cable) vs. 1) along channel wind stress and 2) water level at Key West; b) transport over Transect B vs. 1) cross channel (N-S) wind stress at Key West and 2) along channel water level gradient between Miami and Key West.

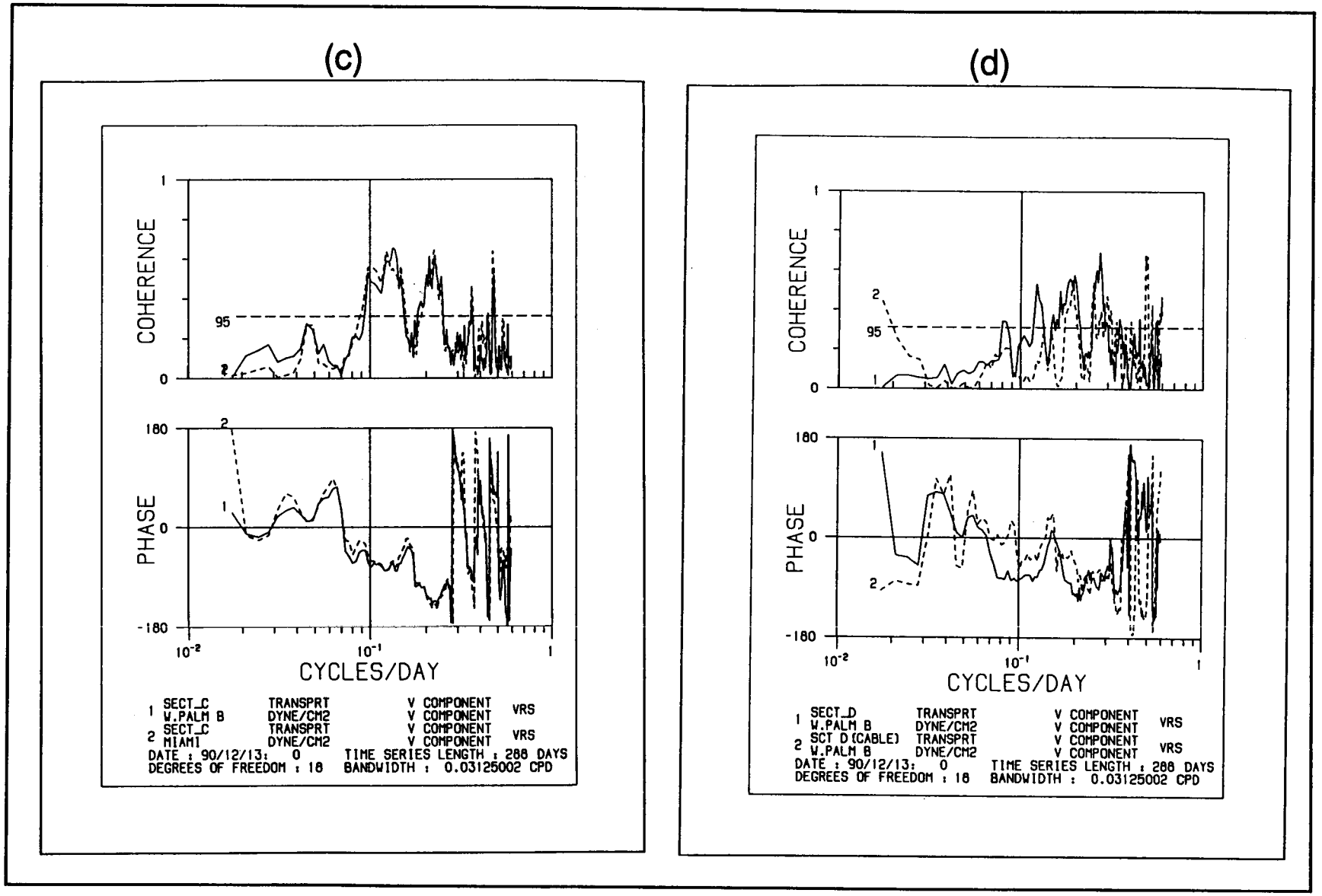

Figure 5.3-8c,d Phase and coherence for: c) transport over Transect C vs. along channel wind stress at 1) West Palm Beach and 2) Miami; d) along channel wind stress at West Palm Beach vs. transport over Transect D as estimated by 1) current meters and 2) cable.

and D, but the lag is much less at Transect A. The reason for the shorter lag time in the transport response to the wind at Transect A is not clear at this time.

The two subsidiary channels (SC and NWPC) have less well defined relationships with wind and sea level in the wind-forced frequency band. The highest coherences are seen between Transect E transports and the eastward wind stress from West Palm Beach, but only at the five-day and three-day spectral peaks (Figure 5.3-9a). The transport at Transect F in the wind-forced band is only marginally coherent with the northward wind stress off Miami (Figure 5.3-9b). The coherence of transports at Transects E and F with sea level from Settlement Point are similar to those of the wind except for a low frequency peak at around 25 to 40 days. This is again an indication of transports into the east side of FC from the SC, which seems to be contributing to fluctuations in the NWPC transports at these frequencies.

Thus, local winds affect local transport at 3- to 12-day periods in a similar manner in the FC off Key West, Miami and Jupiter. There is almost no evidence of wind-forced transport at Transect B where flow is constricted by the Cay Sal Bank or at Transect F in the SC. The NWPC transport over Transect E, however, is coherent at the 5-day period with easterly winds. Therefore, the Cay Sal Bank region seems to act as a partial block to wind-forced transport in the east-west and north-south part of the FC channel where the Lee and Williams (1988) coastal Ekman-response model is a reasonable explanation of the first-order, wind-forced transports. This helps to explain the limited memory of the two parts of the channel to winds even though along-channel wind components are moderately to strongly coherent in the 4- to 12-day period band.

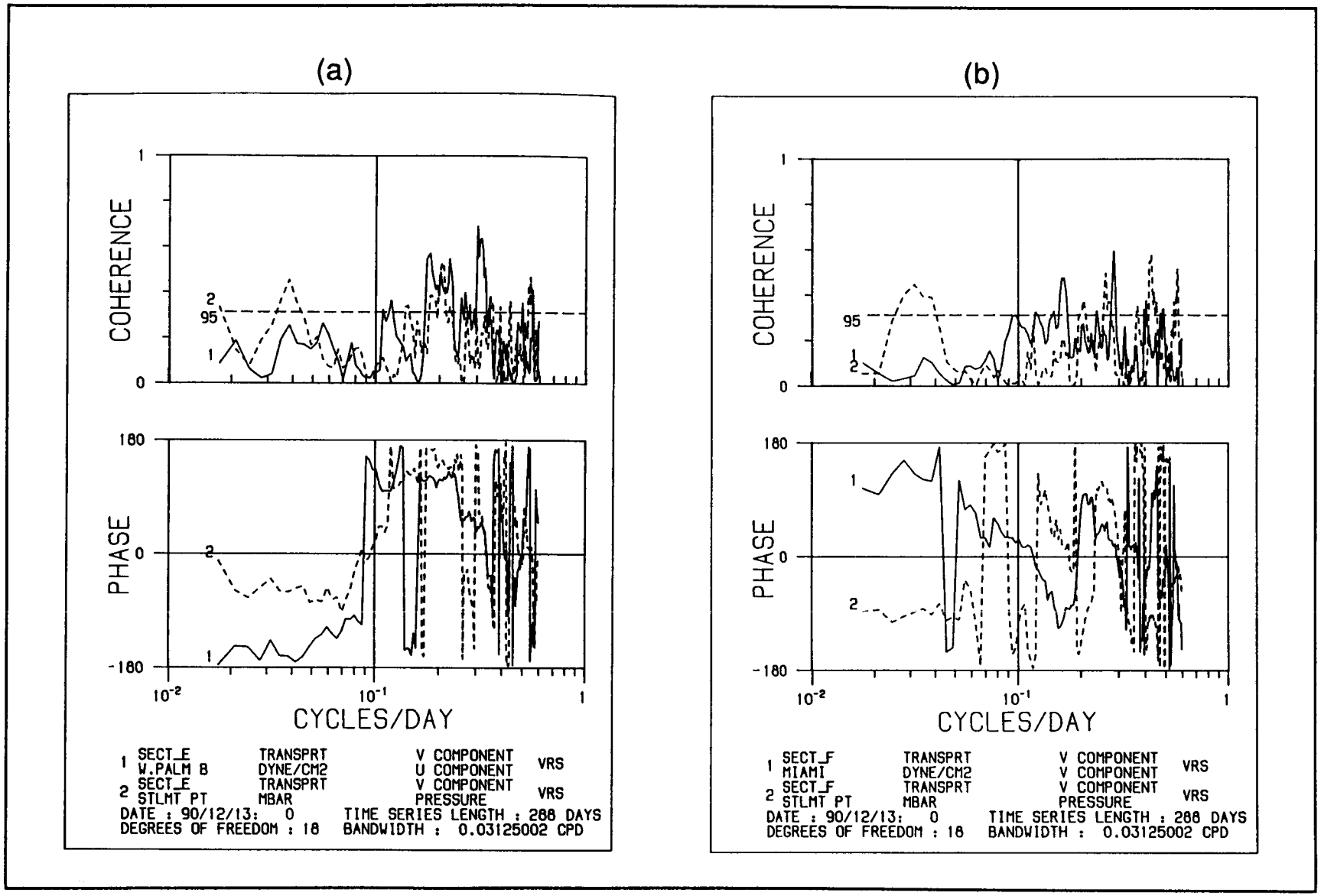

Figure 5.3-9 Phase and coherence for: a) transport over Transect E and 1) along channel wind stress and 2) water level at Settlement Point, and b) transport over Transect F and 1) along channel wind stress at Miami and 2) water level at Settlement Point.

VI. SUMMARY

6.1 Introduction

The Gulf Stream has a major role in maintaining a meridional heat transport as well as being a primary influence on circulation patterns along the Atlantic coast of the United States. The precursor of the Gulf Stream, the Loop Current, enters the Gulf of Mexico via the Yucatan Straits and exits by the SoF. While in the SoF, this major western boundary current is called the Florida Current. The present study area is the SoF and the primary oceanographic features documented are the FC and related circulation patterns in the region.

As a result of the present study, a comprehensive data base is available to: a) support future numerical modeling activities in this key region connecting the Gulf of Mexico and the Atlantic Ocean, and b) provide an improved understanding of dynamic physical oceanographic process occurring in the study area.

The first (and primary objective) study objective of providing data to support modeling has been accomplished. It is the discussion of oceanographic conditions in the study area that is the focus of this report. This discussion identifies and describes some of the major, coherent, current patterns and transports as they vary in location and with time.

An effort has been made in this report to present the data in a concise manner. It should be realized however, that with time and reflection substantial additional insights can be developed from this excellent and comprehensive data base. It is the opinion of the project team that these data which are available from NODC, will provide oceanographers with a valuable resource well into the future.

6.2 Current Patterns

A combined analyses of satellite imagery, subsurface currents and hydrography helped identify an important pattern of the northern boundary of the FC and an associated circulation. Prior investigators documented the presence of a fairly regularly occurring and persistent cold-dome off the southwestern corner of the west Florida shelf (Tortugas Gyre). While some evidence suggests that the Tortugas Gyre forms in conjunction with Loop Current boundary features, until now it was not clear what happened to it and "where it went." In addition, we now have a better understanding of the impact which migration of this gyre can have on the larger scale circulation in the southern portion of the Florida Straits.

Study results show that the Tortugas Gyre is eventually advected to the east along the northern wall of the FC. In this movement, the dimension of its E-W oriented elliptical shape diminishes. In the region of Transect B, this feature becomes what has been previously thought to be an independent feature called the Portales Gyre. In this eastward advection, a cyclonic rotation moves with the feature and can be a mechanism for exchange of water between the outer shelf and upper slope.

Project data do not provide evidence that this boundary feature "makes the turn" from the E-W channel to the N-S channel in the Florida Straits. Spectral analysis of velocity data indicates that the long period fluctuations in FC

position seen in the southern part do not occur in the northern part of the Florida Straits.

The Tortugas Gyre tends to keep the main portion of the FC deflected to the south (offshore) toward Cuba. As the gyre migrates eastward, the FC stays offshore. If this deflection is sufficiently large, the FC can become bifurcated by Cay Sal Bank such that a substantial portion (as much as one half) of the FC flows counter clockwise around Cay Sal Bank (via Nicolas Channel to Santaren Channel) and rejoins the main FC just south of Transect C.

Santaren Channel is also the conduit for the persistent (almost continuous) northward directed mid-depth currents in the OBC. The temperature/salinity of the water comprising these mid-depth currents are often different from those found in the Loop Current and the FC south and west of Transect B. It is more saline (up to 37 psu) and sometimes relatively warmer at this maximum salinity. This higher salinity water tends to move through Santaren Channel on the eastern side at a depth of about 100-200m depth. This pattern may result in Santaren Channel water moving into NW Providence Channel on the southern side of the entrance in conjunction with an often seen cyclonic (counter clockwise) circulation over Transect E in the channel entrance.

OBC surface and near surface currents alternately flow toward and away from the FC. It is only below approximately 100-125m that currents are persistently directed northward (toward the FC). Near surface currents measured in OBC are considerably stronger than previously suspected, reaching 2 kts (100 cm s^{-1}) and a 3 kt range (reversal) in approximately one day. These reversals are often associated with strong tidal and inertial currents.

Currents in Santaren Channel show a definite maximum in the magnitude of mean currents on the eastern side centered about a depth of 250-300m in this 550m deep channel. Similarly, mean currents in the entrance to the NW Providence Channel were a maximum at mid-depth such that flow is out (toward FC) on the north side and in (away from the FC) in the southern half of the channel.

Some of the structure of the currents in the main channel (Transects A, B, C and D) have been documented previously, especially in the northern portion of the study area. The difference in behavior of the FC between southern and northern sections is dependent, in part, on the change in the direction of channel orientation relative to regional wind fields. In addition, the primary flow in the north seems more constrained by channel geometry such that the large lateral shifts documented in the southern region can not occur.

6.3 Transport

Computation and estimation of transport in and through the study area was a major objective of the program design and a key component of the analysis effort. The high overall data return for subsurface currents supported a transport computation scheme which has provided results that are consistent with other independent estimates and historical data.

Previous studies of FC transport (e.g. STACS) have focused on water passing through a section at approximately 27°N. In addition, there was a calibrated cross channel cable which could provide historical and concurrent estimates of transport out of the study area. The availability of this data caused a major

component of this study to be directed toward estimating transport through all the other sections that were instrumented with subsurface current meters.

Using transport from instrumented transects and a continuity assumption, estimates of transport were made for sections which were not completely instrumented, e.g. Transect A. There was a strong statistical agreement between cable-based estimates of transport over Transect A and that based on current meters. In addition, the estimated contributions of the main and lateral channels (input vs. output) balance quite closely at the study boundaries.

An important point is the lack of correlation between transport at Transect D as estimated by cable and current meters. The calibrated cable which has historically provided transport estimates ceased functioning so a new active cable was utilized. This new cable may not provide the same quality of data as the previous (abandoned) cable. During the study, comparison of the cable with transport estimates, based on Pegasus velocity profiles taken by NOAA, showed the cable data did not reproduce some fairly large variations in transport which the current meter data documented.

Correlations also provide added support for the inverse correlation of currents and transport over Transects B and F. There is evidence that FC boundary features can deflect the main body of the FC sufficiently far south that a counterclockwise circulation is set-up around Cay Sal Bank which at times can be quite large (11.1 Sv). This is associated with reduced transport over Transect B (minimum of 10.3 Sv). The relative dominance of this pattern in flow through Transect F is further illustrated by a lack of significant correlation between transport through the OBC (Transect G) and Santaren Channel (Transect F).

The important contributions of flow through OBC is shown by the magnitude and range of the transport. An average of almost 2 Sv flows into the FC system through this channel with a maximum of 6.6 Sv. This is large enough that it may be necessary to account for it during modeling exercises. In addition, the unique temperature/salinity character of some of this OBC inflow adds to its importance as a tracer.

In the southern portion of the study area, the various methods of estimating transport agree quite well. For Transect A, the major difference between the cable- and current-meter based estimates occurs during the latter three months of observations. Because this cable is not well calibrated this difference may point to some changes in the cable rather than the current meters. Certainly, on Transect D the transports from current meters reproduced better the large transport fluctuations detected by Pegasus profiling.

Winds acting on the water surface are an important mechanism for causing variability of transport. The frequency bands in which the along channel component of wind energy is concentrated often shows a strong coherence (correlation) with transport. This is true in the northern and southern portions of the study area even though the channel orientation changes by 90°.

6.4 Hydrography

Hydrographic data showed aspects of conditions in the main part of the FC which have been documented previously. It is data from the lateral channels which provided new insight concerning water mass types and sources. In particular, the

OBC is a source for high salinity water (37 psu) which enters the study area at mid-depth and moves through Santaren Channel (Transect F) on the eastern side and joins the main body of the FC just south of Transect C. There are some indications that this high salinity water may be drawn into the NW Providence Channel along the southern side of the channel entrance.

6.5 Tides

Current meter/transport data indicate that a mixed (diurnal and semidiurnal) tide is common throughout the study area. On Transects B, D and F, the primary diurnal and semidiurnal constituents are similar contributors to sectional transport. On Transects C, E and G, the diurnal component substantially exceeds the transport contribution by the semidiurnal component. The maximum total transport due to tides can be a substantial portion of the subtidal transport, e.g. about 20% over Transect B.

REFERENCES

Anderson, D. L. T., and R. A. Corry. 1985. Seasonal transport variations in the Florida Straits. J. Phys. Oceanogr. 15:773-786.

Boudra, D., R. Bleck and F. Schott. 1987. Study of transport fluctuations and meandering of the Florida Current using an isopycnic coordinate numerical model. In Three Dimensional Models of Marine and Estuarine Dynamics, Edited by J.C.J. Nihoul and B.M. Jimart, Elsevier Oceanography Series 45: 149-168.

Boudra, D., R. Bleck and F. Schott. 1988. A Numerical Model of Instabilities in the Florida Current. J. Mar. Res. 46: 715-751.

Brooks, I. H., and P. P. Niiler. 1975. The Florida Current at Key West: Summer 1972. J. Mar. Res. 33(1): 83-92.

Brooks, I. 1979. Fluctuations in the transport of the Florida Current at periods between tidal and two weeks. J. Phys. Oceanogr. 9: 1048-1053.

Brooks, D. A. and C. N. K. Mooers. 1977a. Wind forced continental shelf waves in the Florida Current. J. Geophys. Res. 82: 2569-2576.

Brooks, D. A. and C. N. K. Mooers. 1977b. Free, stable continental shelf waves in a sheared, barotropic boundary current. J. Phys. Oceanogr. 7(3): 380-388.

Chew, F. 1974. The turning process in meandering currents: A case study. J. Phys. Oceanogr. 4: 27-57.

Cochrane, J. D. 1972. Separation of an anticyclone and subsequent developments in the Loop Current (1969). Texas A&M Univ. Dept. Oceanogr. Studies, Vol 2, Chap. 4: 91-106.

Csanady, G. T. 1982. Circulation in the Coastal Ocean. D. Reidel Publishing Co., 279 pp.

Düing, W. 1975. Synoptic studies of transients in the Florida Current. J. Mar. Res. 33: 53-73.

Düing, W., C. N. K. Mooers and T. N. Lee. 1977. Low-frequency variability in the Florida Current and relations to atmospheric forcing from 1972 to 1974. J. Mar. Res. 35: 129-161.

Foreman, M. G. G. 1979. Manual for Tidal Currents Analysis and Prediction. Pacific Marine Science Report 78-6. Institute of Ocean Sciences, Patricia Bay, Sidney, B.C. 70 pp.

Godin, G. 1972. The Analysis of Tides. University of Toronto Press, Toronto.

Hamilton, Peter. 1990. Deep Currents in the Gulf of Mexico. J. Phys. Oceanogr. 20(7): 1087-1104.

Hurlburt, H. E. and J. D. Thompson. 1980. A Numerical Study of Loop Current Intrusions and Eddy Shedding. J. Phys. Oceanogr. 10: 1611-1651.

Johns, W. E. and F. Schott. 1987. Meandering and transport variations of the Florida Current. J. Phys. Oceanogr. 17: 1128-1147.

Larsen, J. C. and T. B. Sanford. 1985. Florida Current volume transports from voltage measurements. Science, 227, 302-304.

Larsen, J. C. 1992. Transport and heat flux of the Florida Current at 27°N derived from cross-stream voltages and profiling data: theory and observations. Phil. Trans. R. Soc. Lond. 338: 169-236.

Leaman, K., R. Molinari and P. Vertes. 1987. Structure and variability of the Florida Current at 27°N: April 1982-July 1984. J. Phys. Oceanogr. 17: 565-583.

Leaman, K. D., E. Johns, and H. T. Rossby 1989. The average distribution of volume transport and potential vorticity with temperature at three sections across the Gulf Stream. J. Phys. Oceanogr., 19(1): 36-51.

Leaman, K. D., and R. Molinari. 1987. Topographic modification of the Florida Current by Little Bahama and Great Bahama Banks. J. Phys. Oceanogr. 17(10): 1724-1736.

Lee, T. N. 1975. Florida Current spin-off eddies. Deep-sea Res. 22: 753-763.

Lee, T. N., and L. P. Atkinson. 1983. Low-frequency current and temperature variability from Gulf Stream frontal eddies and atmospheric forcing along the southeast U.S. outer continental shelf. J. Geophys. Res. 88: 4541-4568.

Lee, T. N. and D. A. Mayer. 1977. Low-frequency current variability and spin-off eddies off Southeast Florida. J. Mar. Res. 35(1): 193-220.

Lee, T. N., and E. Waddell. 1983. On Gulf Stream variability and meanders over the Blake Plateau at 30°N. J. Geophys. Res. 88: 4617-4632.

Lee, T. N., J. A. Yoder and L. P. Atkinson. 1991. Gulf Stream frontal eddy influence on productivity of the southeast U. S. continental shelf. J. Geophys. Res., 96, 22191-22205.

Lee, T. N., F. Schott and R. Zantopp. 1985. Florida Current: Low-frequency variability of the Florida Current as observed with moored current meter stations during April 1982-June 1983. Science, 227, 298-301.

Lee, T. N. and E. Williams. 1988. Wind forced transport fluctuations of the Florida Current, J. Phys. Oceanogr., 18(7): 937-946.

Lee, T. N., C. Rooth, E. Williams, M. McGowan, A. F. Szmant and M. E. Clarke. 1992. Influence of Florida Current, gyres and wind-driven circulation on transport of larvae and recruitment in the Florida Keys coral reefs. (In Press, Cont. Shelf. Res.)

Leipper, D. F. 1970. A sequence of current patterns in the Gulf of Mexico. J. Geophys. Res. 75(3): 637-657.

Leipper, D. F., J. Cochrane and J. F. Hewitt. 1972. A detached eddy and subsequent changes (1965), in L. Capurro and J. Reid, eds. Contributions to the Physical Oceanography of the Gulf of Mexico. Texas A&M Univ. Studies, Gulf Pub. Co.: 107-118.

Maul, G. 1977. The annual cycle of the Gulf Loop Current Part I: Observations during a one-year time series. J. Mar. Res. 35(1): 29-47.

Mayer, D. A., K. D.Leaman and T. N. Lee. 1984. Tidal motions in the Florida Current. J. Phys. Oceanogr. 14(10):1551-1559.

Mitchum, G. T. and W. Sturges. 1982. Wind driven currents on the West Florida Shelf. J. Phys. Oceanogr. 12: 1310-1317.

Molinari, R., and J. P. Cochrane, 1972. The effect of topography on the Yucatan Current, in L. Capurro and J. Reid, eds. Contributions on the Physical Oceanography of the Gulf of Mexico. Gulf Publishing Co. Houston: 149-156.

Molinari, R. L., W. D. Wilson and K. Leaman. 1985. Volume and heat transports of the Florida Current: April 1982 through August 1983. Science, 227, 295-297.

Morrison, J. M. and W. D. Nowlin. 1977. Repeated nutrient, oxygen, and density sections through the Loop Current. J. Mar. Res. 35(1): 105-128.

Niiler, P. P. and W. S. Richardson. 1973. Seasonal variability of the Florida Current. J. Mar. Res. 31: 144-167.

Nowlin, W. D. 1971. Water masses and general circulation of Gulf of Mexico. Oceanology International 6(2): 28-33.

Nowlin, W., J. Hubertz, and R. Reid. 1968. A detached eddy in the Gulf of Mexico. J. Mar. Res. 26(2): 185-186.

Nowlin, W. and J. Hubertz. 1972. Contrasting summer circulation patterns for the eastern Gulf-Loop Current vs. anticyclone ring. In L. Capurro and J. Reid, eds., Contributions to the Physical Oceanography of the Gulf of Mexico, Texas A&M Univ. Studies, Gulf Pub. Co.: 119-138.

Nowlin, W. and H. McLellan. 1967. A characterization of the Gulf of Mexico Waters in Winter. J. Mar. Res. 25(1): 29-59.

Oey, L. 1988. A model of Gulf Stream frontal instabilities, meanders and eddies along the continental slope. J. Phys. Oceanogr. 18: 211-229.

Paluszkiewicz, T., L. P. Atkinson, E. S. Posmentier and C. R. McClain. 1983. Observations of a Loop Current Frontal Eddy intrusion onto the West Florida Shelf. J. Geophys. Res. 88: 9639-9652.

Richardson, W. S. and J. R. Finlen. 1967. The transport of Northwest Providence Channel. Deep-Sea Res. 14: 361-367.

SAIC. 1987. Gulf of Mexico Physical Oceanography Program, Final Report, Year 4, SAIC Report No. SAIC-87/1027: 226 pp.

SAIC. 1989. Gulf of Mexico Physical Oceanography Program, Final Report: Year 5. Volume II: Technical Report. OCS Report/MMS 89-0068. U.S. Department of the Interior, Minerals Management Service, Gulf of Mexico OCS Regional Office, New Orleans, LA. 333 pp.

SAIC. 1992. Straits of Florida Physical Oceanographic Field Study, Data Report. OCS Report/MMS . U.S. Department of the Interior, Minerals Management Service, Gulf of Mexico OCS Regional Office, New Orleans, LA pp.

Schmitz, W. J., Jr., and W. S. Richardson. 1968. On the transport of the Florida Current. Deep-Sea Res. 15: 679-693.

Schmitz, W. and P. L. Richardson. 1991. On the sources of the Florida Current. Deep-Sea Res., 38 (Suppl.1): 5379-5409.

Schott, F. and W. Düing. 1976. Continental shelf waves in the Florida Straits. J. Phys. Oceanogr. 6: 451-460.

Schott, F., T. N. Lee and R. Zantopp. 1988. Variability of structure and transport of the Florida Current in the period range of days to seasonal. J. Phys. Oceanogr. 18(9): 1209-1230.

Spain, P. F., D. L. Dorson and H. T. Rossby. 1981. PEGASUS: A simple, acoustically tracked, velocity profiler. Deep-Sea Res. 28A(12): 1553-1567.

Sturges, W. 1992. An estimate of the spectrum of Loop Current variability from gappy data. (accepted Jr. Phy. Ocean.)

Vukovich, F. M. 1988. On the formation of elongated cold perturbations off the Dry Tortugas. J. Phys. Oceanogr. 18: 1051-1059.

Wennekins, M. P. 1959. Water mass properties of the Straits of Florida and related waters. Bulletin of Marine Science of the Gulf and Caribbean. 9(1): 1-52.

Williams, E. and T. N. Lee. 1992. SEFCAR Current Meter Data Report for deployment number 6, April - Sept. 1991.

Worthington, L. V. 1976. On the North Atlantic Circulation, The Johns Hopkins Oceanographic Studies, V. 6, The Johns Hopkins University Press, Baltimore. 110pp.

Zantopp, R., K. D. Leaman and T. N. Lee, 1987. Facts on Florida Current Meanders: a close look in June/July 1984. J. Phys. Oceanogr. 17(5): 584-595.